THE
PHYSICAL REVIEW
A Journal of Experimental and Theoretical Physics Established by E. L. Nichols in 1893
VOL. 60, NO. 2 JULY 15, 1941 SECOND SERIES

Fission Yield by Fast Neutrons*

M. AGENO,† E. AMALDI,† D. BOCCIARELLI,‡ B. N. CACCIAPUOTI,† AND G. C. TRABACCHI‡
Istituto di Sanità Pubblica, Rome, Italy
(Received April 30, 1941)

The fission cross section of uranium was measured for neutrons produced in the following reactions: Rn+Be, D+C, D+D, D+Be, D+B, D+Li. From the fact that the mean cross section has about the same value for neutrons of the D+D, D+Be, D+B reactions, it was concluded that the fission cross section has a value σ_f which remains nearly constant between 1 and 10 Mev. For neutrons of the Rn+Be and D+C reactions the fission cross sections seem to be respectively, about $\frac{1}{3}\sigma_f$ and $\frac{1}{8}\sigma_f$. Finally, for neutrons of the D+Li reaction the mean cross section is equal to $1.4\sigma_f$. This fact was interpreted by N. Bohr as due to successive transformations which are possible for energies of the impinging neutrons larger than 10 Mev. A similar increase of the fission cross section was observed also in case of thorium, in very good agreement with the theoretical prediction by Bohr.

ROBERTS, Meyer, Hafstad[1] and Ladenburg, Kanner, Barschall, Van Voohris[2] have performed a few measurements on the dependence of the fission cross section on the energy of the impinging neutrons. The first group of researchers have compared qualitatively the fission yield of neutrons produced in different reactions. Ladenburg and others have measured the fission cross section of U and Th for neutrons of 2.4-Mev energy (D+D) and found, respectively, 0.5×10^{-24} and 0.1×10^{-24} cm^2.

These researchers were also able to show that the fission cross section of U remains constant for energies of the impinging neutrons between 2.1 and 3.1 Mev in agreement with the calculations of Bohr and Wheeler.[3] According to these authors, the fission cross section is negligible for excitation energies of the compound nucleus smaller than a critical value E_f. For excitation energies close to E_f, the fission cross section increases very rapidly to a value σ_f which remains constant also for excitation energies considerably larger than E_f.

The theoretical values of E_f for U^{238}, Pa^{232} and Th^{233} are, respectively, 0.7, 1, 1.7 Mev. The experimental values seem to be slightly lower.[4] In case of U the fission can be produced also by slow neutrons. Bohr[5] pointed out, on theoretical considerations, and Nier, Booth, Dunning, Von Grosse[6] confirmed experimentally, that the isotope responsible for this phenomenon is U^{235};

* Our measurements on uranium fission were performed in April–May, 1940. The measurements on thorium and protoactinium fission were performed in January, 1941.
† Istituto Fisico della R. Università.
‡ Istituto di Sanità Pubblica.
[1] R. D. Roberts, R. C. Meyer and L. R. Hafstad, Phys. Rev. **55**, 416 (1939).
[2] R. Ladenburg, M. H. Kanner, H. Barschall and C. C. Van Voorhis, Phys. Rev. **56**, 168 (1939).
[3] N. Bohr and J. A. Wheeler, Phys. Rev. **56**, 426, 1065 (1939).
[4] R. O. Haxby, W. E. Shoupp, W. E. Stephens, W. H. Wells and M. Goldhaber, Phys. Rev. **57**, 1088 (1940).
[5] N. Bohr, Phys. Rev. **55**, 418 (1939).
[6] A. V. Grosse, E. T. Booth and J. R. Dunning, Phys. Rev. **56**, 382 (1939).

our experiments, however, do not refer to this problem.

In this paper we give an account of some experiments on the dependence of the fission cross section on the energy of the impinging neutrons.[7] Our measurements are more quantitative than those of Roberts and others and refer to a larger range of energy than the experiments of Ladenburg and others. We did not perform any absolute measurement of the cross section; the energy of the impinging neutrons was in all experiments larger than 0.2 Mev.

For our purpose it would be very convenient to have homogeneous groups of neutrons and repeat the measurements of the fission cross section for different values of their energy. Unfortunately only the neutrons emitted in the $D+C$ and $D+D$ reactions are approximately homogenous (we use a thick target). In all other reactions, obtained by bombarding light elements with deuterons, the spectrum of the emitted neutrons is rather complicated and extends from zero to several million electron volts of energy. If we assume, however, the theoretical dependence of the fission cross section on the energy of the impinging neutrons, we must expect to find the same experimental mean cross section independently of the spectrum of the neutrons, provided it extends only above the critical energy E_f. If the neutron spectrum extends from zero to several million electron volts, in order to check the theory of Bohr and Wheeler it will be sufficient to know the percentage α of the total number of impinging neutrons which have an energy larger than E_f. The remaining fraction $1-\alpha$ of the impinging neutrons does not give any contribution to the experimental mean cross section. Therefore the ratio of the number of fission processes produced in a given amount of uranium to the number of impinging neutrons is proportional to $\alpha\sigma_f$. By measuring this ratio with different neutron spectra it is possible to check, in outline if not in detail, the constancy of the fission cross section for energies larger than E_f. The method would also permit, in principle, the determination of the critical energy E_f. However, this determination would require the knowledge of the low energy part of the spectrum of the neutrons with a much higher accuracy than is now available.

[7] M. Ageno, E. Amaldi, D. Bocciarelli, B. N. Cacciapuoti and G. C. Trabacchi, Ricerca Scient. **11**, 302 (1940); M. Ageno, E. Amaldi, D. Bocciarelli and G. C. Trabacchi, Ricerca Scient. **11**, 413 (1940); E. Amaldi, D. Bocciarelli and G. C. Trabacchi, Ricerca Scient. in press.

2. Principle of the Method

The best method which permits a measurement of the number of neutrons emitted from a source independently of their energy, consists in slowing down all neutrons in a hydrogenated substance and then measuring the density of thermal neutrons by means of a convenient detector. The integral of the density of thermal neutrons over all the volume of the hydrogenated substance is proportional to the total number of the emitted neutrons. In order to use this method of measuring the number of the impinging neutrons, the experiments on uranium were performed on the following principle. Let us consider a spherical shell, coated with uranium and having its center on the target. The ratio of the number n of fissions produced in the uranium layer to the number of impinging neutrons is proportional to $\alpha\sigma_f$. The number of impinging neutrons can be measured by substituting for the uranium layer a water cylinder so large that all neutrons emitted from the target are slowed down to thermal energy.

We point out the necessity of performing both measurements (of the total number of fissions and of the density of thermal neutrons) in all directions with respect to the direction of the deuterons impinging on the target, because the slowing down process in water partially cancels the anisotropy of the neutrons impinging on the uranium layer.

3. Experimental Data

Our neutrons were produced by bombarding with deuterons accelerated in the 1100-kv tube of the Istituto di Sanità Pubblica,[8] different targets, namely D, Li, Be, B, C. The deuterium target was obtained by adsorbing about 3 liters of D_2 in 20 g of zirconium powder at the temperature of 200°C.[9] This powder was cooled and compressed in a brass cup of 3.5-cm diameter and

[8] E. Amaldi, D. Bocciarelli, F. Rasetti and G. C. Trabacchi, Ricerca Scient. **10**, 623 (1939).

[9] F. H. Penning and J. H. A. Moubis, Physica **4**, 1190 (1937).

2-mm depth which was placed in the lower part of the tube. We have used this method, which presents several inconveniences, among them the low intensity and the rather complicated preparation, because the use of a target of heavy water with liquid air must be excluded on account of the geometry of the arrangement.

Li, Be and C were used in form of disks of the elements; B in form of a disk of B_2O_3. The electrodes of the ionization chambers used for counting the number of fissions in different heavy elements were two disks of 5-cm diameter, 3 cm apart from one another. One of the electrodes was connected to the grid of the first tube of an amplifier and the other was maintained to a voltage of 3800 volts by means of a stabilized system. This electrode was coated with a layer of the heavy element; for U and Th we used thick layers of U_3O_8 and ThO_2.

For Pa we evaporated on a silver electrode 3.5 cc of a solution of 7 percent H_2SO_4 containing less than a hundred micrograms of Pa.[10] By substituting for the electrode coated with a heavy element a blank electrode, we could check the absence of electrical disturbances. The primary ions produced in the gas of the ionization chamber by the fission products gave rise to a weak multiplication on account of the relatively high voltage applied to the chamber. The pulses were recorded by means of a scale-of-four or a scale-of-six and were simultaneously observed by means of an oscillograph.

As the lower part of the tube was cooled by means of a thin layer of water (4 mm thick), we surrounded completely the lower part of the tube and the ionization chamber with Cd of 0.52 g/cm² thickness in order to absorb all neutrons of thermal energy. These, however, in our conditions, were negligible; in fact by removing the cadmium layer we could not observe any increase of the number of counts.

In some of the experiments we will describe below, we measured the number of neutrons impinging on heavy elements by means of the activity of 44 sec. induced in Rh by slow neutrons. All these measurements were performed with three Rh detectors 5×5.5 cm² of area and 0.36 g/cm² thick. The activity of these detectors was measured with an ionization chamber containing carbon dioxide at 2.5 atmos. pressure connected to an Edelman electrometer. The activities given in the tables are defined as the total activity (namely the activity measured from zero time to infinite time) of the detector after 1 minute irradiation. We assume the activity of a preparation of 85 g of U_3O_8 equal to unity. This standard was 42.1 times larger than the standard preparation used in other researches.[11]

[10] We are indebted to Professor A. V. Grosse of the University of Chicago for this protoactinium preparation.

4. Experiments with Uranium

In the case of uranium, we performed two experiments based on the principle described in Section 2.

(a) In the first experiment we measured the number of fissions produced in uranium by means of the ionization chamber described in Section 3 and the density of thermal neutrons by means of the activity of 44-sec. period of Rh. Instead of measuring both these quantities in all directions in order to evaluate their integral with respect to θ and φ, the experiments were actually performed only at $\theta=90°$ and $\theta=0°$ with the direction of the impinging neutrons.

From the following simple geometrical consideration it is easy to recognize that the largest contribution to the above-mentioned integrals comes from the measurements at 90°, while the measurements in the forward direction give only a small contribution. If we call l the linear dimension of the detector (Rh or electrode coated with uranium) and r its distance from the center of the target, the solid angle subtended by the detector is l^2/r^2 for each direction θ, φ. In order to evaluate the integral with respect to the azimuth φ, we must multiply the data at $\theta=0°$ by 1 and the data at $\theta=90°$ by the factor $\delta=2\pi r\times l/l^2$. As the distance r of the detector from the center of the target was 5.7 cm, we find for the Rh detector (5×5.5 cm²) $\delta=6.5$ and for the uranium layer (disk of 5-cm diameter) $\delta=9.1$.

As will appear below, the measurements in forward directions give results slightly different from the measurements at $\theta=90°$, showing that both the number of fissions per minute and the activity of the Rh detector are functions changing only very slowly with the angle θ. It seems,

[11] E. Amaldi and E. Fermi, Phys. Rev. **50**, 899 (1936).

TABLE I. ($\theta=90°$) *summary of data.*

REACTION	ENERGY OF D^+, MEV	a	$K\times10^{-3}$	n	$n\times10^3/Ka$
$D+C$	0.85	184 ± 5	0.41 ± 0.03	3.2 ± 0.5	0.042
$D+C$	0.85	273 ± 2	0.41 ± 0.03	5.2 ± 0.7	0.046
$D+C$	1.0	669 ± 7	0.46 ± 0.03	11.4 ± 1	0.037
$D+C$	1.0	621 ± 6	0.46 ± 0.03	9.3 ± 0.9	0.033
$D+D$	0.50	80.7 ± 2	0.96 ± 0.05	18.2 ± 1	0.24
$D+Be$	0.85	2217 ± 23	1.03 ± 0.05	580 ± 7	0.25
$D+B$	0.85	514 ± 11	0.76 ± 0.05	101 ± 2	0.26
$D+Li$	0.75	1627 ± 30	1.11 ± 0.03	660 ± 8	0.37
$D+Li$	0.60	780 ± 6	1.11 ± 0.03	310 ± 5	0.36

therefore, reasonable to substitute the integrals of these two quantities with the mean value of the results at $\theta=90°$ and $\theta=0°$ weighted with the above-mentioned factors. As the difference of the data obtained by this method from the data at 90° is of the same order of magnitude as the error of the experimental results, we shall use in the discussion the data obtained at 90°. We will, however, give also the data obtained in the forward directions in order to justify the approximations used.

The measurements were actually performed as follows: with the ionization chamber placed in a well-reproducible position with respect to the target at a distance $r=5.7$ cm at 90° (or 0°) we counted the number n of fissions per minute. Then we removed rapidly the ionization chamber and surrounded the lower part of the tube containing the target with a cylindrical vessel of 28-cm diameter and 25-cm depth filled with water. A Rh detector in the same position as previously occupied by the coated electrode of the ionization chamber (at 5.7 cm at 90° or 0°) was irradiated for 1 minute and its activity a was measured. These two measurements with U and Rh were repeated alternately many times in order to check the constancy during the experiment of the intensity of the emitted neutrons. The activity a of the Rh detector, however, is not simply proportional to the total number of neutrons emitted from the target because the spatial distribution of slow neutrons in water has a different distance dependence for different neutron sources. Therefore, at a later time, we placed around the target a vessel of $38\times80\times28$ cm³ for the experiments at 90° and a cylindrical vessel 70 cm deep and 50 cm in diameter for the measurements at $\theta=0°$ and we measured the activity $A(r)$ of the Rh detector as a function of the distance from the target (in this paper by r we mean the root-mean-square distance between points on the detector and on the target). Then we calculated both at 90° and 0° the ratio

$$K=\int_0^\infty A(r)r^2dr \Big/ A(5.7).$$

The product $K\cdot a$ is proportional to the total number of neutrons as long as we neglect the anisotropy of the emission from the target.

The results of our measurements are summarized in Table I ($\theta=90°$) and Table II ($\theta=0°$). In the third column we give the activity a of the Rh detector, in the fourth column the factor K multiplied by 10^{-3} and in the fifth column the number n of fissions per minute. The sixth column contains the quantity $n10^3/Ka$ calculated from the preceding data.

As it appears from Table II, we also performed an experiment with the photo-neutrons of Rn+Be. As the emission of neutrons in this case is certainly isotropic we performed this experiment only in one direction. We put in a brass tube having the same shape of the lower part of the tube a layer of beryllium powder 5 cm thick in which we plunged a small glass tube containing initially 500 millicuries of radon. The geometry of the experiment was the same as that used with the tube in the forward direction.

As the observed effect was very weak, we counted the number of pulses given by our ionization chamber, alternately with and without the γ-ray source close to the chamber. We counted 75 pulses (corrected to 79 for the decay of radon) in 980 minutes with the γ-ray source, against 1 pulse in 709 minutes without the γ-ray source.

We shall discuss in Section 6 the results obtained with photo-neutrons and neutrons of the $D+C$ reaction. From the data of Table I it appears that the quantity $n\times10^3/Ka$ has about the same value for neutrons of the $D+D$, $D+Be$

TABLE II. ($\theta=0°$) *summary of data.*

REACTION	ENERGY OF D^+ MEV	a	$K\times10^{-3}$	n	$n\times10/Ka$
$D+C$	0.85	241 ± 2	0.34 ± 0.03	6.9 ± 0.8	0.084
$D+C$	1.0	705 ± 11	0.47 ± 0.03	17 ± 2	0.051
$D+D$	0.50	26.4 ± 0.5	1.1 ± 0.06	12.2 ± 1	0.42
$D+Be$	0.85	2790 ± 40	0.90 ± 0.05	669 ± 6	0.27
$D+B$	0.85	640 ± 5	0.71 ± 0.04	164 ± 3	0.36
$D+Li$	0.75	2400 ± 50	1.07 ± 0.01	1070 ± 7	0.42
γ Rn+Be		3.95 ± 0.04	0.39 ± 0.04	0.08 ± 0.009	0.052

and $D+B$ reactions while for neutrons of the $D+Li$ reactions this quantity seems to be about 1.4 times larger.

(b) We thought it convenient to compare the mean cross section for fission of the neutrons from the $D+Be$ and $D+Li$ reactions by means of an improved method. On account of the low intensity it was impossible to use this second method in the case of the $D+D$ and $D+B$ reactions.

Experiment (a) is open to some criticism because of the anisotropy of the emitted neutrons for which we did not correct the experimental data. Therefore we mounted the ionization chamber with the electrode coated with uranium on a wooden arm which could turn around the center of the target. The distance of the U_3O_8 layer from the center of the target was 11 cm. By means of this disposition we measured the number of fissions n per minute for θ equal to 0°, 22°.5, 45°, 67°.5, 90°, 112°.5, 135°. The ratio

$$s=\frac{\sum n(\theta)\sin\theta}{n(90°)\sum\sin\theta}$$

represents the factor by which we must multiply the number n of fissions per minute observed in the 90° direction and given in column 5, Table I, in order to correct in a complete way for the anisotropy of the emitted neutrons. In Table III, column 4, we give the values of this factor s for the $Be+D$ and $Li+D$ reactions. In column 5 we give the values of the quantity ns/a calculated by using for n and a the values already given in Table I and reproduced in columns 2 and 3 of Table III.

In order to measure the total number of neutrons emitted from the target we dissolved 30 kg of $MgCl_2$ in 100 liters of water and put this solution in the form of a water cylinder 50 cm high and 50 cm in diameter, around the target. This solution was irradiated 40 min. in order to activate the 37-min. period of Cl. During the irradiation the solution was continuously mixed by blowing with a small pump some air close to the bottom of the container.

TABLE III.

REACTION	a	n	s	$\frac{n\cdot s}{a}$
$Be+D$ 0.85 Mev	2217±23	580±7	1.04±0.03	0.272±0.010
$Li+D$ 0.75 Mev	1627±30	660±8	0.98±0.03	0.398±0.015
$Li+D$ 0.60 Mev	780±6	310±5	0.98±0.03	0.390±0.014

TABLE IV.

	REACTION	i	b	i/b	$\frac{ns}{a}\frac{i}{b}$ ×10⁴	$\frac{d\sigma_{Li}}{a\sigma_{Be}}$
1.	Be+D	.8312±116	408±11	20.4±0.6	133	1.37±0.09
	Li+D	.6063±107	280±6	21.6±0.6	182	
2.	Be+D	.8247±115	388±6	21.2±0.5	128	1.49±0.09
	Li+D	.5197±100	252±3	20.6±0.5	191	
3.	Be±D	.7474±112	1430±30	5.23±0.01	520	1.34±0.08
	Li±D	.8128±114	1440±30	5.65±0.01	697	
						1.40±0.05

It is clear that the activity of a given amount of the solution is proportional to the integral with respect to the distance from the target as well as to the angles θ, φ, of the density of slow neutrons and therefore to the total number of emitted neutrons. Therefore, after the irradiation we placed the solution in a small glass vessel having the shape of a hollow cylinder 20 cm long which could be put on a thin-walled Geiger counter of 20-mm diameter. Then the counting system was started 3 min. after the end of the irradiation and we measured the total number of pulses observed in 40 min. We were very careful to keep constant both the time of observation as well as the 3 minutes of delay because our solution showed a rather complicated decay curve due to the superposition of many periods. In fact our $MgCl_2$ was not very pure and contained also some potassium. Therefore the zero effect of the counter (63 pulses/min.) was always measured by putting on the counter our thin-walled glass vessel filled with non-activated solution.

In Table IV, column 2, we give the total number i of pulses observed in 40 min. in three successive experiments; the zero effect has already been subtracted. In order to check the constancy of the emission of neutrons during the irradiation and in order to be able to compare results obtained with different reactions, we measured, every fifth minute, the activity of a Rh detector, after 1-min. irradiation, in a well-reproducible position with respect to the target in the solution of $MgCl_2$.

In column 3 of Table IV we give the mean value b of these activities.

In experiments 1 and 2 the Rh detector was placed at 13.2 cm from the target at 90° with the direction of the impinging deuterons: in experiment 3 it was put in the same direction but at a distance of only 5.7 cm. As our curves of the activity as a function of the distance r show that the ratio $A(5.7)/A(13.2)$ has the same value for neutrons of $D+$Li and $D+$Be reactions, the data of experiment 3 can be compared with that of experiments 1 and 2. We checked also that the presence of the salt did not change appreciably the spatial distribution of slow neutrons.

In column 4, Table IV, we give the values of the quantity i/b and in column 5 a quantity proportional to $\alpha\sigma$, namely the ratio of the data of column 5, Table III, to the data of column 4, Table IV, $(ns/a)/(i/b)\times 10^4$.

Finally in column 6, Table IV, we give for each of the three experiments the ratio $\alpha\sigma_{\mathrm{Li}}/\alpha\sigma_{\mathrm{Be}}$. We find for this quantity the value 1.4 as from experiment (a).

5. Experiments with Thorium and Protoactinium

In a first attempt we performed with Th an experiment similar to experiment (a) (on U) described in Section 4. The precision of this experiment was too low and did not allow, therefore, any definite conclusion.

Recently we again worked on this subject and we thought it more convenient to compare the fission cross section of Th and Pa with the fission cross section of U with neutrons produced in different reactions. For this purpose we used two similar ionization chambers, as described in Section 3, connected to two linear amplifiers, one with the electrode coated with uranium, the other with the electrode coated with Th (or Pa).

When these two ionization chambers were put in a given position with respect to the target, we counted by means of a scale-of-six and a scale-of-four the number of fissions observed in a given time, respectively in U and Th (or Pa). The ratio $n_{\mathrm{U}}/n_{\mathrm{Th}}$ of these numbers of pulses was measured with neutrons produced in the $D+$Be and $D+$Li reactions. The experiment was repeated, alternatively, five times with these two targets.

In the experiments on Th the two layers of U and Th were placed symmetrically in a horizontal plane, below the lower part of the tube, at 10 cm from the center of the target. In Table V we give results obtained in five successive experiments and the corresponding mean values.

Table V. *Ratio of number of fission in* U *and* Th.

$D+$Be	$D+$Li
4.46	3.17
4.57	2.82
4.04	3.53
4.37	3.03
4.19	3.45
4.34 ± 0.10	3.20 ± 0.13

From these data we conclude that the fission cross section of Th increases, with increasing energy of the impinging neutrons, more than the fission cross section of U by a factor

$$\frac{4.34\pm0.10}{3.20\pm0.13}=1.35\pm0.08.$$

As mentioned above, we tried a similar experiment with Pa.

Although the electrode coated with this element was placed as close as possible to the target, and neutrons produced in the $D+$Be reaction were used, we observed only 1 fission every second or third minute. On account of the larger number of the impinging neutrons, in the case of the $D+$Li reaction we observed about 2 or 3 fissions per minute. We counted, altogether, 120 counts with neutrons produced in the $D+$Be reaction and 345 counts with neutrons produced in the $D+$Li reaction and found that the ratio of fission cross section of U and Pa is slightly higher with neutrons of the $D+$Li than with neutrons of the $D+$Be reaction. The difference is, however, of the same order of magnitude as the statistical error and therefore can be considered only as an indication.

6. Discussion

Let us first consider the data obtained in the case of U with neutrons of the $D+$D, $D+$Be and $D+$B reactions, given in Table I, column 6.

We see that the mean cross section obtained with neutrons of the $D+$Be reaction (0–4.6 Mev) is equal to the cross section obtained with neutrons of the $D+$D reaction which, in our condition, gave an approximatively homogeneous

group of neutrons of 2.6 Mev. From this fact we conclude that the percentage α of the neutrons, produced in the $D+$Be reaction, having an energy larger than the critical energy for fission E_f of U is about equal to one: $\alpha \sim 1$ and that the fission cross section remains practically constant for energies of the impinging neutrons between E_f and the upper limit of the spectrum of the $D+$Be reaction. In fact, by correcting for the proton-neutron elastic cross section the data of Bonner and Brubaker,[12] which extend on the low energy side to 0.6 Mev, we find that the neutrons having energy below 1 Mev, represent only about 5 percent. As the theoretical value of the critical energy E_f is 0.7 Mev we conclude that we must expect $\alpha \sim 1$ as we found experimentally.

In a similar way we can discuss the result obtained with the neutrons of the $D+$B reaction. This spectrum has an upper limit at 13.5 Mev and was measured, on the low energy side, down to 2 Mev.[12] The extrapolation of the spectrum to zero energy is, in this case, rather uncertain and therefore we cannot evaluate the percentage α of neutrons having energy higher than E_f. We can, however, presume that α will differ not very much from 1, since E_f is rather low. Therefore, considering the fact that the mean fission cross section obtained in this case is slightly higher than that obtained with neutrons of the $D+$D and $D+$Be reactions (the difference is of the same order of magnitude as the experimental errors) we can conclude that the fission cross section of uranium is practically constant up to energies of the impinging neutrons higher than 10 Mev.

In order to have some information on the value of the fission cross section for energies of the impinging neutrons of the order of 0.5 Mev we carried out a similar experiment with neutrons of the $D+$C reaction for 1-Mev and 0.85-Mev energy of the impinging ions. At 90° the energies of the emitted neutrons are, respectively, 0.55 and 0.40 Mev.[13] As we see from Table I, for higher energy of the impinging neutrons we find a lower value of the fission cross section. This very strange result can be explained as due to contamination of the C target with deuterium. Such a contamination, not very important at 1-Mev energy of the impinging deuterons, cannot be neglected at lower energy, as the yield of the $D+$C reaction decreases more rapidly than that of the $D+$D reaction.

We can try to correct the data obtained with neutrons of the $D+$C reaction in the following way: let us call N_D the number of neutrons of the $D+$D reaction emitted from our contaminated carbon target, and $N_C(0.85)$, $N_C(1)$ the numbers of neutrons of the $D+$C reaction emitted, respectively, for 0.85- and 1-Mev energy of the impinging deuterons. Assuming N_D and the fission cross section σ_f as constant in this small interval of energy, we have that the sums $N_C(0.85)+N_D$, $N_C(1)+N_D$ represent the total numbers of emitted neutrons and therefore are proportional to the rhodium activity integrated to all the volume. On the other side the quantities $N_C(0.85)\sigma_f+N_D 0.25$, $N_C(1)\sigma_f+N 0.25$ are equal to the observed cross sections. Solving these four equations we find

$$\sigma_f \sim 0.03, \quad N_D \sim 28, \quad N_C(0.85) \sim 38, \quad N_C(1) \sim 280.$$

We conclude by this rather indirect method that the fission cross section of U for energies of the impinging neutrons of 0.5 Mev is about $\frac{1}{8}(=0.03/0.25)$ of the cross section obtained between 1 and 10 Mev. This value seems to be considerably higher than the one given by other authors.[3] Therefore we thought it convenient to perform a similar experiment with photo-neutrons emitted from a Rn+Be source, having 0.200-Mev energy.

We can compare the result obtained with photo-neutrons with the data obtained for $\theta = 0°$ with neutrons of the $D+$Be reaction. In fact, as we see from the data given in Tables I and II and as it appeared from the measurements of the angular distribution,[14] the neutrons emitted in the $D+$Be reaction are nearly isotropic. Therefore from the data of Table II we can conclude that the fission cross section for photo-neutrons is about $\frac{1}{5}(=0.05/0.27)$ of the cross section obtained with neutrons having energies between 1 and 10 Mev.

These rather high values of the fission cross section found both at 0.2 and 0.5 Mev energy of the impinging neutrons seem to indicate that the

[12] T. W. Bonner and W. M. Brubaker, Phys. Rev. **50**, 308 (1936).
[13] T. W. Bonner, Phys. Rev. **53**, 496 (1938).
[14] M. Ageno, E. Amaldi, D. Bocciarelli and G. C. Trabacchi, Atti R. Acc. Ital. In press.

fission cross section decreases, for energies below the critical energy E_f, less rapidly than expected.[3] In this connection we point out that, in the meantime, Haxby, Shoupp, Stephens and Wells[4] have measured the critical energy E_f for U and found 0.35 ± 0.1 Mev.

Let us now compare the results obtained with $D+$Be and $D+$Li reactions and given in Table I. We see that, in case of the $D+$Li neutrons, the mean cross section is larger by a factor 1.4 than in case of the $D+$Be neutrons. This result is confirmed by experiment (b) whose results are summarized in Table IV. The interpretation of this fact is due to N. Bohr[15] who pointed out that, for sufficiently high energy of the impinging neutrons, a new process becomes possible, as follows: The capture of the impinging neutron by a nucleus U^{238} gives rise to an excited U^{239}. The excitation energy is given by the sum of the energy E of the impinging neutrons and of the binding energy W_n of a neutron in the nucleus, which is equal to 5.2 Mev. The probability of fission of the compound nucleus U^{239} is determined by the competition with other disintegrative processes, among which the most important is the evaporation of a neutron. The ratio of the probabilities of fission and of evaporation of a neutron, is for U^{239} according to Bohr and Wheeler equal to 1 : 4. For energies of the impinging neutrons of the order of a few Mev after the evaporation of a neutron the residual nucleus U^{238} has such a low excitation energy that fission is impossible.

If the energy of the impinging neutrons is sufficiently high, however, the excitation energy of the residual nucleus U^{238} can be larger than its critical energy for fission. Also, in this case, the fission probability is determined of course by the competition with the evaporation of a neutron. As U^{238} is a nucleus containing an even number of particles, the ratio ρ of the probabilities of fission and evaporation will be larger than in case of U^{239}. According to Bohr we have $\rho = 3 : 1$. Therefore, if we indicate by σ_0 the cross section for formation of the compound system U^{239}, the fission cross section will be

$$\sigma_f = \tfrac{1}{5}\sigma_0, \tag{1}$$

when the impinging neutrons are of low energy (a few Mev).

For sufficiently high energies of the impinging neutrons, two different fission processes are possible: namely, the direct fission of U^{239} with cross section σ_f, and the fission of the system U^{238} residual of the evaporation of a neutron from U^{239}. The cross section corresponding to the second process is given by

$$\sigma_f' = \tfrac{4}{5}\tfrac{3}{4}\sigma_0, \tag{2}$$

where $\frac{4}{5}\sigma_0$ represents the cross section for evaporation of a neutron from U^{239} and the numerical factor $\frac{3}{4}$ corresponds to the above given ratio ρ of the probability of fission and evaporation of a neutron for the residual system U^{238}. Therefore for high energy of the impinging neutrons, the fission cross section must be equal to

$$\sigma_f + \sigma_f' = 4\sigma_f. \tag{3}$$

Let us now combine this theoretical result of Bohr with our data obtained with $D+$Li neutrons. Assuming, roughly, that the successive fission process of U^{238} takes place only above a definite energy E' of the impinging neutrons with cross section given by (2), we can indicate by α' the fraction of impinging neutrons having energy higher than E'. The mean cross section we must expect to find experimentally with a continuous spectrum of neutrons is given by

$$\sigma_f(1-\alpha') + (\sigma_f + \sigma_f')\alpha' = \sigma_f + \alpha'\sigma_f' = \sigma_f(1+3\alpha').$$

Comparing this theoretical result with the ratio of the fission cross sections obtained with neutrons, respectively, of the $D+$Li and $D+$Be reactions we conclude

$$1+3\alpha' = 1.4; \quad \alpha' = 0.13.$$

From the inspection of the spectrum of neutrons of the $D+$Li reaction[16] we see that about 13 percent of the emitted neutrons have energies larger than 12 Mev. This value is slightly higher than theoretically expected. In fact, taking into account that in the case of U^{238} the critical energy E_f for fission is equal to 5.7 Mev, we could expect that the successive fission

[15] N. Bohr, Phys. Rev. **58**, 864 (1940). We are indebted to Professor Bohr for sending us his manuscript.

[16] T. W. Bonner and W. H. Brubaker, Phys. Rev. **47**, 973 (1935); **48**, 742 (1935). We used the data of these authors instead of that of W. E. Stephens, Phys. Rev. **53**, 223 (1938), because they are more complete on the low energy side (recoil protons were observed down to 0.5 Mev instead of 3 Mev).

of U^{238} can take place for energies of the impinging neutrons larger than

$$E' = 5.7 + 2.6 = 8.3 \text{ Mev},$$

where the second term represents the energy carried out by the evaporating neutron from the compound system U^{239} which was calculated as two times the nuclear temperature. The difference between our experimental data and the theoretically expected value of E' is certainly due, in great part, to experimental errors.

As it was pointed out by Bohr, we must expect a similar behavior of the fission cross section in case of Th and Pa. For Th, Bohr gives the following values of the partial cross section for direct fission of Th^{233} and successive fission of Th^{232}

$$\sigma_f = \frac{1}{25}\sigma_0, \quad \sigma_f' = \frac{8}{25}\sigma_0.$$

In the reasonable assumption that the successive fission process of Th^{232} begins to be possible for about the same energy E' of the impinging neutrons as found in case of uranium, we must expect that the mean experimental cross section for fission of Th obtained with the $D+Li$ neutrons be

$$1 + 8\alpha' = 1 + \gamma \times 0.13 = 2$$

times larger than the same quantity measured with neutrons of the $D+Be$ reactions. Combining the data of Table IV and the result of Section 5, we obtain

$$(1.40 \pm 0.05) \times (1.35 \pm 0.08) = 1.9 \pm 0.2,$$

which seems to agree very well with the theoretical expectation.

Finally we point out that, although our data in case of Pa do not permit any definite conclusion, they seem to indicate that by increasing the energy of the impinging neutrons the fission cross section increases less than the fission cross section of uranium, as we must expect according to the data given by Bohr.

JULY 15, 1941 PHYSICAL REVIEW VOLUME 60

The Nuclear Magnetic Moments of C^{13}, Ba^{135} and Ba^{137} *

ROBERT HENDERSON HAY
Columbia University, New York, New York

(Received May 28, 1941)

The nuclear gyromagnetic ratios for C^{13}, Ba^{135} and Ba^{137} have been measured by the molecular beam magnetic resonance method. The signs of the nuclear magnetic moments have also been determined. For C^{13} the g value is 1.402 ± 0.004 and the moment is positive. When this fact is considered with the results of theoretical treatments of the C^{13} nucleus, $I = \frac{1}{2}$ seems to be the preferable value for C^{13}. The resultant nuclear magnetic moment is $+0.701 \pm 0.002$ n. m. The moments for both Ba^{135} and Ba^{137} are positive. The g values are 0.5575 ± 0.0017 and 0.6236 ± 0.0019 respectively. Using $I = \frac{3}{2}$ for both nuclei, the corresponding nuclear magnetic moments are $+0.8363 \pm 0.0026$ and $+0.9354 \pm 0.0029$, respectively. The ratio of the moments is 1.1174 ± 0.0010. All g values are referred to that for Li^7 of 2.1688. Careful examination of the barium beam intensity as a function of homogeneous field strength with constant oscillating field frequency revealed only two resonance minima.

INTRODUCTION

DIRECT experimental data on the nuclear spin and magnetic moment of C^{13} have more than intrinsic interest, for this isotope is one of the light nuclei to which theoretical calculations can be applied with some hope of success. Rose and Bethe[1] have used the Hartree model with Thomas spin-orbit coupling to predict a value of $\frac{1}{2}$ for the nuclear spin while Sachs,[2] on the other hand, obtains the value $\frac{3}{2}$

* Publication assisted by the Ernest Kempton Adams Fund for Physical Research of Columbia University.

[1] M. E. Rose and H. A. Bethe, Phys. Rev. **51**, 205 (1937).
[2] R. G. Sachs, Phys. Rev. **55**, 825 (1939).

by the use of the alpha-particle model and the same type of coupling. Inglis[3] has pointed out that for C^{13} the Larmor coupling term may be as important as, if not more so than, the Thomas term and that if it is taken into account, one obtains $I=\frac{1}{2}$ from either the Hartree or the alpha-particle model. A definite experimental value for the nuclear spin would provide sufficient ground for choice between the theoretical bases of the three calculations, but the only value for this observable is that of Townes and Smythe[4] which was based on measurements of the alternating intensities of lines in an incompletely resolved band spectrum. They selected 3/2 as the best of three possibilities: 1/2, 3/2 and 5/2. Therefore, when Hutchison, Stewart and Urey[5] made available NaCN and KCN in which the abundance of C^{13} was as high as 25 percent, it was considered highly desirable to add to the existing experimental data by applying the molecular beam magnetic resonance method[6-8] to the determination of (a) the nuclear gyromagnetic ratio and (b) the sign of the nuclear magnetic moment of C^{13}. A brief account of the results of these measurements has already appeared;[9] part of this paper will be devoted to an amplification of that report.

Since McLennan and Allen[10] reported hyperfine structure in a number of the arc and spark lines of barium, several workers have used the h.f.s. patterns to evaluate the nuclear spins of the odd isotopes of barium. Schüler and Jones[11] deduced the value $\frac{3}{2}$ for both isotopes from the measurements of Ritschl and Sawyer[12] on the resonance lines of Ba II, $6^2S_{\frac{1}{2}}-6^2P_{\frac{1}{2},1\frac{1}{2}}$. Kruger, Gibbs and Williams[13] repeated intensity measurements on these same lines and concluded that $3/2 \leqq I < 7/2$ with $I=5/2$ as the most probable value. Murakawa[14] made intensity measurements on these and other lines and gives $\frac{3}{2}$ as the value for both isotopes. In 1937 Benson and Sawyer[15] obtained new data from a study of the intensity ratios, the separation of the components from the center of gravity and the nature of the patterns for the $6^2S_{\frac{1}{2}}$, $6^2P_{\frac{1}{2}}$, $7^2S_{\frac{1}{2}}$, 5^3D_3, 6^3P_2 and other terms and they conclude that the spin of each isotope is $\frac{3}{2}$.

Data from the paper by Kruger, Gibbs and Williams have been used by Bethe and Bacher[16] in the Fermi-Segrè-Goudsmit formula to compute the nuclear magnetic moments of the odd isotopes. They give $\mu=+1.06$ and $+0.82$ for Ba^{135} and Ba^{137}, respectively. In their tables of nuclear magnetic moments, however, both moments appear as 1 (or 0.9 with $I=\frac{3}{2}$). Part of the inability to resolve the two moments is undoubtedly due to the fact that the even isotopes of barium result in a very heavy structureless component that almost obscures the h.f.s. components due to the odd isotopes, and part is due to the impossibility of resolving the splitting of the $6^2P_{\frac{1}{2},1\frac{1}{2}}$ terms by optical methods. The problem thus posed is one which the molecular beam magnetic resonance method is particularly well able to solve, for it does not respond to effects due to nuclei of zero spin or zero moment and its resolution is well beyond that of spectroscopy. In addition, barium possesses a $^1S_0$ ground state which means that atomic beams can be used instead of molecular beams. Thus the complications which arise from intramolecular interactions and possible rotational states are eliminated and the results can be expected to give some check on the theory of the method.

Experimental

The apparatus and the experimental technique which were used to obtain the results set forth in this paper are those which have been described by others[6,7] and that description need not be repeated here except for a review of the procedure

[3] D. R. Inglis, Phys. Rev. **56**, 1175 (1939).
[4] C. H. Townes and W. R. Smythe, Phys. Rev. **56**, 1210 (1939).
[5] C. A. Hutchison, D. W. Stewart and H. C. Urey, J. Chem. Phys. **8**, 532 (1940).
[6] I. I. Rabi, S. Millman, P. Kusch and J. Zacharias, Phys. Rev. **55**, 526 (1939).
[7] S. Millman, Phys. Rev. **55**, 628 (1939).
[8] A. F. Stevenson, Phys. Rev. **58**, 1062 (1940).
[9] R. H. Hay, Phys. Rev. **58**, 180 (1940).
[10] J. C. McLennan and E. Allen, Phil. Mag. **8**, 515 (1929).
[11] Kallman and Schüler, Ergeb. d. exact. Naturwiss. **11**, 134 (1932).
[12] R. Ritschl and R. A. Sawyer, Zeits. f. Physik **72**, 36 (1931).
[13] P. G. Kruger, R. C. Gibbs and R. C. Williams, Phys. Rev. **41**, 322 (1932).
[14] K. Murakawa, Sci. Pap. Inst. Phys. Chem. Research, Tokyo **18**, 304 (1932).
[15] A. N. Benson and R. A. Sawyer, Phys. Rev. **52**, 1127 (1937).
[16] H. A. Bethe and R. F. Bacher, Rev. Mod. Phys. **8**, 222 (1936).

used to determine the sign of the magnetic moments. Some information will be given, in addition, about the compounds used for the C^{13} measurements, the way in which the C^{13} resonance minimum was identified and the difficulties encountered in detecting the barium beams.

The resonance minima can be obtained in either of two ways: by observing beam intensity as a function of the strength of the homogeneous field with the frequency of the oscillating field held constant (constant frequency method), or by observing the beam intensity as a function of the oscillating field frequency with the homogeneous field strength held constant (constant field method). In each case, the curves must be taken in pairs to avoid errors due to the end effects of the oscillating field. One member of the pair is taken with the applied fields in what has been designated the Normal direction, while the other is taken with the fields in the opposite, or Reverse, direction. Millman[7] has pointed out that this procedure for obtaining accurate g values also gives information about the sign of the nuclear magnetic moment to be associated with a minimum, for the direction in which the minima shift with reversal of the applied field directions depends upon the sign of the moment. If it is to low field values, when the fields are changed from Normal to Reverse, the moment is positive. In the case of C^{13}, the curves were all obtained by the use of the constant frequency method since it is usually more convenient from an experimental point of view. In the case of the barium isotopes, however, it was found that when this method was used the minima were so narrow and the end effects so small that the shifts in minima were obscured by the errors caused by the demagnetization procedure. For that reason, and also because the ratio of the g values is much more accurately calculated from curves obtained by the constant field method, some of the barium curves were taken in this way.

C^{13}

The cyanides procured from Professor Urey's laboratory were formed by titrating a condensate of HCN with KOH and NaOH. The chemical purity of all of the substances used was at least equal to that of the KOH, the maker's analysis of which is given below:

Na_2CO_3	2.5	percent
Cl	0.010	"
SO_4	0.005	"
PO_4	0.005	"
SiO_2 and NH_4OH ppt. (SiO_2, Al_2O_3, Fe_2O_3)	0.020	"
N	0.001	"
Fe	0.002	"
Heavy metals	0.003	"

The molecular beams were formed by heating the cyanides in iron ovens to about 700°C and the greatest experimental difficulties arose from the excessive dissociation of the NaCN at that temperature and its tendency to condense on the oven slit jaws. The cure lay in careful drying and moderate preheating under vacuum.

The surface ionization detector used in these experiments has so far been successfully used to detect only the alkali metals, gallium, indium and barium. Fortunately, it will detect the alkali elements when they are combined with other elements to form compounds stable enough to give molecular beams. This circumstance makes possible the application of the molecular beam magnetic resonance method to the measurement of the nuclear g value of elements which are not directly detected by the surface ionization detector but which combine stably with the alkalis. Kusch, Millman and Rabi[17] have reported such measurements on the nuclei of chlorine, aluminum, nitrogen and other elements. As they point out, the correct assignment of observed resonance minima to nuclei is usually possible only if a given minimum is observed with two or more compounds which have nothing in common but the element of immediate interest. In the case of C^{13} only two compounds were available. Had either of these been obtainable in large amounts, it would have been desirable to use that one to form a third compound such as LiCN or RbCN in the hope that it, too, would form usable molecular beams and thus make easier the task of identifying new minima. Since this course was impracticable because of the limitation of supply, the following procedure was substituted: The first step was to study the intensity of the KCN beam as a

[17] P. Kusch, S. Millman and I. I. Rabi, Phys. Rev. **55**, 1176 (1939) and subsequent papers.

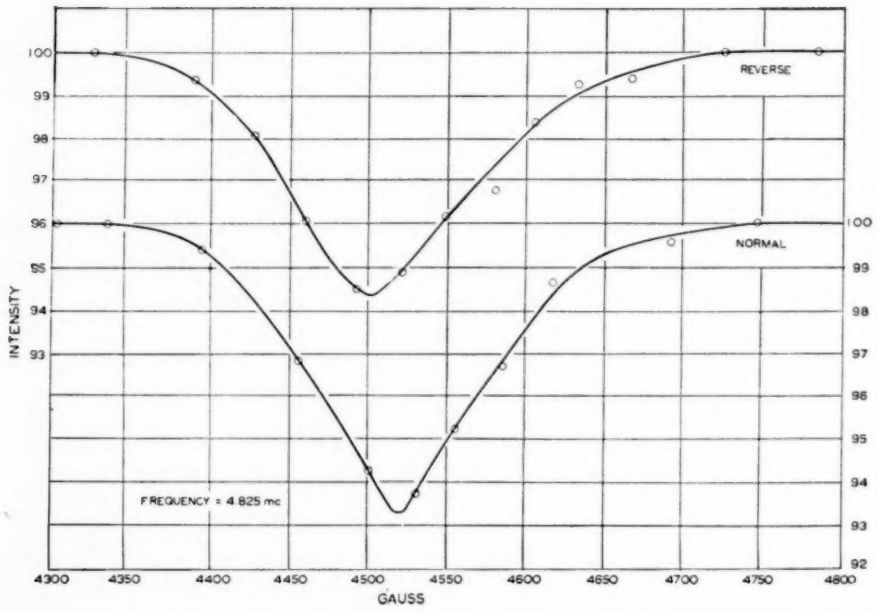

FIG. 1. Beam intensity as a function of homogeneous field strength for beams of KCN enriched in C^{13}. The lower curve is taken with the applied fields in the Normal direction, the upper, with them in the opposite, or Reverse, direction.

function of the homogeneous field strength with the frequency being kept fixed for each curve. Only three resonance minima were seen, two of which were at once identified as being due to K^{39} and N^{14}. The third, curves for which are given in Fig. 1, did not correspond to any g value recorded in this laboratory so it was tentatively assigned to C^{13}. Next, the intensity of the NaCN beam was plotted as a function of the field strength but the new minimum turned out to be so close to that due to Na^{23} that it was visible only as an asymmetry on the high field side of the latter. Two of the curves for the region near the Na^{23} minimum are shown in Fig. 2. They indicate that the asymmetry is not due to end effects of the oscillating magnetic field, for it does not change from the high field side of the minimum to the low with reversal of the field directions. The third step was to obtain beams of KCN and NaCN containing only the normal amount (1.06 percent) of C^{13}. Beam intensity curves of normal KCN showed only two resonance minima, that for K^{39} and that for N^{14}. The new one assigned to C^{13} was absent. The two curves given in Fig. 3 are typical of the normal NaCN beam intensity for the region near the Na^{23} minimum. They reveal no trace of the asymmetry to be seen in the curves of Fig. 2.

The problem is to identify the new minimum with the nucleus of C^{13}. It can be done by eliminating all other alternatives. The chance that a chemical impurity is responsible is negligible, for the NaCN and the KCN used were prepared from substances free from all but the merest traces of impurities important in these experiments. Nor can the new minimum be due to C^{12} for that nucleus possesses no magnetic moment. Even if it did, its minimum should appear in the beams of ordinary KCN in which only two minima were found. There remains the possibility that the minimum is due to the moment arising either from the rotation of the molecules as a whole or from the decoupled rotation of a group, such as CN, common to both molecules. To be valid, the first hypothesis would require that the moments of inertia of NaCN and KCN molecules be equal, which is unlikely. The second would demand complete decoupling of such a rotation from the rotation of the molecule as a whole, which would seem rather difficult to accomplish at the low fields used (not over 5000 gauss). In any case, it is interesting to repeat the computation which

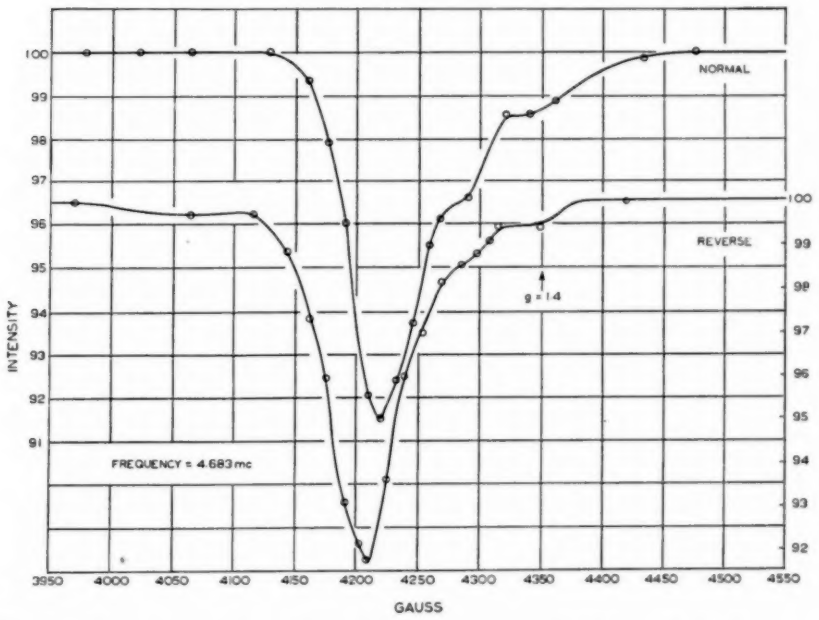

FIG. 2. Beam intensity as a function of homogeneous field strength for beams of NaCN enriched in C^{13}. The main resonance minimum is due to Na^{23}. The asymmetry caused by the C^{13} nucleus is indicated by the arrow marked "$g=1.4$."

Kusch, Millman and Rabi[17] have made of the probable nuclear magnetic moment of the CN group, in which they postulated that the observed minimum is due to such a rotation. The separation of the carbon and the nitrogen atoms is known[18] to be 1.15×10^{-8} cm in the HCN molecule and it seems reasonable to assume this same value for the KCN molecule. The moment of inertia of the CN group then is $I=14.2\times10^{-40}$ g cm^2. From the relation, $Jh/2\pi=(2IkT)^{\frac{1}{2}}$, the most probable value for the rotational angular momentum for an oven temperature of 1000°K comes out to be $19h/2\pi$. The new minimum gives a g value of about 1.4, which leads to a magnetic moment of $19\times1.4=26.6$ nuclear magnetons. By observing the deflection of the molecular beam caused by a single inhomogeneous field one can form an estimate of the approximate magnetic moment of the KCN molecule. Experimental values are about one nuclear magneton, not even the same order of magnitude as the result calculated above. Thus, rotational states may be ruled out as possible causes of the new minimum observed in the enriched KCN beam. At very low values of the homogeneous field, minima yielding g values which are integral multiples of the true g value have been observed in molecular beams for nuclei the spins of which are greater than $\frac{1}{2}$. The new minimum observed in these experiments cannot be attributed to any such phenomenon, however, for it was seen at high field values while both theory and experimental observation show that multiple g value minima are not. This exhausts the alternatives and, therefore, the third minimum seen in the beams of enriched KCN was assigned to the C^{13} nucleus.

[18] H. Sponer, *Molekulspectren* (J. Springer, 1935).

Ba^{135} and Ba^{137}

The barium metal used in these experiments was procured from Eimer and Amend and was over 99 percent pure when bought. The chief impurity was oxygen. As a check, the barium residues left in two ovens after use were analyzed spectroscopically. Silicon, iron, tin, lead and aluminum were found to be present to less than 0.09 percent while strontium, calcium, zinc, sodium and potassium were not found. The beams were formed in the usual manner by heating the metal in an iron oven to about 950°C.

Barium has an ionization potential of 5.16 volts and, therefore, the surface ionization

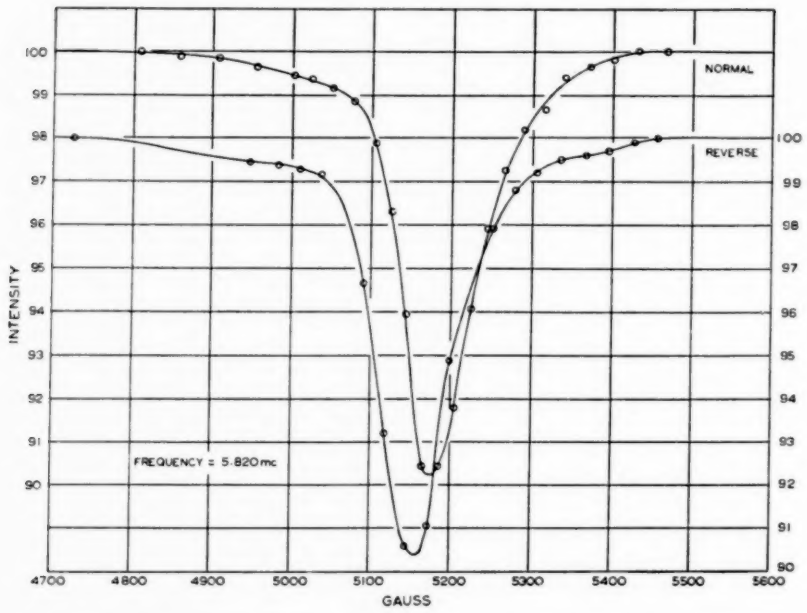

FIG. 3. Beam intensity curves of the region near the Na^{23} minimum for beams of NaCN containing only normal amounts of C^{13}. Note the absence of the asymmetry so noticeable in the curves of Fig. 2.

detector should not detect it.[19,20] An oxide-coated filament will detect elements such as sodium and lithium, whose ionization potentials are higher than 4.5 volts, the work function of tungsten, but it will not work for barium, probably because BaO is an efficient agent for lowering the apparent work function of the filament. However, in 1936 Guthrie[21] reported that, contrary to current theories of surface ionization, barium could be detected by a clean tungsten filament if the latter were kept at sufficiently high temperatures. The precautions which he listed as necessary to secure satisfactory detection were observed with success, although considerable experience was required before the best results were obtained.*

The barium beams were usually very unsteady. Figure 4 gives some idea of the degree of unsteadiness, especially when it is noted that each point on the curve is the average of several observations any one of which may be a rather bad fluctuation. This unsteadiness was due in part to the high filament temperature which caused the barium beam to be superimposed on a background of continuously fluctuating positive

[19] J. B. Taylor, Zeits. f. Physik **57**, 242 (1929).

[20] R. G. J. Fraser, *Molecular Rays* (Cambridge University Press, 1931).

[21] A. N. Guthrie, Phys. Rev. **49**, 868 (1936).

* Guthrie made some calculations based on the geometry of his apparatus, the measured positive ion current and the kinetics of the beam which led him to state that when it was above 2000°K, the filament converted all of the neutral barium atoms striking its surface into positive ions. The temperature, estimated from electrical conditions, at which the filament was maintained for detection in my experiments was at least 2000°K. If the filament, after some steady use as a barium detector, was used for lithium, the detection of which requires an oxide coat, it was found impossible to maintain the required coat and detect lithium until after the filament had been subjected for two or three hours to a temperature well above that used for barium detection and dangerously close to that which experience has shown will burn it out in a short while. This odd behavior of the tungsten was inexplicable until it was recalled that barium in combination with oxygen is a very efficient agent for lowering the apparent work function of tungsten. During the time it had been used as a barium detector, the tungsten had adsorbed a coat of barium with which the oxygen promptly combined to form barium oxide which, in turn, had the opposite effect on the work function of the filament to that necessary for the detection of lithium. The phenomenon was described to Dr. J. A. Becker of the Bell Telephone Laboratories who immediately recalled the results of some unpublished measurements he had made on the ability of tungsten to ionize barium atoms. He found that the conversion from neutral atoms to positive ions at the surface of a hot tungsten wire was by no means equal to 100 percent but was only a third to a half that much. The methods used both in these and in Guthrie's experiments to determine filament temperatures are too inexact to permit one to say that my experience invalidates his statements. It does suggest, however, that tungsten is an inefficient barium detector and requires higher oven pressures and greater beams than would have been necessary with a more efficient detector, and that the phenomena of barium detection will bear more examination.

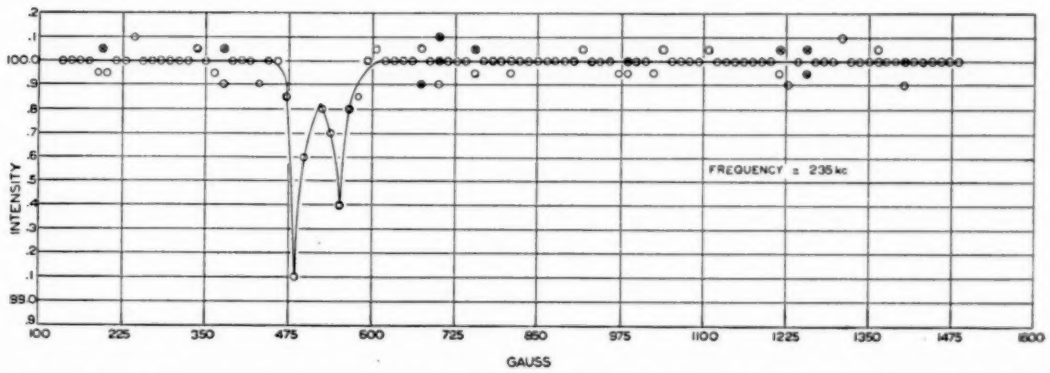

FIG. 4. An exploratory curve giving the barium atomic beam intensity as a function of homogeneous field strength. The frequency of the oscillating field was held constant at 235 kilocycles. Points marked ⊗ are those taken as repeat observations to make sure that beam decreases indicated by several of the original points were not due to resonance minima but only to beam fluctuations.

ion current. Another contributing factor was the excessive oven pressure necessitated by the inefficient detection process. Unprecedented quantities of barium, to judge by experience with other elements and compounds, had to be evaporated from the ovens to maintain a beam of even moderate intensity for a matter of six or seven hours.

To add to these difficulties, it was discovered that the power of a single inhomogeneous field to deflect atoms from the beam was extremely small, being, even with a collimating slit 0.02 mm wide, a matter of less than six percent. This figure set an upper limit not only to the depth of any minimum but also to the sum of the depths if more than one minimum were seen, and meant that extreme care would have to be taken in order that no small minima would be skipped. Each reading of beam intensity represents the difference between the intensity with the oscillating field off and that immediately after with the field on. Furthermore, each of these readings is the average of as many as eight or ten separate observations. In most cases, the averaging was done mentally, but it is interesting to note that what was done with the aid of an adding machine indicated that the extra time and labor involved in the use of the machine was not justified by any significant gain in accuracy.

RESULTS

C^{13}

The resonance curves shown in Fig. 1 are typical of those obtained from observations of the intensity of beams of KCN enriched in C^{13}. They were obtained by the use of the constant frequency method. The shift of the minimum with reversal of the direction of the applied fields is easily seen and indicates that the nuclear magnetic moment of C^{13} is positive. The proper field value to be used in calculating the apparent g value is, of course, the average of the minimal abscissae of the two curves. Data from seven pairs of such curves were used in the formula,

$$g=\frac{1.3122\times10^{-3}\times f}{H}$$

to calculate the apparent g value for C^{13}. H is the value of the homogeneous field at resonance and f is the resonant frequency. Referred to the value 2.1688[22] for Li^7, it is, $g=1.402\pm0.004$ in units of $e/2Mc$.

Ba^{135} and Ba^{137}

Figure 4 is a curve of beam intensity *vs.* homogeneous field strength for the barium atomic beam. The frequency of the oscillating magnetic field was 235 kc and the range of homogeneous field values was such as to cover g values from 0.2 to 6 in units of $e/2Mc$. There are only two resonance minima, nor did more than these two appear in any of the other exploratory curves that were taken. The total range of g values covered was from 0.1 to 9 and for the low values, care was taken to keep the strength of the oscillating magnetic field inversely proportional to the g value in accordance

[22] Private communication from S. Millman and P. Kusch.

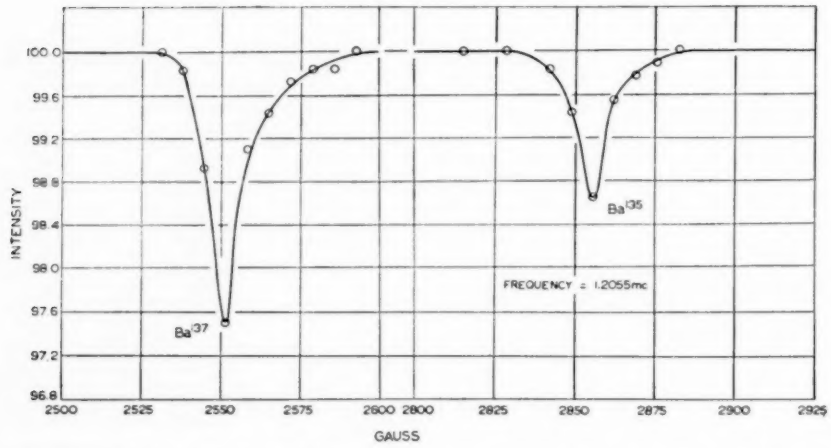

FIG. 5. Beam intensity as a function of homogeneous field strength for the two resonance minima seen in the barium atomic beams. Note their extreme narrowness and the very slight asymmetry.

with the theory of the method. When these two minima were examined in detail, curves such as those of Figs. 5 and 6 were obtained. The curves of Fig. 5 were taken in rapid succession so that they might be used to get the ratio of the minimal ordinates. They also indicate the narrowness of the barium curves, their half-widths being about 0.47 and 0.42 percent (approximately 4.5 kc), respectively. Curves taken in this manner were not satisfactory for determining the signs of the moments, for they showed only slight asymmetries and no shifts of minima with reversal of the directions of the applied fields, the shifts being so small as to be totally obscured by the demagnetization error in the homogeneous field values. Therefore, the curves of Fig. 6 were taken with the frequency of the oscillating field as the independent variable and the strength of the homogeneous field constant. These curves are as narrow as the others (half-widths = 0.43 percent) but not only do the asymmetries due to oscillating field end effects appear more pronounced but also the shifts in minima with reversal of applied field directions are easily discerned. In addition to those of Fig. 6, two more curves were taken for the shallower minimum. The first was with an oscillating field of about 5 gauss and the second with a field four times that strength. The minimum for the second curve was located 1.4 kc higher in frequency than was that for the first, a clear indication that the moment associated with this minimum is positive. The sign of the moment for the deeper minimum is determined by the curves of Fig. 6 to be positive.

The following apparent nuclear g values were calculated from all of the curves taken: 0.5537 $\pm$0.0016 for the smaller minimum and 0.6193 $\pm$0.0018 for the other. The units in both cases are those of the fraction $e/2Mc$, and both values are referred to the value 2.1688 for Li^7. The ratio of the g values was determined from the curves of Fig. 6 and is 1.1174$\pm$0.0010. Four values for the ratio of the decreases in intensity at resonance were obtained: 1.60, 1.84, 2.09 and 1.76, the average being 1.82. Three sets of figures for the abundances of the isotopes of barium are given in Table I, those of Aston,[23] of Sampson and Bleakney[24] and of Nier.[25] The only two isotopes whose abundance ratio is near 1.8 are Ba^{137} and Ba^{135}; their ratio is given in the final column of the table.

The evidence and the arguments upon the basis of which the g value 0.5537 was assigned to Ba^{135} and the value 0.6193 to Ba^{137} are as follows:

(1) The resonance minima observed for the nuclei of Li^6 and Li^7, B^{10} and B^{11}, Cl^{35} and Cl^{37} and Rb^{85} and Rb^{87} show that for each of these isotope pairs, the ratio of the decrease in intensity at resonance is fairly closely proportional

[23] F. W. Aston, Proc. Roy. Soc. **134**, 571 (1932).
[24] M. B. Sampson and W. Bleakney, Phys. Rev. **50**, 456 (1936).
[25] A. O. Nier, Phys. Rev. **54**, 275 (1938).

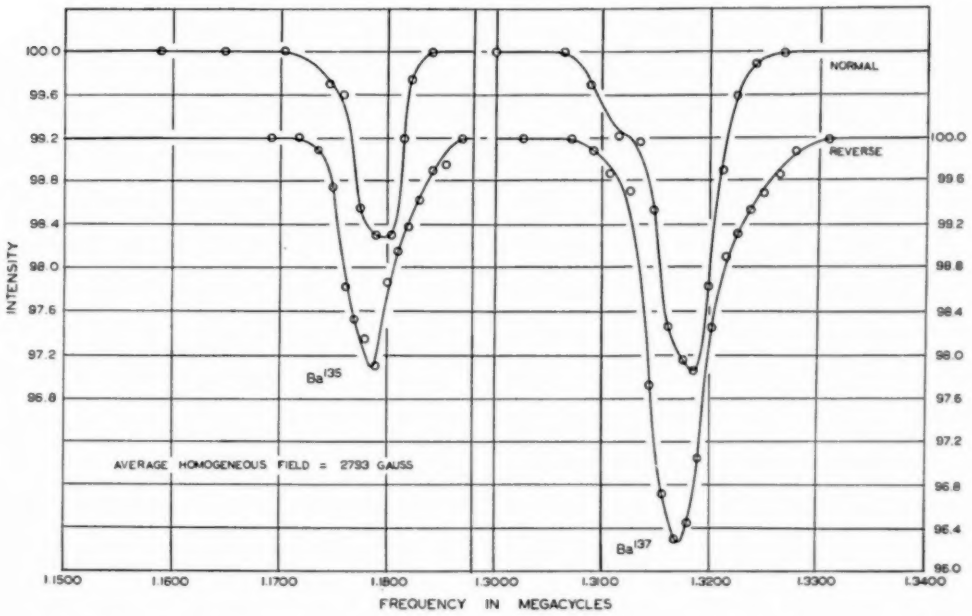

FIG. 6. Beam intensity as a function of oscillating field frequency with the homogeneous field strength held constant. These curves indicate clearly the positive sign of the nuclear magnetic moment to be associated with each minimum.

to the isotope abundance ratio. These minima were observed in the intensity curves of molecular beams and are therefore subject to broadenings and complications arising from intramolecular interactions. What holds for them can confidently be expected to hold for the much narrower minima seen in the barium atomic beam intensity curves, for none of the molecular complications are present.

(2) It is very unlikely that Ba^{138} is responsible for either of the observed minima, for if it were, its abundance is such that a single inhomogeneous field would deflect past the detector more than 6 percent of the total beam. This argument does not apply to the isotopes Ba^{134} and Ba^{136} but there remains a third which is applicable to all the even isotopes.

(3) If either of the two minima is attributed to one of the even isotopes, we can reasonably expect to find a third minimum for the odd isotope with which no minimum would then be associated. Furthermore, in view of the abundance ratios, it should be of about the same depth. No such minimum was found. This bears out the view of spectroscopists that the h.f.s. patterns seen in barium spectra are caused by the two odd isotopes. From these patterns it has been established that these isotopes have equal spins and so nearly equal moments that it is impossible to resolve them optically.

DISCUSSION

Precision

An estimate of the precision of these measurements of nuclear g values involves consideration of errors in four factors: the constant factor, 1.3122×10^{-3}, into which are lumped all atomic physical constants appearing in the formula for calculating g values;[6] the frequency of the oscillating magnetic field; the homogeneous field calibration constant by means of which the potential drop across a shunt in the windings is converted to field strength, and the location of the minimal abscissae for the resonance curves. As far as these results are concerned, errors in the constant factor are entirely negligible. Frequencies were measured with a heterodyne frequency meter capable of an accuracy of 0.005 percent and the oscillator used was stable to better than 500 cycles for the time necessary to take a curve, so that errors in frequency are small enough to be ignored. The homogeneous field was not measured absolutely but was

TABLE I. *Abundance of isotopes.*

Mass Number	130	132	133	134	135	136	137	138	Ratio 137/135
Abundance, Aston	—	—	—	—	5.9	8.9	11.1	74.2	1.88
Abundance, Sampson and Bleakney	0.16	0.015	0.1	1.72	5.7	8.5	10.8	73.1	1.90
Abundance, Nier	0.101	0.097	—	2.42	6.59	7.81	11.32	71.66	1.71

calibrated so that the g values were referred to that for Li^7. Before and after the measurements on C^{13} and again after the measurements on the barium isotopes, the resonance frequency of the Li^7 minimum was determined for field values which covered the working range of the homogeneous field. Since the field strength is indicated in practice by the potential drop across a shunt in the field windings, this calibration procedure results in a curve of a certain factor (by means of which millivolt readings are converted to field strength) as a function of millivolts drop across the shunt. The experimental points were scattered due to small variations in demagnetization procedure, but the greatest deviation from the average for any one field value was 0.3 percent and the average deviation for all points and all three calibrations was 0.15 percent. Location of the minimal abscissae introduces more error than does any other factor since this error depends on such things as the nature of the curves, their widths and the number of points close to the minimum. A conservative estimate of the precision of the location of the C^{13} minimal abscissae is 0.3 percent. The curves for the barium isotopes are considerably sharper than those for C^{13} but, except for those of Fig. 6, no greater precision of location is claimed for them because the minima are, in too many cases, dependent on one point. If all of the errors are combined in the usual way, the value for the probable error is 0.3 percent.

It will be noticed that the precision of the ratio of the g values of the barium isotopes is somewhat greater than that of the values themselves. This ratio was determined from the curves of Fig. 6 and such a determination eliminates errors due to all but very short time changes in the homogeneous field and reduces practically to the measurement of two frequencies.

A correction must be applied to the observed nuclear g values to take into account the diamagnetic property of the atom concerned. Lamb's expression[17] is,

$$\bar{H}/H=0.320\times10^{-4}\times Z^{4/3},$$

where Z is the atomic number and $\bar{H}/H$ is the correction to the external magnetic field H due to the field $\bar{H}$ created at the nucleus by the rotating electrons. For C^{13} this correction is less than 0.04 percent and so is neglected, but for the barium isotopes it amounts to 0.7 percent and the corrected g values become: $g=0.5575\pm0.0017$ for Ba^{135} and $g=0.6236\pm0.0019$ for Ba^{137}, both in units of $e/2Mc$.

The nuclear magnetic moment of C^{13}

When the nuclear spin is known, the measured g value leads at once to the value of the nuclear magnetic moment. Unfortunately, the spin of C^{13} is not known with certainty. Townes and Smythe, who made the only experimental determination, give the value $\frac{3}{2}$ as more probable than the value $\frac{1}{2}$, but their data do not rule out the latter altogether. Of the three theoretical predictions that have been made, it is possible to eliminate Sachs' at once, for, by his theory, the negative moment of the extra neutron is added algebraically to the smaller moment due to the rotational angular momentum and the resultant nuclear magnetic moment is always negative, in direct contradiction to the experimentally determined fact that it is positive. Inglis[26] has pointed out additional support for the view that the nuclear spin of C^{13} is $\frac{1}{2}$. It is derived from the empirical rule that all hitherto known magnetic moments of odd nuclei lie between the limits for the simple single-particle model. The corresponding limits for the gyromagnetic ratio, g, would be, for the odd neutron case,

$$\mu_n/I<g<-\mu_n/(I+1),$$

where $\mu_n=-1.96$, is the lower limit of the

[26] D. R. Inglis, Phys. Rev. **58**, 577 (1940).

neutron moment. The observed g value for C^{13} exceeds the upper limit of 1.30 only slightly for $I=\frac{1}{2}$ but it exceeds it by a factor of two or more for any higher spin value. These arguments strongly support the acceptance of $\frac{1}{2}$ as the most likely value for the nuclear spin of C^{13}, but it must be emphasized that they do not by any means constitute an experimental determination which is contradictory to that of Townes and Smythe.

If the nuclear spin is taken as $\frac{1}{2}$, the value for the nuclear magnetic moment of C^{13} is, $\mu=+0.701\pm0.002$ nuclear magneton, a value in fair agreement with that calculated by Rose and Bethe which is $\mu=+1.05$ n.m.

In view of the recent experimental work by Staub, Tatel and Stevens[27,28] on the anomalous scattering of neutrons by helium, and Dancoff's[29] theory of spin-orbit coupling in He^5 which involves tensor forces of a magnitude sufficient to account for the anomaly, it is unnecessary to make a choice between the calculations of Rose and Bethe and those of Inglis, for both are likely incomplete and not to be relied on too heavily. Not that Rose and Bethe's value for the magnetic moment will be affected much by the addition of the tensor forces, however, for they will determine which level of the ^2P state lies lower while the g value formula will give a moment which is largely due to neutron spin.

The nuclear magnetic moments of Ba^{135} and Ba^{137}

The spectroscopic determinations of the spins of the odd isotopes of barium have already been reviewed. The work of Benson and Sawyer was undertaken to resolve the uncertainty created by the value 5/2 which Kruger, Gibbs and Williams gave. Since the former authors' value 3/2 is based on evidence additional to that presented by the latter authors and is supported by two other independent determinations, it will be used in this paper. Accordingly, the nuclear magnetic moments of the two odd barium isotopes are: $\mu=+0.8363\pm0.0026$ nuclear magneton for Ba^{135} and $\mu=+0.9354\pm0.0029$ nuclear magneton for Ba^{137}. Their ratio is 1.1174 ± 0.0010.

The Fermi-Segrè-Goudsmit formulas have been used to calculate these nuclear magnetic moments from the observed separation factors for the $6^2S_{\frac{1}{2}}$ and $6^2P_{\frac{1}{2}}$ terms. Bethe and Bacher's results, calculated with $I=5/2$, have already been given; with $I=3/2$ they can be corrected to $\mu=+0.954$ and $+0.74$ n.m. for Ba^{135} and Ba^{137}, respectively. That the alteration in moment with change in spin is slight is due to the fact that μ is proportional to $I/(I+\frac{1}{2})$. The g value, on the other hand, is much more sensitive since it is proportional to $1/(I+\frac{1}{2})$. Since they can be compared to experimental values, g values calculated from barium h.f.s. separations for spin values of 5/2 and 3/2 should yield additional information to support the choice of $I=3/2$. Table II gives the results of such a calculation:

TABLE II. *g values.*

		$6^2S_{\frac{1}{2}}$	$6^2P_{\frac{1}{2}}$
$\Delta\nu$ (obs)		0.260 cm^{-1}	0.038 cm^{-1}
$(I+\frac{1}{2})g$		1.25	0.95
g (for $I=3/2$)		0.62	0.42
g (for $I=5/2$)		0.42	0.32
g (obs)	Ba^{135}	0.56	0.56
	Ba^{137}	0.62	0.62

The spin value $I=3/2$ gives a g value in satisfactory agreement with the experimental values, but $I=5/2$ results in a g value too discordant to be acceptable, especially when the $6^2S_{\frac{1}{2}}$ term alone is considered. The values obtained from the $6^2P_{\frac{1}{2}}$ state are low but, according to Goudsmit,[30] this is to be expected. The g values calculated from spectroscopic data emphasize the lack of resolution of the optical method, for one cannot distinguish a separate value for each isotope. The extension in resolution offered by the molecular beam magnetic resonance method is strikingly demonstrated by the ease with which the two minima observed in the barium atomic beams could be resolved. The potentialities of the method are shown by the following figures. Assume that the half-widths of the minima will not exceed 5 kc and that it is desirable to have the minima separated by a frequency increment

[27] H. Staub and W. E. Stevens, Phys. Rev. **55**, 131 (1939).
[28] H. Staub and H. Tatel, Phys. Rev. **58**, 820 (1940).
[29] S. M. Dancoff, Phys. Rev. **58**, 326 (1940).
[30] S. Goudsmit, Phys. Rev. **43**, 636 (1933).

equal to about two or three times the half-widths. The convenient limit of the homogeneous field strength is about 6500 gauss; at that field the Ba^{137} minimum would occur at about 3 mc and it would be quite easy to observe another minimum 15 kc away, provided both were as sharp as are the two barium minima. This separation corresponds to a g value ratio of 1.0050. In other words, had the moments differed by only 0.5 percent, the difference would have been detected with certainty and without extraordinary demands upon experimental technique.

One of the most important parts of the work on the barium isotopes is the search that was made for resonance minima other than the two that were seen. It has already been pointed out that barium is of particular interest. In the first place, it is possible to work with atomic beams and what minima there are should be ideally sharp uncomplicated by anything but the Maxwellian velocity distribution of the beam itself. In the second place, most of the isotopes are of even mass number, and, within the limits mentioned below, the experiments should provide some test of the assumption that the even isotopes are of zero spin or do not possess a magnetic moment. Rough calculations indicated that the smallest moment which would allow either of the inhomogeneous fields alone to deflect atoms past the detector would be of the order of 0.3 nuclear magneton, which means that with a spin of $\frac{3}{2}$, the smallest g value likely to be seen would be of the order of 0.2. To be on the safe side, the lower limit to which the search was extended was $g=0.1$ in units of $e/2Mc$. The upper limit was 9. The theory of the method requires that the strength of the oscillating field be inversely proportional to the g value. Consequently, for one of the exploratory curves, the oscillating magnetic field strength was increased so as to be always at least the proper magnitude, the starting point being the field strength necessary to give a reasonably sharp minimum for Ba^{137}. The positive ion current from the detecting filament was never steady but was always subject to random fluctuations whose magnitudes were such as to make it unwise to claim that minima of depth less than 0.5 percent of the beam intensity could have been recognized. A caution altogether natural in view of the detection difficulties which were encountered dictates that the smallest recognizable minimum be put at about half that due to Ba^{135}. These experiments establish, then, that if any of the isotopes of barium other than 135 and 137 possesses a gyromagnetic ratio, that ratio must be less than 0.2 and is likely less than 0.1, in units of $e/2Mc$, or else the g value is due to an isotope of less than 2.5 percent abundance. Further evidence that only the isotopes 135 and 137 have gyromagnetic ratios is to be found in the close correspondence which exists between the sum of the decreases in beam intensity at resonance and the decrease in intensity caused by a single inhomogeneous field. The latter decrease sets an upper limit to the sum of the decreases due to resonance minima. It was difficult to measure with any accuracy because of the lateral shift of the beam which arose from the diamagnetism of the barium beam, but it amounted to about 6 percent. The sum of the two decreases at resonance was observed in one curve to be 5.8 percent leaving 0.2 percent to be accounted for by another isotope, by inaccuracies in the determination of the single field decrease or by the fact that the strength of the oscillating field was greater than necessary and thus caused a diminution of the intensity decrease at resonance. Of these three probable explanations the second and third are by far the more important.

Acknowledgment

Professor I. I. Rabi suggested the measurements described in this paper and, during their course, has helped with discussion and suggestions. It is a pleasure to acknowledge his kindness here. The molecular beam apparatus which was used is one which is most productive when used cooperatively. Dr. Millman and Dr. Kusch have most generously provided the assistance which rendered such use possible. The manner in which they made freely available their skill, experience and knowledge contributed in no small degree to the successful completion of these measurements.

The Induced Radioactivity of Krypton and Xenon

EDWARD P. CLANCY
Harvard University, Cambridge, Massachusetts
(Received May 14, 1941)

Irradiation of krypton with deuterons of 11 Mev produces krypton activities with half-lives of 102 minutes, 4.0 hours, and about 35 hours. When selenium is bombarded with 22-Mev alpha-particles, there appear krypton activities of 114 minutes and about 33 hours. The 114-minute period coincides with that reported by other investigators as due to a krypton isotope growing out of Br^{83}, and hence is assigned to Kr^{83*}. The 102-minute period observed in deuteron irradiation is considered to be the same activity. Kr^{87}, an isotope which cannot be formed from alpha-particle reactions with selenium, is probably the source of the 4.0-hour activity. The weak 33–35 hour activity is due to Kr^{79} or Kr^{81}. Kr^{85} is presumed to have an activity long or fairly short. Irradiation of xenon with deuterons produces xenon activities of 68 minutes, 9.6 hours, and 5.4 days. Of these, the last also appears in the irradiation of tellurium with alpha-particles, and is due to Xe^{133}. The 9.6-hour activity is assigned to Xe^{135}. Xe^{137} is the most probable source of the 68-minute activity.

APPARATUS

A STUDY has been made of the induced radioactivity of the rare gases krypton and xenon. The results, many of which have already been reported briefly,[1,2] are here presented in more detail. Bombardments were made with the Harvard cyclotron, at energies of 11 Mev for deuterons and 22 Mev for alpha-particles.

A target chamber for irradiating the gases was constructed in the following way (Fig. 1). A flanged Pyrex pipe of two inches internal diameter was cut off and closed four inches from one of the flanged ends. This forms the bombardment chamber proper; a tube and stopcock permit the introduction of gas. By means of a cast bronze collar lined with a cushioning material, the flanged end is pressed down upon a brass plate, the seal being accomplished with a rubber gasket. In the center of the plate is a rectangular hole through which the beam comes. To prevent the bombarding particles from striking the glass at the end of the chamber, a shallow molybdenum cup is provided. The wire supporting this cup may be connected to the beam galvanometer at the control desk to give a measure of the current traversing the chamber. Since no provision is made for cooling the cup, the beam current must be limited to about 10 microamperes.

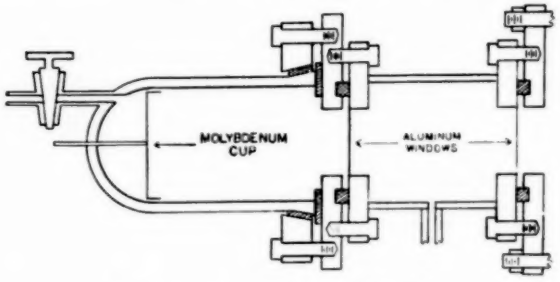

FIG. 1. Gas bombardment chamber.

Figure 1 shows that there is an intervening chamber which the beam must traverse. This chamber, kept evacuated, has holes at each end closed by 1-mil aluminum windows supported on grids. The latter are not shown. Were there only one window between the target chamber and the cyclotron chamber, fracture of this window would mean losing a quantity of rather expensive gas, and possible damage to the cyclotron itself. The whole assembly is sealed with rubber gaskets, and is bolted to the target opening of the cyclotron.

A glass ionization chamber for the radioactive gases was made as shown in Fig. 2. The outer electrode consists of a platinum film on the inside of the glass, covering some two-thirds of the surface. The film was formed from "platinizing paint." Between this film and the point where the central electrode enters the chamber

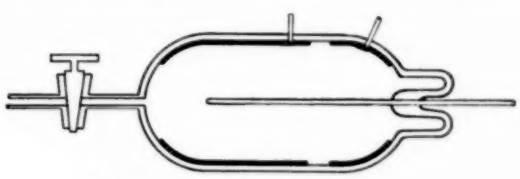

FIG. 2. Gas ionization chamber.

[1] Edward P. Clancy, Phys. Rev. **58**, 88 (1940).
[2] Edward P. Clancy, Phys. Rev. **59**, 686A (1941).

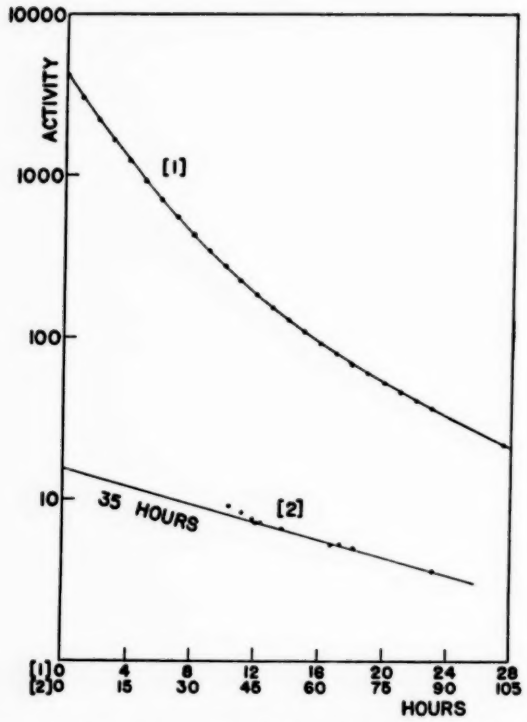

FIG. 3. Total activity of Kr from Kr+D. Activity is expressed in arbitrary units.

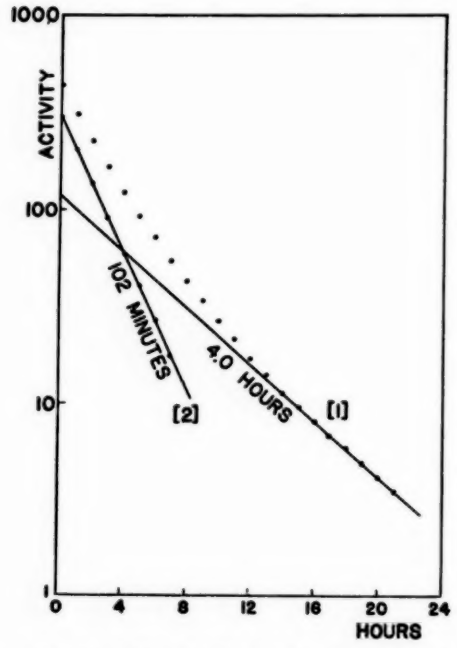

FIG. 4. Kr from Kr+D. Curve (1) represents the total activity indicated in Fig. 3, minus the 35-hour component. Curve (2) is the result of subtracting from (1) the 4.0-hour component.

there is a strip of film which forms a guard ring. Wires sealed in the glass wall make contact on the inside with the films. A supporting clamp holds the device in a vertical position above an ordinary ionization chamber, whose window has been removed to permit the central electrode of the glass ionization chamber to be fastened to the same electrode of the ordinary chamber. The latter chamber is connected to a d.c. amplifier using an FP54 electrometer tube. Recording is done automatically by means of a revolving drum covered with sensitized paper, upon which the galvanometer spot falls. An auxiliary device causes a zero reading to be taken every six minutes.

The transfer of gas from bombardment chamber to ionization chamber is effected by means of a Toepler pump. Connections are made with ground glass joints.

RADIOACTIVE KRYPTON ($Z=36$)

Irradiation of krypton with deuterons produced strong activities with periods of 102 minutes and 4.0 hours, and a weak activity of about 35 hours. The decay curve is shown in Fig. 3, and the subtracted curves in Fig. 4. These results are only in rough agreement with

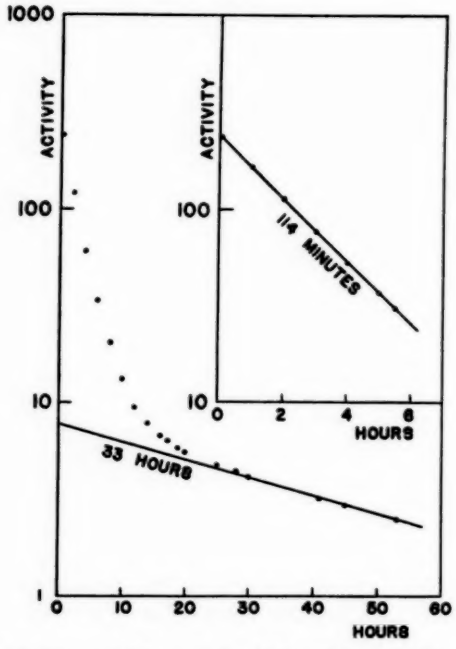

FIG. 5. Kr activities produced by alpha-particle irradiation of Se. The 114-minute activity is the result of subtracting the 33-hour component from the total activity.

those of Snell,[3] who, in the only previous irradiation of krypton, reported deuteron-induced activities of 74 minutes, 4.5 hours, and about 18 hours.

In the hope of obtaining further information to make possible isotope assignments, selenium ($Z=34$) was irradiated with alpha-particles. Such bombardment might be expected to produce krypton isotopes by (α, n) reactions. At the end of the irradiation the selenium was placed in a glass tube, the tube was evacuated, and the selenium was boiled to drive out the active krypton. Then the tube was cooled in CO_2-acetone slush to condense any active bromine ($Z=35$) that might have been formed by an (α, p) reaction, and finally the krypton was allowed to flow into the ionization chamber. A strong activity with a period of 114 minutes was observed, and also a weak activity of about 33 hours. These are shown in Fig. 5.

The 114-minute period can be assigned to the excited level of the stable isotope Kr^{83} (which decays by a gamma-ray transition to the ground state), since the period coincides with that reported for this isotope by Langsdorf and Segrè.[4] These investigators found a radioactive Kr^{83}, of 113-minute period, growing out of Br^{83}. In the present work, Kr^{83*} is being formed, either directly by the reaction

$$Se^{80}(\alpha, n)Kr^{83*},$$

or indirectly according to the reactions

$$Se^{80}(\alpha, p)Br^{83}$$
$$Br^{83}\rightarrow Kr^{83*}+e^{-}.$$

The 102-minute period observed in deuteron irradiation of krypton is obtained upon the second subtraction from the decay curve, and the margin of error is therefore likely to be large. It is probable that this activity is really that of Kr^{83*}, formed by a (d, p) or (d, d) reaction. The fact that the 4.0-hour period is not produced in the alpha-particle bombardment of selenium means that this activity must be assigned to Kr^{87}, an isotope which cannot be formed from alpha-particle reactions with selenium.

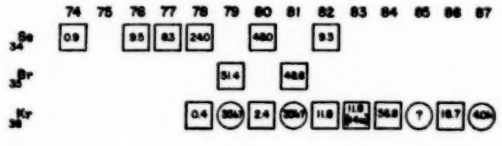

FIG. 6.

Other investigators[5] have irradiated bromine with protons, separated the krypton product, and observed a long period of 34 hours due to Kr^{79} or Kr^{81} formed by a (p, n) reaction. The weak 35-hour period found in the present work can probably be assigned to the same isotopes. When this activity is produced by alpha-particle bombardment, the reaction has therefore been

$$Se^{76,78}(\alpha, n)Kr^{79,81}.$$

We should expect Kr^{85} to appear from Se^{82} as the result of an (α, n) reaction when selenium is irradiated with alpha-particles. Since no activity other than the 114-minute and 33-hour periods was apparent, one must presume that the period of Kr^{85} is long or fairly short. In the latter case it might easily have been undetected in the present work, since there was necessarily a delay of several minutes between the end of the bombardment and the first reading.

RADIOACTIVE XENON ($Z=54$)

Deuteron irradiation of xenon produces activities with periods of 68 minutes, 9.6 hours, and

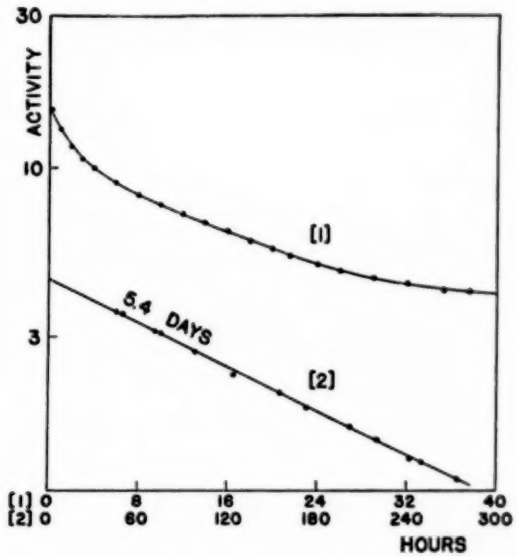

FIG. 7. Total activity of Xe from Xe+D.

[3] Arthur H. Snell, Phys. Rev. **52**, 1007 (1937).
[4] Alexander Langsdorf, Jr., and Emilio Segrè, Phys. Rev. **57**, 105 (1940).
[5] E. C. Creutz, L. A. Delsasso, R. A. Sutton, M. G. White and W. H. Barkas, Phys. Rev. **58**, 481 (1940).

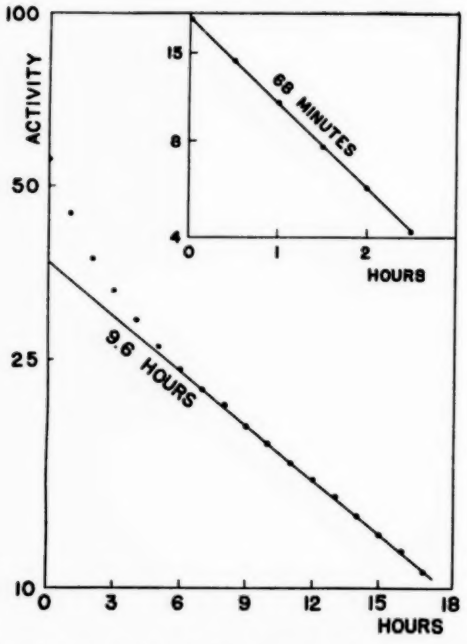

FIG. 8. Xe from Xe+D. The lower curve represents the total activity indicated in Fig. 7, minus the 5.4-day component. The curve in the inset is the result of subtracting the 9.6-hour component.

5.4 days. The decay curve is shown in Fig. 7, and the subtracted curves in Fig. 8. Of these periods, the longest is unambiguously due to Xe^{133}, since Wu[6] has found a 5-day period when activating the single isotope of caesium through an (n, p) reaction. This isotope has also been formed in the present investigation by bombarding tellurium with alpha-particles, through the reaction

$$Te^{130}(\alpha, n)Xe^{133}.$$

The experimental procedure here was practically the same as that used in the case of selenium, except that tellurium, on account of its high boiling point, could not be boiled directly in a glass tube. Instead, a small cup was constructed of sheet Nichrome. After irradiation, the tellurium was put in the cup, and the cup, placed in an evacuated glass vessel, was heated almost white-hot by means of an induction furnace. In addition to the long period due to Xe^{133}, there appeared an activity of about three hours. Definite assignment of this activity cannot be made, because it might result from any of several possible (α, n) reactions. It is not due to Xe^{137}, an isotope which cannot be formed in such a reaction. It is probably not due to Xe^{127}, since others[5] irradiated the single isotope of iodine with protons and found an active xenon with periods of 75 seconds and 34 days. A possible source is Xe^{125}, produced in the reaction $Te^{122}(\alpha, n)Xe^{125}$.

The 9.6-hour period produced in deuteron bombardment is undoubtedly the same as Wu's 9.4-hour xenon[6] obtained from an (n, α) reaction on barium, and assigned by her to Xe^{135}.

Assignment of the 68-minute period resulting from deuteron bombardment is uncertain. It can most logically be ascribed to Xe^{137}, since it did not appear among the activities produced in alpha-particle irradiation. No daughter activity

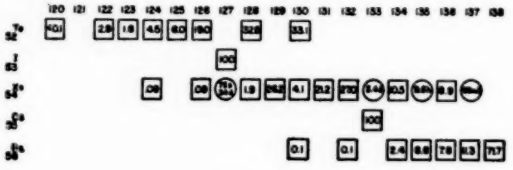

FIG. 9.

corresponding to the unstable decay product Cs^{137} has been found.

It is interesting that the 9.6-hour and 5.4-day periods correspond to xenon periods observed in uranium fission.[7, 8]

The assistance and encouragement of Professor K. T. Bainbridge during the course of this work is gratefully acknowledged.

[6] C. S. Wu, Phys. Rev. **58**, 926 (1940).

[7] E. Segrè and C. S. Wu, Phys. Rev. **57**, 552 (1940).

[8] R. W. Dodson and R. D. Fowler, Phys. Rev. **57**, 966 (1940).

On the Precision Measurement of Nuclear Magnetic Moments by the Molecular Beam Magnetic Resonance Method

The Moments of H^1, Li^7, F^{19}, and Na^{23} ‡

S. MILLMAN,* *Columbia University and City College, New York, New York*

AND

P. KUSCH,† *Columbia University, New York, New York*

(Received June 2, 1941)

A direct comparison of nuclear magnetic moments with the electronic moment is made. This is done by the measurement of the Larmor precession frequency of the nucleus and the frequencies of some of the lines of the radiofrequency spectra of the alkali atoms in the same magnetic field. In this way the magnetic moment of the proton is found to be 2.7896 ± 0.0008 nuclear magnetons. The precision of this value is very much greater than that which has heretofore been obtained by measurement of magnetic field by usual methods. The same methods are used in a redetermination of the magnetic moments of Li^7, F^{19} and Na^{23}. Since the nuclear gyromagnetic ratio of Li^7 has previously served as a standard in terms of which other g values were expressed, an improvement in the precision of this g value makes it possible to restate, with improved precision, the g values and magnetic moments of other nuclei.

INTRODUCTION

THE gyromagnetic ratios of a number of nuclei have been determined by the molecular beam magnetic resonance method.[1] The limitations on the precision of these measurements arose, for the most part, from uncertainties in the determination of magnetic fields by the usual methods, involving the use of flip coils and standards of mutual inductance. It was thus found difficult to determine, with the apparatus at hand, any nuclear g with a precision better than 0.5 percent. The relative values of many nuclear moments were much more precisely determined since such determinations could be made by measuring two frequencies at a fixed field.

Recent work[2,3] on the radiofrequency spectra of the alkali atoms suggested the possibility of making a direct comparison between nuclear and electronic magnetic moments. In the experiments to be described, such a comparison was made by utilizing the field dependence of some of the lines in the radiofrequency spectra for the determination of the magnetic field in which the precession frequencies of nuclear magnetic moments were observed. This determination of magnetic field could be made with considerable precision and led to a greatly improved precision in the values of the nuclear magnetic moments of H^1, Li^7, F^{19} and Na^{23}. The improvement in precision of the proton moment is particularly desirable for the purpose of comparing the neutron moment obtained from the difference of the deuteron and proton moments with the value measured for free neutrons by the method of Alvarez and Bloch.[4] An improvement in the accuracy of the g value of Li^7 automatically improves the precision of the g values of many other nuclei, since all gyromagnetic ratios determined by the resonance method have heretofore been referred to the g value of Li^7 as a standard.

METHOD

The hyperfine separations of the ground states of the alkali atoms have been previously reported. These $\Delta\nu$'s were determined either by an observation of the Zeeman lines in very low magnetic field, or by the study of lines in the

‡ Publication assisted by the Ernest Kempton Adams Fund for Physical Research of Columbia University.

* Now at Queens College, Flushing, New York.

† Now at Westinghouse Electric and Manufacturing Company, Bloomfield, New Jersey.

[1] I. I. Rabi, S. Millman, P. Kusch, and J. R. Zacharias, Phys. Rev. **55**, 526 (1939).

[2] P. Kusch, S. Millman, and I. I. Rabi, Phys. Rev. **57**, 765 (1940).

[3] S. Millman and P. Kusch, Phys. Rev. **58**, 438 (1940).

[4] L. W. Alvarez and F. Bloch, Phys. Rev. **57**, 111 (1940).

intermediate and Paschen-Back regions of field. In the cases of Li^7 and K^{39} both methods were used. In each of these experiments the choice of line or lines used in the determination of $\Delta\nu$ was such that the calculated values of $\Delta\nu$ did not depend on a precise knowledge of the magnetic fields at which the lines were observed. However, for purposes of calibrating a magnetic field, lines which have frequencies markedly dependent on magnetic field are used. If the frequency of such a line is measured and if the $\Delta\nu$ of the ground state is known, the magnetic field can at once be calculated by use of the quantum-mechanical expressions which give the energy of an alkali atom in a magnetic field. These expressions are given in Eqs. (9–12) of an earlier paper.[2] The lines chosen in our experiments are those represented by the transition $(2, -2) \leftrightarrow (1, -1)$ of Na^{23}, $(3, -3) \leftrightarrow (2, -2)$ of Rb^{85} and $(4, -2) \leftrightarrow (4, -1)$ of Cs^{133}. The notation is the same as that previously employed; the first symbol in the parenthesis indicates the F value of a state and the second symbol the m value.

In Figs. 1, 2 and 3 are plotted the frequencies of these lines as a function of field. The particular region of field employed in each of these cases covered the highest fields compatible with a marked dependence of the frequency of the line on field and with readily obtainable oscillator frequencies. The use of high magnetic fields is, of course, important since the error in locating the minimum of a nuclear resonance curve, obtained by varying frequency for a fixed field, decreases with increasing field. This arises from the fact that the width of the nuclear resonance curve is independent of the magnetic field. Li^7 and K^{39} are not suitable calibrating atoms for the present purposes, because no lines in the radiofrequency spectra of these two atoms show a marked dependence on field at values of the magnetic field above 1000 gauss and for frequencies not exceeding 1100 megacycles.

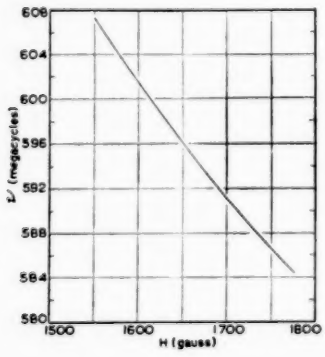

FIG. 1. The frequency of the line $(2, -2) \leftrightarrow (1, -1)$ of Na^{23} as a function of the magnetic field. $\Delta\nu(Na^{23}) = 1771.75 \times 10^6$ sec.$^{-1}$ has been assumed in the construction of the curve.

The equations which describe the curves merely give the ratio of the frequency of the line ν to $\Delta\nu$, in terms of the parameter x, which is related to the field by the expression:

$$H = \frac{4\pi\Delta\nu}{(e/mc)(g_j - g_i)} x.$$

Clearly, the curves in Figs. 1, 2 and 3 are constructed for assumed values of $\Delta\nu$ and g_i. We have used for the values of $\Delta\nu$ the following: $\Delta\nu(Na^{23}) = 1771.75 \times 10^6$ sec.$^{-1}$; $\Delta\nu(Rb^{85}) = 3035.7 \times 10^6$ sec.$^{-1}$; $\Delta\nu(Cs^{133}) = 9192.6 \times 10^6$ sec.$^{-1}$. The $\Delta\nu$ of Rb^{85} has been redetermined for the purposes of this work and the value found to be as previously reported[3] but with the somewhat better precision of 0.005 percent. We have also redetermined the $\Delta\nu$ of Cs^{133} and find it to be as above instead of 9191.4×10^6 sec.$^{-1}$ as previously reported.[3] The present value is undoubtedly better and has a precision of about 0.005 percent.

Any uncertainty in the value of $\Delta\nu$ will, of course, be reflected in a corresponding uncertainty in the field calculated from the line frequency. The percent error of the value of the parameter x, determined from an observation of the frequency ν of the atomic line, is given by the percent error in $\Delta\nu$ multiplied by the percent change in x for unit percent change in the ratio $\nu/\Delta\nu$. It follows from Figs. 1, 2 and 3 that an increase of 0.1 percent in the assumed values of the respective $\Delta\nu$'s will result in an increase in the x value, calculated from a given frequency of the atomic line, of 0.38 percent in the case of Na^{23}, 0.2 percent in the case of Rb^{85} and a decrease of 0.22 percent in the x value associated with a line of given frequency of Cs^{133}. Since the value of $\Delta\nu$ also enters linearly into the expression which converts x into H, an increase in the assumed value of $\Delta\nu$ by 0.1 percent will result in an additional increase in H by 0.1 percent in all cases. It follows, therefore, that an error in $\Delta\nu$ is reflected by an error in H which is 4.8 times as large for the case of Na^{23}, 3.0 times as large for the case of Rb^{85} and only 1.2 times as large for the case of Cs^{133}. Since all the $\Delta\nu$'s are known to

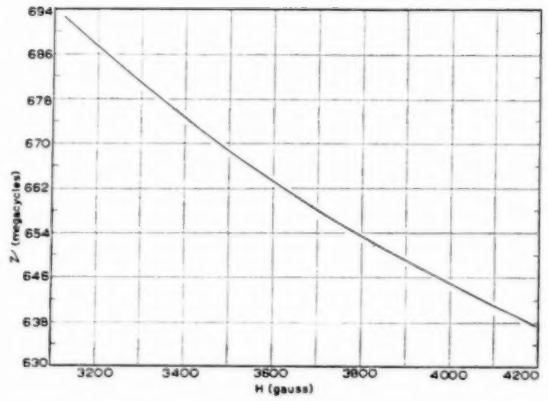

FIG. 2. The frequency of the line $(3, -3) \leftrightarrow (2, -2)$ of Rb^{85} as a function of the magnetic field. $\Delta\nu(Rb^{85}) = 3035.7 \times 10^6$ sec.$^{-1}$ has been assumed in the construction of the curve.

within 0.005 percent, the error in field due to uncertainty in $\Delta\nu$ alone will be about 0.024 percent in the Na^{23} calibration, 0.015 percent in the Rb^{85} calibration and 0.006 percent in the Cs^{133} calibration.

The values of g_i of the calibrating atoms enter both into the calculation of the ratio $\nu/\Delta\nu$ as a function of x and into the conversion from x to H. We have used for these g's the values listed in Table III. The contribution of terms involving g_i is so small that the indicated uncertainties in g_i introduce uncertainties in the field of only 0.001 percent in the case of Na^{23}, 0.002 percent in the case of Rb^{85} and 0.001 percent in the case of Cs^{133}. These uncertainties, therefore, do not affect the precision of our results.

In addition to the errors introduced by uncertainties in the values of $\Delta\nu$, the calculated values of the field will be subject to observational errors of the frequencies ν of the atomic lines. For any given atomic line the percent error in the field will be equal to the percent error in the frequency of the line multiplied by the percent change in x for unit percent change in $\nu/\Delta\nu$ as given earlier. Since the frequencies of lines may be determined to within 0.005 percent, the error arising from this factor should not exceed 0.02 percent for Na^{23}, 0.01 percent for Rb^{85} and 0.01 percent for Cs^{133}. The net precision within which the atomic lines may be used to determine the value of a magnetic field is about 0.035 percent for Na^{23}, 0.02 percent for Rb^{85} and 0.015 percent for Cs^{133}.

The determination of a field value from the observed frequency of an atomic line also depends on the value used for the constant e/mc. We have used for this quantity[5] the value 1.7591×10^7 e.m.u. per gram.

The value of any nuclear g is found by the expression:

$$g = \frac{4\pi}{(e/Mc)} \times \frac{f}{H},$$

where f is the frequency at resonance of the nucleus in a magnetic field H. The best way of obtaining the constant e/Mc is by use of the faraday. For this quantity we have used the most recent value of Birge,[5] 9650.6 e.m.u. per gram equivalent, on the physical scale. On the same scale the atomic weight of H^1 is 1.00813. After correction for the mass of the electron, the quantity e/Mc becomes 9578.0 e.m.u. per gram. The above expression then becomes,

$$g = 1.31200 \times 10^{-3} f/H.$$

The nuclear g value is, of course, the ratio of the nuclear magnetic moment expressed in units of the nuclear magneton, $eh/(4\pi Mc)$, and the angular momentum in units of $h/2\pi$. If we use for h the most recent value given by Birge,[5] 6.6237×10^{-27} erg sec., the nuclear magneton, in terms of which our magnetic moments are given, is 5.049×10^{-24} e.m.u. It is to be noted that the constant h does not enter into our calculations as long as magnetic moments are expressed in terms

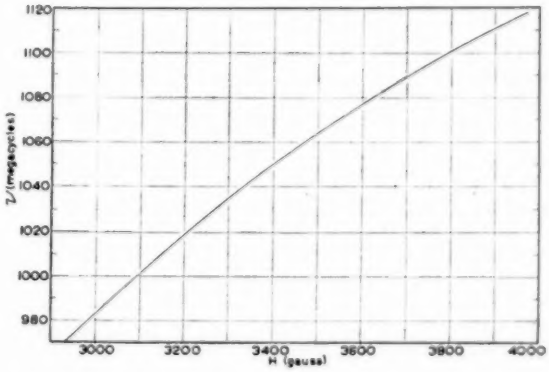

FIG. 3. The frequency of the line $(4, -2) \leftrightarrow (4, -1)$ of Cs^{133} as a function of the magnetic field. $\Delta\nu(Cs^{133}) = 9192.6 \times 10^6$ sec.$^{-1}$ has been assumed in the construction of the curve.

[5] For the fundamental constants used in this paper we have used the values given by R. T. Birge in a privately circulated tabulation of August, 1939.

of the nuclear magneton; it is only when these moments are expressed in absolute units that the quantity h enters.

The nuclear g values which we find depend directly on the ratio of the quantities e/mc and e/Mc and therefore on M/m. For the values of e/mc and e/Mc that we have used, the ratio M/m is equal to 1836.6. Any increase in this quantity will result in a proportional increase in the g values reported in this paper.

Finally it is assumed in all our calculations that the magnitude of the electronic gyromagnetic ratio for an alkali atom in the ground state, g_J, is exactly 2. Dr. M. Phillips[6] discusses the validity of this assumption in a paper in this journal.

Determination of the Gyromagnetic Ratios of Li^7, F^{19} and Na^{23}

Even though the value of a magnetic field may be determined within very narrow limits, as pointed out in the previous section, the use of such field values for the purpose of accurate determination of nuclear gyromagnetic ratios presents considerable difficulties. We have used two distinct methods of utilizing a field calibration in the determination of g values. The first method has been applied to the cases of Li^7, F^{19} and Na^{23} and the second method to the case of H^1.

For the purposes of determining the nuclear gyromagnetic ratios of Li^7 and F^{19}, runs were made by loading the oven with two substances, one of which produced the atomic portion of the beam and the other of which produced the molecular portion. Since a beam of the calibrating atom was produced at a lower temperature than the molecular beam, it was necessary to make the calibration of the field before the observation of any nuclear resonance curves. In the case of Na^{23}, a molecular beam of Na_2 accompanies a beam of atomic Na, so that calibration of field and observation of nuclear resonance curves may be accomplished at the same oven temperature.

In order that nuclear transitions may produce an appreciable drop in intensity at the detector, it is necessary that the inhomogeneous fields have large gradients. Such gradients will, however, serve to remove atoms from the beam, since the moment of an alkali atom is about 1000 times as great as that of a nucleus. It is, therefore, necessary that the deflecting fields have different values for the observation of nuclear and atomic transitions. However, because of the proximity of the deflecting magnets to the transition field, a change in the inhomogeneous field has a slight, but not negligible, effect on the value of the field in the transition magnet. This effect was found to be least when the transition field was demagnetized in the presence of the appropriate inhomogeneous field and was then raised to its final value.

The procedure which was followed in the determination of nuclear g values was to determine the calibration constant (field per unit current in the magnet coils) of the magnet in which the transitions occurred. This calibration constant was modified slightly for use in determining nuclear g values by an amount which depended on the difference between the value of the inhomogeneous field used for the observation of atomic and nuclear transitions. This correction was determined by flip coil measurements. In the region of 1600 gauss, where calibrations were made with the use of atomic transitions of Na^{23}, the correction was about 0.04 percent. In the region of 3200 gauss, where calibrations were made with the use of atomic transitions of Rb^{85}, the correction was about 0.10 percent. To average out effects arising from the non-reproducibility of the field as a function of the current in the field coils, all observations which were used in the determination of the calibration constant were repeated a large number of times, each for an independent demagnetization of the field.

The nuclear resonance curves were then observed at the same value of the field as that at which the calibration was made. Errors arising

TABLE I. *The nuclear g's of* Li^7, F^{19} *and* Na^{23} *as found by a direct determination. Each line in the table represents the results of a distinct run.*

Calibrating Substance	Molecule	Nucleus	Observed g Value
Na^{23}	Na_2	Na^{23}	1.4768
Na^{23}	Li_2	Li^7	2.1695
Na^{23}	NaF	F^{19}	5.2496
Na^{23}	Na_2	Na^{23}	1.4762
Rb^{85}	LiCl	Li^7	2.1691
Rb^{85}	LiCl	Li^7	2.1701
	Mean $g(Li^7)$	$=2.1696$	
	$g(F^{19})$	$=5.2496$	
	$g(Na^{23})$	$=1.4765$	

[6] M. Phillips, Phys. Rev. **60**, 100 (1941).

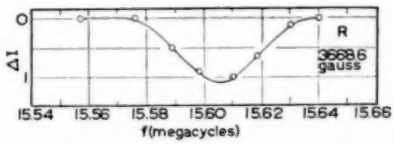

FIG. 4. Typical proton resonance curve in KOH observed for such values of the inhomogeneous fields that Rb^{85} atoms in the state $m=-2$ pass through each field without deflection.

from the non-reproducibility of the field as a function of the current in the coils were reduced, as in the calibration procedure, by observing resonance curves for many independent demagnetizations of the field. It was also necessary to observe the resonance minima for each of the two directions of the homogeneous field perpendicular to the beam direction. In this way asymmetries in the resonance curves arising from end effects in the wires which produce the oscillating field may be averaged out.[7]

In Table I are listed the observed nuclear g's. The error in any one of the tabulated g's does not exceed 0.1 percent. The consistency of the observed g values of Na^{23} obtained from two distinct runs may be noted. In the case of Li^7 such consistency is particularly significant since the individual results depend on different calibrating atoms, the $\Delta\nu$'s of which have been independently measured, on different molecules and on independently determined corrections to the transition field arising from the inhomogeneous field.

Any errors arising from uncertainties in fundamental constants have not been included in the above estimates of precision.

DETERMINATION OF THE PROTON MOMENT

The chief source of error in the experiments just described arose from the circumstance that the detection of atomic transitions requires very low gradients in the deflecting fields while nuclear reorientations produce appreciable changes in the path of the molecule only when large field gradients are used. Errors arising from the correction due to the presence of the deflecting fields, as well as those arising from the non-reproducibility of the transition field, would be eliminated if both nuclear and atomic transitions could be observed at the same setting of the homogeneous transition field as well as at the same setting of the deflecting fields. It was, therefore, thought worthwhile to investigate the possibility of observing nuclear transitions with low deflecting fields. Hydrogen is particularly favorable for such experiments since it has a large nuclear g value. Moreover, it was thought desirable to obtain the proton moment directly without any dependence on the moment of an intermediate nucleus.

In the attempt to obtain a proton resonance curve we have tried to obtain beams of a number of molecules containing an alkali atom as well as hydrogen. The alkali atom is essential for the detection of the beam by the surface ionization method. When LiH was heated in an iron or in a silver oven the beam which was detected was unsteady and practically 100 percent Li atoms. Similar results were obtained when $NaNH_2$ was heated in an iron or in a silver oven. In each case an atomic beam was produced with the evolution of large quantities of gas. NaOH and KOH were also completely dissociated when heated in iron or nickel ovens. However, when a silver oven was used, good molecular beams of NaOH and KOH were obtained. The dissociation in these cases was such that about one-third of the beam was molecular and about two-thirds atomic. This gave ample beam intensity of sufficient steadiness

TABLE II. *Results of the determination of the proton moment by direct measurement. Column 1. Calibrating atom and transition. Hydrogen-containing molecule used. Column 2. Field direction. Column 3. Observed atomic transition frequency. $\nu\times10^{-6}$ (sec.$^{-1}$). Column 4. H (gauss) calculated from $\nu/\Delta\nu$. Column 5. Frequency of proton resonance minimum. $f\times10^{-6}$ (sec.$^{-1}$). Column 6. Proton g in units of e/2Mc. $g=1.3120\times10^{-3}\,f/H$. Column 7. Mean g values found for the field directions N and R separately. Column 8. Mean g value for each run.*

1	2	3	4	5	6	7	8
Rb^{85}	*N*	659.98	3665.1	15.583	5.5782		
$(3,-3)\leftrightarrow(2,-2)$		659.99	3664.9	15.585	5.5792		
KOH		659.98	3665.1	15.581	5.5775	5.5783	
	R	659.76	3669.6	15.606	5.5796		
		659.81	3668.6	15.606	5.5811		
		659.81	3668.6	15.605	5.5808	5.5805	5.5794
Na^{23}	*N*	588.97	1723.2	7.3251	5.5771		
$(2,-2)\leftrightarrow(1,-1)$		588.94	1723.5	7.3257	5.5766	5.5769	
NaOH							
	R	588.12	1729.1	7.3594	5.5841		
		588.38	1729.5	7.3600	5.5833	5.5837	5.5803
Cs^{133}	*N*	1056.04	3450.3	14.665	5.5764		
$(4,-2)\leftrightarrow(4,-1)$		1055.98	3449.9	14.665	5.5771		
KOH		1056.19	3453.5	14.679	5.5766	5.5767	
	R	1055.46	3446.2	14.657	5.5800		
		1056.12	3450.9	14.681	5.5815		
		1056.41	3453.0	14.688	5.5808	5.5808	5.5788

[7] S. Millman, Phys. Rev. **55**, 628 (1939)

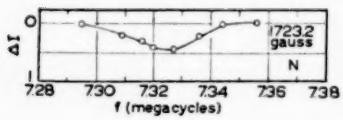

FIG. 5. Typical proton resonance curve in NaOH observed for such values of the inhomogeneous fields that Na^{23} atoms in the state $m=-1$ pass through each field without deflection.

for the observation of resonance curves of the proton. The partial dissociation of NaOH served a useful purpose in the determination of the proton moment with the use of atomic lines of Na^{23} for field calibration. In this case one oven charge gave the appropriate atomic and molecular beams in about the right proportion for the calibration of the magnet and the observation of proton resonance curves.

A preliminary study of the proton resonance curves obtained with KOH and NaOH showed that these could be observed with values of gradients in the deflecting fields as low as 3000 gauss/cm, compared with 100,000 gauss/cm normally employed for detecting nuclear transitions. The reduction of deflecting power of the magnets merely results in the lowering of the depth of the resonance curve but does not affect its width. In our apparatus such gradients are still too large for use with atoms having magnetic moments of the order of one Bohr magneton. However, if we take advantage of the fact that alkali atoms in some states have zero magnetic moment[8] for certain values of magnetic field, we can, with a suitable choice of atom and state, use deflecting fields that will not be excessive for observing certain atomic transitions and at the same time be sufficiently large for the purpose of detecting nuclear reorientations.

The first atom used for calibrating the field in this manner was Rb^{85}. In order to observe atomic and nuclear reorientations in rapid succession, so that errors due to field drift are minimized, it is important to arrange for simultaneous detection of the atomic Rb beam and the molecular KOH beam. It is, therefore, essential that the Rb atoms produce a beam at approximately the same temperature of the oven as the alkali hydroxide. It is clearly impossible to use metallic rubidium for this purpose, since the temperature at which the vapor pressure is of the order of 1 mm of Hg is about 600°C for KOH, 680°C for NaOH while only 200°C for metallic Rb. However, if instead of placing metallic Rb in the oven, we insert RbCl and Ca in a silver oven, we find that a rubidium beam is obtained at approximately the same temperature as a KOH beam. If RbCl and Ca are inserted in an iron oven, similar Rb vapor pressures are obtained at temperatures 50°C to 75°C higher than those required for the silver oven. We have, accordingly, constructed a silver oven containing two separate compartments, merging only at the slit. This prevents any possible reaction between KOH and the ingredients necessary for the production of the Rb beam. It was found that a beam of atomic Cs could be produced at the same time as a beam of molecular KOH by use of the same methods.

The atomic transition used for the calibration with Rb^{85} is the line $(3, -3) \leftrightarrow (2, -2)$. The magnetic moment of an atom in the state $m=-3$ is independent of the field and has a value of one Bohr magneton. Atoms in the state $m=-2$ have zero moment[9] at a field of about 725 gauss, which, in our apparatus, means a gradient of about 6000 gauss/cm. If, in the homogeneous field between the two deflecting magnets, atoms in the state $m=-2$ make a transition to the state $m=-3$, they will be deflected away from the original direction by the second deflecting field and will not reach the detector.

The procedure followed in these experiments was to observe the atomic transition at some fixed value of the homogeneous field, and then, without any changes except that involved in switching oscillators, to observe a proton resonance curve. We have obtained three such curves for one field direction and three curves for the reversed field direction. In each case a calibration was made between the successive curves. The procedure of using the transition field in each of two directions is necessary in order to eliminate errors in locating minima of resonance curves due to asymmetries introduced by end effects in the oscillating field. Figure 4 shows a typical proton resonance curve obtained in this way for the field direction which we designate as R. Evidently the value of the proton g as calculated from this curve will not coincide with the value finally arrived at. The drop in beam intensity ΔI is plotted in arbitrary

[8] V. W. Cohen, Phys. Rev. **46**, 713 (1934).

[9] S. Millman and M. Fox, Phys. Rev. **50**, 220 (1936).

units. The results of the KOH-Rb run are tabulated in Table II.

The constancy of the g value for either field direction is a measure of the internal consistency of the results. Errors due to small changes in the homogeneous field between the calibration and the observation of the resonance curve, uncertainty in the location of the resonance minima, or in the readings of the wave meter, will cause variations in the observed g value. Errors in the assumed value of the $\Delta\nu$ of Rb^{85} and in the assumed value of M/m are, of course, common to all observations. The precision of the gyromagnetic ratio of the proton as determined from a calibration with Rb^{85} is about 0.04 percent. This includes all factors except the uncertainty in M/m.

The second calibrating atom used in these experiments was Na^{23}. We have used the transition $(2, -2) \leftrightarrow (1, -1)$, and therefore set the deflecting magnets at such a field value that the moment of atoms in the state $m=-1$ is zero. This field is about 320 gauss[10] and in our apparatus corresponds to a gradient of about 2600 gauss/cm. This gradient is less than half of that used for deflection in the KOH-Rb run and will, therefore, result in a very shallow proton resonance curve, thus introducing greater errors in the location of the minimum. Since the sensitivity of the frequency of the calibrating line to field demands that the calibration with Na^{23} be made at about half the value of the homogeneous field used for Rb^{85}, the ratio of the half-width of the resonance curve to the frequency at resonance is about twice as great for curves obtained in the NaOH-Na run as for curves obtained in the KOH-Rb run. This occurs because the half-width of the curve in frequency units is independent of the field. The net effect is that the g value of the proton as obtained by use of a calibration with the atomic line of Na^{23} is considerably less precise than that obtained by use of a calibration with the atomic line of Rb^{85}. Figure 5 shows a proton resonance curve, for the field direction which we designate as N, obtained in a molecular beam of NaOH under the conditions outlined above. The drop in beam intensity ΔI is plotted on the same scale as in the case of the KOH-Rb run. The generally low intensity drop is indicative of the difficulty of obtaining a precise value of g from these data. The precision of the g value of the proton as obtained from this calibration is probably not better than about 0.08 percent. The results obtained in this run are given in Table II.

Finally we have used the caesium atom for our field calibration. This atom is even more favorable for these experiments than Rb^{85}, since "zero moment peaks" of the former occur at considerably higher field values than do those of the latter. Since we are making use of the transition $(4, -2) \leftrightarrow (4, -1)$ we may set our deflecting fields so that the moment of atoms in either the state $m=-2$ or in the state $m=-1$ shall be equal to zero. However, since the zero moment peak for $m=-2$ occurs at twice the field as that for which the zero moment peak for $m=-1$ occurs, it is evidently desirable to use the former of the two peaks for our present purposes. This peak occurs at a field of about 1650 gauss.[8] An atom in this state suffers no deflection in the first of the two inhomogeneous fields. If a transition has taken place in the region between the two inhomogeneous fields, the moment of the atom will be considerably different from zero in the second deflecting field. The gradients are sufficiently strong to remove such an atom from the beam. The great advantage of this calibration lies in the fact that the relatively large gradients give rise to a fairly deep resonance minimum for the proton and a corresponding improvement in the precision of locating a minimum. A proton resonance curve for the field direction R taken in the KOH-Cs run is shown in Fig. 6. The results obtained in this run are tabulated in Table II. The g value of the proton as obtained from the Cs calibration can probably be expressed to a precision of 0.03 percent.

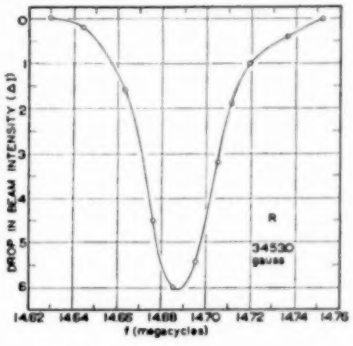

FIG. 6. Typical proton resonance curve in KOH observed for such values of the inhomogeneous fields that Cs^{133} atoms in the state $m=-2$ pass through each field undeflected.

[10] M. Fox and I. I. Rabi, Phys. Rev. **48**, 746 (1935).

The difference between the apparent g values of the proton as obtained for the field directions R and N will depend on a number of factors.[7] For identical beams and for identical amplitudes of the oscillating fields the shift in the resonance minimum will be represented by a constant frequency difference. The apparent shift in the g value due to the end effects of the wires which produce the oscillating field will, therefore, be inversely proportional to the field at which the resonance curve is observed. This is apparent in Table II where the discrepancy between the two observed g values for the NaOH-Na run is about twice as great as in the case of the KOH-Cs run. The difference between the two observed values of the proton g for the KOH-Rb run is appreciably smaller than it is in the case of the KOH-Cs run. This may possibly result from lower oscillating currents in the first of the two cases. We believe that the mean of the apparent g's for the field direction R and N represents the true g value in all of the cases, since the magnitude of the oscillating currents used is of no importance if the same currents are used in the observation of resonance curves for each of the two field directions. We have fulfilled this requirement in all cases.

We also believe that the minima of the resonance curves represent the resonance of the Larmor precession frequency of the proton at the indicated values of the constant field with the frequency of the oscillating field. The small half-widths of the curves (32 kc for KOH-Rb and 36 kc for KOH-Cs) indicate that broadening arising from molecular interactions with the proton is very small indeed, and the generally symmetrical character of the curves indicates that such broadening is not likely to shift the minimum of the true proton resonance curve by any significant amount.

In arriving at the final result for the proton g value we average the results obtained with the three different calibrating atoms. We believe the proper weight factors to be about 6, 1 and 8 for the Rb^{85}, Na^{23} and Cs^{133} runs, respectively. The g value of the proton can then be given as: 5.5791 ± 0.0016. The proton moment is then 2.7896 ± 0.0008 nuclear magnetons. The precision measures do not include uncertainties in M/m.

TABLE III. *The values of nuclear gyromagnetic ratios observed by the molecular beam magnetic resonance method, the values of the nuclear spin and the resulting values of nuclear magnetic moments.*

Nucleus	Observed g Value	Spin i	Moment μ	Diamagnetic Correction (%)	Ref.
$_1H^1$	5.5791 ± 0.0016	1/2	2.7896	0	15
$_1H^2$	0.8565 ± 0.0004	1	0.8565	0	15
$_3Li^6$	0.8213 ± 0.0005	1	0.8213	0.01	1
$_3Li^7$	2.1688 ± 0.0010	3/2	3.2532	0.01	1
$_4Be^9$	0.784 ± 0.003	3/2	−1.176	0.02	a
$_5B^{10}$	0.598 ± 0.003	1	0.598	0.03	b
$_5B^{11}$	1.791 ± 0.005	3/2	2.686	0.03	b
$_6C^{13}$	1.402 ± 0.004	1/2	0.701	0.03	c
$_7N^{14}$	0.403 ± 0.002	1	0.403	0.04	14
$_7N^{15}$	0.560 ± 0.006	1/2	0.280	0.04	13
$_9F^{19}$	5.250 ± 0.005	1/2	2.625	0.06	1
$_{11}Na^{23}$	1.4765 ± 0.0015	3/2	2.215	0.08	14
$_{13}Al^{27}$	1.452 ± 0.004	5/2	3.630	0.10	d
$_{17}Cl^{35}$	0.547 ± 0.002	5/2	1.368	0.14	e, f
$_{17}Cl^{37}$	0.454 ± 0.002	5/2	1.136	0.14	e, f
$_{19}K^{39}$	0.260 ± 0.001	3/2	0.391	0.16	14
$_{19}K^{41}$	0.143 ± 0.001	3/2	0.215	0.16	2, 16, 17
$_{37}Rb^{85}$	0.536 ± 0.003	5/2	1.340	0.39	e
$_{37}Rb^{87}$	1.822 ± 0.006	3/2	2.733	0.39	e
$_{55}Cs^{133}$	0.731 ± 0.002	7/2	2.558	0.67	14
$_{56}Ba^{135}$	0.558 ± 0.002	3/2	0.837	0.68	g
$_{56}Ba^{137}$	0.624 ± 0.002	3/2	0.936	0.68	g

[a] P. Kusch, S. Millman, and I. I. Rabi, Phys. Rev. **55**, 666 (1939).
[b] S. Millman, P. Kusch, and I. I. Rabi, Phys. Rev. **56**, 165 (1939).
[c] R. Hay, Phys. Rev. **58**, 180 (1940).
[d] S. Millman and P. Kusch, Phys. Rev. **56**, 303 (1939).
[e] P. Kusch and S. Millman, Phys. Rev. **56**, 527 (1939).
[f] E. F. Shrader, S. Millman, and P. Kusch, Phys. Rev. **58**, 925 (1940).
[g] R. Hay, Phys. Rev. **59**, 686 (1941).

Nuclear g Values and Magnetic Moments Referred to the New Scale

All the values of nuclear g's previously published are subject to a rather large uncertainty arising from the difficulty of determining the absolute value of a field at resonance. Since the ratio of two nuclear g values may, in general, be determined to a higher order of precision than the g value itself, it has been the custom to report all g values relative to that of Li^7. The g value of Li^7 was chosen as a standard because the resonance curve associated with the nuclear g of Li^7 may readily be observed in a great variety of molecular beams, and because the resonance curve is generally deep and narrow. In view of the fact that the absolute value of the hydrogen moment has been established to a high order of precision, it seems desirable to tabulate all the moments, obtained by the molecular beam magnetic resonance method, referred to our new standard. For this purpose the g value of Li^7 will serve as a secondary or intermediate standard. Since its

value is very well known, no appreciable error is introduced by use of this value. In the first column of Table III are listed the nuclei for which data are available. In the second column are listed the observed g values corrected to the scale for which the g value of the proton is 5.5791. The corresponding values of the spin are listed in the third column. Most of these have been determined by reliable experimental procedures. Exceptions occur in the cases of Be^9, B^{10}, B^{11} and C^{13} where the tabulated values of the spin are the result of theoretical calculations, and in the cases of Cl^{35} and Cl^{37} where the tabulated spins are those obtained from an observation[11,12] of the alternating intensities of lines in the band spectra of the homonuclear diatomic molecules of chlorine. The last of these procedures may not be conclusive for spins as large as 5/2. The fourth column lists the magnetic moments obtained from the observed g value and the spin. The signs of the moments have been experimentally determined[7] for all nuclei except N^{15}.[13] They are all positive except that of Be^9. A diamagnetic correction, which serves to increase the value of the moment, must be applied, as discussed in an earlier paper.[14] This correction has not been applied to the values of the moments listed in Table III. The magnitude of the correction is indicated in each case in the fifth column of the table. A brief discussion of some of the g values follows.

$_1H^2$. The value of the deuteron moment has been determined from our value of the proton moment and from the value $\mu_P/\mu_D = 3.257 \pm 0.001$ gives by Kellogg, Rabi, Ramsey, and Zacharias.[15]

$_3Li^7$. We have made a careful determination of the ratio $g(H^1)/g(Li^7)$ which we find to be 2.5729 ± 0.0008. If this ratio is applied to the known g of the proton we obtain for the g of Li^7 the value 2.1684. The directly determined value of the g of Li^7 is 2.1696. The discrepancy lies well within the experimental error of the determinations. It is to be noted that the two determinations are entirely independent and involve only the common values of $\Delta\nu$. The first of the two indicated values is somewhat more precise, and we have given this value a weight of two as compared to a weight of one assigned to the second of the two values. The g of Li^7 then becomes 2.1688 ± 0.0010. The discrepancy between this value and that previously reported is 0.10 percent.

$_3Li^6$. For the determination of the nuclear g value of Li^6 we have used the previously published value[2] of the ratio $\mu(Li^7)/\mu(Li^6) = 3.9601 \pm 0.0015$. This gives $g(Li^6) = 0.8213 \pm 0.0005$.

$_9F^{19}$. The previously published value[1] for the g of F^{19}, when corrected to the present scale, becomes 5.247. The new and independently determined value is 5.250. We believe this agreement to be fortuitous and adopt the new value as the better one.

$_{11}Na^{23}$. The previously published value[14] for the g of Na^{23}, when corrected to the present scale, becomes 1.4771. This value is to be compared to the present directly determined value of 1.4765. The agreement is better than is to be expected and may be regarded as fortuitous. We believe the value determined by methods described in this paper to be the better one and shall adopt it.

$_7N^{14}$. The present value of the nuclear g of N^{14} depends on a new determination of the ratio, $g(Li^7)/g(N^{14}) = 5.37$. This leads to the value $g(N^{14}) = 0.403$, which is in good agreement with that previously published.[14] We believe the present value to be the better one.

$_{19}K^{41}$. The nuclear g of K^{41} has not been directly determined. However, since the spin[16] of K^{41} is the same as that of K^{39},[17] the g value of the former can be obtained from the measured g value of the latter by multiplying by the ratio of the observed[2] $\Delta\nu$'s of the ground state of these atoms.

All other nuclear g values listed in Table III are simply the previously published g values corrected to the new scale.

The Magnetic Moment of the Neutron

A simple subtraction of the proton moment from the deuteron moment gives the value -1.933 ± 0.001 for the moment of the neutron.

[11] A. Elliot, Proc. Roy. Soc. **A127**, 638 (1930).
[12] E. F. Shrader, Phys. Rev. **58**, 475 (1940).
[13] J. R. Zacharias and J. M. B. Kellogg, Phys. Rev. **57**, 570 (1940).
[14] P. Kusch, S. Millman, and I. I. Rabi, Phys. Rev. **55**, 1176 (1939).
[15] J. M. B. Kellogg, I. I. Rabi, N. F. Ramsey and J. R. Zacharias, Phys. Rev. **56**, 728 (1939).
[16] J. H. Manley, Phys. Rev. **49**, 921 (1936).
[17] S. Millman, Phys. Rev. **47**, 739 (1935).

If we take the expression given by Rarita and Schwinger[18] for the calculation of the neutron moment from the observed values of μ_P and μ_D,

$$\mu_n=\frac{\mu_D-\frac{3}{4}\times 0.039}{1-\frac{3}{2}\times 0.039}-\mu_P,$$

we obtain the value -1.911 ± 0.001 for μ_n, wherein the precision measure includes only experimental errors in the determination of μ_P and μ_D. These results are to be compared with the value of 1.935 ± 0.02 obtained by Alvarez and Bloch[4] for the magnetic moment of the free neutron. The uncertainty in the latter experiment is thus too great to yield an experimental check on the theoretical predictions. It is highly desirable that the moment of the free neutron be measured with a precision comparable to that obtained for the difference $\mu_D-\mu_P$.

We wish to thank Professor I. I. Rabi for his interest in this work and Mr. R. H. Hay and Dr. A. W. Lawson for their assistance in part of the work. The research has been aided by a grant from the Research Corporation.

[18] W. Rarita and J. Schwinger, Phys. Rev. **59**, 436 (1941).

JULY 15, 1941 PHYSICAL REVIEW VOLUME 60

On Electronic g Factors for Alkali Atoms

M. PHILLIPS
Brooklyn College, Brooklyn, New York

(Received June 2, 1941)

Possible theoretical deviations from $g_J=2$ for the ground state of the alkalis are investigated, and it is concluded that none is large enough to affect measurably the experimental results.

IT is assumed by Millman and Kusch[1] that for the ground level of an alkali atom $g_J=2$ is good to the accuracy of the experiments. This value of the gyromagnetic ratio for the electronic system follows at once from the description of an alkali atom in terms of a single electron moving in the central static field of the nucleus and core electrons. The energy level scheme predicted on this model is generally satisfactory, but inverted or anomalously narrow doublets occur frequently in alkali spectra,[2] indicating that the simple picture is not always justified. In view of this the question of possible perturbations of the magnetic moment must be considered seriously when high experimental accuracy is involved.

The anomalous doublet separations are adequately explained by taking into account the excitation of core electrons.[3] Possible dependence of the magnetic moment of the ground state on core excitation is here investigated. Two other aspects of the atom which are neglected in first approximation, the motion of the nucleus and relativistic effects, are also considered.

It can be easily shown that departures of the core from rigidity do not affect the mean value of the magnetic moment operator $(e/2mc)(L_z+2S_z)$ in this case. Such an effect would arise only if the ground state were not pure $^2S_{\frac{1}{2}}$ but contained some admixture of other $J=\frac{1}{2}$ states with different L or S. Perturbations due to excited levels may be found by writing the normal state wave function as $\Psi=\psi_0+\sum_i[V_{0i}/(E_0-E_i)]\psi_i$. Here ψ_0 is the approximate function for the lowest configuration, ψ_i that for some excited state i, and V_{0i} is the interconfiguration matrix element of the perturbing energy. The possible interacting configurations must be even, and the lowest of these would differ from the ground state only in that one of the core electrons has its total quantum number increased by unity. (No even states characterized by one-half unit of total angular momentum arise from excitation of the valence electron except for higher $^2S_{\frac{1}{2}}$

[1] S. Millman and P. Kusch, Phys. Rev. **60**, 91 (1941).
[2] Bowen and Millikan, Phys. Rev. **25**, 301 (1925).
[3] M. Phillips, Phys. Rev. **44**, 644 (1933).

levels.) It remains to consider the various possibilities for V_{0i}.

Electrostatic polarization of the core cannot be responsible for mixing into the ground state excited levels with $L\neq 0$ and $S\neq\frac{1}{2}$, since the electrostatic interaction commutes with the orbital and spin angular momenta separately, and hence will have no matrix elements non-diagonal with respect to L and S. Neither will the ordinary vector couplings, $\mathbf{l}_1\cdot\mathbf{s}_2$, $\mathbf{s}_1\cdot\mathbf{s}_2$, $\mathbf{l}_1\cdot\mathbf{l}_2$. Even the spin-orbit-spin interaction,[4] which in general has mean values non-diagonal in the total spin, does not perturb ^2S states, since the J value for a quartet S level is $\frac{3}{2}$. It follows that although there may be some mixture of excited configurations in the ground state the g_J factor is essentially unperturbed.

If the wave equation for the entire atom, including the nucleus, is used to determine the dependence of the energy E on a weak magnetic field H and dE/dH is then computed there is a small term due to the motion of the nucleus. This term is of the form $(e/2mc)(2m/M)[y_ip_{xj}+y_jp_{xi}-x_ip_{yj}-x_jp_{yi}]$, and is analogous to the Hughes-Eckart term which describes the specific isotope effect.[5] There will be non-vanishing matrix elements if i refers to the s electron and j to a p shell electron of parallel spin, but since both the s orbit and the closed p shell are spherically symmetric there will be no net contribution to the magnetic moment of the ground state. (The quantity in brackets has so small a mean value, besides having as a coefficient the ratio of the electron mass to that of the nucleus, that the estimated effect on the g factor for a P state of sodium is of the order 10^{-6}.)

Relativistic corrections have already been treated by Margenau.[6] For a $^2S_1$ level his formula reduces to $g_J=2(1-\frac{1}{3}v^2/c^2)$. This correction term is roughly the same for Na, Rb and Cs, and amounts to about 10^{-5}. This is too small to affect the measurements of Millman and Kusch.[1]

[4] E.g. H. A. Bethe, *Handbuch der Physik* Vol. XXIV, 1, 380.

[5] D. S. Hughes and C. Eckart, Phys. Rev. **36**, 69, 694 (1930).

[6] H. Margenau, Phys. Rev. **57**, 383 (1940).

JULY 15, 1941 PHYSICAL REVIEW VOLUME 60

The Thundercloud as a Source of Penetrating Particles

E. C. HALLIDAY
University of the Witwatersrand, Johannesburg, South Africa

(Received April 28, 1941)

The paper describes cloud-chamber experiments designed to test the hypothesis that the electrostatic fields in thunderclouds can produce showers of electrons with energies as great as those found in the penetrating radiation. Sixty-five thunderstorms were observed and five thousand photographs of electron tracks were taken, together with four thousand five hundred control photographs. A statistical examination of the relative number of penetrating electron tracks seen in the two sets of photographs indicates that there is a very strong possibility that penetrating electrons *are* ejected from thunderclouds and reach the earth at considerable distances from the clouds. Evidence is thus obtained that storm clouds act as a source of penetrating electrons, but it is not known whether they are the only source. The experiments indicated that the simple hypothesis, that the penetrating electrons, after their ejection from the storm clouds travel in helical paths about the earth's magnetic field, is untenable.

INTRODUCTION

IN 1925 and again in 1929, C. T. R. Wilson suggested that it was possible for thunderclouds, by reason of their very high potentials, to produce a shower of high speed electrons, with energies as high as 5×10^9 electron volts.[1,2] As the polarity of thunderclouds is predominantly positive (the positive charge being above the

[1] C. T. R. Wilson, Proc. Camb. Phil. Soc. **22**, 534 (1925).
[2] C. T. R. Wilson, J. Frank. Inst. **208**, 1 (1929).

negative charge), the process envisaged by Wilson involves the projection of the electrons in a more or less upward direction at the instant that the electric moment of the cloud is destroyed by the action of a lightning flash. The electron is accelerated upwards by the field between the positive and negative charges of the cloud, and when it passes above the upper positive charge it enters a reversed field which would retard its speed and reduce its energy. At the instant of the lightning flash, however, the electric moment of the cloud is destroyed and all the electrons which are traveling through the cloud are freed from the action of the reverse field above the cloud, and so escape with their full energy.

TABLE I. *High energy electrons.*

	STORM CONDITIONS	CONTROL CONDITIONS
No. of photographs M	918	928
No. of high energy tracks N	430	395
Probability of capture P	0.468	0.425
$P_s - P_c$	0.043	
Std. dev. for $P_s - P_c$	0.030	
Confidence coefficient	0.8	

In his Franklin Society lecture[2] Wilson suggested that the electrons would then describe helical paths round the lines of force of the earth's magnetic field, subsequently returning to the earth at great distances from the cloud which had produced them. The work which has been carried out during recent years on the production of high energy secondaries by high energy primary radiation indicates that high energy electrons produced by stormclouds may be the parent particles for a number of generations of secondary particles, and that finally there may come to earth, not the original electrons, but the products of this process of secondary production.

This hypothesis has been the subject of three experimental investigations: by Schonland in 1930,[3] by Schonland and Viljoen in 1933,[4] and by Halliday in 1934.[5] This paper describes a fourth set of observations designed to test the hypothesis still further.

The method used was to expand a cloud chamber on a large number of occasions at the same instant as the occurrence of a lightning flash, and also to expand the chamber a further large number of times quite at random. The argument was as follows: if the destruction of the electric moment of the cloud by a lightning flash releases high energy electrons from the cloud, then, when the chamber is expanded at the instant of the flash, the chance that one of these electrons will pass through the chamber and produce an electron track is higher than it would be if the chamber were to be expanded at any other time. Thus, in the expansions made at the instant of a lightning flash, we would expect the number of electron tracks seen in every 100 expansions to be greater than in the case of the expansions made quite at random. If the storm has no action in producing high speed electrons these figures for the two sets of experiments should be the same.

APPARATUS

A simplified type of cloud chamber was constructed, similar to that described by C. T. R. Wilson.[6] The pressure in the chamber was raised to a fixed value above atmospheric pressure, and, when a large valve was opened by means of an electromagnetic trigger, the pressure fell very rapidly to atmospheric. The chamber was connected to a mercury manometer which had movable electric contacts in the open limb connected to a relay. The relay controlled the air pump for the chamber and so the expansion ratio could be set and maintained, by setting the contacts.

In order to check the satisfactory operation of the chamber it was customary, at regular intervals, to make an expansion with a small gamma-ray source near the chamber and see that satisfactory photographs of tracks were obtained.

For synchronizing the expansion of the chamber with the lightning flashes, a three-valve amplifier was connected to a small aerial and tuned to a frequency of 30 kilocycles per sec., as Schonland has shown that this is the frequency emitted by the stepped leader which initiates a "ground-flash." The output of the amplifier operated a

[3] B. F. J. Schonland, Proc. Roy. Soc. **A130**, 37 (1930).
[4] B. F. J. Schonland and J. P. T. Viljoen, Proc Roy. Soc. **A140**, 314 (1933).
[5] E. C. Halliday, Proc. Camb. Phil. Soc. **30**, 206 (1934).
[6] C. T. R. Wilson, Proc. Roy. Soc. **A142**, 88 (1933).

gas-filled relay and caused the expansion of the cloud chamber. During the first set of observations this amplifier was part of a radio direction finder so that it was possible to record the compass bearing of almost every flash which caused the chamber to expand. During the second set of observations the direction finder was dispensed with, and the cloud chamber was placed between the poles of an electromagnet capable of producing a horizontal field of 1000 gauss fairly uniformly over the whole volume of the chamber. This meant that the stereoscopic camera which was used during the first set of observations had to be discarded, and photographs were taken with a single camera by means of an inclined mirror between the pole face of the magnet and the front of the chamber. The information obtained with the direction finder and with the stereoscopic camera was used for two secondary lines of investigation which are discussed later in the paper.

The Relative Number of Tracks Seen Under Two Conditions of Chamber Operation

During the first set of observations (made during the summer of 1936–7) 24 thunderstorms were studied and 918 photographs of electron tracks were taken. The control observations consisted of 928 expansions made in small groups of 30 to 40 on various occasions between the days on which the storms occurred.

It was not possible to eliminate radioactive contamination from the room in which the cloud chamber was operated, and as a result each photograph taken during an expansion was liable to show electron tracks of relatively low energy, as well as the tracks of penetrating electrons. An energy measurement by means of magnetic bending would have separated the electron tracks of radioactive origin from those of the higher energy penetrating electrons; but no magnetic field was then available, so the tracks were divided into two categories by inspection. Any track which showed any sign of bending was placed in the class of "low energy" and all others were taken to be of "high energy."

The observations are summarized in the case of "high energy" electrons in Table I. Here the first line shows the number of photographs taken under "storm" conditions and under "control" conditions. The second line shows how many "high energy" tracks appeared in these photographs. In the third line, the probability of capture (P) means the average number of tracks seen per photograph, and is therefore the quotient of the first two lines. It will be seen that the probability of capture during storms (P_s) is greater than the probability of capture under control conditions (P_c). The difference between the probabilities is 0.043, and it is necessary to decide whether this difference is significant or merely due to chance.

In an experiment in which M_s photographs are taken under storm conditions, let the number of tracks obtained be N_s. If the experiment were repeated again and again, the same number of photographs M_s being taken every time, the value of N_s would vary about its ultimate mean value $\bar{N}_s$ with a distribution that is almost "normal" and with an ultimate standard deviation $\sqrt{\bar{N}_s}$.

Similarly, if a control experiment with M_c photographs were repeated a large number of times, the value of the number of tracks obtained (N_c) would be distributed almost "normally" about its ultimate mean value $\bar{N}_c$ with an ultimate standard deviation $\sqrt{\bar{N}_c}$.

From this it may be shown that the value of

Table II. *Low energy electrons.*

	Storm Conditions	Control Conditions
No. of photographs M	918	928
No. of low energy tracks N	508	527
Probability of capture P	0.554	0.567
P_s-P_c	−0.013	
Std. dev. for P_s-P_c	0.035	
Confidence coefficient	0.3	

P_s-P_c for successive pairs of experiments will be distributed normally about its ultimate mean value, with an ultimate standard deviation given by

$$\left(\frac{\bar{N}_s}{M_s^2}+\frac{\bar{N}_c}{M_c^2}\right)^{\frac{1}{2}}.$$

This expression, with N_s and N_c used as estimates of $\bar{N}_s$ and $\bar{N}_c$ gives the standard deviation in the fifth line of Table I.

TABLE III. *High energy electrons.*

	STORM CONDITIONS	CONTROL CONDITIONS
No. of photographs M	4053	3611
No. of high energy tracks N	722	499
Probability of capture P	0.178	0.138
P_s-P_c	0.040	
Std. dev. for P_s-P_c	0.009	
Confidence coefficient	0.99	

Considering the hypothesis that the process of synchronizing the expansion of the cloud chamber with a lightning flash does *not* affect the number of tracks observed, we then have a quantity P_s-P_c with an ultimate mean value of zero, observed to be as large as 0.043, when its standard deviation is only 0.030. Tables[7] show that in repeated experiments such a large deviation from zero would occur in only 16 percent of the experiments performed. We can therefore state with a confidence coefficient of 0.84 that the differences between the storm count and the control count *is significant.*

It is of considerable interest to apply the above reasoning to the "low energy" class of electrons which are presumably of local origin so that their frequency of appearance should be the same, no matter at what moment the cloud chamber is operated. The observations are summarized in Table II, where the successive lines have the same meaning as in Table I.

In this case the statistical tables show that with a standard deviation of 0.035, a deviation from zero of 0.013 would occur in 70 percent of a series of such experiments. It is therefore clear that the deviation which was observed is of *no significance*, a result which we expected to find on our hypothesis that the low energy electrons were of local origin. This in itself helps to make the results for the "high energy" electrons more significant than they would perhaps have appeared by themselves.

During the 1938–9 storm season, 41 thunderstorms were observed. At this time the electromagnet was in use so that it was possible to divide the tracks more precisely into two classes (high and low energy). The value 10^6 ev as a dividing line between the two categories was chosen arbitrarily, because it was the highest energy which could be measured with the magnetic field, and because it is just possible to consider 10^6 ev as the lower limit of the penetrating ray spectrum. The results for the "high energy" and the "low energy" electron tracks appear in Tables III and IV, where the significance of the various lines in the tables is as before.

It will be seen that though four times as many photographs were taken as in the 1936–7 storm season, the yield of high energy tracks was only 1.5 times as great. This is probably due to two causes. First, the pole pieces of the electromagnet constituted a fairly thick screen for any particles which entered the chamber either through the front or the back. Thus many particles at the low energy end of the spectrum must have had their energy so reduced that they appeared in the "low energy" class. Second, the chamber in its new set-up between the poles of the magnet, had a slightly smaller effective volume than in the earlier set of observations.

In Table III, it will be seen that the difference (P_s-P_c) is 0.040, a value nearly the same as that obtained in Table I. The standard deviation, however, is much lower, on account of the larger number of photographs taken, and so the reliability of the result is greater. Once again, starting with the hypothesis that the synchronizing of the expansions with lightning flashes does *not* affect the number of tracks observed, we see from statistical tables that a deviation of 0.040 from the expected value zero for the quantity (P_s-P_c) would be observed in only 1 percent of a series of observations. Thus it can be said with a confidence coefficient of 0.99 that the observed deviation *is significant.*

TABLE IV. *Low energy electrons.*

	STORM CONDITIONS	CONTROL CONDITIONS
No. of photographs M	4053	3611
No. of low energy tracks N	2148	1992
Probability of capture P	0.531	0.552
P_s-P_c	−0.021	
Std. dev. for P_s-P_c	0.017	
Confidence coefficient	0.77	

The values for the "low energy" tracks in Table IV show, as in Table II, a negative value

[7] R. A. Fisher, *Statistical Methods for Research Workers* (Oliver and Boyd, Edinburgh, 1938), seventh edition.

for $P_s - P_c$. According to statistical theory this value (-0.021), would be obtained in about 23 percent of a series of observations.

Here again it is important to notice the tremendous difference between the "high energy" and the "low energy" tracks. The first are very much affected by the process of synchronizing the cloud-chamber expansion with a lightning flash, while the second are only slightly affected by the process, and in the reverse manner.

It will almost certainly be asked, "Was it not possible that the observer, when scrutinizing the photographs and counting the tracks seen, was influenced by a knowledge of what should happen, and when he examined 'storm' photographs counted too many 'high energy' tracks and too few 'low energy' tracks? This would account for the value ($P_s - P_c$) being positive for the 'high energy' tracks and negative for the 'low energy' tracks." The answer to that is that all the photographs were numbered in code before they were examined at the end of the season, so that the scrutineer did not know the category into which any photograph fell, and thus an unbiased count was obtained.

It is therefore claimed that reliable evidence has been obtained that thunderclouds are instrumental in producing penetrating particles at the surface of the earth, at a considerable distance from the scene of the storm activity.

Two Tests of the Magnetic Bending Hypothesis

1. Analysis of the compass bearings of lightning flashes which produced penetrating electrons

The work described was designed to test the simple hypothesis of Wilson that the electrons, after leaving the cloud, traveled in helical paths about the direction of the earth's magnetic field. The later discoveries of the production of secondary and tertiary, etc., particles necessitates a more complex hypothesis and it will be seen that the evidence offered here *does* indicate that the helical path is too simple a picture of the manner in which the penetrating particles travel from the cloud to the ground.

If particles are ejected from the cloud, they will be traveling in a general upward, though not necessarily vertical, direction. One certain statement can be made, however. If the particles are negative electrons they must return to the earth at some point to the *east* of the cloud. Thus a test of the hypothesis is to compare the number of tracks observed in photographs taken when the flashes were to the *west* of the cloud chamber with the number observed when the flashes were to the *east* of the cloud chamber.

Table V. *Directional effects for high energy electrons.*

Bearing of Flashes	Number of Photographs Taken	Number of Tracks Observed
NW to SW	273	74
NE to SE	272	72

Table VI. *Angle of arrival of high energy electrons.*

Angular Interval	Control Observations: No. of Tracks	Control Observations: Mean Angle × No. of Tracks	Storm Observations: No. of Tracks	Storm Observations: Mean Angle × No. of Tracks
90– 80	4	340	3	255
80– 70	13	975	18	1350
70– 60	17	1105	21	1365
60– 50	17	935	13	715
50– 40	16	720	30	1350
40– 30	8	280	21	735
30– 20	10	250	16	400
20– 10	11	165	8	120
10– 0	4	20	11	55
0–(−10)	6	− 30	14	− 70
−10–(−20)	7	−105	8	−120
−20–(−30)	2	− 50	3	− 75
Totals	*115*	*4605*	*166*	*6080*
Average angle		= 40°		36.6°

Here only "high energy" tracks are shown.

The meteorological conditions made it difficult to obtain a great many storms to east and west of the laboratory, for most of the storms started many miles to the south of the city and traveled rapidly to the north, so that they were to east and west for only a short part of their existence.

During 1936–7 a radio direction finder was used to note compass bearings of flashes which produced an expansion of the cloud chamber and the information obtained is shown in Table V.

Here, as in the work done at Cambridge, the total number of tracks is rather too small to warrant the application of statistical theory for

the calculation of standard deviations. Thus the result is not conclusive, but the magnetic bending hypothesis is not supported.

2. Study of the directions of arrival of penetrating electrons

A further consideration of the paths of electrons ejected from thunderclouds and spiralling about the direction of the earth's magnetic field shows that the only particles which could reach the ground at a point approximately to the east of the cloud would be those electrons which started their journey in a plane at right angles to the magnetic field, or very nearly in that plane. These particles, when they arrived at the cloud chamber, would still be in that plane, or nearly in it.

Accordingly, during 1936–7, stereoscopic photographs were taken of the electron tracks, and all those "high energy" tracks which could be seen in both photographs were plotted in space. The angle which the track made with the plane at right angles to the earth's magnetic field was measured. When the track showed that the particle had approached the chamber on the *north* side of the plane, the angle was called positive, while a negative sign was given to the angle when the particle had approached from the *south* side of the plane. The tracks were classified in groups, all those which had angles to the plane between ten-degree limits being gathered together, and the results of this process are shown in Table VI.

In the table the observations have been treated as follows: The first column gives the angular intervals into which the tracks were classified. The second column shows the number of tracks which fell in that interval in the case of the control observations, while the third column gives the result of multiplying the number of tracks by the mean angle of the interval. The fourth and fifth columns repeat columns 2 and 3 for the case of the storm observations. At the bottom of each column appears the sum of the figures, and from these is obtained what has been called an average angle, the result of dividing the column 3 sum by the column 2 sum.

It will be seen that the average angle for the storm observations is less than that for the control observations, leading to the suggestion that more of the tracks were close to the plane at right angles to the earth's magnetic field than in the case of the control observations.

It remains to test if this reduction of angle is real and ascribable to any cause other than the variation of two samples from the same population of electron tracks. Standard statistical methods, based on the student distribution were used to evaluate the confidence interval to be associated with the quantity $(\bar{\theta}_s - \bar{\theta}_c)$. For the control sample $\delta = 29°$ and $n = 115$ while, for the storm sample, $\delta = 28°$ and $n = 166$. Using these figures, we have $(\bar{\theta}_s - \bar{\theta}_c) = 3.4° \pm 6.8°$ with a confidence coefficient of 0.95. It will be seen at once that there is no reason to suppose that the two samples labeled "storm" and "control" were from two different populations of electron tracks, as far as direction of arrival is concerned, so that there is no evidence for the simple theory of magnetic deviation of the electrons ejected from storm clouds.

Grateful thanks are due to Professor H. H. Paine, who gave laboratory facilities at the University of the Witwatersrand, to Professor B. J. Schonland and Dr. G. G. Wiles, who supplied most helpful and constructive criticism as the work proceeded, and to Mr. P. C. Roberts who made the cloud chamber and other auxiliary apparatus. The expenses of the work were met by a grant from the Research Grant Board of the Union of South Africa, and from the Joule Fund of the Royal Society, through Professor Schonland.

Quenching and Depolarization of Resonance Radiation by Collisions with Molecules of a Foreign Gas

A. ELLETT, *State University of Iowa, Iowa City, Iowa*
LEONARD O. OLSEN, *Case School of Applied Science, Cleveland, Ohio*
RAYMOND PETERSEN,* *State University of Iowa, Iowa City, Iowa*

(Received May 28, 1941)

A semi-classical theory describing the quenching and depolarization of resonance radiation by collisions with foreign gas molecules is presented. The total depolarizing probability is divided into two parts to allow for adiabatic and nonadiabatic depolarization. The equations for polarization are generalized in order to apply to the case in which the observed polarization results from several lines belonging to a hyperfine group. The effect of a magnetic field applied along the direction of observation is also included in the treatment. Experimental results on the polarization of the λ2537A mercury line as a function of gas pressure and as a function of magnetic field at various fixed gas pressures show good agreement with the theory. Cross sections for quenching and depolarization have been calculated for the gases investigated and are presented in Table VI.

THEORY

WHEN resonance radiation is excited in a gas at pressures such that the probability of collision is of the same order of magnitude as that for the emission of radiation, the polarization and intensity of the emitted radiation are affected.[1,2] Collisions with atoms of a foreign gas may result in either depolarization or quenching. In collisions of atoms of the resonating gas, the passing on of excitation and all the phenomena connected with the possibility of coherent excitation of neighboring atoms complicate the situation. The present paper deals with the effect of foreign gases only. Clearly, in this case, it makes sense to speak of quenching collisions and a cross section for quenching. We shall assume that the mechanism of depolarization is such that after a depolarizing collision the excited atom, on the average, emits isotropic and unpolarized radiation. Quenching collisions obviously shorten the mean life of the excited state. With depolarizing collisions this is not necessarily true, as the depolarization may be the result of an adiabatic process.

If, however, depolarization is the result of a nonadiabatic process, the excited atom, while still excited after the collision, is in a new excited state having no coherence with the state which existed before the collision. Collisions giving rise to such noncoherent excited states must be counted as transitions from the original excited state and so lead to a shortening of the mean life of the excited atom. To sum up, an atom in an excited state may emit radiation with probability $1/\tau_0$, or it may suffer a collision of any of three types: (1) Quenching, probability αp proportional to the pressure of foreign gas; (2) Adiabatic depolarizing leading to no loss of coherence, probability $\alpha'' p$; (3) Nonadiabatic depolarizing, leading to a noncoherent excited state, probability $\alpha' p$. The total transition probability from the original excited state is then

$$1/\tau = 1/\tau_0 + \alpha p + \alpha' p. \qquad (1)$$

By exciting resonance radiation with plane polarized light in a weak magnetic field parallel to the magnetic vector of the exciting light and observing either the polarization or rotation of the plane of maximum polarization of the radiation emitted along the applied magnetic field we may measure τ. For we have

$$P = P_{0,p}/[1+(eHg\tau/mc)^2],$$

TABLE I.

ATOM TYPE	N_τ	A_τ	B_τ
Nonspin	0.613	1	0
199 $f=\frac{1}{2}$	0.211	0.111	0.111
199 $f=\frac{3}{2}$	0.211	0.444	0.111
201 $f=\frac{1}{2}$	0.176	0.050	0.050
201 $f=\frac{3}{2}$	0.176	0.182	0.075
201 $f=5/2$	0.176	0.260	0.120

* Deceased. Data for hydrogen and oxygen were obtained by Mr. Petersen.

[1] R. W. Wood, Phil. Mag. **44**, 1109 (1922).

[2] V. Von Keussler, Ann. d. Physik **87**, 793 (1927).

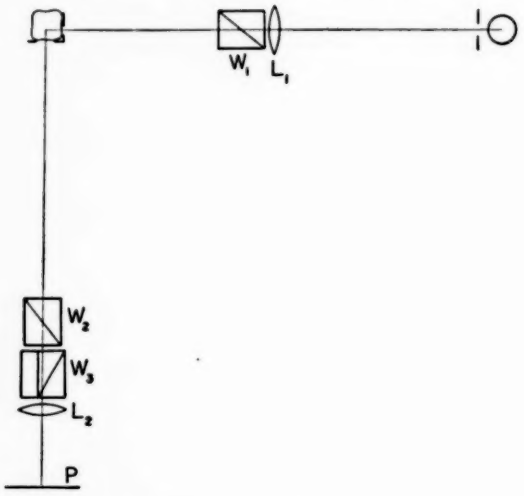

FIG. 1. Diagrammatic sketch of apparatus.

where $P_{0,p}$ is the polarization of the radiation in zero magnetic field at a pressure p of the foreign gas, and H is the magnetic field strength. For the angle of rotation of the polarization maximum ϕ

$$\tan 2\phi = eHg\tau/mc. \tag{3}$$

In order to obtain the dependence of P upon p we must estimate the relative amounts of radiation coming from atoms in the original excited state, before suffering collision of *any* type, and from atoms which have suffered either type of depolarizing collision. The competing processes have probabilities $1/\tau_0$ and $(\alpha+\alpha'+\alpha'')P$, so that a fraction $(1/\tau_0)/[1/\tau_0+(\alpha+\alpha'+\alpha'')p]$ emits before collision. A fraction

$$\frac{(\alpha'+\alpha'')p}{1/\tau_0+(\alpha+\alpha'+\alpha'')p}$$

is left in a condition such that the atoms either emit unpolarized light or are quenched. The fraction emitting is $(1/\tau_0)/(1/\tau_0+\alpha p)$ so that the ratio of the numbers of emissions giving rise to polarized and nonpolarized radiation is

$$\beta=\frac{1/\tau_0+\alpha p}{(\alpha'+\alpha'')p}. \tag{4}$$

Excited atoms emitting before collision give rise to intensities A, polarized parallel to the electric vector of the exciting light, and B, perpendicular thereto. If they emit after a depolarizing collision the intensity plane polarized in any azimuth is $\frac{1}{3}(A+2B)$. The relative intensities of radiation polarized parallel and perpendicular to the electric vector of plane polarized exciting light are then:

$$\frac{I_{\parallel}}{I_{\perp}}=\frac{A\beta+\frac{1}{3}(A+2B)}{B\beta+\frac{1}{3}(A+2B)}, \tag{5}$$

so that

$$P_{0,p}=P_{0,0}\Big/\left[1+(1-\tfrac{1}{3}P_{0,0})\frac{(\alpha'+\alpha'')p}{1/P_0+\alpha p}\right]. \tag{6}$$

For sufficiently small gas pressures, $\alpha p \ll 1/\tau_0$

$$P_{0,p}=\frac{P_{0,0}}{1+(1-\frac{1}{3}P_{0,0})(\alpha'+\alpha'')p\tau_0}. \tag{7}$$

Von Keussler[2] attempted to represent his data on polarization *vs.* gas pressure with an equation of this form. If it is fitted merely to the initial part of the curve, or if quenching is negligible, it will give good values for the total depolarizing efficiency. If quenching is not negligible, such a curve will not fit at higher pressures. As pressure increases, the polarization will not approach zero but will approach

$$P_{0,\infty}=\frac{P_{0,0}}{1+(1-\frac{1}{3}P_{0,0})(\alpha'+\alpha'')/\alpha}. \tag{8}$$

The equations above require modification if the observed polarization is due to several lines having different g values and different initial polarizations. Equation (5) will apply to any one line and the modification required is merely that the polarization is now

$$P=(\textstyle\sum I_{\parallel}-\sum I_{\perp})/(\sum I_{\parallel}+\sum I_{\perp}), \tag{9}$$

where $\sum I_{\parallel}$ and $\sum I_{\perp}$ signify the total radiation due to all lines polarized in the specified azimuth. If, in zero magnetic field at zero gas pressure, the normalized parallel and perpendicular intensities due to the sth line of the rth isotope are A_{rs} and B_{rs}, respectively, and N_r the relative number of atoms of this isotope present, then

for a broad line exciting source we have

$$P_0=\frac{\sum_r\sum_s N_r\left(\dfrac{A_{rs}-B_{rs}}{1+\left(\dfrac{e}{m}\dfrac{H}{c}\tau g_{rs}\right)^2}\right)}{\sum_r\sum_s N_r\left[A_{rs}+B_{rs}+\tfrac{2}{3}(A_{rs}+2B_{rs})\dfrac{(\alpha'+\alpha'')p}{1/\tau_0+\alpha p}\right]}. \tag{10}$$

The corresponding generalization of Eq. (3) may be written

$$\tan 2\phi=\frac{\sum_r N_r\sum_s \dfrac{(eHg_{rs}/mc)(A_{rs}-B_{rs})}{[(\alpha+\alpha')p+1/\tau_0]^2+(eHg_{rs}/mc)^2}}{\sum_r N_r\sum_s \dfrac{[(\alpha+\alpha')p+1/\tau_0](A_{rs}-B_{rs})}{[(\alpha+\alpha')p+1/\tau_0]^2+(eHg_{rs}/mc)^2}}. \tag{11}$$

In applying the above equation to the λ2537A mercury resonance line we have used values of N_r given in Table I. These are not in agreement with Aston's[3] isotope ratios—the relative number of atoms of nonspin isotopes has been arbitrarily reduced in order that $P_{0,0}$ may be brought into agreement with the observed value. It should be mentioned that the values of the quantities α are not very sensitive to change in the N_r. The use of the simple equations (2), (3) with $g=\frac{3}{2}$ and $P_{0,0}=0.80$ will give values of the α's differing from those obtained with Eqs. (10), (11) by ten percent, at most.

Experimental Procedure

A diagrammatic sketch of the apparatus is shown in Fig. 1. The earth's magnetic field was counteracted in the vicinity of the resonance bulb by means of a large Helmholtz coil, the axis of which was parallel to the direction of the earth's field. The necessary current to reduce the field to zero was determined by means of a flip coil operated in the position to be occupied by the resonance bulb.

The applied field was produced by a smaller Helmholtz coil which was accurately calibrated. The current in this coil was measured with a precision ammeter. The mercury vapor pressure was kept low by means of ice and salt mixtures surrounding the reservoirs. One reservoir containing a drop of mercury consisted of a U-tube bent in the pumping line. The second reservoir was a tube attached to the bottom of the resonance bulb. The resonance bulb was constructed

Table II. *Depolarization in hydrogen for various fields (H) and pressures (p).*

H	p=0.12	0.188		0.442		0.743		2.37	3.67	5.93
0	0.68	0.64		0.57		0.53		0.46	0.45	0.45
0.4		0.44	*0.63*	0.47	*0.44*	0.48	*0.33*			
0.8		0.25	*1.17*	0.33	*0.83*	0.37	*0.58*			
1.2			*1.73*		*1.22*		*0.93*			
1.6		0.10		0.17		0.23				

Table III. *Depolarization in deuterium for various fields (H) and pressures (p).*

H	p=0.19	0.52	0.84	0.86	2.40	3.50	4.54	5.63
0	0.71	0.59		0.55	0.46	0.44	0.40	0.39
0.406	0.33	0.40	*0.46*	0.44				
0.812	0.16	0.24	*0.91*	0.29				
1.218	0.11	0.16	*1.23*	0.20				
1.624	0.08	0.12	*1.44*	0.15				

[3] F. W. Aston, Proc. Roy. Soc. **126**, 523 (1930).

Table IV. *Depolarization in nitrogen for various fields (H) and pressures (p).*

H	p=0.096	p=0.3	0.47	p=0.58	0.76	2.05	3.16	4.7
0	0.71	0.53	0.47	0.41	0.38	0.23	0.18	0.11
0.203	0.57	0.49	0.44	0.38				
0.406	0.36 *0.96*	0.37 *0.66*	0.34 *0.58*	0.32 *0.54*	0.30			
0.812	0.16 *1.85*	0.21 *1.26*	0.21 *1.10*	0.20 *0.97*	0.21			
1.218	*2.48*	*1.62*	*1.62*	0.13 *1.46*				
1.624	0.07	0.09	0.09	0.10	0.11			

Table V. *Depolarization in oxygen for various fields (H) and pressures (p).*

H	p=0.41	0.99		1.86	3.49
0	0.68	0.61		0.57	0.53
0.4		0.52	*0.37*		
0.8		0.38	*0.82*		
1.2			*1.06*		
1.6		0.20			

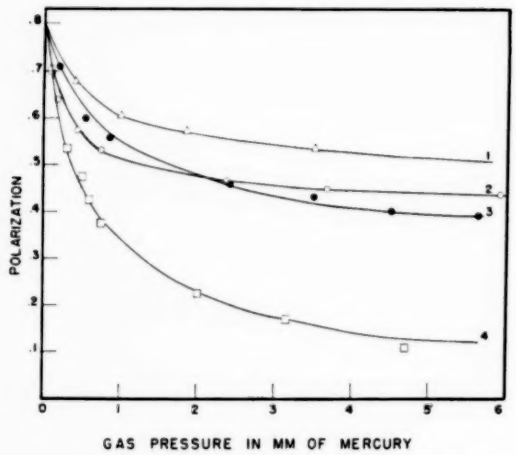

FIG. 2. Polarization of mercury resonance radiation as a function of gas pressure. The curves are drawn using the α's given in Table VI. Curve 1 (△) oxygen; 2 (○) hydrogen; 3(●) deuterium; 4 (□) nitrogen.

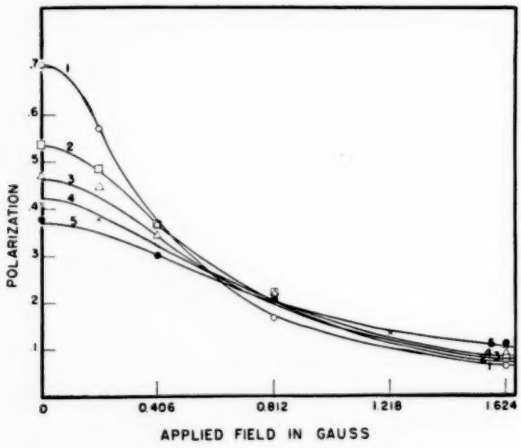

FIG. 3. Effect of magnetic fields on polarization of mercury resonance radiation at fixed nitrogen pressures. The curves are drawn using $\alpha=0.1\times10^7$, $\alpha'=1.55\times10^7$ and $\alpha''=0.55\times10^7$. Curve 1 (○) N_2 pressure=0.096 mm of Hg; curve 2 (□) $p=0.305$ mm of Hg; curve 3 (△) $p=0.47$ mm of Hg; curve 4 (+) $p=0.58$ mm of Hg; curve 5 (●) $p=0.76$ mm of Hg.

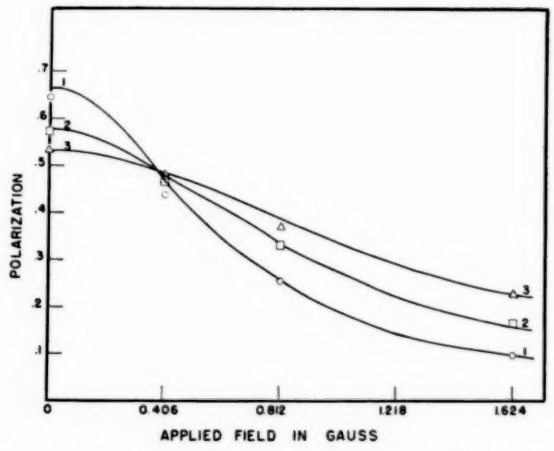

FIG. 4. Effect of magnetic fields on polarization of mercury resonance radiation at fixed hydrogen pressures. The curves are drawn using $\alpha=1.39\times10^7$, $\alpha'=1.81\times10^7$ and $\alpha''=0$. Curve 1 (○) H_2 pressure=0.188 mm of Hg; curve 2 (□) $p=0.443$ mm of Hg; curve 3 (△) $p=0.743$ mm of Hg.

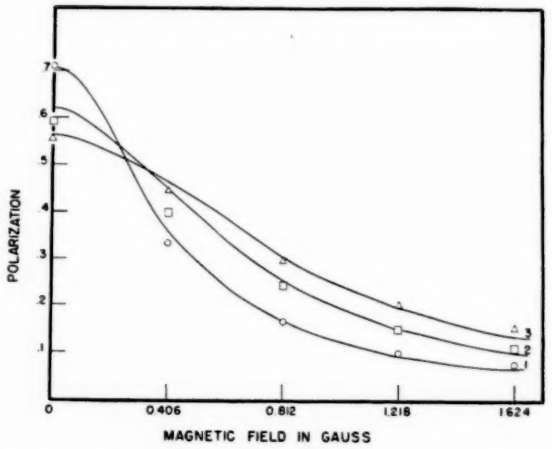

FIG. 5. Effect of magnetic fields on polarization of mercury resonance radiation at fixed deuterium pressures. The curves are drawn with $\alpha=0.45\times10^7$, $\alpha'=0.9\times10^7$ and $\alpha''=0$. Curve 1 (○) pressure=0.19 mm of Hg; curve 2 (□) $p=0.52$ mm of Hg; curve 3 (△) $p=0.864$ mm of Hg.

from a round quartz cell (about 70 cc capacity) by flattening four sides, giving it the approximate rectangular shape shown in the figure.

The polarization was determined by the Cornu method. Four images of a small area of the resonance bulb were produced by the Wollastons W_2, W_3 and the quartz lens L_2. W_3 was rotated about the direction of observation until two of the images on the photographic plate were equal in intensity. Experimentally, five photographs were taken near the probable match position. The difference in intensity was plotted against the angle and a straight line drawn through the points. The intersection of this line and the zero intensity line determined the match point.

In order to measure the intensity of the images, which were approximately one-eighth inch square, the images were placed over a square slit of approximately the same size and illuminated from beneath. The transmitted light fell on a photronic cell connected to a galvanometer. The difference in galvanometer readings for the

two images was assumed proportional to the intensity difference when working near the match point.

The experimental method was checked by determining the polarization as a function of applied field with no foreign gas present. Good agreement with H. F. Olson's[4] data was obtained.

The nitrogen used was secured by decomposing sodium azide in a vacuum. Deuterium was prepared electrolytically from 99.5 percent pure heavy water.

Results

The observed polarization of the λ2537A mercury line for various pressures of H_2, D_2, N_2, O_2, and in various applied magnetic fields is given in Tables II to V. In these double-entry tables values of the polarization are printed in roman type and tangents of twice the angle of maximum polarization in italics. The same data are presented graphically in Figs. 2 to 7 together with curves computed from Eqs. (10), (11), with values of the α's which appear to give the best fit. These values are presented in Table VI together with cross sections computed in the usual way by means of the relation:[5]

$$\sigma_\alpha^2 = \frac{\alpha}{2.608}\left(\frac{M_1 M_2}{M_1+M_2}\right)^{\frac{1}{2}} \cdot 10^{-22}.$$

It will be noticed that the quenching cross sections given here differ considerably from those obtained by less direct methods. Where depolarizing cross sections differ significantly from those of von Keussler, the difference is due to the fact that the condition $\alpha p \ll 1/\tau_0$ was not always satisfied in his experiments, and to the high mercury pressure in his resonance lamp.

Table VI. *Collision probabilities* ($\times 10^{-7}$ *sec.*$^{-1}$) *and cross sections* ($\times 10^{16}$ *cm*^{2}).

Gas	Quenching α	Quenching σ_α^2	Nonadiabatic Depolarizing α'	Nonadiabatic Depolarizing $\sigma_{\alpha'}^2$	Adiabatic Depolarizing α''	Adiabatic Depolarizing $\sigma_{\alpha''}^2$	Total Depolarizing $\sigma_{\alpha'}^2+\sigma_{\alpha''}^2$
Hydrogen	1.39	7.5	1.81	9.80	0.00	0.00	9.80
Deuterium	0.45	3.4	0.90	6.82	0.00	0.00	6.82
Nitrogen	0.10	1.92	1.55	29.60	0.55	10.50	40.1
Oxygen	0.85	17.2	0.78	15.70	0.00	0.00	15.70

[4] H. F. Olson, Phys. Rev. **32**, 443 (1928).
[5] Sir James Jeans, *Introduction to Kinetic Theory of Gases* (Macmillan Company, New York, 1940), p. 137.

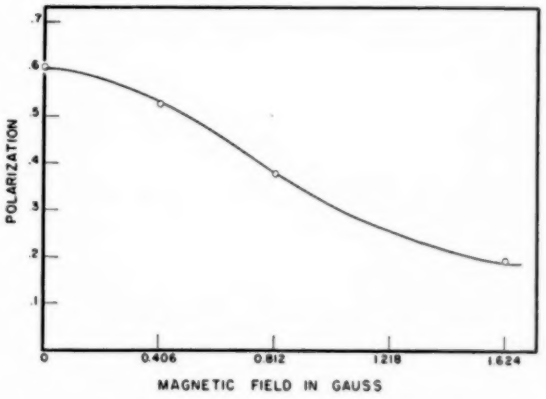

Fig. 6. Effect of magnetic fields on polarization of mercury resonance radiation at an oxygen pressure of 0.994 mm of Hg. The curve is drawn with $\alpha=0.85\times10^7$, $\alpha'=0.78\times10^7$ and $\alpha''=0$.

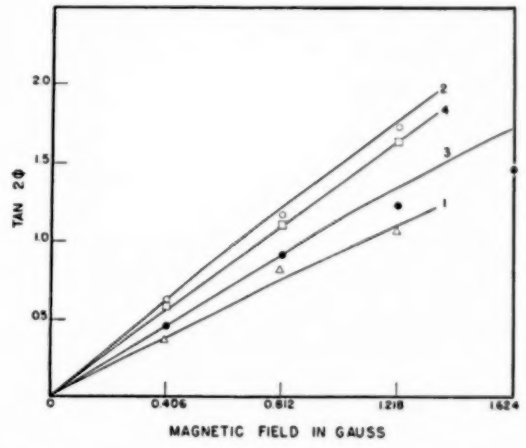

Fig. 7. Rotation of the plane of maximum polarization as a function of magnetic fields for various gases. The curves are drawn with the α's given in Table VI. Curve 1 (△) oxygen at $p=0.994$ mm of Hg; 2 (○) hydrogen at $p=0.188$ mm of Hg; 3 (●) deuterium at $p=0.84$ mm of Hg; 4 (□) nitrogen at $p=0.47$ mm of Hg.

One of the authors (L. O. O.) wishes to express his sincere appreciation to the Department of Physics of the State University of Iowa and especially to Professor G. W. Stewart, head of the department, for a summer lecturing and research appointment at which time some of the experimental results were obtained. He is also very grateful for a loan of the necessary optical equipment which has enabled him to continue the investigation.

The Isotopic Constitution of Lead and the Measurement of Geological Time. III

ALFRED O. NIER, ROBERT W. THOMPSON AND BYRON F. MURPHEY
Department of Physics, University of Minnesota, Minneapolis, Minnesota

(Received June 5, 1941)

A mass spectrographic measurement of the relative abundances of the isotopes in eight samples of radiogenic lead and thirteen samples of common lead has been made. As five of the radiogenic lead samples originated from minerals containing both uranium and thorium, three independent determinations of the age could be made. One of the samples was the oldest so far studied and appears to have an age close to two billion years. The common lead samples were found to have large variations in the relative abundances of the same sort as were reported in a previous investigation of twelve other samples.

THE well-established fact that uranium and thorium disintegrate naturally to form, ultimately, isotopes of lead makes possible the measurement of the geological age of uranium and thorium minerals. As the decay constants of uranium and thorium are accurately known, a knowledge of amounts of lead, uranium, and thorium contained in a given mineral enables one to compute its age provided the atomic weight, or alternately, the isotopic constitution of the lead, is known. As common lead is often present as an impurity it is important to know its isotopic constitution also. In this paper will be discussed the results obtained from the isotopic analyses of a number of radiogenic and common lead samples.

Apparatus and Procedure

The mass spectrometer used in this work was essentially identical with one described earlier.[1] As a source of lead ions, lead iodide vapor is bombarded with low energy electrons. The mass analyses of the ions is accomplished by a 180° magnetic analyzer. As the analyzed ion currents are measured with an electrometer tube amplifier, rapid and accurate measurements of the relative abundances are possible. The general procedure used in analyzing lead has already been described.[2,3]

[1] A. O. Nier, Phys. Rev. **52**, 933 (1937).
[2] A. O. Nier, J. Am. Chem. Soc. **60**, 1571 (1938).
[3] A. O. Nier, Phys. Rev. **55**, 153 (1939). Several errors have been found in this paper. Equation (5) should have the coefficient 1/139 instead of 139. In Table I, for sample 9, column 3 should have 3.09 instead of 0.309; for sample 20, columns 17 and 18 should have 0.0106 and 235, respectively, instead of 0.016 and 355. In Table II the headings 206 and 208 should be interchanged. In footnotes 23 and 29 the initials should be A. D. rather than E. W. Bliss.

Analysis of Radiogenic Lead

Because the intermediate members of the radioactive families have short half-lives in comparison with the ages of the minerals with which we are concerned one can write the following equations relating the numbers of atoms of radiogenic lead, thorium and uranium isotopes:

$$N(\mathrm{Pb}^{206}) = N(\mathrm{RaG}) = N(\mathrm{U\ I})(\exp[\lambda(\mathrm{U\ I})t]-1), \quad (1)$$

$$N(\mathrm{Pb}^{207}) = N(\mathrm{AcD}) = N(\mathrm{AcU})(\exp[\lambda(\mathrm{AcU})t]-1), \quad (2)$$

$$N(\mathrm{Pb}^{208}) = N(\mathrm{ThD}) = N(\mathrm{Th})(\exp[\lambda(\mathrm{Th})t]-1). \quad (3)$$

A chemical analysis of the mineral gives the relative amounts of U, Th and Pb. An isotopic analysis of the lead, after being corrected for common lead contamination, yields the relative amounts of RaG, AcD and ThD. Thus, as the decay constants are known, three independent determinations of a mineral's age are possible provided it contains both uranium and thorium in sufficient amounts to permit an accurate chemical analysis.

It is customary to apply Eqs. (1) and (3) directly whereas (2) is applied indirectly by dividing (2) by (1) to give

$$\frac{\mathrm{AcD}}{\mathrm{RaG}} = \frac{N(\mathrm{AcU})}{N(\mathrm{U\ I})} \frac{\exp[\lambda(\mathrm{AcU})t]-1}{\exp[\lambda(\mathrm{U\ I})t]-1}. \quad (4)$$

As $\lambda(\mathrm{AcU})$ is not known directly it may be evaluated by means of the expression

$$R = \lambda(\mathrm{AcU})N(\mathrm{AcU})/\lambda(\mathrm{U\ I})N(\mathrm{U\ I}), \quad (5)$$

TABLE Ia. *Isotopic abundances in radiogenic lead.*

1 No.	2 MINERAL AND SOURCE*	3 ISOTOPIC ABUNDANCES 208	4 207	5 206	6 204	7 ThD RELATIVE TO TOTAL $Pb^{208}=100$†	8 AcD	9 RaG
8a.	Curite[1] Katanga, Africa	0.178 ±0.005	6.18	100	—			
22.	Uraninite[2] Parry Sound, Canada	1.52	7.40	100	0.0062 ±0.0008	1.28	7.30	99.9
23.	Samarskite[3] Glastonbury, Conn.	21.3	7.60	100	0.167 ±0.01	14.9	5.03	96.9
24.	Pitchblende[4] Woods Mine, Colo.	38.0	19.4	100	1.01 ±0.05	−0.6	3.8	81.3
25.	Pitchblende[4] Gilpin County, Colo.	44.5	22.0	100	1.17 ±0.03	−0.2	4.0	78.4
26.	Thucholite[5] Parry Sound, Canada	6.90	5.88	100	0.024 ±0.005	5.98	5.51	99.5
27.	Monazite[6] Mt. Isa Mine, Australia	100	1.03 ±0.05	5.82	0.041 ±0.003	98.4	0.40	5.05
28.	Monazite[4] Huron Claim, Manitoba, Canada	100	2.11 ±0.05	11.6	0.011 ±0.002	99.6	1.94	11.4
29.	Monazite[4] Las Vegas, New Mexico	100	1.25 ±0.05	10.1	0.028 ±0.002	98.9	0.82	9.6

TABLE Ib. *Analysis and ages of minerals.*

No.	MINERAL AND SOURCE	10 MINERAL ANALYSIS % U	11 % Th	12 % Pb	13 RATIO OF NOS. OF ATOMS RaG/U I	14 ThD/Th	15 AcD/RaG	16 AGES IN 10^6 YR. FROM RaG/U I	17 ThD/Th	18 AcD/RaG[7]
22.	Parry Sound Uraninite	69.0	2.95	10.8	0.166	0.0483	0.0731 ±1%	1003	945	1030 ±15
23.	Conn. Samarskite	6.91	3.05	0.314	0.0396	0.0134	0.0518 ±3%	253	266	280 ±60
24.	Woods Mine Pitchblende	72.3	0.11	1.063	0.0088	—	0.0467 ±25%	57	—	—
25.	Gilpin Co. Pitchblende	38.28	0.053	0.643	0.0091	—	0.051 ±25%	59	—	—
26.	Parry Sound Thucholite	4.63	0.903	0.187	0.0414	0.0123	0.0553 ±2%	265	245	430 ±40
27.	Mt. Isa Monazite	0.0	5.73	0.285	—	0.051	0.0792 ±25%	—	1000	1190 ±400
28.	Huron Claim Monazite	0.281	15.63	1.524	0.628	0.0955	0.170 ±4%	3180	1830	2570 ±70
29.	Las Vegas Monazite	0.122	9.39	0.372	0.303	0.0392	0.0855 ±10%	1730	770	1340 ±200

* References for this column refer to analysis of minerals appearing in columns 10, 11, and 12.
† Except for samples 27, 28 and 29 in which the amounts are relative to total $Pb^{208}=100$.
[1] This sample was one referred to in reference 3 of text and was analyzed here only as a check on the present apparatus.
[2] H. V. Ellsworth, *Canadian Geologic Survey*, Economic Geology Bull. 11, 268 and 174 (1932).
[3] R. C. Wells, *Report of the Committee on Determination of Geologic Time* (National Research Council, April, 1935, and September, 1936). The atomic weight of the lead from this sample was found by Baxter, Faull and Tuemmler, J. Am. Chem. Soc. **59**, 702 (1937) to be 206.34. The value computed from the isotopic abundances is 206.36 if the P. F. of lead is taken as +1.55, reference 2 of text.
[4] O. B. Muench, *Report of the Committee on the Measurement of Geologic Time*, 1939–1940, p. 88.
[5] O. B. Muench, J. Am. Chem. Soc. **59**, 2269 (1937).
[6] Private Communication to Professor A. C. Lane, from R. Blanchard and F. E. Connah.
[7] The estimates of error are based upon error in AcD/RaG ratio which in turn depends upon the errors given in columns 4 and 6.

where R is the present day ratio of the activities of the actinium and uranium series. Since $N(\text{U I})/N(\text{AcU})$ has been shown to be 139.0[4] Eq. (4) may be written as

$$\frac{\text{AcD}}{\text{RaG}}=\frac{1}{139}\,\frac{\exp[139R\lambda(\text{U I})t]-1}{\exp[\lambda(\text{U I})t]-1}. \qquad (6)$$

[4] A. O. Nier, Phys. Rev. **55**, 150 (1939).

In Tables Ia and Ib are listed the minerals investigated together with isotope analyses and other pertinent data needed for age computations. Unless otherwise designated the numbers in columns 3, 4, 5, and 6 are believed to be correct within one percent.

Since Pb^{204} may, as far as is known, be attributed entirely to common lead, it is used as

an index of the common lead impurity in the samples. Accordingly the data in columns 7, 8, and 9 are found by correcting the measured abundances for common lead. In each case common lead was assumed to have a constitution of 204 : 206 : 207 : 208 :: 1 : 18.5 : 15.4 : 38.2. This set of values corresponds to a type of common lead which would be an average between samples 13 and 14 of Table II, the two samples exhibiting the widest differences in isotopic abundances. Actually, except for samples 24 and 25 so little common lead is present that it makes little difference which type is assumed in making the corrections. In samples 24 and 25 so much common lead is present that the AcD/RaG ratio cannot be computed with sufficient accuracy to have significance even if a better assumption could be made as to the type of common lead present.

In making the age computations the decay constants of Th and U I were chosen as 4.99×10^{-11} yr.$^{-1}$,[5] and 1.535×10^{-10} yr.$^{-1}$,[6] respectively.

In employing Eq. (6) for computing the ages from the AcD/RaG ratio R was assumed to be 0.046 as in the earlier work.[3] It is interesting to compare the ages as computed by the three different methods. It is to be recalled that a close agreement between the three methods may be considered as a good indication that the mineral has not suffered alterations. Conversely, discrepancies in the numbers in columns 16, 17, and 18 are indicative of some alteration, unless the quantities in columns 10 or 11 are so small that the limit of chemical accuracy becomes important, as for the uranium in a monazite and thorium in some uraninites and pitchblendes.

The close agreements in samples 22 and 23 indicate no serious alterations have taken place. Unfortunately, samples 24 and 25 contain so little thorium and so much common lead that age computations are possible only from the RaG/U I ratio. The presence of the large amounts of common lead in these is especially unfortunate as an accurate computation of AcD/RaG cannot be made. It had been hoped that as AcD/RaG is not critically dependent upon t for low ages in Eq. (6), it would have been possible to use Eq. (6) in reverse manner to obtain an accurate check upon the assumed value of R.

It is not surprising that the AcD/RaG age for sample 26 does not agree with the other two ages. An earlier investigation (reference 5, Table I) of the material indicated that alterations probably had taken place.

As sample 27 contained very little uranium a determination of the amount had not been made. Thus the age from RaG/U I could not be computed. Unfortunately the mass spectrometer does not have sufficient resolution to permit a more accurate measurement of Pb^{207} in the presence of so large a Pb^{208} ion current. Thus the AcD/RaG ratio cannot be measured with the accuracy that might be desired. This same difficulty was encountered in sample 29.

Sample 28 is especially interesting as it comes from a region known to be very old geologically. The analysis of a sample of uraninite from the same locality gave[3] for the age in millions of years as computed from RaG/U I, ThD/Th and AcD/RaG the values 1570, 1252 and 2200, respectively. It is to be recalled that it has been suggested[3] that in the case of the alteration of a mineral AcD/RaG is least affected and hence should serve as the most reliable index of the age. From the present results it appears that the high RaG/U I age may be accounted for by a leaching of uranium. It must be mentioned that such an alteration would give an AcD/RaG age which was also somewhat high. Thus one has some justification in assuming the mineral to be close to two billion years old. A comparison of the three age determinations for the two samples shows that only the AcD/RaG ages are in reasonable agreement.

Analysis of Common Lead

In Table II are shown the isotopic abundances obtained for a group of common lead samples having different geographical origins. The abundance of Pb^{204} has been arbitrarily chosen as a reference, as it is not produced, as far as is known, by natural radioactive decay. An examination of the table reveals that in spite of a

[5] A. F. Kovarik and N. I. Adams, Phys. Rev. **53**, 928 (1938).

[6] This value is based on the new determination of the rate of emission of alpha-particles from uranium given by Kovarik and Adams, J. App. Phys. **12**, 296 (1941). For method of calculation see reference 4.

TABLE II. *Isotopic abundances in common lead.*

No.	Source of Lead[1] Locality	Isotopic Abundances Referred to $Pb^{204}=1.000$ 206	207	208	Excess over Ivigtut Galena 206	207	208	Excess 207/206	208/206	Mean[2] Mass Number
13.	Galena[3] Ivigtut, Greenland	14.54 14.75	14.60 14.70	34.45 34.5						207.261
14.	Galena III[4] Joplin, Missouri	22.37 22.28	16.10 16.20	41.8 41.8	7.70	1.50	7.36	0.19	0.96	207.203
15.	Galena[5] Tetreault Mine, Canada	16.27	15.16	35.6	1.62	0.50	1.08	0.31	0.67	207.239
16.	Bournonite[6] Casapalca, Peru	18.65 18.69	15.49 15.40	38.15 38.15	4.02	0.80	3.68	0.20	0.91	207.225
17.	Galena Casapalca, Peru	18.86 18.83	15.71 15.61	38.75 38.5	4.20	1.01	4.16	0.24	0.99	207.226
18.	Galena[7] Clausthal, Harz Mts., Germany	18.46	15.66	38.6	3.81	1.01	4.13	0.27	1.08	207.233
19.	Galena[8] Przibram, Bohemia	17.95	15.57	37.9	3.31	0.92	3.43	0.28	1.04	207.235
20.	Galena[9] Franklin, New Jersey	17.15	15.45	36.53	2.50	0.80	2.06	0.32	0.82	207.233
21.	Galena[10] Mexico	18.71	15.70	38.5	4.06	1.05	4.08	0.26	1.00	207.227
22.	Native Lead[11] Langban, Sweden	15.83	15.45	35.6	1.18	0.80	1.16	0.68	0.99	207.249
23.	Galena[12] Arizona	19.22	16.17	39.15	4.57	1.53	4.68	0.33	1.03	207.226
24.	Galena[13] Freiberg, Saxony	18.07	15.40	38.0	3.42	0.75	3.48	0.22	1.02	207.234
25.	Galena[14] Alpine Trias, Austria	17.75	16.21	38.05	3.10	1.56	3.58	0.50	1.15	207.237
					Average			0.32	0.97	
8a.	Galena II	21.72	15.74	40.3						
8b.	Joplin, Missouri	21.62	15.74	40.4						
14a.	Galena III Joplin, Mo.	22.48	16.15	41.3						

[1] As the bulk of the samples listed below were obtained from the Harvard Mineralogical Museum through the courtesy of Dr. H. Berman, the number given in the footnotes describing the individual samples is the Harvard catalog number.
[2] The chemical atomic weight may be computed from the mean mass number by subtracting 0.025 (see reference 2 of text).
[3] 80014. Occurred in pegmatite, associated with cryolite and siderite; Lindgren's *Mineral Deposits*, p. 765.
[4] Galena, Charles Palache collector; 8a and 8b are from the father of G. P. Baxter.
[5] Galena, Tetreault Mine near Montaubon les Mines, Port Neuf Company, Quebec, from J. N. Herring, Superintendent (letter April 15, 1938). Recommended by J. A. Dresser as an old vein, not pre-Grenville.
[6] From Casapalca Mine, M vein, 600 foot level, Peru; Tertiary or later? From L. C. Graton.
[7] 88919 late Paleozoic, page 574 Lindgren, with siderite.
[8] 81731 Mesothermal deposits from Przibram, Bohemia.
[9] Galena. See Palache reports on Franklin Furnace.
[10] 91074 Galena and anglesite, Durango, Mexico. General type discussed by Lindgren, pages 598–599.
[11] Native lead with iron ores. Langban, Sweden; Precambrian (Wahl). See Palache and Flink, *American Mineralogist*, 1926, p. 195.
[12] 90486 Galena, Sonora Mine, Castle Dome, Arizona, with fluorite; H. H. Chen, collector.
[13] 81725 Mesothermal deposit, like 91074 probably of younger formation, Freiberg, Saxony; Lindgren, page 577.
[14] 84456, Galena in sedimentary rocks,—dolomites of the Austrian Triassic.

nearly constant atomic weight (see column marked "Mean Mass Number") the isotopic abundances vary between rather wide limits. That these variations are not the result of errors in analyses may be seen from the fact that in the five cases, samples 13, 14, 16, 17, and 8, where check runs were made at a later time, the results are almost identical with the original ones. In the repeat analyses the samples were given to the operator of the mass spectrometer as unknowns so there was no chance for prejudice. It may be seen that, in general, results are reproducible within one-half percent. As all samples are studied under conditions as nearly identical as possible, systematic discriminations in the mass spectrometer should not play a part in comparing samples. The absolute values of the abundances should be correct within two percent.

The analysis of Joplin galena III, sample 14,

was intended as an intercheck between the present and earlier results. However, it was not until the mass spectrometer tube had been dismantled and rebuilt that it was learned that Joplin III was not identical with either of the previous[2] Joplin galenas studied. Hence, the analysis of Joplin III, 14a, was repeated in the rebuilt tube. This was followed by a re-examination of Joplin II, (from earlier work[2]), 8a. No. 8b gives the analysis found previously for Joplin II. From the figures it may be inferred that there was no appreciable discrimination or systematic differences between the performances of the several mass spectrometer tubes used and that the new results may be compared directly with the older ones.

It is quite apparent that the present samples exhibit large variations similar to those found in the earlier work. Those samples containing relatively more Pb^{206} also contain relatively more Pb^{207} and Pb^{208}. As an explanation for this it was proposed[2] that one could consider any common lead sample as made up of "uncontaminated" or "primal" lead to which had been added a certain quantity of radiogenic lead composed of approximately equal amounts of uranium and thorium lead. The added radiogenic lead could not be due to U and Th impurities, as a simple calculation reveals that the samples did not contain enough to account for the results in any of the cases. As the Great Bear Lake galena[2] contained the least amounts of Pb^{206}, Pb^{207} and Pb^{208}, it was chosen, tentatively, as "uncontaminated." Its isotopic constitution is approximately the same as sample 22 of the present work. In the present investigation sample 13, the Ivigtut galena was found to contain even less Pb^{206}, Pb^{207} and Pb^{208} than the Great Bear Lake galena. Thus it has been chosen as "uncontaminated" for the new comparisons. The justification for the assumption that the "excess" is made up of equal quantities of ThD and RaG is seen in the close agreement of the numbers in the excess 208/206 column with unity. If one assumes that these excess isotopes were generated in the period one to two billion years ago then the average ratio 0.97 corresponds to a Th/U ratio in the source as would be measured today of 3.4. It is interesting to note that recent average values for the Th/U ratio for granitic and basaltic rocks range from 2.6 to 4.3.[7,8] The results of the isotopic study are thus not in disagreement with the theory that ore lead has its origin in the igneous rocks or magmas of these rocks.

The average excess Pb^{207}/Pb^{206} ratio of 0.32 is difficult to account for in view of the fact that the relative rates of production of Pb^{207} and Pb^{206} have varied only between 0.046 (at present) and 0.24[3] two billion years ago, the time usually taken as the earth's beginning. The fact that the Ivigtut galena has an isotopic constitution so far different from any other sample so far studied may mean that it is anomalous in some way. If the Great Bear Lake galena were used as "uncontaminated" as it was in the earlier work,[2] one would find very little difference in the excess Pb^{208}/Pb^{206} ratio whereas the excess Pb^{207}/Pb^{206} would be near to 0.1, a value somewhat lower than one might expect for old uranium lead.

It is a pleasure to acknowledge the interest taken by Professor Alfred C. Lane, Chairman of the Committee on the Measurement of Geologic Time, through whose efforts many of the specimens were obtained. The radiogenic lead iodides and some of the common lead iodides were very kindly prepared by Professor G. P. Baxter of the Harvard Chemistry Department. The bulk of the common lead samples was obtained from Professor H. Berman of the Harvard Mineralogical Museum and were converted to PbI_2 by Dr. Charles Sage of the University of Minnesota. The senior author expresses his appreciation to the graduate school for financial support.

[7] N. B. Keevil, Economic Geology **33**, 685 (1938).
[8] R. D. Evans, J. App. Phys. **12**, 297 (1941).

The Spectra of Cd IV, In V and Sn VI in the Isoelectric Sequence Rh I to Sn VI

MILTON GREEN
Department of Physics, University of California, Berkeley

(Received May 12, 1941)

The spectra of Cd IV, In V and Sn VI were photographed in the region 270A to 1800A with a three-meter, normal incidence, vacuum spectrograph, with a highly condensed, high voltage vacuum spark as a source of light. The irregular doublet law and the law of constant second difference were applied in the classification of many of the lines of these three ions. The separation of the $4d^9\ ^2D$ multiplet of the ground state has been found for all three ions. Most of the odd terms arising from the $4d^8 5p$ electron configuration and some of the even terms arising from the $4d^8 5s$ electron configuration have been determined. Classifications have been made for one hundred eighty-five lines of Cd IV, forty-three lines of In V and thirty-nine lines of Sn VI, making possible the assignment of fifty-one term values for Cd IV, thirty-two for In V and twenty-five for Sn VI.

THE spectra of Rh I, Pd II and Ag III have been analyzed by Sommers,[1] Shenstone[2] and Gilbert,[3] respectively. With the data on these three spectra in conjunction with the law of constant second difference and the irregular doublet law, the analyzed spectra of this isoelectronic sequence has been extended three more elements, i.e., through Sn VI. The predicted and observed terms for the spectra of

TABLE I. *Predicted and observed terms in* Cd IV, In V *and* Sn VI.

Electron Config.	Predicted Terms	Parent Term in Ion	Observed Terms: Cd IV	In V	Sn VI
$4d^9$	^2D	^1S	^2D	^2D	^2D
$4d^8 5s$	^2S	^1D	—	—	—
	^2D	^1G	^2G		
	^2G	^3P			
	2 and ^4P	^3F	2 and ^4F		
	2 and ^4F	^1S	—	—	—
	$^2P^\circ$	^1D	$^2(P^\circ D^\circ F^\circ)$	$^2(P^\circ D^\circ F^\circ)$	$^2(P^\circ D^\circ F^\circ)$
$4d^8 5p$	$^2(P^\circ D^\circ F^\circ)$	^1G	$^2(F^\circ H^\circ)$	$^2F^\circ$	$^2F^\circ$
	$^2(F^\circ G^\circ H^\circ)$	^3P	$^2(S^\circ P^\circ D^\circ)$	$^2(S^\circ P^\circ D^\circ)$	$^2(S^\circ P^\circ D^\circ)$
	2 and $^4(S^\circ P^\circ D^\circ)$	^3F	2 and $^4(D^\circ F^\circ G^\circ)$	2 and $^4(D^\circ F^\circ)$ $^4G^\circ$	$^2D^\circ$ 2 and $^4F^\circ$ $^4G^\circ$
	2 and $^4(D^\circ F^\circ G^\circ)$				

TABLE II. *Radiated frequencies with first and second differences. First series members.*

Ion	$4d^9\ ^2D_3 - 4d^8(^3F)5p\ ^2D^\circ_2$			$4d^9\ ^2D_3 - 4d^8(^3F)5p\ ^4F^\circ_4$		
Rh I	28,737			29,867		
		43,995			41,379	
Pd II	72,732		8365	71,246		11,003
		52,360			52,382	
Ag III	125,092		6850	123,628		6,963
		59,209			59,345	
Cd IV	184,301		6134	182,973		6,197
		65,343			65,542	
In V	249,644		5735	248,515		5,805
		71,076			71,345	
Sn VI	320,720			319,860		

[1] L. A. Sommers, Zeits. f. Physik **45**, 147 (1927).
[2] A. G. Shenstone, Phys. Rev. **32**, 30 (1928).
[3] W. P. Gilbert, Phys. Rev. **48**, 338 (1935).

TABLE III. *A comparison of the* $4d^9\ ^2D_{3,2}$ *splitting with the difference* $4d^9\ 5s\ ^3D_3 - 4d^9\ 5s\ ^3D_1$ *of the same element.*

Ion	$^2D_{3,2}$(cm^{-1})		Ion	$^3D_{3,1}$(cm^{-1})	
Rh I	2350				
		1190			
Pd II	3540		Pd I	3530	
		1070			1045
Ag III	4610		Ag II	4575	
		1200			1195
Cd IV	5810		Cd III	5770	
		1350			1340
In V	7160		In IV	7110	
		1550			1510
Sn VI	8710		Sn V	8620	

TABLE IV. *Term values in* Cd IV.

Term Symbol	Relative Term Values (cm^{-1})	Term Symbol	Relative Term Values (cm^{-1})
$4d^9\ ^2D_3$	0	$4d^8(^3F)5p\ ^2D^\circ_2$	187,213
$^2D_2$	5,812	$^2G^\circ_4$	188,147
$4d^8(^3F)5s\ ^4F_5$	108,704	$^2F^\circ_3$	188,296
$^4F_4$	111,734	$(^3P)5p\ ^4P^\circ_1$	189,404
$^4F_3$	114,758	$^4P^\circ_2$	190,411
$^4F_2$	116,125	$^4P^\circ_3$	190,694
$^2F_4$	118,333	$(^1D)5p\ ^2F^\circ_3$	191,953
$^2F_3$	120,557	$^2P^\circ_1$	194,212
$(^1G)5s\ ^2G_5$	133,860	$^2F^\circ_4$	194,367
$^2G_4$	134,010	$^2P^\circ_2$	195,542
$(^3F)5p\ ^4D^\circ_4$	172,387	$^2D^\circ_3$	196,255
$^4G^\circ_5$	175,319	$(^3P)5p\ ^4D^\circ_1$	196,370
$^4D^\circ_3$	177,252	$(^1D)5p\ ^2D^\circ_2(?)$	196,485
$^4G^\circ_6$	179,173	$(^1G)5p\ ^2H^\circ_5$	196,560
$^4G^\circ_4$	179,375	$(^3P)5p\ ^4D^\circ_4$	197,508
$^4G^\circ_3$	180,812	$^4D^\circ_2$	198,220
$^4D^\circ_2$	180,868	$^4D^\circ_3$	198,338
$^4F^\circ_5$	181,672	$^2D^\circ_3$	199,525
$^4F^\circ_2$	182,176	$^2D^\circ_2$	200,743
$^4D^\circ_1$	182,864	$(^1G)5p\ ^2H^\circ_6$	201,293
$^4F^\circ_4$	182,973	$(^3P)5p\ ^2P^\circ_2$	201,967
$^2D^\circ_3$	184,301	$^2S^\circ_1$	202,655
$^2G^\circ_5$	185,366	$(^1G)5p\ ^2F^\circ_4$	202,836
$^4F^\circ_3$	186,307	$^2F^\circ_3$	204,196
$^2F^\circ_4$	187,168	$(^3P)5p\ ^4S^\circ_2$	204,294
		$^2P^\circ_1$	206,402

TABLE V. *Classified lines in* Cd IV.

INT.	λ VAC.	ν VAC.	CLASSIFICATION
1	1929.70	51,821	$4d^8(^3F)5s\ ^2F_3 - 4d^8(^3F)5p\ ^4D^\circ_4$
1	1850.40	54,043	$^2F_4 - \quad ^4D^\circ_4$
6	1763.67	56,700	$^2F_3 - \quad ^4D^\circ_3$
0	1735.42	57,623	$^4F_3 - \quad ^4D^\circ_4$
4	1700.14	58,819	$^2F_3 - \quad ^4G^\circ_4$
4	1697.07	58,925	$^2F_4 - \quad ^4D^\circ_3$
6	1659.51	60,259	$^2F_3 - \quad ^4G^\circ_3$
4	1658.08	60,311	$^2F_3 - \quad ^4D^\circ_2$
2	1648.58	60,658	$^4F_4 - \quad ^4D^\circ_4$
4	1638.19	61,042	$^2F_4 - \quad ^4G^\circ_4$
0	1635.81	61,132	$^4F_2 - \quad ^4D^\circ_3$
8	1622.87	61,619	$^2F_3 - \quad ^4F^\circ_2$
4	1602.20	62,414	$^2F_3 - \quad ^4F^\circ_4$
10	1600.42	62,484	$^2F_4 - \quad ^4G^\circ_3$
4	1600.13	62,495	$^4F_3 - \quad ^4D^\circ_3$
10	1598.73	62,550	$(^1G)5s\ ^2G_4 - \quad (^1G)5p\ ^2H^\circ_5$
6	1594.86	62,701	$^2G_5 - \quad ^2H^\circ_5$
6	1578.90	63,335	$(^3F)5s\ ^2F_4 - \quad (^3F)5p\ ^4F^\circ_5$
6	1572.69	63,585	$^4F_4 - \quad ^4G^\circ_5$
10	1570.20	63,686	$^4F_5 - \quad ^4D^\circ_4$
6	1547.62	64,615	$^4F_3 - \quad ^4G^\circ_4$
6	1547.01	64,641	$^2F_4 - \quad ^4F^\circ_4$
6	1545.79	64,691	$^4F_2 - \quad ^4G^\circ_3$
2	1544.52	64,745	$^4F_2 - \quad ^4D^\circ_2$
6	1526.15	65,520	$^4F_4 - \quad ^4D^\circ_3$
2	1520.88	65,750	$^2F_3 - \quad ^4F^\circ_3$
6	1515.77	65,973	$4d^8(^3F)5s\ ^2F_4 - 4d^8(^3F)5p\ ^2D^\circ_3$
6	1513.92	66,054	$^4F_2 - \quad ^4F^\circ_2$
6	1513.75	66,057	$^4F_3 - \quad ^4G^\circ_3$
6	1512.57	66,113	$^4F_3 - \quad ^4D^\circ_2$
6b	1501.13	66,616	$^2F_3 - \quad ^2F^\circ_4$ $^4F_5 - \quad ^4G^\circ_5$
4	1500.11	66,662	$^2F_3 - \quad ^2D^\circ_2$
4	1498.39	66,738	$^4F_2 - \quad ^4D^\circ_1$
10	1491.79	67,034	$^2F_4 - \quad ^2G^\circ_5$
0	1483.28	67,418	$^4F_3 - \quad ^4F^\circ_2$
8	1482.95	67,433	$(^1G)5s\ ^2G_5 - \quad (^1G)5p\ ^2H^\circ_6$
6	1479.37	67,596	$(^3F)5s\ ^2F_3 - \quad (^3F)5p\ ^2G^\circ_4$
6	1478.32	67,644	$^4F_4 - \quad ^4G^\circ_4$
6	1476.22	67,741	$^2F_3 - \quad ^2F^\circ_3$
6	1471.08	67,978	$^2F_4 - \quad ^4F^\circ_3$
8	1466.67	68,182	$^4F_2 - \quad ^2D^\circ_3$
8	1465.97	68,214	$^4F_3 - \quad ^4F^\circ_4$
2	1452.90	68,828	$(^1G)5s\ ^2G_4 - \quad (^1G)5p\ ^2F^\circ_4$
10	1452.63	68,841	$(^3F)5s\ ^2F_4 - \quad (^3F)5p\ ^2F^\circ_4$
6	1449.71	68,979	$(^1G)5s\ ^2G_5 - \quad (^1G)5p\ ^2F^\circ_4$
10	1447.54	69,083	$(^3P)5s\ ^4F_4 - \quad (^3F)5p\ ^4G^\circ_3$
6	1437.90	69,546	$^4F_3 - \quad ^2D^\circ_3$
4	1432.23	69,821	$^2F_4 - \quad ^2G^\circ_4$
4	1431.55	69,854	$^2F_3 - \quad (^3P)5p\ ^4P^\circ_2$
8	1429.83	69,938	$^4F_4 - \quad (^3F)5p\ ^4F^\circ_5$
6	1429.28	69,965	$^2F_4 - \quad ^2F^\circ_3$
6	1425.73	70,139	$^2F_3 - \quad (^3P)5p\ ^4P^\circ_3$
6	1424.92	70,179	$4d^8(^1G)5s\ ^2G_4 - 4d^8(^1G)5p\ ^2F^\circ_3$
4	1424.81	70,185	$(^3F)5s\ ^4F_2 - \quad (^3F)5p\ ^4F^\circ_5$
16	1418.89	70,478	$^4F_5 - \quad ^4G^\circ_6$
6	1414.83	70,680	$^4F_5 - \quad ^4G^\circ_4$
8	1406.58	71,094	$4d^8(^3F)5s\ ^4F_2 - 4d^8(^3F)5p\ ^2D^\circ_2$
12	1403.68	71,239	$^4F_4 - \quad ^4F^\circ_4$
6	1400.72	71,392	$^2F_3 - \quad (^1D)\ ^2F^\circ_3$
10	1397.65	71,549	$^4F_3 - \quad (^3F)\ ^4F^\circ_3$
6	1385.55	72,173	$^4F_2 - \quad ^2F^\circ_3$
2	1381.88	72,365	$^2F_4 - \quad (^3P)\ ^4P^\circ_3$
12	1380.98	72,412	$^4F_3 - \quad (^3F)\ ^2F^\circ_4$
16	1370.48	72,967	$^4F_5 - \quad ^4F^\circ_5$
4	1364.37	73,294	$^4F_2 - \quad (^3P)\ ^4P^\circ_1$
12	1362.55	73,392	$^4F_3 - \quad (^3F)\ ^2G^\circ_4$
4	1359.86	73,537	$^4F_3 - \quad ^2F^\circ_3$
6	1358.49	73,611	$^2F_4 - \quad (^1D)\ ^2F^\circ_3$
10	1358.11	73,632	$^4F_4 - \quad (^3F)\ ^2G^\circ_5$
12	1354.78	73,813	$^2F_3 - \quad (^1D)\ ^2F^\circ_4$
4	1346.45	74,269	$^4F_5 - \quad (^3F)\ ^4F^\circ_4$
8	1346.15	74,286	$^4F_2 - \quad (^3P)\ ^4P^\circ_2$
12	1340.97	74,573	$^4F_4 - \quad (^3F)\ ^4F^\circ_3$ $^4F_2 - \quad (^3P)\ ^4F^\circ_3$
6	1333.53	74,989	$^2F_3 - \quad (^3P)\ ^2P^\circ_2$
10	1325.55	75,440	$4d^8(^3F)5s\ ^4F_4 - 4d^8(^3F)5p\ ^2F^\circ_4$
8	1321.85	75,651	$^4F_3 - \quad (^3P)\ ^4P^\circ_2$
4	1318.94	75,818	$^4F_2 - \quad (^1D)\ ^2F^\circ_3(?)$
4	1316.99	75,931	$^2F_3 - \quad (^1D)\ ^2D^\circ_2(?)$
8	1316.89	75,935	$^4F_3 - \quad (^3P)\ ^4P^\circ_3$
4	1315.12	76,039	$^2F_4 - \quad (^1D)\ ^2F^\circ_4$
12	1306.07	76,566	$^4F_4 - \quad (^3F)\ ^2F^\circ_3$
14	1304.36	76,666	$^4F_5 - \quad ^2G^\circ_5$
10	1299.46	76,955	$^2F_3 - \quad (^3P)\ ^4D^\circ_4$
10	1287.58	77,665	$^2F_3 - \quad ^4D^\circ_2$
10	1285.63	77,783	$^2F_3 - \quad ^4D^\circ_3$
4	1283.23	77,928	$^2F_4 - \quad (^1D)\ ^2D^\circ_2$
00	1280.50	78,094	$^4F_2 - \quad ^2P^\circ_1$
8	1274.41	78,468	$^2F_4 - \quad (^3F)\ ^4F^\circ_5$
12b	1266.47	78,960	$^4F_4 - \quad (^3P)\ ^4P^\circ_3$
2	1266.25	78,973	$^2F_3 - \quad (^3P)\ ^2D^\circ_3$
6	1262.98	79,178	$^2F_2 - \quad (^3P)\ ^4D^\circ_4$
6	1259.14	79,421	$^4F_2 - \quad (^1D)\ ^2P^\circ_2$
	(OV)(?)		
1	1256.16	79,608	$4d^8(^3F)5s\ ^4F_3 - 4d^8(^1D)5p\ ^2F^\circ_4$
8	1249.94	78,004	$^2F_4 - \quad (^3P)\ ^4D^\circ_3$
2	1247.39	80,195	$^2F_3 - \quad ^2D^\circ_2$
	(CIII)(?)		
8	1246.56	80,220	$^4F_4 - \quad (^1D)\ ^2F^\circ_3$
10	1246.06	80,253	$^4F_2 - \quad (^3P)\ ^4D^\circ_1$
4	1237.87	80,784	$^4F_3 - \quad ^2P^\circ_2$
0	1231.51	81,201	$^2F_4 - \quad ^2D^\circ_3$
0	1228.40	81,407	$^2F_3 - \quad ^2P^\circ_2$
4	1227.07	81,495	$^4F_3 - \quad (^1D)\ ^2D^\circ_3$
10	1223.52	81,731	$^4F_3 - \quad ^2D^\circ_2$
1	1218.04	82,099	$^4F_2 - \quad ^4D^\circ_2$
8	1215.38	82,279	$^2F_3 - \quad (^1G)\ ^2F^\circ_4$
6	1210.24	82,638	$^4F_4 - \quad (^1D)\ ^2F^\circ_4$
3	1208.43	82,752	$^4F_3 - \quad (^3P)\ ^4D^\circ_4$
10	1198.93	83,408	$^4F_2 - \quad ^2D^\circ_3$
3	1198.15	83,462	$^4F_1 - \quad ^2D^\circ_2$
12	1196.47	83,579	$^4F_3 - \quad ^4D^\circ_3$
10	1195.63	83,638	$^2F_3 - \quad (^1G)\ ^2F^\circ_3$
14	1194.13	83,743	$^2F_3 - \quad (^3P)\ ^4S^\circ_2$
20	1183.40	84,502	$4d^8(^3F)5s\ ^2F_4 - 4d^8(^1G)5p\ ^2D^\circ_2$
8	1183.07	84,526	$^4F_4 - \quad ^2D^\circ_3$
4	1181.66	84,627	$(^3F)\ ^4F_2 - \quad (^3P)\ ^2D^\circ_2$
10	1179.73	84,765	$^4F_3 - \quad ^2D^\circ_3$
14	1167.30	85,668	$^4F_5 - \quad ^2F^\circ_4$
10	1165.78	85,780	$^4F_4 - \quad ^4D^\circ_4$
0	1164.89	85,845	$^4F_2 - \quad ^2P^\circ_2$
20	1164.65	85,863	$^2F_4 - \quad (^1G)\ ^2F^\circ_3$
4	1162.87	85,994	$^4F_3 - \quad (^3P)\ ^2D^\circ_2$
7	1155.73	86,525	$^4F_2 - \quad ^2S^\circ_1$
10	1154.64	86,607	$^4F_4 - \quad ^4D^\circ_3$
2	1146.71	87,206	$^4F_3 - \quad ^2P^\circ_2$
8	1139.04	87,793	$^4F_4 - \quad ^2D^\circ_3$
2	1135.46	88,070	$^4F_2 - \quad (^1G)\ ^2F^\circ_3$
10	1134.08	88,177	$^4F_2 - \quad (^3P)\ ^4S^\circ_2$
12	1126.00	88,810	$^4F_5 - \quad ^4D^\circ_4$
24	1118.16	89,433	$^4F_3 - \quad (^1G)\ ^2F^\circ_3$
2	1116.88	89,535	$^4F_3 - \quad (^3P)\ ^4S^\circ_2$
0	1107.76	90,272	$^4F_2 - \quad ^2P^\circ_1$
6	1097.53	91,114	$4d^8(^3F)5s\ ^4F_4 - 4d^8(^1G)5p\ ^2F^\circ_4(?)$
2	1081.50	92,464	$^4F_4 - \quad ^2F^\circ_3$
10	1062.23	94,142	$^4F_5 - \quad ^2F^\circ_4$
3	583.30	171,438	$4d^9\ ^2D_2 - \quad (^3F)\ ^4D^\circ_3$

TABLE V.—*Continued.*

INT.	λ VAC.	ν VAC.	CLASSIFICATION		INT.	λ VAC.	ν VAC.	CLASSIFICATION	
3	580.09	172,387	$^2D_3-$	$^4D^\circ_4$	14	525.18	190,411	$^2D_3-$	$(^3P)\ ^4P^\circ_2$
3	571.43	175,000	$^2D_2-$	$^4G^\circ_3$	17	525.09	190,444	$^2D_2-$	$(^1D)\ ^2D^\circ_3$
6	571.25	175,055	$^2D_2-$	$^4D^\circ_4$	14	524.77	190,560	$^2D_2-$	$(^3P)\ ^4D^\circ_1$?
18	567.03	176,358	$^2D_2-$	$^4F^\circ_2$	14	524.46	190,672	$^2D_2-$	$(^1D)\ ^2D^\circ_2$?
3	564.80	177,054	$^2D_2-$	$^4P^\circ_1$	14	524.40	190,694	$^2D_3-$	$(^3P)\ ^4P^\circ_3$
11	564.17	177,252	$^2D_3-$	$^4D^\circ_3$	9	520.96	191,953	$^2D_3-$	$(^1D)\ ^2F^\circ_3$
14	560.25	178,492	$^2D_2-$	$^2D^\circ_3$	14	519.41	192,526	$^2D_2-$	$(^3P)\ ^4D^\circ_3$
9	557.49	179,375	$^2D_3-$	$^4G^\circ_4$	1	516.22	193,716	$^2D_2-$	$(^3P)\ ^2D^\circ_3$
18	554.04	180,493	$^2D_2-$	$^4F^\circ_3$	17	514.49	194,367	$^2D_3-$	$4d^8(^1D)5p\ ^2F^\circ_4$
17	553.06	180,812	$^2D_3-$	$^4G^\circ_3$	17	512.99	194,936	$^2D_2-$	$(^3P)\ ^2D^\circ_2$
10	552.89	180,868	$^2D_3-$	$^4D^\circ_2$	17	511.40	195,542	$^2D_3-$	$(^1D)\ ^2P^\circ_2$
11	551.26	181,403	$^2D_2-$	$^2D^\circ_2$	3	509.80	196,155	$^2D_2-$	$(^3P)\ ^2P^\circ_2$
10	548.92	182,176	$^2D_3-$	$^4F^\circ_2$	17	509.54	196,255	$^2D_3-$	$(^1D)\ ^2D^\circ_3$
11	548.00	182,482	$^2D_2-$	$^2F^\circ_3$	17	508.01	196,847	$^2D_2-$	$(^3P)\ ^2S^\circ_1$
25	546.53	182,973	$^2D_3-$	$^4F^\circ_4$	19	506.31	197,508	$^2D_3-$	$(^3P)\ ^4D^\circ_4$
9	544.68	183,594	$^2D_2-4d^8(^3P)5p$	$^4P^\circ_1$	17	504.49	198,220	$^2D_3-$	$^4D^\circ_2$
25	542.59	184,301	$^2D_3-$	$(^3F)\ ^2D^\circ_3$	11	504.19	198,338	$^2D_3-$	$^4D^\circ_3$
18	541.73	184,594	$^2D_2-$	$(^3P)\ ^4P^\circ_2$	14	504.09	198,377	$^2D_2-$	$(^1G)\ ^2F^\circ_3$
17	540.89	184,881	$^2D_2-$	$^4P^\circ_3$	3	503.81	198,488	$^2D_2-$	$(^3P)\ ^4S^\circ_2$
14	537.22	186,144	$^2D_2-$	$(^1D)\ ^2F^\circ_3$	1	501.19	199,525	$^2D_3-$	$^2D^\circ_3$
17	536.75	186,307	$^2D_3-$	$(^3F)\ ^4F^\circ_3$	17	498.53	200,590	$^2D_2-$	$^2P^\circ_1$
17	534.28	187,168	$^2D_3-$	$^2F^\circ_4$	17	498.15	200,743	$^2D_3-$	$^2D^\circ_2$
18	531.50	188,147	$^2D_3-$	$^2G^\circ_4$	17	495.13	201,967	$^2D_3-$	$^2P^\circ_1$
18	531.08	188,296	$^2D_3-$	$^2F^\circ_3$	17	493.00	202,840	$^2D_3-$	$(^1G)\ ^2F^\circ_4$
14	530.78	188,402	$^2D_2-$	$(^1D)\ ^2P^\circ_1$	2	489.76	204,182	$^2D_3-$	$^2F^\circ_3$
18	527.06	189,732	$^2D_2-$	$^2P^\circ_2$	10	489.49	204,294	$^2D_3-$	$(^3P)\ ^4S^\circ_2$

these ionized atoms are shown in Table I. In Table II are listed the frequencies of the two strong transitions $4d^9\ ^2D_3-4d^8(^3F)5p^2D^\circ_3$, and $4d^9\ ^2D_3-4d^8(^3F)5p^4F^\circ_4$ with first and second differences. The data in the second difference column show an approach toward a constant value for increasing ionization. The displaced frequency diagram for $4d^9-4d^85p$ transition is shown in Fig. 1.

The data in Table III give a comparison of the over-all separation of the triplet levels of the $4d^95s$ electron configuration with the doublet separation of the normal $4d^9\ ^2D$ state of the ion, indicating the existence of nearly pure *jj*-coupling between the $4d^9$ ion and the $5s$ electron for the ionized atoms isoelectronic with Pd I.

The spectrograms of cadmium, indium and tin were taken with a three-meter normal incidence vacuum spectrograph. The electrodes used for obtaining the spectra of cadmium and tin were cast from the pure molten metals while those for indium were made by packing an alloy of indium and aluminum into aluminum shells. All elec-

TABLE VI. *Term values in* In V.

TERM SYMBOL		RELATIVE TERM VALUES (CM^{-1})	TERM SYMBOL		RELATIVE TERM VALUES (CM^{-1})
$4d^9$	$^2D_3$	0	$(^1D)5p$	$^2F^\circ_4$	261,260
	$^2D_2$	7,165		$^2P^\circ_2$	262,082
$4d^8(^3F)5p$	$^4D^\circ_4$	236,317		$^2D_3$	262,971
	$^4D^\circ_3$	241,051	$(^1D)5p$	$^2D^\circ_2$(?)	263,555
	$^4G^\circ_4$	243,315	$(^3P)5p$	$^4D^\circ_4$	264,124
	$^4G^\circ_3$	245,128		$^4D^\circ_2$	265,908
	$^4D^\circ_2$	246,145		$^4D^\circ_3$	266,071
	$^4F^\circ_2$	246,713		$^2D^\circ_2$	268,226
	$^4F^\circ_4$	248,515		$^2D^\circ_3$	268,894
	$^2D^\circ_3$	249,644	$(^3P)5p$	$^2P^\circ_2$	270,197
	$^2D^\circ_2$	252,648		$^2S^\circ_1$	270,850
	$^4F^\circ_3$	252,691	$(^1G)5p$	$^2F^\circ_4$	271,245
	$^2F^\circ_4$	253,878		$^2F^\circ_3$	272,565
$(^3P)5p$	$^4P^\circ_3$	257,129	$(^3P)5p$	$^4S^\circ_2$	273,867
	$^4P^\circ_2$	257,294		$^2P^\circ_1$	275,305
$(^1D)5p$	$^2F^\circ_3$	258,598			
	$^2P^\circ_1$	261,220			

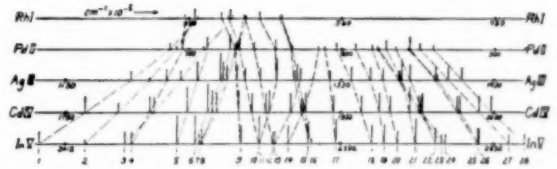

1. $^2D_2-(^3F)^2F^\circ_2$
2. $^2D_2-\ \ ^2D^\circ_2$
3. $^2D_3-\ \ ^4G^\circ_3$
4. $^2D_2-\ \ ^4F^\circ_2$
5. $^2D_3-\ \ ^4F^\circ_4$
6. $^2D_3-\ \ ^2D^\circ_3$
7. $^2D_3-(^3P)^4P^\circ_2$
8. $^2D_2-\ \ ^4P^\circ_2$
9. $^2D_3-(^3F)^4F^\circ_3$
10. $^2D_3-\ \ ^2F^\circ_4$
11. $^2D_3-(^3F)^2F^\circ_3$
12. $^2D_2-\ \ ^2G^\circ_4$
13. $^2D_2-(^1D)^2P^\circ_2$
14. $^2D_2-\ \ ^2D^\circ_3$
15. $^2D_3-(^3P)^4P^\circ_3$
16. $^2D_2-\ \ ^4P^\circ_2$
17. $^2D_2-\ \ ^4D^\circ_3$
18. $^2D_3-(^1D)^2F^\circ_4$
19. $^2D_3-(^1D)^2P^\circ_2$
20. $^2D_2-\ \ ^2D^\circ_2$
21. $^2D_3-(^3P)^4D^\circ_4$
22. $^2D_3-(^1G)^2F^\circ_2$
23. $^2D_3-(^3P)^4D^\circ_2$
24. $^2D_3-(^3P)^4D^\circ_3$
25. $^2D_2-\ \ ^2P^\circ_1$
26. $^2D_3-\ \ ^2D^\circ_2$
27. $^2D_3-\ \ ^2P^\circ_2$
28. $^2D_3-(^1G)^2F^\circ_4$

FIG. 1. Displaced frequency diagram, law of constant second differences for $4d-5p$ electron transition.

TABLE VII. *Classified lines in* In V.

INT.	λ VAC.	ν VAC.	CLASSIFICATION
2	423.16	236,317	$4d^9\ ^2D_3 - 4d^8(^3F)5p\ ^4D^\circ_4$
0	420.16	238,005	$^2D_2 - (^3F)\ ^4G^\circ_3$
2	418.45	238,977	$^2D_2 - (^3F)\ ^4D^\circ_2$
9	417.43	239,561	$^2D_2 - (^3F)\ ^4F^\circ_2$
0	414.85	241,051	$^2D_3 - (^3F)\ ^4D^\circ_3$
0	412.41	242,477	$^2D_2 - (^3F)\ ^2D^\circ_3$
9	407.95	245,128	$^2D_3 - \ ^4G^\circ_3$
3	407.36	245,483	$^2D_2 - (^3F)\ ^2D^\circ_2$
9	407.28	245,531	$^2D_2 - \ ^4F^\circ_3$
3	405.33	246,713	$^2D_2 - (^3F)\ ^2F^\circ_3$ and $^2D_2 - (^3F)\ ^4F^\circ_2$
25	402.39	248,515	$^2D_3 - (^3F)\ ^4F^\circ_4$
25	400.57	249,644	$^2D_3 - (^3F)\ ^2D^\circ_3$
9	400.05	249,969	$^2D_2 - (^3P)\ ^4P^\circ_3$
10	399.79	250,131	$^2D_2 - (^3P)\ ^4P^\circ_2$
3	397.73	251,427	$^2D_2 - (^1D)\ ^2F^\circ_3$
11	395.74	252,691	$^2D_3 - (^3F)\ ^4F^\circ_3$
25	393.89	253,878	$^2D_3 - (^3F)\ ^2F^\circ_3$ and $^2D_3 - (^3F)\ ^2F^\circ_4$
1	393.60	254,065	$^2D_2 - (^1D)\ ^2P^\circ_1$
9	392.46	254,803	$^2D_3 - (^3F)\ ^2G^\circ_4$
9	392.29	254,914	$^2D_2 - (^1D)\ ^2P^\circ_2$
11	390.92	255,807	$4d^9\ ^2D_2 - 4d^8(^1D)5p\ ^2D^\circ_3$
11	390.03	256,391	$^2D_2 - (^1D)\ ^2D^\circ_2$(?)
14	388.91	257,129	$^2D_3 - (^3P)\ ^4P^\circ_3$
3	388.66	257,294	$^2D_3 - (^3P)\ ^4P^\circ_2$
10	386.70	258,598	$^2D_3 - (^1D)\ ^2F^\circ_3$
17	386.21	258,927	$^2D_2 - (^3P)\ ^4D^\circ_3$
	(CIII)(?)		
10	383.05	261,063	$^2D_2 - (^3P)\ ^2D^\circ_2$
11	382.76	261,260	$^2D_3 - (^1D)\ ^2F^\circ_4$
9	382.14	261,684	$^2D_2 - (^3P)\ ^2D^\circ_3$
11	381.56	262,082	$^2D_3 - (^1D)\ ^2P^\circ_2$
9	380.27	262,971	$^2D_3 - (^1D)\ ^2D^\circ_3$
3	379.24	263,685	$^2D_2 - (^3P)\ ^2S^\circ_1$
17	378.61	264,124	$^2D_3 - (^3P)\ ^4D^\circ_4$
10	376.79	265,400	$^2D_2 - (^1G)\ ^2F^\circ_3$
6	376.07	265,908	$^2D_3 - (^3P)\ ^4D^\circ_2$
6	375.84	266,071	$^2D_3 - (^3P)\ ^4D^\circ_3$
2	374.95	266,702	$^2D_2 - (^3P)\ ^4S^\circ_2$
10	372.94	268,140	$^2D_2 - (^3P)\ ^2P^\circ_1$
10	372.82	268,226	$^2D_3 - (^3P)\ ^2D^\circ_2$
6	370.10	270,197	$^2D_3 - (^3P)\ ^2P^\circ_2$
6	368.67	271,245	$^2D_3 - (^1G)\ ^2F^\circ_4$

TABLE VIII. *Term values in* Sn VI.

TERM SYMBOL	RELATIVE TERM VALUES (CM^{-1})	TERM SYMBOL	RELATIVE TERM VALUES (CM^{-1})
$4d^9\ ^2D_3$	0	$(^1D)5p\ ^2P^\circ_1$	334,183
$^2D_2$	8,715	$^2P^\circ_2$	334,348
$4d^8(^3F)5p\ ^4G^\circ_3$	315,060	$^2D^\circ_3$	335,638
$^4F^\circ_2$	317,581	$^2D^\circ_2$	336,530
$^4F^\circ_4$	319,857	$(^3P)5p\ ^4D^\circ_4$	336,678
$^2D^\circ_3$	320,718	$^4D^\circ_2$	339,443
$^4F^\circ_3$	324,925	$^2D^\circ_2$	341,729
$^2F^\circ_3$	326,712	$^2D^\circ_3$	342,861
$(^3P)5p\ ^4P^\circ_3$	329,131	$^2P^\circ_2$	344,400
$^4P^\circ_2$	330,098	$^2S^\circ_1$	344,883
$(^1D)5p\ ^2F^\circ_3$	331,356	$(^1G)5p\ ^2F^\circ_4$	345,770
$^2F^\circ_4$	333,868	$^2F^\circ_3$	347,021
		$(^3P)5p\ ^2P^\circ_1$	350,245

trodes had a hard pencil lead inserted as a core. The power for the vacuum spark was supplied from a bank of condensers (3 mf capacity) which were charged through a kenotron to a peak potential of 25 kv. The primary of the transformer was operated at 110 volts and 10 amperes.

Prior to the analysis given here L. Bloch and E. Bloch[4] had photographed and measured many of the lines of Cd IV using a high frequency electrodeless discharge as a source. Classifications for some of the stronger lines were suggested by them, none of which turned out to be correct.

[4] L. Bloch and E. Bloch, Ann. de physique **5–6**, 332 (1936).

TABLE IX. *Classified lines in* Sn VI.

INT.	λ VAC.	ν VAC.	CLASSIFICATION
4	326.43	306,344	$4d^9\ ^2D_3 - 4d^8(^3F)5p\ ^4G^\circ_3$
1	323.82	308,814	$^2D_2 - \ ^4F^\circ_2$
0	321.15	311,381	$^2D_2 - \ ^2D^\circ_3$
18	317.40	315,060	$^2D_3 - \ ^4G^\circ_3$
16	316.23	316,226	$^2D_2 - \ ^4F^\circ_3$
1	314.88	317,581	$^2D_3 - \ ^4F^\circ_2$
12	312.64	319,857	$^2D_3 - \ ^4F^\circ_4$
10	312.41	320,092	$^2D_2 - (^3P)5p\ ^4P^\circ_1$
15	312.10	320,410	$^2D_2 - \ ^4P^\circ_3$
17	311.80	320,718	$^2D_3 - (^3F)5p\ ^2D^\circ_3$
16	311.15	321,388	$^2D_2 - (^3P)5p\ ^4P^\circ_2$
5	309.94	322,643	$^2D_2 - (^1D)5p\ ^2F^\circ_3$
17	307.77	324,920	$^2D_3 - (^3F)5p\ ^4F^\circ_3$
15	307.43	325,277	$^2D_3 - (^3F)5p\ ^2F^\circ_3$
3	307.25	325,468	$^2D_2 - (^1D)5p\ ^2P^\circ_1$
15	307.12	325,606	$^2D_2 - \ ^2P^\circ_2$
10	306.08	326,712	$^2D_3 - (^3F)5p\ ^2F^\circ_4$
12	305.87	326,936	$^2D_2 - (^1D)5p\ ^2D^\circ_3$
13	305.51	327,322	$^2D_3 - (^3F)5p\ ^2G^\circ_4$
15	305.05	327,815	$^2D_2 - (^1D)5p\ ^2D^\circ_2$
15	303.83	329,131	$4d^9\ ^2D_3 - 4d^8(^3F)5p\ ^4P^\circ_3$
3	302.94	330,098	$^2D_3 - \ ^4P^\circ_2$
10	302.33	330,764	$^2D_2 - \ ^4D^\circ_2$
9	302.00	331,126	$^2D_2 - \ ^4D^\circ_3$
10	301.79	331,356	$^2D_3 - (^1D)5p\ ^2F^\circ_3$
10	300.34	332,956	$^2D_2 - (^3P)5p\ ^2D^\circ_2$
12	299.52	333,868	$^2D_3 - (^1D)5p\ ^2F^\circ_4$
8	299.27	334,146	$^2D_2 - (^3P)5p\ ^2D^\circ_3$
8	299.09	334,348	$^2D_3 - (^1D)5p\ ^2P^\circ_2$
5	297.94	335,638	$^2D_3 - \ ^2D^\circ_3$
4	297.47	336,168	$^2D_2 - (^3P)5p\ ^2S^\circ_1$
10	297.02	336,678	$^2D_3 - \ ^4D^\circ_4$
10	295.59	338,306	$^2D_2 - (^1G)5p\ ^2F^\circ_3$
5	294.60	339,443	$^2D_3 - (^3P)5p\ ^4D^\circ_2$
5	294.24	339,859	$^2D_3 - \ ^4D^\circ_3$
1	292.80	341,530	$^2D_2 - \ ^2P^\circ_1$
1	292.63	341,729	$^2D_3 - \ ^2D^\circ_2$
10	290.36	344,400	$^2D_3 - \ ^2P^\circ_2$
2	289.21	345,770	$^2D_3 - (^1G)5p\ ^2F^\circ_4$

They did obtain, however, the correct value for the $4d^9\ ^2D_{3,2}$ splitting of the ground state, namely 5810 cm^{-1}.

The term values of Cd IV, In V and Sn VI are listed relative to the $4d^9\ ^2D_3$ level of the ground state of each ion and are to be found in Tables IV, VI and VIII. The estimated intensities of all classified lines are given in Tables V, VII and IX along with the wave-lengths and corresponding frequencies reduced to vacuum.

The writer is very much indebted to Professor H. E. White for suggesting the problem and for his valuable advice during the course of the investigation.

JULY 15, 1941 PHYSICAL REVIEW VOLUME 60

Finite Self-Energies in Radiation Theory. Part I

ALFRED LANDÉ
Mendenhall Laboratory, Ohio State University, Columbus, Ohio

(Received March 8, 1941)

According to Dirac, electric particles display a finite radius $r_0=2e^2/3mc^2$ as the result of the damping term $(2e^2/3mc^3)d^3x/dt^3$ in the equation of motion. If the finite radius is due to radiative damping, the same must necessarily be true for the finite self-energy that is inversely proportional to the radius. An infinitely large self-energy and an infinitely small radius (Coulomb's law e^2/r) results from *Fermi's* Fourier representation of classical electrodynamics. A certain change is necessary, but the change is to produce at once a finite self-energy and a finite radius r_0. Now, an electric particle vibrating in a field of frequency ν suffers a reduction R_ν of its vibrational energy due to radiative damping, the energy reduction factor being $R_\nu=1/[1+(\nu/\nu_0)^2]$ where $\nu_0=3mc^3/4\pi e^2$. In view of the uncertainty of position due to damping we propose that the Fourier terms in the expression for the *energy* in Fermi's classical radiation theory be reduced by the same factor R_ν with Doppler effect for particles in motion. The result of this reduction is that Dirac's finite radius r_0 now occurs in a modified Coulomb energy $(e^2/r)[1-\exp(-r/r_0)]$, and the finite self-energy of a single particle becomes $e^2/2r_0=(3/4)mc^2$. Whereas the force between charged particles of finite mass remains finite for $r=0$, the force on an ideal test charge of infinite mass becomes infinite for $r=0$. This is analogous to the difference between the field E and the displacement D in Born's unitary field theory. Of interest for nuclear reactions are the electrostatic forces between particles of different masses m and M. The results are related to Sommerfeld's fine-structure constant and to the theory of mesons.

1. INTRODUCTION

ELECTRIC particles can be treated from the unitary or dualistic point of view. In the unitary theory a particle is but a spherically symmetric solution of certain modified field equations, without singularity at $r=0$. Born-Infeld's new field equations yield a finite maximum field e/r_0^2 at $r=0$. The electronic radius r_0 can be adjusted so that the total field energy is $\kappa\cdot mc^2$; the fraction κ can be chosen at will. This adjustable parameter is a disadvantage since we cannot know beforehand what fraction of the total mass is of electromagnetic origin. We prefer the dualistic point of view in which particles of various masses m are taken for granted, and the field produced by them, the "radius" and the self-energy, are to be expressed in terms of e and m.

One general point is common to all theories of electric particles. The smaller the radius, the larger the mass, the product r_0mc^2 being proportional to the square of the universal charge. However, the accepted (dualistic) radiation theory leads to an infinitely large self-energy and to an infinitely small radius, as expressed in Coulomb's energy $e^2/r=\infty$ for $r=0$. *If there are any reasons for having a finite radius then the same reasons must also be responsible for the finite self-energy.*

A radius dependent on the charge and mass occurs in Thomson's formula for the scattering cross section of an electric particle as the result of *radiative damping*. A similar radius occurs in Dirac's re-examination of the classical Lorentz theory.[1] Due to the damping term

[1] P. A. M. Dirac, Proc. Roy. Soc. **A167**, 148 (1938).

$(2e^2/3mc^3)d^3x/dt^3$ in the equation of motion, the universal length

$$r_0 = 2e^2/3mc^2$$

plays the rôle of an apparent radius in Dirac's discussion. The same radius measures the uncertainty of position due to the natural line breadth. *If the finite electronic radius is the result of radiative damping*, the same cause then must also be responsible for the finite electromagnetic energy. Our task is to find the quantitative relation between radius and self-energy in terms of e and m.

In particular we have tried to answer the following questions. (1) If m is the total inertia of a particle, what part of m is of electromagnetic origin? (in contrast to the infinite field energy of the present theory). (2) What is the mutual electrostatic energy of two electric particles of equal or different masses? (in contrast to the Coulomb energy e^2/r that is ∞ for $r=0$).

An answer different from the impossible result of radiation theory can only be obtained by means of a *formal* change of this theory, introduced *ad hoc* for the purpose of getting rid of the infinities.

We are proposing a cutting-off method based on the analogy to the classical Lorentz theory. If an electric particle of charge e and mass m is put into a periodic electric field of frequency ν then the vibrational energy of the particle depends on whether we do or do not account for radiative damping. With damping the energy is reduced (§ 2) by a factor

$$R_\nu = 1/[1+(\nu/\nu_0)^2], \quad \text{where} \quad \nu_0 = 3mc^3/4\pi e^2.$$

On the other hand, in Fermi's classical field theory the electromagnetic energy produced by the particles consists of Fourier terms of wavelength c/ν. Our hypothesis is that each of these Fourier terms of the energy is to be reduced by the same factor R_ν that reduces the energy of a vibrating electron because of radiative damping. For a particle in motion ν is replaced by the Doppler frequency ν' for reasons of invariance.

The result of this formal modification is so simple that it might be considered correct even if the method of deduction is not yet satisfactory. The mutual energy of two equal particles at distance r is found (§ 3) to be

$$E_{jk} = (e^2/r)[1-\exp(-r/r_0)]$$

where

$$r_0 = 2e^2/3mc^2.$$

The same $\exp(-r/r_0)$ appears in Dirac's investigation. For $r=0$ we have the finite value

$$E_{jk}(r=0) = e^2/r_0.$$

For the self-energy of one particle at rest we obtain

$$E_{jj} = \tfrac{1}{2}e^2/r_0,$$

intimately connected with the modification of Coulomb's mutual energy. With the former value of r_0 we also can write $E^0 = \frac{3}{4}mc^2$. That is, if the modified Coulomb law is correct (in view of its great simplicity it probably is) then only $\frac{3}{4}$ of the total energy mc^2 can be of electromagnetic origin. A result like this is not unexpected in view of neutral particles that have mass without field.

Our discussion throws an interesting sidelight on Sommerfeld's *constant* $\alpha = 1/137$. The characteristic frequency ν_0 occurring in R_ν may be considered as the *central frequency* between $\nu=0$ and $\nu=\infty$ for the particle. Indeed, according to Dirac[1] Eq. (35) the spectral intensity emitted by a self-accelerated particle is proportional to R_ν and the total recorded intensity $\int R_\nu d\nu$ consists of two equal parts, integrals from $\nu=0$ to ν_0, and from ν_0 to $\nu=\infty$. The characteristic time period $t_0 = 1/\nu_0 = 4\pi e^2/3mc^3$ leads to an approximative value ($\alpha \sim 1/140$) of the fine-structure constant when used in the proper value theory[2] of the electronic charge.

There is also a relation between our results and the *theory of the meson*. The modified Coulomb potential resulting from the damping effect consists of two terms

$$V - U = (e/r) - (e/r)\exp(-r/r_0).$$

V yields the ordinary Coulomb repulsion between like charges whereas U leads to an attraction between like charges at nuclear distances. V

[2] A. Landé, Phys. Rev. **59**, 434 (1941); J. Frank. Inst. **229**, 767 (1940); **231**, 63 (1940). Part III is to appear soon. The proper value theory of M. Born starts from a different background and arrives at different results (Proc. Roy. Soc. Edinburgh **59**, 219 (1939) **60**, 100 and 141 (1940).

and U are solutions of the differential equations

$$\nabla^2 V - \partial^2 V/\partial ct^2 = -4\pi\rho,$$

$$\nabla^2 U - \partial^2 U/\partial ct^2 = -4\pi\rho + k^2 U,$$

with

$$k = 1/r_0 = 3mc^2/2e^2.$$

The latter differential equation of Yukawa is the Schrödinger-Klein-Gordon equation for a free particle of mass

$$M = kh/2\pi c = (3mc^2/2e^2)(h/2\pi c) = (3m/2)(hc/2\pi e^2) = m\cdot(3/2)\cdot 137 = m\cdot 205,$$

perhaps identical with the meson mass.

2. Energy of Scattering Particles

The equation of motion for a particle of charge e and mass m is

$$m\ddot{x} - (2e^2/3c^3)d^3x/dt^3 = eE \qquad (1)$$

for small accelerations. For a periodic field

$$E = E_\omega \cos(\omega t)$$

the solution reads

$$x = (eE_\omega/m\omega^2)\cos\zeta_\omega \cos(\omega t - \zeta_\omega), \qquad (1')$$

where

$$\zeta_\omega = \mathrm{tg}^{-1}(\omega/\omega_0), \quad \cos\zeta_\omega = [1+(\omega/\omega_0)^2]^{-\frac{1}{2}}, \qquad 2\pi\nu_0 = \omega_0 = 3mc^3/2e^2. \qquad (2)$$

The average vibrational energy thus is

$$\tfrac{1}{2}m(\dot{x})^2_{\text{Mw}} = (e^2E_\omega^2/4m\omega^2)\cos^2\zeta_\omega. \qquad (3)$$

$\cos^2\zeta_\omega$ is identical with the reduction factor R_ν mentioned before. Periodic terms also occur in the classical Fermi theory[3] under the heading "mutual energy." There, however, the terms appear without the reducing factor $\cos\zeta_\omega$ and without the phase lag ζ_ω. We are trying to rectify this situation in an *invariant* way. For this purpose we need the proper value ζ'_{sj} of the phase shift for a particle e_j moving with velocity β_j in the direction of ϑ_{sj} through the wave s of frequency ω_s. Since the proper frequency felt by the particle according to Doppler is

$$\omega'_{sj} = \omega_s(1-\beta_j\cos\vartheta_{sj})(1-\beta_j^2)^{-\frac{1}{2}}, \qquad (4)$$

we have a phase lag and amplitude reduction

$$\zeta'_{sj} = \mathrm{tg}^{-1}(\omega'/\omega_0); \quad \cos\zeta'_{sj} = [1+(\omega'/\omega_0)^2]^{-\frac{1}{2}}. \qquad (4')$$

The terms describing the mutual energy between field and particles in Fermi's classical theory of radiation can be transformed (§7) into

$$H' = 4\pi c^2\Omega^{-1}\sum_s \omega_s^{-2}\{(\sum_i e_i\beta_i\sin\vartheta_{si}\sin\Gamma_{si})^2 + (\sum_i e_i\cos\Gamma_{si})^2\}. \qquad (5)$$

Here Ω is the total volume in which the proper vibrations of frequency ω_s take place; ϑ_{si} is the angle between the wave s and the velocity β_i, and

$$\Gamma_{si} = \omega_s r_i\cos\theta_{si}/c + \text{phase}$$

contains the angle θ_{si} between the wave direction s and the radius vector r_i from the zero point to the particle e_i. Replacing the summation over all waves s by an integration over $(\Omega/2\pi^2c^3)\omega_s^2 d\omega_s$ one obtains

$$H' = (e_1e_2/r_{12}) + \cdots + \text{infinite self-energies}.$$

This is Fermi's explanation of the Coulomb law in wave fashion, accompanied by infinite self-energies of every single particle.

We propose to modify Fermi's mutual energy (5) into the form:

$$H' = 4\pi c^2\Omega^{-1}\sum_s \omega_s^{-2} \times\{(\sum_i e_i\beta_i\sin\vartheta_{si}\cos\zeta'_{si}\sin(\Gamma_{si}+\zeta'_{si}))^2 + (\sum_i e_i\cos\zeta'_{si}\cos(\Gamma_{si}+\zeta'_{si}))^2\} \qquad (6)$$

making use of the invariant phase shift and amplitude reduction (4) (4'). We remark that all *electrostatic* results obtained from (6) could as well be obtained from an energy expression half-way between (5) and (6) in which the reduction ζ'_{si} is applied only to ***one*** factor of the squares $(\sum\cdots)^2$. We even could omit the phase lag altogether.

Another justification for the factor $\cos^2\zeta' = R_\nu$ is this. Due to the classical uncertainty $\delta\lambda = r_0$ wave functions at the place $\times$ are to be replaced by their averages with density $\exp(-r/r_0)$, *viz.*

$$\sin(\omega x/c)_{\text{Mw}} = \frac{1}{2}\int_{-\infty}^{\infty}\exp(-|\xi|r_0^{-1})\cdot\sin[\omega(x+\xi)/c]d\xi = \sin(\omega x/c)\cdot[1+(\omega/\omega_0)^2]^{-1}.$$

[3] E. Fermi, Rev. Mod. Phys. **4**, 87 (1932).

3. Self-Energy and Mutual Energy of Particles

For a single particle at rest, $\beta_i=0$ and $\zeta'_{si}=\zeta_s$ we obtain from (6)

$$E_i{}^0=(4\pi c^2/\Omega)e_i{}^2\sum_s \omega_s{}^{-2}\cos^2\zeta_s\cos^2(\Gamma_{si}+\zeta_s).$$

Replacing the sum by an integral we obtain

$$E_i{}^0=\frac{e_i{}^2}{2c}\cdot\frac{2}{\pi}\int_0^\infty\left(1+\frac{\omega^2}{\omega_0{}^2}\right)^{-1}d\omega=\frac{e_i{}^2\omega_0}{2c}=\tfrac{3}{4}m_ic^2. \quad (7)$$

Next we consider the mutual energy of two particles at rest in the distance r_{ij}. Here

$$\cos(\Gamma_{si}+\zeta_s)\cos(\Gamma_{sj}+\zeta_s)=\tfrac{1}{2}\cos(\omega_s r/c\cos\theta_s)+\tfrac{1}{2}\cos(\text{phase})$$

where θ_s is the angle between the wave s and the direction of r_{ij}. Replacing the summation by the integration $\frac{1}{2}d(\cos\theta_s)(\Omega/2\pi^2c^3)\omega_s{}^2d\omega_s$, and using the abbreviations

$$\omega/\omega_0=u,\quad \omega r/c=ux_0,\quad x_0=r/r_0,\qquad r_0=2e^2/3mc^2,\quad \cos\zeta=(1+u^2)^{-\frac{1}{2}}, \quad (8)$$

we obtain from (6) the mutual energy

$$E^0_{ij}=(e^2/r)(2/\pi)\int_0^\infty du\,\sin(ux_0)u^{-1}(1+u^2)^{-1}=(e^2/r)[1-\exp(-r/r_0)]. \quad (9)$$

For large r this is the Coulomb energy. For small r the mutual energy tends toward the constant value $e^2/r_0=\frac{3}{2}mc^2$. The mutual plus the self-energies of a pair of electrons at the distance zero is equal to the self-energy of a charge $2e$. If an electron and a positron approach to $r=0$ the energy $2\cdot(\frac{3}{4}mc^2)$ is released, but the system would still retain its original non-electromagnetic mass. This process has nothing to do with annihilation. In general, a point charge acts on another point charge like an exponentially shading-off charge cloud of radius $r_0=2e^2/3mc^2$.

For the mutual energy of two electric particles of masses m and M we obtain from (6) with $X_0=r/R_0$ and $R_0=2e^2/3Mc^2$

$$E^0_{mM}=(e^2/r)(2/\pi)\int_0^\infty dw\,\sin w\,w^{-1}\times(1+w^2/x_0{}^2)^{-\frac{1}{2}}(1+w^2/X_0{}^2)^{-\frac{1}{2}}. \quad (10)$$

We discuss this integral in the limit $M=\infty$ where $X_0=\infty$. Here (10) reduces to

$$E^0_{m\infty}=(e^2/r)(2/\pi)\int_0^\infty dw\,\sin w\,w^{-1}(1+w^2/x_0{}^2)^{-\frac{1}{2}}=(e^2/r)(2/\pi)\int_0^{x_0}dw\int_0^\infty dt\,\cos(wt)(1+t^2)^{-\frac{1}{2}}=(e^2/r)(2/\pi)\int_0^{x_0}dwK_0(w),$$

where K_0 is the Bessel function. For $x_0=r/r_0=\infty$ this reduces to e^2/r. In general one can say that a test charge of mass ∞ in the distance r from the charge e of mass m feels a Coulomb potential of the smaller charge

$$e'=e(2/\pi)\int_0^{r/r_0}dwK_0(w)<e. \quad (11)$$

Since $K_0(w)$ for small w is $-\lg w+\lg 2-\gamma=-\lg w+0.11593$, the potential energy at small distance becomes

$$E^0_{m\infty}=(e^2/r_0)(2/\pi)[1.11593+\lg(r_0/r)]=(3mc^2/\pi)\lg(3.052\,r_0/r).$$

For $M\gg m$ one obtains approximately

$$E^0_{M\gg m}=(3mc^2/\pi)\lg(3.052\,M/m). \quad (12)$$

Whether the formulae (10, 11, 12) for particles of different masses have any physical significance depends on whether the protonic mass is or is not of electromagnetic character. It seems more reasonable to assume that the mass of the proton is mainly that of a neutron, plus a small electron mass. In this case the *electric* forces between electrons and protons, and between protons and protons, would be of the same type (9) as between electronic particles, with r_0 being the *electronic* radius.

The potential energy between two electrons remains finite and differentiable even for $r=0$, whereas the potential energy $E^0_{m\infty}$ between the electron and a test charge of infinite mass ($R_0=0$) becomes logarithmically infinite for $r=0$. This is a distinction similar to that between the potential of the vector E (which remains finite), and the potential of the vector D (that becomes infinite for $r=0$) in the unitary theory of *Born* and *Infeld*[4]).

[4] M. Born, Proc. Roy. Soc. **A143**, 410 (1934).

4. Self-Energy of Particles in Motion

In order to find the electromagnetic self-energy of a particle in motion we need the average of $(\cos\zeta'_{sj})^2$ over all angles ϑ_{sj}. Expanding (4′) into powers of β^2 we obtain the average

$$(\cos\zeta'_{sj})_{Av}=\cos^2\zeta_s + \frac{4}{3}\beta^2\left(\frac{\omega_s^2}{\omega_0^2}\cos^4\zeta_s-\frac{\omega_s^4}{\omega_0^4}\cos^2\zeta_s\right)+\cdots,$$

if we neglect terms in β^4. Remembering that the average of $\cos^2\vartheta_{sj}$ is $\frac{1}{3}$ and that of $\sin^2\vartheta_{sj}$ is $\frac{2}{3}$ we obtain from (6) the self-energy of a moving particle

$$E=(2e^2\omega_0/c)\left[\beta^2\frac{2}{3}\frac{1}{2}\frac{\pi}{2}+\frac{1}{2}\left(\frac{\pi}{2}+\frac{4}{3}\beta^2\frac{3\pi}{16}-\frac{4}{3}\beta^2\frac{\pi}{4}\right)\right]$$

$$=\tfrac{3}{4}mc^2(1+\tfrac{1}{2}\beta^2) \qquad (13)$$

in agreement with relativity if β^4 is neglected. The result is mainly due to the *invariance* of the phase and amplitude reduction.

Our considerations yield definite values for the self- and mutual-energies. We cannot expect that quantum theory will change these values materially. In particular, there is no reason why the self-energy should be multiplied by a factor of order 1000 on account of the magnetic dipole energy of a spinning charge cloud. This expectation would be just as wrong as the expectation of an infinite self-energy from the picture of a point charge.

In conclusion: The electromagnetic self-energy of a charged particle is finite. Hence there must also be a deviation from Coulomb's law so as to eliminate Coulomb's singularity for $r=0$. We have tried to find the modified interaction energy and the corresponding finite self-energy by a modification of Fermi's radiation theory, taking account of the classical uncertainty of position due to the natural line breadth.

Our next task is that of trying to deduce the modified energy expression (6) from a corresponding modification of the general set-up of radiation theory. Fermi's theory is based on standing waves rather than on incoming and outgoing waves. Since standing waves account for retarded and advanced potentials in a symmetrical fashion, they cannot adequately describe the very radiation damping that was the starting point of our approach. Indeed, radiation damping is due to transforming an incoming plane wave into an outgoing spherical wave. (The corresponding difficulties in the unreduced theory are much greater due to the *infinite* self-field of the electron.)

5. Modified Fermi Theory

Fermi[3] Eq. (140) introduces a Fourier expansion of the scalar and vector potential into standing waves in a large volume Ω:

$$V(r,t)=c(8\pi/\Omega)^{\frac{1}{2}}\sum_s Q_s(t)\cos\Gamma_{sr},$$
$$U(r,t)=c(8\pi/\Omega)^{\frac{1}{2}}\sum_s[\alpha_s\chi(t)+A_sq_s(t)]\sin\Gamma_{sr}, \qquad (14)$$
$$\Gamma_{sr}=\omega_s(\alpha_s\cdot r)/c+\text{phase}.$$

α_s and A_s are unit vectors longitudinal and transversal to the wave s. Substitution of (14) into the Maxwell equations with $\operatorname{div}U-\partial V/\partial ct=0$ leads to the following differential equations for Q_s, χ_s and q_s:

$$d^2Q_s/dt^2+\omega_s^2Q_s=c(8\pi/\Omega)^{\frac{1}{2}}\sum_i e_i\cos\Gamma_{si},$$
$$d^2\chi_s/dt^2+\omega_s^2\chi_s=(8\pi/\Omega)^{\frac{1}{2}}\sum_i e_i(\alpha_s\dot r_i)\sin\Gamma_{si}, \qquad (15)$$
$$d^2q_s/dt^2+\omega_s^2q_s=(8\pi/\Omega)^{\frac{1}{2}}\sum_i e_i(A_s\dot r_i)\sin\Gamma_{si}.$$

Equation (15) has homogeneous solutions Q^0, χ_s^0, q_s^0 superposed by solutions of the inhomogeneous

equation which are

$$Q_s^1(t)=c(8\pi/\Omega)^{\frac{1}{2}}\sum_i e_i\omega_s^{-2}(1-\beta_i^2\cos^2\vartheta_{si})^{-1}\cos\Gamma_{si},$$

$$\begin{matrix}\chi^1\\ q_s\end{matrix}(t)=c(8\pi/\Omega)^{\frac{1}{2}}\sum_i e_i\beta_i\begin{matrix}\sin\\ \cos\end{matrix}\vartheta_{si}\omega_s^{-2}(1-\beta_i^2\cos^2\vartheta_{si})^{-1}\sin\Gamma_{si}, \tag{16}$$

when we suppose that $\dot r_i/c=\beta_i$ and $\ddot r_i=0$. ϑ_{si} is the angle between s and β_i. By virtue of (16) and (14) the field at every point r is composed of contributions of every single particle in a *symmetric* fashion, aside from the pure field derived from Q^0, χ^0, q^0.

Referring to the amplitude reduction and the phase lag (4′) we now define reduced quantities $\mathbf{Q}_s$, $\boldsymbol{\chi}_s$, $\mathbf{q}_s$ as the solutions of the following differential equation

$$d^2\mathbf{Q}_s/dt^2+\omega_s^2\mathbf{Q}_s=c(8\pi/\Omega)^{\frac{1}{2}}\sum_i e_i\cos\zeta'_{si}\cos(\Gamma_{si}+\zeta'_{si}), \tag{17}$$

etc. Compare these with (15). The solutions are $\mathbf{Q}_s=\mathbf{Q}_s^0+\mathbf{Q}_s^1$, etc. Here $\mathbf{Q}_s^0$ is identical with the former Q_s^0 whereas $\mathbf{Q}_s^1$ is reduced in amplitude and lags in phase:

$$\mathbf{Q}^1(t)=c(8\pi/\Omega)^{\frac{1}{2}}\sum_i e_i\omega_s^{-2}(1-\beta_i^2\cos^2\vartheta_{si})^{-1}\cos\zeta'_{si}\cos(\Gamma_{si}+\zeta'_{si}), \tag{17′}$$

etc., to be compared with (16). We also define reduced potentials at the place of the particle e_i.

$$\begin{aligned}\mathbf{V}(i,t)&=c(8\pi/\Omega)^{\frac{1}{2}}\sum_s\mathbf{Q}_s\cos\zeta'_{si}\cos(\Gamma_{si}+\zeta'_{si}),\\ \mathbf{U}(i,t)&=c(8\pi/\Omega)^{\frac{1}{2}}\sum_s(\alpha_s\boldsymbol{\chi}_s+A_s\mathbf{q}_s)\cos\zeta'_{si}\sin(\Gamma_{si}+\zeta'_{si}).\end{aligned} \tag{17″}$$

Given positions and given velocities of the particles produce Fourier components (17′) satisfying (17). Equations (15) are the Fourier representation of Maxwell's equations including $\mathrm{div}\,U-\partial V/\partial ct=0$. Since (15) for $\mathbf{Q}_s$ is equivalent to (17) for Q_s, Eqs. (17) are only another form of Maxwell's equations as long as $\ddot r=0$.

6. Energy of Particles in a Field

In Fermi's (154) we write $\dot r_i$ for $-c\gamma_i$, 1 for δ_i, which is immaterial for our main task, which is to *deduce* (6) *from a Hamiltonian*. We propose the following modification of Fermi's Hamiltonian (154):

$$\begin{aligned}H=&\sum_i m_ic^2+\sum_s\sum_i(\dot r_ip_i)+c(8\pi/\Omega)^{\frac{1}{2}}\sum_s\mathbf{Q}_s\sum_i e_i\cos\zeta'_{si}\cos(\Gamma_{si}+\zeta'_{si})\\ &-(8\pi/\Omega)\sum_s\sum_i(\dot r_i,\alpha_s\chi_s+A_s\mathbf{q}_s)\cos\zeta'_{si}\sin(\Gamma_{si}+\zeta'_{si})\\ &+\tfrac{1}{2}\sum_s[(\mathbf{p}_s^2+\xi_s^2-\mathbf{P}_s^2)+\omega_s^2(\mathbf{q}_s^2+\chi_s^2-\mathbf{Q}_s^2)].\end{aligned} \tag{18}$$

H differs in the terms containing ζ'_{si} from the unreduced Fermi Hamiltonian. Nevertheless, as we shall see in (20), the energy of the pure field is the same as in Maxwell's theory, and only the mutual energy is changed. As "coordinates" we consider the reduced quantities $\mathbf{Q}_s$, $\boldsymbol{\chi}$, $\mathbf{q}_s$; the conjugate "momenta" are $\mathbf{P}_s$, ξ_s, $\mathbf{p}_s$. As equations of motion $\partial H/\partial\mathbf{Q}_s=-d\mathbf{P}_s/dt$, $\partial H/\partial\mathbf{P}_s=d\mathbf{Q}_s/dt$ we obtain the former Eqs. (17) which, as we saw before, are equivalent to Maxwell's equations for $\ddot r_i=0$. Furthermore, the first four terms of (18) can be written

$$\begin{aligned}&\text{Energy}=\text{rest}+\text{potential}+\text{kinetic energy}\\ &E=\sum_i[m_ic^2+e_i\mathbf{V}(i)+(\beta_i,p_i-e_i\mathbf{U}(i)/c)],\end{aligned} \tag{18′}$$

representing the Hamiltonian of a system of electric particles under the reduced potentials $\mathbf{V}$ and $\mathbf{U}$, defined in (17″) with the Fourier amplitudes $\mathbf{Q}_s=\mathbf{Q}_s^0+\mathbf{Q}_s^1$, etc. and $\mathbf{Q}_s^0=Q_s^0$. According to (18′) a monochromatic external potential Q_s acts on the particle with a potential $\mathbf{V}$ that is reduced by the factor $\cos\zeta'_{si}$ and has a phase lag ζ'_{si} behind the phase of Q_s. At the same time there is no damping term in (18′). The motion of the electron under this reduced external potential then is the same as its motion according to the usual theory where the effect of the unreduced potential is accompanied by that of a damping term. The terms $\mathbf{Q}_s^1$ in $\mathbf{V}$ calculated for vibrating electrors have no phase

lag and will not produce an additional damping effect. This result seems very inconsistent indeed. But we must remember that the method of standing waves accounts for advanced and retarded potentials simultaneously, not only for an external potential Q_s^0 but also for the potential $\mathbf{Q}_s^1$ produced by a particle on itself. The whole problem needs further clarification.

7. Transformation of the Energy

We now turn to transforming the energy (18) into a more convenient form in which the Hamiltonian form is abandoned, however. p_i is the total momentum, $p_i - e_i\mathbf{U}(i)/c$ is the kinetic momentum $(p_i)^{\text{kin}}$. It does not matter in (17) that $(p_i)^{\text{kin}}$ and m_ic^2 split up into an electromagnetic and a mechanical part in the ratio of 3 to 1 (see below). Only the mechanical part is to be carried in m_ic^2 and $(\dot{r}_ip_i)^{\text{kin}}$, the electromagnetic part being contained in the other terms of (18). The potential momentum is a part of the second sum in (18) and cancels the negative potential momentum represented by the fourth sum of (18). This leaves for the total energy:

$$E=\sum_i m_ic^2+\sum_i (\dot{r}_ip_i)^{\text{kin}}+c(8\pi/\Omega)^{\frac{1}{2}}\sum_i e_i\sum_s \mathbf{Q}_s\cos(\Gamma_{si}+\zeta'_{si})\cos\zeta'_{si}$$
$$\times\tfrac{1}{2}\sum_s[(\mathbf{p}_s^2+\boldsymbol{\xi}_s^2-\mathbf{P}_s^2)+\omega_s^2(\mathbf{q}_s^2+\boldsymbol{\chi}_s^2-\mathbf{Q}_s^2)]. \quad (19)$$

A further simplification is obtained by virtue of [Fermi's (160)(161)]

$$\omega_s\boldsymbol{\chi}_s-\mathbf{P}_s=0, \quad \boldsymbol{\xi}_s=\omega_s\mathbf{Q}_s-(c/\omega_s)(8\pi/\Omega)^{\frac{1}{2}}\sum_j e_j\cos\zeta'_{sj}\cos(\Gamma_{sj}+\zeta'_{sj}),$$

which results in

$$E=\sum_i m_ic^2+\sum_i(\dot{r}_ip_i)^{\text{kin}}+(4\pi c^2/\Omega)\sum_s\omega_s^{-2}(\sum_i e_i\cos\zeta'_{si}\cos(\Gamma_{si}+\zeta'_{si})+\tfrac{1}{2}\sum_s(\mathbf{p}_s^2+\omega_s^2\mathbf{q}_s^2).$$

At last we can use the relations $\dot{\mathbf{q}}_s=\mathbf{p}_s$ so that

$$\mathbf{q}_s^2=(\mathbf{q}_s^0)^2+(\mathbf{q}_s^1)^2+2\mathbf{q}_s^0\mathbf{q}_s^1,$$
$$\mathbf{p}_s^2=(\dot{\mathbf{q}}_s^0)^2+(\dot{\mathbf{q}}_s^1)^2+2\dot{\mathbf{q}}_s^0\dot{\mathbf{q}}_s^1.$$

When summing over s the double products vanish because of independent phases. q_s' can be taken from (16) whereas $(\dot{q}_s')^2$ is small and of order β^4. Thus the energy becomes (if we neglect β^4)

$$E=\sum_i m_ic^2+\sum_i(\dot{r}_ip_i)^{\text{kin}}+\tfrac{1}{2}\sum_s[(p_s^0)^2+\omega_s^2(q_s^0)^2]$$
$$+(4\pi c^2/\Omega)\sum_s\omega_s^{-2}\{(\sum_i e_i\beta_i\sin\vartheta_{si}\sin(\Gamma_{si}+\zeta'_{si})\cos\zeta'_{si})^2+(e_i\cos(\Gamma_{si}+\zeta'_{si})\cos\zeta'_{si})^2\}. \quad (20)$$

E consists of the mechanical rest and kinetic energy of the particles, the pure field energy, and the mutual energy between field and particles. For the latter (20) yields the expression used before in (6) *q.e.d.*

The attempt to incorporate the phase lag and the amplitude reduction into the general set-up of the radiation theory cannot be considered as satisfactory because of inherent difficulties of the standing wave method. Nevertheless the results obtained in the case of particles at rest or in uniform motion may be considered as a supplement to Dirac's investigation[1] of the classical electron. Dirac has shown that the "own radiation field" of a particle leads to a self-accelerated motion in which the term $\exp(-r/r_0)$ plays a major rôle. We have tried to show here that radiation damping when accounted for by the modified energy (6), leads to a mutual energy between two particles of the extremely simple form

$$E_{12}=(e^2/r)[1-\exp(-r/r_0)].$$

The corresponding electromagnetic self-energy ($E_1=\frac{1}{2}E_{12}$ for $r=0$) is $\frac{3}{4}mc^2$ contradicting those who think that the mass ought to be completely of electromagnetic origin, and confirming the present idea[1,5] that only a part of the mass can be electromagnetic.

[5] W. Heitler, *Quantum Theory of Radiation* (Oxford, 1936), p. 33. See also reference 1.

The Forces Between Neutral Molecules and Metallic Surfaces

H. MARGENAU, *Yale University, New Haven, Connecticut*

AND

W. G. POLLARD, *University of Tennessee, Knoxville, Tennessee*

(Received May 23, 1941)

A general formula is developed for the interaction between a neutral molecule and a metal, and its relation to the image force law is exhibited, (Section III). The latter is shown to be valid only for molecules containing slowly moving charges, such as rigid permanent dipoles. A fairly accurate evaluation of the general formula involving empirical polarizabilities, f values, and resonance frequencies is made in Section IV. The numerical values for a number of gases and metals are collected in Tables I and II.

I. INTRODUCTION

EXAMINATION of the rapidly growing experimental[1] material dealing with the adsorption of gases on metallic surfaces has brought into evidence the action of two types of forces which cause neutral molecules to be attracted to metals: unsaturated valences and van der Waals interactions. The former produce the phenomena often referred to as *chemisorption*, the latter give rise to what is now commonly called *physical* or *van der Waals* adsorption. The two types occur generally in different ranges of temperature; physical adsorption is usually predominant at low, while chemisorption sets in strongly at high, temperatures, a fact which is most easily explained by supposing that chemisorption requires activation but physical adsorption does not. (For this reason chemisorption is sometimes called "activated adsorption.") The energy liberated by physical adsorption is much smaller than that evolved in chemisorption; the values of the heats of adsorption for the former type are in the neighborhood of 4000 cal./mole (=0.17 electron volt/molecule) while the latter leads to values between 10,000 and 200,000 cal./mole.

The distinction here discussed is best clarified, perhaps, by reference to a typical graph (Fig. 1) in which the volume of gas adsorbed on a metal surface is plotted against the temperature at which adsorption occurs. At low temperatures, van der Waals forces attract a large amount of gas to the surface. Because of the weak binding produced by these forces, these molecules are easily driven off when the temperature rises. But at sufficiently high temperatures the chemical forces, which come into play only when the kinetic energy of the molecules is great enough to supply the heat of activation, cause larger volumes of gas to be occluded to the metal. These, in turn, are released at very high temperatures when the kinetic energy of the molecules becomes comparable with the heats of chemisorption.

Accessory features, such as the phenomenon of surface catalysis and the dependence of heats on the nature of the crystal face, complicate the problem of chemisorption. Even aside from these, a detailed calculation of the attractive valence forces between the gas molecules and the metal surface is hardly feasible at present and will not be undertaken here. The van der Waals forces, on the other hand, are amenable to reasonably accurate treatment; they are the object of the present study. Attention will be given only to the attractive part of these forces, operative at distances of separation greater than the diameter of the molecules. And even here, only the long range constituent proportional to D^{-7} (dipole-dipole force) will be considered. In a subsequent paper by one of us[2] a composition of the attractive van der Waals with the re-

[1] For a summary of experimental work see: N. K. Adams, *The Physics and Chemistry of Surfaces*, second edition (Oxford University Press, 1938), *The Adsorption of Gases by Solids* (The Faraday Society, 1932); also in Trans. Faraday Soc. **28**, 131–447 (1932); J. K. Roberts, *Some Problems in Adsorption* (Cambridge Physical Tracts No. 7, 1939).

[2] W. G. Pollard, to be submitted.

pulsive exchange forces will be undertaken, a procedure which leads to a numerical evaluation of the minimum potential energy thus created and hence to an estimate of the heats of van der Waals adsorption.

One of the first attacks upon the problem was made by Lennard-Jones[3] who calculated the interaction between a molecule and a metal by the image method, a procedure which implies that the electrons in the molecule create images of opposite charge within the metal and that these images move in definite phase relations with the molecular charges. The result obtained for the potential energy of interaction has the simple form

$$W = -e^2\langle R^2\rangle_{Av}/12D_0^3 \qquad (1)$$

where $\langle R^2\rangle_{Av}$ is the mean square displacement of all electrons in the molecule and D_0 the distance of the molecule from the metal surface. Specific properties of the metal do not enter into the formula because all metals are assumed to be perfect conductors.

There is, of course, an obvious criticism of the assumptions leading to (1). The electrons in the metal can adjust themselves to form images of static or slowly moving external charges, but because of their finite relaxation time they are incapable of simulating the very rapid motions of the instantaneous dipoles composing a non-polar molecule. In fact while a metal is a reasonably perfect conductor with respect to alternating fields of low frequencies, it takes on the properties of non-conductors at frequencies not far beyond the visible range, and this happens in a manner peculiar to each metal. Now the molecules and atoms whose heats of adsorption have been investigated, particularly the rare gases, have resonance frequencies far in the ultraviolet, so that one would expect a metal to behave in these interactions not so much like a perfect conductor characterized by image forces, but more like an insulator. We note in this connection that the method of London[4] for computing heats of adsorption of non-conductors, which takes no account whatever of the presence of free electrons, yields even for metals numerical values that are comparable with experimental data.

[3] J. E. Lennard-Jones, Trans. Faraday Soc. **28**, 334 (1932).
[4] F. London, Zeits. f. physik. Chemie, **B11**, 222 (1930).

Two conclusions may be drawn from these qualitative considerations: Because the metallic electrons cannot maintain the proper phase with the rotating molecular dipoles, the correct interaction law will yield smaller values than (1); the properties of the metal must enter explicitly. These expectations were verified in a calculation the results of which have been reported by the present authors.[5]

A result perhaps somewhat at variance with these considerations was reported by Prosen, Sachs, and Teller.[6] More recently, Bardeen[7] has made a careful analysis of the problem in which particular attention is directed to the interaction of the electrons within the metal. It also leads to the conclusion that the image force generally yields too strong an attraction. Bardeen's results agree on the whole with those presented in this paper. Although there are several points of contact, the method here used is different and somewhat more in line with the theory of van der Waals forces; we also believe it to be simpler.

II. Preliminary Considerations

We consider the classical interaction energy ΔV between a molecule situated at the origin of coordinates and an elementary portion ω of metal at **D**. By an elementary portion is meant a volume of smaller dimensions than the wavelength of radiation corresponding to the pre-

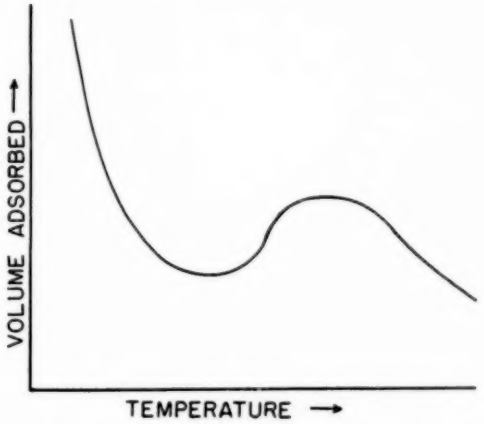

FIG. 1. Typical dependence on temperature of gaseous volume adsorbed.

[5] W. G. Pollard and H. Margenau, Phys. Rev. **57**, 557 (1940).
[6] E. J. R. Prosen, R. G. Sachs, and E. Teller, Phys. Rev. **57**, 1066 (1940).
[7] J. Bardeen, Phys. Rev. **58**, 727 (1940).

dominant resonance frequencies of the molecule, but large enough to possess the bulk properties of the metal. The latter supposition will permit us to compute the total interaction between molecule and metal by summing over the elementary portions; the former requirement is needed to make the formulas for the polarizability, stated [cf. Eq. (5)] and used below, meaningful. With the molecule there is associated, at every instant, a displacement vector $\mathbf{R}^{(1)}$ defined by postulating that the dipole moment be $e\mathbf{R}^{(1)}$. Thus if the molecule is monatomic, $\mathbf{R}^{(1)}=\sum_i \mathbf{r}_i^{(1)}$, the summation extending over the displacements of the individual electrons.

The potential at $\mathbf{D}$ due to the molecular charges at 0 is $\phi(\mathbf{D})=e\mathbf{R}^{(1)}\cdot\mathbf{D}/D^3$. Therefore, if the portion of metal, ω, contains n positive charges at D_i^+ and n negative charges at D_i^- where $i=1, 2, \cdots n$, the mutual potential energy between the molecule and ω will be

$$V=-e^2\sum_i^n[\mathbf{R}^{(1)}\cdot\mathbf{D}_i^+/(D_i^+)^3]+e^2\sum_i^n[\mathbf{R}^{(1)}\cdot\mathbf{D}_i^-/(D_i^-)^3]. \quad (2)$$

If $\mathbf{D}$ is the vector to some fixed point in ω and

$$\mathbf{D}_i^+=\mathbf{D}+\mathbf{r}_i^+, \quad \mathbf{D}_i^-=\mathbf{D}+\mathbf{r}_i^-;$$

V may be expanded provided $|r_i^\pm|\ll D$, yielding the familiar dipole energy

$$V=-e(\mathbf{R}^{(1)}-(\mathbf{R}^{(1)}\cdot\mathbf{D}/D^2)\mathbf{D})\cdot\sum_i e(\mathbf{r}_i^+-\mathbf{r}_i^-)/D^3.$$

The summation appearing here is the dipole moment of ω for which we shall henceforth write $e\mathbf{R}^{(2)}$. When, furthermore, the Z-axis is taken along $\mathbf{D}$, V becomes

$$V=-e^2(X^{(1)}X^{(2)}+Y^{(1)}Y^{(2)}-2Z^{(1)}Z^{(2)})/D^3, \quad (3)$$

$X^{(1)}$, $X^{(2)}$, etc., being the components of the vectors $\mathbf{R}^{(1)}$, $\mathbf{R}^{(2)}$, respectively.

If we assume that the molecule has no permanent dipole moment, the integral of V over the charge distribution of the molecule is zero. The state function of metal+molecule may, for the purpose of calculating van der Waals forces, be taken to be a product of $\psi(1)$ and $\psi(2)$, the former depending only on the state of the molecule, the latter only on the metal. The first-order perturbation is then zero, and the interaction energy is given by

$$\sum_\kappa{}' \frac{|V_{k\kappa}|^2}{E_k-E_\kappa}.$$

Since each state κ depends on the quantum numbers of the molecule (κ_1) and of the metal (κ_2), the energy may be written more explicitly as follows

$$W_\omega=\sum_{\kappa_1\kappa_2}{}' \frac{|(k_1k_2|\,V\,|\kappa_1\kappa_2)|^2}{E(k_1)-E(\kappa_1)+E(k_2)-E(\kappa_2)}.$$

In view of (3) this becomes

$$W_\omega=-\frac{e^4}{D^6}\sum_{\kappa_1\kappa_2}[E(\kappa_1)-E(k_1)+E(\kappa_2)-E(k_2)]^{-1}\times\{|(k_1|X^{(1)}|\kappa_1)(k_2|X^{(2)}|\kappa_2)|^2+|(k_1|Y^{(1)}|\kappa_1)(k_2|Y^{(2)}|\kappa_2)|^2+4|(k_1|Z^{(1)}|\kappa_1)(k_2|Z^{(2)}|\kappa_2)|^2\}. \quad (4)$$

The cross terms have disappeared from (4) because in the summation over that part of κ_1 on which the energy of the state $E(\kappa_1)$ does not depend, terms like $X_{k_1\kappa_1}{}^{(1)}$ vanish for a molecule possessing no permanent dipole moment. For dipole molecules, the meaning of W_ω must be modified. See remarks after Eq. (7).

As is customary in calculations of this sort, Eq. (4) will subsequently be transformed by the use of well-known formulas for the "atomic" polarizability. The polarizability of a physical system having instantaneous dipole moment $\mathbf{R}$, due to electrical waves of frequency ν and electric vector along X, is given by

$$\alpha_x(\nu)=2e^2\sum_\kappa\frac{|(k|X|\kappa)|^2[E(\kappa)-E(k)]}{[E(\kappa)-E(k)]^2-(h\nu)^2}. \quad (5)$$

The static polarizability, in accordance with (5), takes the form

$$\alpha_x(0)=2e^2\sum_\kappa[|(k|X|\kappa)|^2/E(\kappa)-E(k)]. \quad (5a)$$

Equation (5) holds for the element of metal as well as the molecule if exact metal wave functions are used in the evaluation of $(k|X|\kappa)$. The fact that these are difficult to calculate need not disturb us here, for the values of α may be taken from experiment or expressed in some other computationally more convenient way.

III. Image Force Formula

In this section it will be shown how Eq. (4) reduces to the expression for the image force. One simply assumes that the energy differences $E(\kappa_1)-E(k_1)$ are much smaller than those for the metal. This implies that the charges in the molecule move more slowly than those in the metal. Under these circumstances the summation over κ_1 appearing in (4) may be carried out and (4) becomes

$$W_\omega = -(e^4/D^6)\cdot\tfrac{1}{3}(k_1|R^{(1)^2}|k_1) \cdot\sum_{\kappa_2}[6|(k_2|X^{(2)}|\kappa_2)|^2/E(\kappa_2)-E(k_2)], \quad (6)$$

provided it is proper to put

$$(k_1|X^{(1)^2}|\kappa_1)=(k_1|Y^{(1)^2}|\kappa_1) =(k_1|Z^{(1)^2}|\kappa_1)=\tfrac{1}{3}(k_1|R^{(1)^2}|\kappa_1) \quad (7)$$

for the ground state k_1. Similar relations are assumed to hold for the metal. Eq. (7) is obvious when the molecule has a spherically symmetrical charge distribution. Otherwise it is necessary to perform, in addition to the summation over κ_1 indicated in (4), an average over all orientations of the molecule in state k_1, and (6) represents this average. Assumption (7) with respect to the metal implies equal polarizabilities in all directions. With the use of (5a),

$$W_\omega = -(e^2/D^6)(k_1|R^{(1)^2}|k_1)\alpha^{(2)}(0).$$

The static polarizability of a metal is its volume divided by 2π, as is known from an elementary argument.[8] Therefore, the interaction energy between the molecule and the entire metal, which is taken to be infinite in both the X and Y directions but extends along Z from D_0 to ∞, will be

$$W=-\frac{e^2}{2\pi}(k_1|R^{(1)^2}|k_1)\int\frac{d\tau}{D^6}=-\frac{e^2(k_1|R^{(1)^2}|k_1)}{12D_0^3}.$$

This is Lennard-Jones' formula (1). The present derivation emphasizes its inadequacy for the case of non-polar molecules which have significant energy differences $E(\kappa_1)-E(k_1)$ far greater than the metal, and their neglect falsifies the result completely. On the other hand, if the molecule is rigid and possesses a permanent dipole moment so that its energy differences are those appearing in rotational band lines, the neglect is permissible and (1) should be nearly correct. In physical terms, the electrons in the metal are able to maintain the proper phase with the slowly rotating dipole, but not with the rapidly revolving electrons in a non-polar atom or molecule.

Since $E(k_1)-E(\kappa_1)$ is positive for every κ_1 when k_1 denotes the ground state, it is also clear that the image force law gives too large a result for W.

IV. General Formula

In treating the problem further, restriction will at once be made to molecules having a spherical charge distribution. Equation (4) then reduces to

$$W_\omega = 6S,$$

where

$$S=-\frac{e^4}{D^6}\sum_{\kappa_1\kappa_2}\frac{|(k_1|X^{(1)}|\kappa_1)|^2|(k_2|X^{(2)}|\kappa_2)|^2}{E(\kappa_1)-E(k_1)+E(\kappa_2)-E(k_2)}. \quad (8)$$

After multiplying numerator and denominator of each term in this expression by $[E(\kappa_1)-E(k_1)]-[E(\kappa_2)-E(k_2)]$ there results, on using (5),

$$S=-\frac{e^2}{2D^6}\{\sum_{\kappa_1}\alpha^{(2)}(\nu_{\kappa_1})|(k_1|X^{(1)}|\kappa_1)|^2 +\sum_{\kappa_2}\alpha^{(1)}(\nu_{\kappa_2})|(k_2|X^{(2)}|\kappa_1)|^2=S_1+S_2. \quad (9)$$

Here $\alpha^{(2)}(\nu_{\kappa_1})$ is the polarizability of the metal at the frequency ν_{κ_1} corresponding to the transition of the molecule from the state κ_1 to the ground state k_1; $e|X^{(1)}|$ is the dipole moment connected with that transition. In the second part of (9) the summation is over the polarizabilities of the molecule at the resonance frequencies of the metal, multiplied by the matrix elements of the corresponding transitions.

The first summation occurring in (9) may be evaluated empirically if $\alpha^{(2)}$, obtainable from the optical properties of the metal, is known as a function of the frequency. The matrix elements $|(k_1|X^{(1)}|\kappa_1)|^2$ are simply related to the f values of the molecular transitions. The calculation of S_1 is particularly easy when the visiting molecule is one whose resonance frequencies lie in the ultraviolet and whose dispersive properties are well described by a one-term dispersion formula.

[8] A slab of metal in an electric field E acquires a surface charge of density $\sigma=E/2\pi$. If its thickness is d and its area A its dipole moment is $\sigma Ad=E\tau/2\pi$ where τ denotes its volume.

TABLE I. *Interaction energies, in volts, at a distance 10^{-8} cm from the surface of the metal. Last column for* Na *represents interaction between metal ions and the visiting molecule.*

		W_1	W_2	W	BARDEEN	IMAGE FORCE	W_{ions}
	He	0.01	−0.16	−0.15	−0.12	−0.61	
	Ne	0.01	−0.30	−0.29	−0.24	−1.25	
Cs	A	0.07	−1.25	−1.18	−0.92	−3.54	
	H_2	0.04	−0.62	−0.58	−0.42	−1.40	
	N_2	0.08	−1.33	−1.25	−1.11	−3.95	
	He	0.02	−0.23	−0.21	−0.16	−0.61	−0.013
	Ne	0.03	−0.43	−0.40	−0.32	−1.25	−0.025
Na	A	0.20	−1.80	−1.60	−1.19	−3.54	−0.087
	H_2	0.12	−0.89	−0.77	−0.53	−1.40	−0.038
	N_2	0.24	−1.92	−1.68	−1.42	−3.95	−0.086
	He	0.04	−0.30	−0.26	−0.20	−0.61	
	Ne	0.08	−0.57	−0.49	−0.39	−1.25	
Ag	A	0.47	−2.37	−1.90	−1.42	−3.54	
	H_2	0.28	−1.18	−0.90	−0.62	−1.40	
	N_2	0.55	−2.53	−1.98	−1.78	−3.95	
	He	0.05	−0.31	−0.27	−0.20	−0.61	
	Ne	0.09	−0.59	−0.51	−0.40	−1.25	
Pt	A	0.53	−2.49	−1.96	−1.46	−3.54	
	H_2	0.32	−1.23	−0.92	−0.64	−1.40	
	N_2	0.62	−2.65	−2.03	−1.72	−3.95	
	He	0.06	−0.34	−0.28	−0.21	−0.61	
	Ne	0.11	−0.64	−0.53	−0.42	−1.25	
Cu	A	0.67	−2.69	−2.02	−1.52	−3.54	
	H_2	0.41	−1.34	−0.93	−0.67	−1.40	
	N_2	0.80	−2.88	−2.08	−1.80	−3.95	

Since this is true for most of the simpler molecules, these assumptions will here be made. The summation over κ_1 then reduces to a single term and one obtains

$$S_1=-\frac{e^2h^2}{4mD^6}\alpha^{(2)}(\nu_1)\frac{f_1}{h\nu_1}, \tag{10}$$

since the oscillator strength of the resonance transition having frequency ν_1 is related to the matrix element by

$$f_1=\frac{2mh\nu_1}{h^2}|(k_1|X|\kappa_1)|^2.$$

The second summation in (9) is a little more difficult to handle. First, we shall present a simple evaluation which is rather crude but shows the physical meaning and order of magnitude of the term. Since the metallic transitions ν_{κ_2} are generally of smaller frequency than the resonance frequencies of the molecule, the polarizability of the latter, $\alpha^{(1)}(\nu_{\kappa_2})$, may be approximated by its static value $\alpha^{(1)}(0)$, obtainable from the dielectric constant of the gas. This leaves us with the calculation of $\sum_{\kappa_2}|(k_2|X|\kappa_2)|^2$. If, however, we multiply numerator and denominator of each term in this sum by $[E(\kappa_2)-E(k_2)]$ the result may be written, in view of (5a)

$$\frac{1}{2e^2}\Delta E_{Av}^{(2)}\alpha^{(2)}(0),$$

where $\Delta E_{Av}^{(2)}$ is some rather vague mean excitation energy of the electrons in the metal, which one might estimate to be of the order of several volts. As pointed out in the previous section, $\alpha^{(2)}(0)=d\tau/2\pi$. On substituting these results in (9) one has

$$S=\left[-\frac{e^2h^2}{4m}\frac{f_1}{h\nu_1}A^{(2)}(\nu_1)-\frac{1}{8\pi}\alpha^{(1)}(0)\Delta E_{Av}^{(2)}\right]\frac{d\tau}{D^6}, \tag{11}$$

provided $A^{(2)}$ stands for the polarizability per unit volume of the metal so that $\alpha^{(2)}=A^{(2)}d\tau$. By (8) Eq. (11) must be multiplied by 6 to give W_ω and this is to be integrated over $d\tau$ to yield W. Hence

$$W=-\left[\frac{e^2h}{m}A^{(2)}(\nu_1)\frac{f_1}{\nu_1}+\Delta E_{Av}^{(2)}\alpha^{(1)}(0)\right]\Big/8D_0^3$$
$$=\quad W_1\quad+\quad W_2. \tag{12}$$

A satisfactory estimate of the uncertain $\Delta E_{Av}^{(2)}$ can be obtained from the work of Bardeen.[7] To see the connection between his analysis and the present we return to Eq. (2) which is the same as Bardeen's. This may be written

$$V=\mathbf{R}^{(1)}\cdot\text{grad}V,$$

if by grad$V$ is meant the operation with respect to any one of the $\mathbf{r}_i^{(1)}$, the coordinates of the molecular electrons. It is to be noted that grad$V$ depends only on the metal. If now we follow the procedure which led to Eq. (9) we find, in place of $6S_2$, the expression

$$W_2=-\sum_{\kappa_1\kappa_2}\frac{|(k_1|X^{(1)}|\kappa_1)|^2|(k_2|\text{grad}_xV|\kappa_2)|^2+|(k_1|Y|\kappa_1)|^2|(k_2|\text{grad}_yV|\kappa_2)|^2+|(k_1|Z|\kappa_1)|^2|(k_2|\text{grad}_zV|\kappa_2)|^2}{[E(\kappa_1)-E(k_1)]^2-(h\nu_{\kappa_2})^2}$$
$$\cdot(E(\kappa_1)-E(k_1)),$$

which, for a symmetrical molecule, reduces to

$$-\frac{1}{2e^2}\sum_{\kappa_2}\alpha^{(1)}(\nu_{\kappa_2})\,|(k_2|\ \mathrm{grad}\ V|\kappa_2)|^2,$$

again because of (5). Since all ν_{κ_2} are presumably far from the absorption region of the molecule, $\alpha^{(1)}(\nu_{\kappa_2})$ may be replaced by its static value. Then

$$W_2=-\frac{\alpha^{(1)}(0)}{2e^2}\sum_{\kappa_2}|(k_2|\ \mathrm{grad}V|\kappa_2)|^2$$
$$=-\frac{\alpha^{(1)}(0)}{2e^2}(k_2|(\mathrm{grad}V)^2|k_2).$$

Now the matrix element $(k_2|(\mathrm{grad}V)^2|k_2)$ for the ground state of the metal has been evaluated by Bardeen who finds it to be $Ce^4/8r_sD_0^3$ when computed for the entire metal (from $z=D_0$ to $z=\infty$). Here C is a numerical constant approximately equal to 2.5, r_s is the radius of a sphere containing one metal electron. Hence

$$W_2=-Ce^2\alpha^{(1)}/16r_sD_0^3.$$

This is to be identified with the second term in (12). We see, therefore, that the average excitation energy of the metal is given by

$$\Delta E_{Av}^{(2)}=Ce^2/2r_s. \qquad (13)$$

The energy W_2 appears also in Bardeen's work, it is the same as his W_B; but it enters into his final formula in a different and somewhat less conspicuous way.

It is interesting to compare Eq. (12) with the image force formula. For this purpose we may rewrite W_1 in terms of $\langle\mathbf{R}_1^2\rangle_{Av}$ by using $\hbar f_1/m\nu_1=(4\pi/3)\langle R_1^2\rangle_{Av}$. This converts Eq. (12) into

$$W=-\frac{\pi e^2\langle R_1^2\rangle_{Av}}{6D_0^3}A^{(2)}(\nu_1)+W_2. \qquad (12')$$

In order to compare the image potential with this expression, Eq. (1) may be rewritten so as to include the static polarizability $A^{(2)}(0)=1/2\pi$ of the metal. Equation (1) then becomes

$$W=-\frac{\pi e^2\langle R_1^2\rangle_{Av}}{6D_0^3}A^{(2)}(0). \qquad (1')$$

It is seen that (12') reduces to the image law (1') when W_2 is neglected and ν_1 is equated to 0 in W_1. These errors compensate to a considerable extent. While on the image force picture W_1 accounts for the entire interaction, W_2 is the main constituent of Eq. (12'). Indeed $A^{(2)}(\nu_1)$ is negative for the resonance frequencies of the molecule so that W_1 gives rise to a repulsion, as the tables show. Thus all resemblance of our final formula with the image law is lost.

V. Numerical Values

The resonance frequencies of all the molecules for which computations are made in this section are much higher than those of the absorption bands of the metals. For such frequencies the polarizability $A^{(2)}(\nu_1)$ of the metal is given by the simple relation,[9]

$$A^{(2)}(\nu_1)=-n_0e^2/4\pi^2m\nu_1^2,$$

where n_0 is the actual number of free electrons per unit volume of the metal and m is their true mass. The values of f_1, ν_1 and $\alpha^{(1)}(0)$ have been taken from a tabulation published by one of us.[10] In Table I are listed the values of W_1 and W_2 separately for various gases adsorbed on monovalent metals. The values tabulated are the various energies in volts at a distance of 10^{-8} cm from the surface of the metal and so represent the coefficient in volts of $1/D_0^3$ for

Table II. *Interaction energies, in volts, at a distance 10^{-8} cm from the surface of bivalent metals.*

	W_1	W_2	W	Bardeen	Metal
He	0.19	−0.48	−0.29	−0.26	
Ne	0.32	−0.91	−0.59	−0.53	
A	2.00	−3.79	−1.79	−1.82	Be
H_2	1.22	−1.88	−0.66	−0.78	
N_2	2.38	−4.04	−1.66	−2.13	
He	0.08	−0.38	−0.30	−0.23	
Ne	0.15	−0.72	−0.57	−0.46	
A	0.95	−3.02	−2.07	−1.63	Zn, Cd, Hg,
H_2	0.58	−1.50	−0.92	−0.71	rough average
N_2	1.13	−3.23	−2.10	−1.92	
He	0.04	−0.28	−0.24	−0.19	
Ne	0.06	−0.53	−0.47	−0.37	
A	0.39	−2.22	−1.83	−1.36	Mg, Ca, Sr, Ba
H_2	0.24	−1.10	−0.86	−0.60	rough average
N_2	0.46	−2.37	−1.91	−1.61	

[9] Cf. N. F. Mott and H. Jones, *Theory of the Properties of Metals and Alloys* (Oxford University Press, 1936), p. 115; F. Seitz, *Modern Theory of Solids* (McGraw-Hill, 1940), p. 641.

[10] H. Margenau, Rev. Mod. Phys. **11**, 1 (1939).

each W when D_0 is in angstroms. Table I also shows a comparison of the results here obtained with those of Bardeen and the image force law. The former values were computed from the relation[7]

$$W=-(e^2\langle R_1^2\rangle_{Av}/12D_0^3)(Ce^2/2r_s h\nu_1/1+Ce^2/2r_s h\nu_1)$$

developed by Bardeen, and the latter were obtained from Eq. (1). The agreement with Bardeen's theory appears on the whole satisfactory, although the values obtained from the latter are always lower than ours. Table II contains similar data for divalent metals.

The interaction between the metal ions and the visiting molecule is of course included in the basic formulas (9) and (11). But the approximations made in evaluating $A^{(2)}$ and $\Delta E_{Av}^{(2)}$ ignore this effect. It is therefore of interest to calculate it separately in order to exhibit its order of magnitude. This was done by the methods of reference 4 for the metal Na only. The interaction energy is also proportional to D_0^{-3}; the coefficient, in the same units as the others, is given in the last column of Table I. Clearly, this effect is generally negligible in comparison with that expressed by Eq. (12).

JULY 15, 1941 PHYSICAL REVIEW VOLUME 60

Magnetic Studies of Solid Solutions

II. The Properties of Quenched Copper-Iron Alloys

F. BITTER, A. R. KAUFMANN, C. STARR AND S. T. PAN
Massachusetts Institute of Technology, Cambridge, Massachusetts

(Received April 28, 1941)

The alloys of copper and iron which have been studied show unusual magnetic properties both in the saturation effects at low temperatures and in the apparent change in the magnetic moment of the dissolved iron atoms over the range of temperatures from 14°K to 1300°K. Further research is required on other alloy systems containing transition elements dissolved in the noble metals in order to ascertain whether the phenomena are due to fundamental magnetic properties or due to the state of aggregation of the iron atoms.

IN the first paper of this series[1] the authors described a method of measurement which has been used again for the present experiments. The only difference in this case is that the location of the specimen in the magnet has been changed slightly in order to have stable equilibrium and that the furnace of Fig. 2, Part I, has been replaced by a Dewar flask for low temperature measurements. The specimens were in an atmosphere of hydrogen for all experiments except those below 60°K for which a mixture of hydrogen and helium was used.

Some preliminary results presented in Part I on alloys of copper with small percentages of iron showed that the magnetic properties depended in a complicated way on the heat treatment of the specimens. In an effort to narrow the range of investigation, the present experiments have been confined to that state of the alloys in which all the iron is believed to be in solid solution. This state surely exists in the high temperature measurements above the solubility limits and it is assumed to exist for all the present experiments at room temperature and below because each of the specimens was quenched in water from above the solubility limits.

The alloys for this investigation were made by dissolving iron in molten electrolytic copper in an atmosphere of hydrogen and then chill casting in vacuum. The castings were annealed for 5 days at 1000°C and then quenched after which they were swaged to the desired size. Samples for measurement were cut from this stock and prepared by annealing the low iron alloys at 950°C and the

[1] F. Bitter and A. Kaufmann, Phys. Rev. **56**, 1044 (1939).

alloys with more than 0.5 percent iron at 1030°C for 24 hours and then quenching in water.

Susceptibility measurements at room temperature on these specimens showed the absence of any appreciable ferromagnetism except for the alloy with 2.7 percent iron which had a ferromagnetic moment per unit mass of 0.02 absolute unit. This moment corresponds to less than 0.4 percent of the total iron in the specimen but this value indicates, nevertheless, that the solution heat treatment in this case was not entirely successful, possibly because of an insufficiently rapid cooling rate. The absence of ferromagnetism in the other specimens indicates that the iron is entirely in solution.

Experimental Results

The susceptibility values at room temperature increase rapidly with composition up to 0.7 percent iron and then show little further change at higher compositions as shown by curve *A*, Fig. 1. This peculiar behavior above 0.7 percent iron indicates either that the randomly distributed iron atoms have affected each other in some way or else that the quench has not retained the iron atoms in a random arrangement. The second possibility seems the more plausible for two reasons. In the first place, if randomly distributed iron atoms could influence each other so strongly at room temperature, then some trace of the phenomenon ought to still exist at high temperatures. However, curve *B* shows only a linear increase of susceptibility with iron content at 1300°K, a temperature which is above the solubility limit for all the alloys. In the second place, it is known from the observations in Part I that an incipient or actual precipitation of iron will cause a decrease in susceptibility without the appearance of ferromagnetic iron. Such a condition in the quenched alloys would lead to the observed behavior and would mean simply that the quenching treatment was not entirely effective for iron contents greater than 0.7 percent. Because of this conclusion, the state of the quenched alloys with more than 0.7 percent iron was considered to be doubtful and accordingly only a few low temperature measurements were made on them and none of these results are discussed in the following.

The susceptibility of the quenched alloys showed a large temperature dependence below room temperature as would be expected from the high temperature results in Part I. The interpretation of the data is not straightforward, however, since the susceptibility values showed a considerable field dependence. The extent of this phenomenon is shown by Fig. 2 where the magnetization curves for the specimen with 0.7 percent iron are plotted. The heavy lines going through the points represent the experimental data while the lighter, straight lines show the slope at the origin. Measurements were made up to 30 kilogauss but no definite saturation effects were found even at 14°K. This fact combined with the absence of field dependence at room temperature indicates that the observed behavior cannot be due simply to the presence of ordinary ferromagnetic impurities. From Fig. 2 it can be seen that at a given composition the field dependence becomes greater as the temperature is lowered while other observations show that at a fixed temperature the field dependence becomes less as the iron content decreases. At 14°K the most dilute alloy which still showed a definite field dependence contained about 0.1 percent iron. It is perhaps well to mention that the results shown in Fig. 2 were reproducible, thus removing the possibility that some permanent change in the specimen such as the precipitation of iron during cooling might have caused the observed behavior.

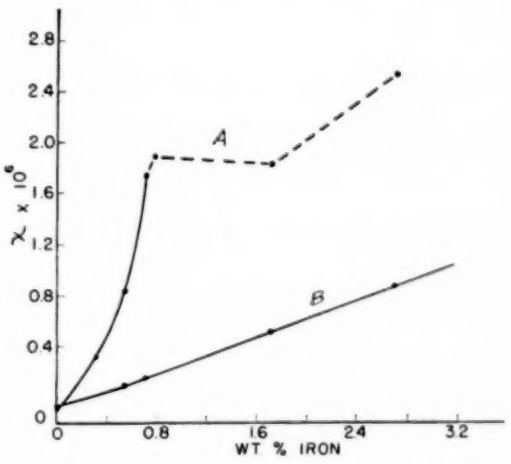

Fig. 1. Mass susceptibility of copper-iron alloys. Curve *A* —quenched alloys at room temperature. Curve *B*—alloys at 1300°K.

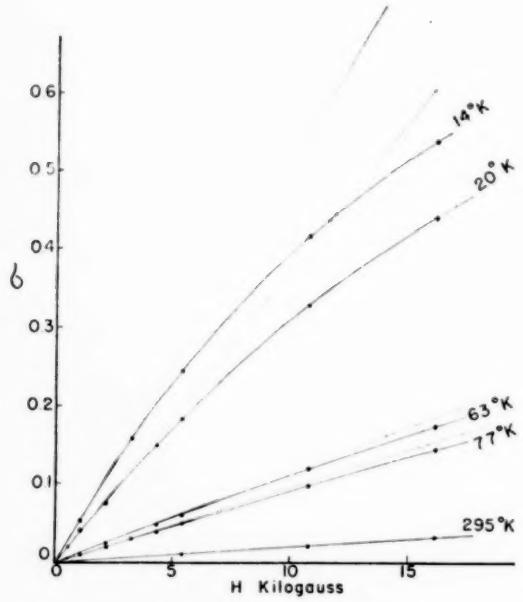

FIG. 2. Magnetization curves of quenched copper containing 0.7 percent iron.

In all cases where a field dependence was observed, the initial susceptibilities as indicated by the straight lines in Fig. 2 were determined. These values as well as those obtained by orthodox methods at higher temperatures are given in Table I.

The susceptibility of "pure" copper was measured over the same temperature range as the alloys in order to be able to make a correction for it. Some typical results are plotted in Fig. 3 and are tabulated in Table I. All the samples showed a nearly linear decrease in diamagnetism between room temperature and 1000°C as mentioned in Part I, but below room temperature the measurements showed a considerable divergence. The first specimens examined were made of the copper used in the alloys and these showed a large change toward paramagnetism at low temperatures. A calculation indicated that the paramagnetism of the dissolved iron impurities could cause this behavior but in order to be sure a sample containing less than 0.00007 percent iron was also measured.[2] The increase in susceptibility at low temperatures in this case cannot be accounted for by the iron or even by the other impurities such

[2] Obtained through the courtesy of Dr. A. J. Phillips of the American Smelting and Refining Company. The specimen contained 99.998 percent copper and a typical analysis is given in A.I.M.E. Tech. Pub. 1289 (1941).

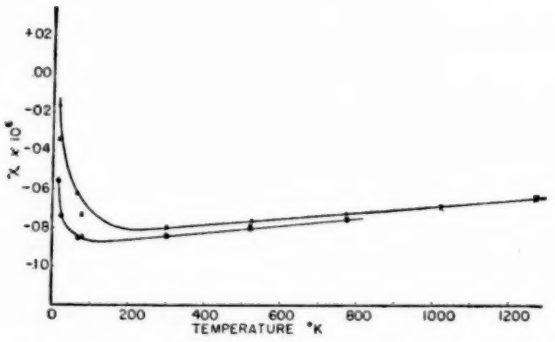

FIG. 3. Susceptibility of "pure" copper. —●— 0.0082 percent iron; —X— 0.0025 percent iron; —⊙— <0.00007 percent iron.

as manganese because of the extremely high purity of the copper. The observed behavior is apparently a property of pure copper but further investigation is required to prove this. The values for "pure" copper that were finally used were obtained by extrapolating the curves in Fig. 4 to zero iron content.

DISCUSSION OF RESULTS

The susceptibility values in Table I between 14°K and 77°K may be represented by an equation of the form

$$\chi = \chi_{Cu} + C/(T-\theta) \qquad (1)$$

as shown by Fig. 5 in which percent iron $/(\chi - \chi_{Cu})$ is plotted as a function of temperature. From the slopes of these lines one can evaluate the constant C and from this the Bohr magneton value per

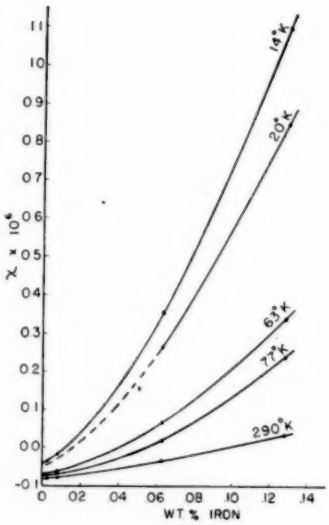

FIG. 4. Mass susceptibility of dilute copper-iron alloys below room temperature.

iron atom can be calculated by using the equation

$$p_B = 2.84(100M/C)^{\frac{1}{2}},$$

where M is the gram atomic weight of iron. The results are given in Table II along with the values of θ, the paramagnetic Curie temperature.

The Bohr magneton values seem to vary linearly with composition although the sample with 0.5 percent iron forms an exception to this. The fact that the 0.7 percent iron specimen has a Bohr magneton value almost equal to the theoretical value for a free, doubly ionized iron ion probably has no special significance in view of the large field dependence of susceptibility. The small values of θ indicate that the initial susceptibility of the dissolved iron atoms behaves almost like that of a perfect Curie substance. According to the usual theories this behavior would indicate that the influence of the iron atoms upon each other is very small.

The experimental data do not lie on the curves of Fig. 5 at high temperatures. This can be seen for the room temperature values in Fig. 5 and more completely from the values obtained above the solubility limits as shown in Fig. 6. No measurements were made in the intervening temperature range because a precipitation of iron would have occurred.

The interesting thing about the high temperature data is that they can also be represented by Eq. (1) but in a way which indicates a different behavior from that at low temperatures. The slopes of all the high temperature curves are almost equal, which means that the magnetic moment per iron atom is the same in all the

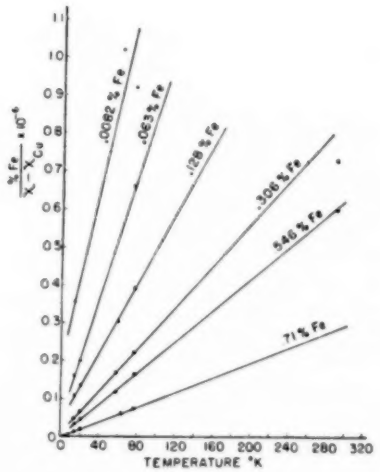

FIG. 5. Reciprocal of susceptibility per gram of iron below room temperature.

alloys. This magnetic moment corresponds to a Bohr magneton value of 4.7, which happens to be the theoretical value for an iron ion in which the electron spins only are contributing to the moment. The extrapolated Curie temperatures are considerably larger in magnitude than those found at low temperatures and they change progressively from negative to positive values as the iron content is increased.

The high temperature data indicate that the iron atoms have a definite magnetic moment when dissolved in copper and that this moment is independent of concentration over the range investigated. Furthermore, the decrease of Curie temperature from positive to negative values may be attributed to a decreasing interaction of some sort between the iron atoms as the iron content becomes less, although the ordinary

TABLE I. *Susceptibility per unit mass—$\chi \times 10^6$.*

T° K	Pure Copper	Weight Percent Iron 0.0025	0.0082	0.063	0.128	0.306	0.546	0.71	1.70	2.69
14.0	−0.056	−0.034	−0.017	0.356	1.10	6.4	15.6	51.0		
20.4	− .074			.263	.845	4.52	12.4	37.5		
58					.338	1.75	4.57			
63.1	− .0863		− .062					11.4		
77.3	− .0850	− .073	− .066	.0197	.238	1.29	3.26	9.42		
295	− .0843	− .0796	− .080	− .033	.0354	.328	.823	1.74	1.82	2.52
380					.0117	.237	.596			
523	− .0809	− .0786	− .0761							
773	− .0760	− .0748	− .0732							
1023		− .0693								
1073		− .0685	− .0685		− .0314	.0346	.1205	.240		
1173		− .0665	− .0665		− .0316	.0292	.1066	.183		
1273		− .0645	− .0646		− .0321	.0251	.0965	.163		
1298									.506	.875

Weiss theory would allow θ only to approach zero but not to become negative. It is interesting to note that the measurements of Gustafsson on manganese dissolved in copper show the same type of variation of Curie temperature with concentration and likewise a constant value for the magnetic moment of the manganese atoms.[3]

The results at low temperatures, as already mentioned, show a different behavior of the iron atoms in that the magnetic moment increases rapidly with concentration while the Curie temperatures are so small as to indicate only a slight mutual influence of the iron atoms. This behavior is difficult to understand with the Curie-Weiss theory and in addition the apparent change in the state of the iron atoms between high and low temperatures is most unusual in magnetic phenomena. Since the alloys at low temperatures were supersaturated, the question arises as to whether or not this condition could produce the observed behavior. This possibility is somewhat discredited by the fact that the most dilute alloys which, of course, are the least supersaturated, still show the same type of change. In order to settle the problem of whether supersaturation produces the above effect or whether it is a real magnetic phenomenon, it would be necessary to examine other similar alloys both supersaturated and in equilibrium.

The dependence of susceptibility upon field strength at low temperatures is further evidence of a peculiar magnetic behavior. The observed effect is much too great to be accounted for by the saturation of an ordinary paramagnetic substance even at 14°K. It is conceivable that the quenching treatment did not succeed in keeping the iron atoms distributed at random and hence that they had formed local regions of high concentration. Such groups of iron atoms might be on the verge of becoming ferromagnetic and hence could show saturation effects in a strong field. This situation seems unlikely, however, since by plotting magnetization against H/T all the curves from 77°K to 14°K can be brought into coincidence, as would be expected for a paramagnetic substance but not for a substance in which interactions have almost produced an intrinsic magnetization.

Another possible way of accounting for the field dependence would be to assume that the iron has actually formed in numerous small regions which are spontaneously magnetized to some fixed intensity. If the orientation of these magnetic moments in an external field was given by the Langevin function as for a paramagnetic gas, then the magnetization would depend upon H/T as found, and since each region would have a large moment compared with a single atom, $\mu H/KT$ could be large enough to give an ordinary paramagnetic saturation effect. There seems to be no way of proving or disproving this idea and hence one can question it only on the basis of the complicated and somewhat unreasonable mechanism required.

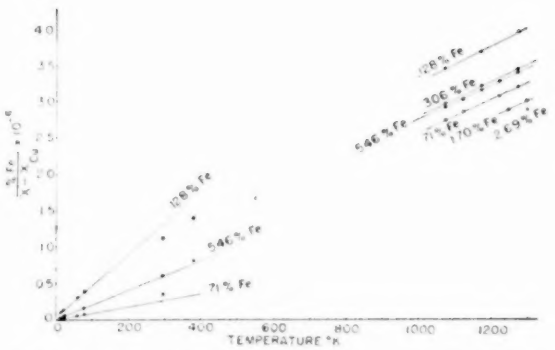

FIG. 6. Reciprocal of susceptibility per gram of iron for quenched alloys below room temperature and for the alloys above the solid-solubility temperature.

TABLE II. *Curie temperatures* (θ) *and Bohr magneton per atom* (p_B).

Wt. % Fe	p_B	θ
0.0082	2.0	−16
0.063	2.4	− 6
0.128	3.1	−10
0.306	4.1	− 4
0.546	4.7	− 2
0.71	6.9	0

[3] E. Vogt, Ann. d. Physik **29**, 362 (1937).

The Effect of Dislocations on Magnetization Near Saturation

WILLIAM FULLER BROWN, JR.
Palmer Physical Laboratory, Princeton University, Princeton, New Jersey
(Received May 24, 1941)

The effect of dislocations on the magnetization curve at high fields is calculated by direct use of dislocation theory. The deviation from saturation is assumed to be due to magnetostrictive forces, localized in the stress field about the dislocation rather than at the dislocation itself; their effect is more complicated than that of the simple "line concentrations of force" considered in an earlier article. Pairs of dislocations of opposite sign, separated by a short distance, contribute a term a/H to the deviation from saturation; in this respect they resemble line concentrations. Pairs separated by a long distance and surplus dislocations of one sign contribute a term b/H^2, with b theoretically not a constant but a logarithmically varying function of H. From data on the variation of the empirical a and b with plastic strain, it is possible to calculate the density of dislocations and the "block" length if a value is assumed for the distance Y between the members of a dislocation pair. The orders of magnitude obtained agree with those obtained in the theory of hardening if Y is taken $\leqq 2\times10^{-6}$ cm. It appears that all but about 1 percent of the dislocations are members of such pairs.

THE magnetic properties of ferromagnetic materials are greatly affected by plastic strain. A theoretical analysis of such effects, developed chiefly by Kersten,[1] has been very successful in correlating a large number of experimental observations. Kersten's theory offers a rather detailed description of the effect of "internal stresses" on magnetic processes, but no description at all of the way in which such stresses arise; they are merely postulated. Meanwhile, other workers have developed a fairly successful theory of plastic strain and hardening, in which the most fruitful concept has been that of "dislocations."[2] It should, therefore, be possible to interpret Kersten's "internal stress" in terms of dislocations, or still better to describe directly the effect of dislocations on the magnetization process.

At low fields the theoretical problem is an extremely complicated one; but as saturation is approached, simplifications may be introduced. The resulting equations are solvable, and data are available from which it is possible to judge the success of such a theoretical analysis. If theory and experiment agree here, then there is some ground for hope that the dislocation concept may also prove useful in interpreting properties of practical importance at lower fields: initial and maximum permeability, hysteresis, remanence, and coercive force.

The magnetization curve at high fields can usually be fitted by an empirical formula $J=J_s-a/H-b/H^2+CH$, where J is the magnetization at a field H, and the other quantities are constants. The "spontaneous" or "intrinsic" magnetization J_s and susceptibility C are satisfactorily explained by atomic theory.[3] The constant b in annealed material can be calculated from data on crystalline and stress-induced anisotropy,[4] but in plastically strained material it has a higher value. The constant a is much more dependent on plastic strain, and quite possibly would vanish for a perfectly annealed specimen. It will be shown in this article that the orders of magnitude of a, and of the part of b not attributable to anisotropy, are consistent with the view that they are due to dislocations. The empirical formula, however, is theoretically far from exact.

1. The Stress Produced by Dislocations

A "positive" line dislocation, of the sort postulated by Taylor[5] to explain plastic flow, is shown in Fig. 1(a). If such a dislocation moves through the crystal from left to right, the atoms above it are displaced to the right, with respect

[1] R. Becker and W. Döring, *Ferromagnetismus* (Julius Springer, Berlin, 1939), pp. 154–167.
[2] F. Seitz and T. A. Read, J. App. Phys. **12**, 100, 170 (1941).
[3] Reference 1, pp. 25–101; T. Holstein and H. Primakoff, Phys. Rev. **58**, 1098 (1940).
[4] Reference 1, pp. 168–171, 175; T. Holstein and H. Primakoff, Phys. Rev. **59**, 388 (1941).
[5] G. I. Taylor, Proc. Roy. Soc. **A145**, 362 (1934).

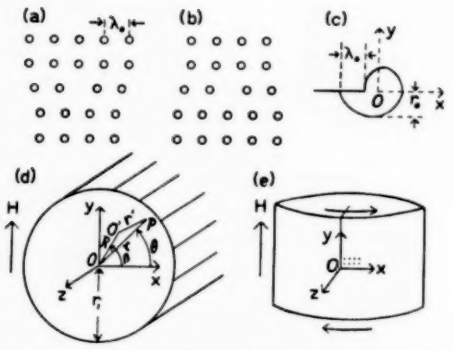

FIG. 1. (a) Approximate positions of atoms in a plane perpendicular to a dislocation line. Positive dislocation. (b) Negative dislocation. (c) The equivalent of (a) for a continuous medium: a "dislocation" in the theory of elasticity. (d) With an excess of dislocations of one sign, the specimen may no longer be treated as having infinite dimensions in the plane perpendicular to the dislocations. The cylindrical specimen shown has been chosen for detailed study. The stress produced at P by a dislocation at O' is to be expressed in terms of polar coordinates referred to the center O. (e) Directions of field, dislocation lines, and reference axes in a twisted wire, in the simplified model adopted here. In the detailed consideration of a microscopic neighborhood of a dislocation, the model is further simplified by supposing that the dislocations are all parallel to Oz and infinitely long.

to the atoms below it, by an amount λ_0. The same result is attained if a "negative" dislocation (Fig. 1(b)) moves through the crystal from right to left. A specimen after plastic strain is supposed to contain dislocations of both signs.

The lattice distortion in the neighborhood of a dislocation may be calculated by elasticity theory at distances r that are large compared with λ_0, that is, with the interatomic distance. In such a calculation the dislocation is pictured as in Fig. 1(c) and may be treated by methods developed by Timpe, Volterra, and others.[6] The internal surface is assumed free from traction; its radius r_0 is of atomic order of magnitude, but disappears in the final formulas, since in the application to Fig. 1(a) it must be supposed that $r \gg r_0$.

In a ferromagnetic material, this distortion of the lattice produces torques that tend to aline the magnetic moments of the atoms along certain directions; the directions change from point to point, since the strain is not uniform. At high fields the effect is a slight deviation of the local magnetization from the field direction, and a consequent decrease of the observed holomagnetization J below the saturation value J_s. Where the spatial variation of the strains is slow, the local direction of magnetization is determined by an equilibrium between the torques due to the lattice distortion and to the field. But in the immediate neighborhood of a dislocation, where the strains vary rapidly, the magnetization is prevented from changing equally rapidly by the interatomic coupling torques, which tend to keep the magnetic moments of neighboring atoms parallel. Thanks to this smoothing out effect, the region $r \leqq \lambda_0$, where the formulas of elasticity theory are not reliable, is precisely the region where the exact nature of the lattice distortion is least important in the magnetic problem; thus for magnetic calculations the elastic formulas may be used at *all* points without serious error.

The dislocation of Fig. 1(c) produces, in an infinite medium, stresses which may be calculated from the Airy stress function[7]

$$\chi = -(G'\lambda_0/2\pi) y \ln(x^2+y^2) = -(G'\lambda_0/\pi) r \ln r \cdot \sin\theta \quad (1)$$

by means of the formulas

$$\begin{aligned} &X_x = \partial^2\chi/\partial y^2, \quad Y_y = \partial^2\chi/\partial x^2, \quad X_y = -\partial^2\chi/\partial x\partial y, \\ &\sigma_{rr} = r^{-2}\partial^2\chi/\partial\theta^2 + r^{-1}\partial\chi/\partial r, \quad \sigma_{\theta\theta} = \partial^2\chi/\partial r^2, \\ &\sigma_{r\theta} = -\partial(r^{-1}\partial\chi/\partial\theta)/\partial r. \end{aligned} \quad (2)$$

A state of plane strain will be assumed; the constant G' is then equal to $\mu(\lambda+\mu)/(\lambda+2\mu)$ in the usual notation for elastic constants.[8] For the magnetic calculation the only stress required is

$$X_y = cx(x^2-y^2)/r^4 = c(\cos\theta+\cos 3\theta)/2r, \quad (3)$$

where $c = G'\lambda_0/\pi$.

[6] A. Timpe, Zeits. f. Math. Physik **52**, 348 (1905); V. Volterra, Ann. Ec. Norm [3] **24**, 401 (1907); A. E. H. Love, *A Treatise on the Mathematical Theory of Elasticity* (Cambridge, 1934), fourth edition, pp. 221–228.

[7] A. Timpe, reference 6; L. N. G. Filon, *British Association Report* (1921), p. 305.

[8] For generalized plane stress, $G' = \mu(3\lambda+2\mu)/4(\lambda+\mu) = \frac{1}{4}\times$Young's modulus. These stresses differ from those given by Taylor, reference 5, p. 376. The incompleteness of Taylor's formulas has been pointed out by J. M. Burgers, Proc. K. Ned. Akad. Wet. **42**, 293 (1939), footnote pp. 305–6. Taylor's Cartesian stresses could be maintained only if surface tractions were applied to the internal boundary $r = r_0$. They appear to have been derived from a preliminary displacement formula given by Volterra, reference 6, p. 463, to which Volterra later added other terms in order to satisfy the boundary conditions. Volterra's complete displacement formula, p. 465, agrees with that of Burgers (except for a rotation of axes) and leads to stress formulas in agreement with those given here. Taylor's polar stresses are inconsistent with his Cartesian; they are incorrect in the sign of σ_{rr} and in the value of the constant (Taylor has μ instead of G').

The displacement corresponding to Eq. (1) becomes logarithmically infinite at $r=\infty$. If the numbers of positive and of negative dislocations are equal, the *resultant* displacement behaves properly at infinity, and a large specimen may be considered infinite in the xy plane; but if there is an excess of dislocations of one sign, the external boundary must be taken into account. A similar situation occurs in the magnetic problem. In most of the following calculations it will be assumed that positive and negative dislocations are present in equal numbers; but one particularly simple case of unequal numbers will be investigated. In this case the boundary is assumed to be a circular cylinder of radius r_1 with center at O, illustrated in Fig. 1(d). The stress may be found as follows.

If the medium were infinite, the stress function for a positive dislocation at O' would be $\chi_1=-cy'\ln r'$. Referred to O as origin, this becomes,[9] for $r>R$,

$$\chi_1=-c\{(r\sin\theta-R\sin\beta)\ln r+C_1r^{-1}\cos\theta+C_1'r^{-1}\sin\theta+\sum_{n=2}^{\infty}[(C_nr^{-n}+D_nr^{-n+2})\cos n\theta+(C_n'r^{-n}+D_n'r^{-n+2})\sin n\theta]\},\quad(4)$$

where

$$\begin{aligned}C_n&=[\sin(n+1)\beta-(n+1)\sin(n-1)\beta]\times R^{n+1}/2n(n+1),\\C_n'&=-[\cos(n+1)\beta-(n+1)\cos(n-1)\beta]\times R^{n+1}/2n(n+1),\\D_n&=[\sin(n-1)\beta]R^{n-1}/2(n-1),\\D_n'&=-[\cos(n-1)\beta]R^{n-1}/2(n-1).\end{aligned}\quad(5)$$

The additional term χ_2 required by the boundary must correspond to a single-valued displacement, must have no singularity at O, and must be such that at $r=r_1$ the sum $\chi_1+\chi_2$ satisfies Michell's boundary conditions[10]

$$\chi=\kappa_1r_1\cos\theta+\kappa_2r_1\sin\theta+\kappa_3,\qquad\partial\chi/\partial r=\kappa_1\cos\theta+\kappa_2\sin\theta,\quad(6)$$

where κ_1, κ_2, and κ_3 are independent of θ. Hence[11]

$$\chi_2=-c\{R\sin\beta\cdot(r^2/2r_1^2)+L_1r^3\cos\theta+L_1'r^3\sin\theta+\sum_{n=2}^{\infty}[(K_nr^n+L_nr^{n+2})\cos n\theta+(K_n'r^n+L_n'r^{n+2})\sin n\theta]\},\quad(7)$$

where

$$\begin{aligned}&L_1=C_1r_1^{-4},\quad L_1'=C_1'r_1^{-4}-\tfrac{1}{2}r_1^{-2};\\&K_n=-(n+1)C_nr_1^{-2n}-nD_nr_1^{-2n+2}\quad(n>1),\\&L_n=nC_nr_1^{-2n-2}+(n-1)D_nr_1^{-2n}\quad(n>1),\end{aligned}\quad(8)$$

with similar equations in the primed constants.

The solution for an arbitrary distribution of dislocations may be found by superposition of the individual solutions with due regard to the sign of each dislocation.[12] The coefficients in the resultant boundary stress function χ_2 contain such sums as $\sum_i s_iR_i^n\cos n\beta_i$, where s_i is $+1$ or -1, according as the ith dislocation is positive or negative. For a macroscopically uniform distribution of dislocations, with an excess N of positive ones, approximate values of the coefficients may be obtained by replacing the sums by integrals, or in other words by treating the dislocation distribution as *continuous* in calculating the effect of the boundary. If this is done, most of the coefficients vanish; and there remains only

$$\chi_b=(Nc/4r_1^2)r^3\sin\theta,\quad(9)$$

whence

$$(X_y)_b=-(Nc/2r_1^2)r\cos\theta.\quad(10)$$

The function $\chi=-c\sum_i s_iy_i'\ln r_i'+\chi_b$ is a good approximation to the actual stress function, except in a region near the boundary, whose width δ is a few times larger than the distance between dislocations. This may be seen as follows. Let A be the region $r<r_1-\delta$ and B the region

[9] W. R. Smythe, *Static and Dynamic Electricity* (McGraw-Hill Book Company, Inc., New York, 1939), p. 64.

[10] J. H. Michell, Proc. Lond. Math. Soc. **31**, 100 (1899).

[11] This is not equivalent to the stress produced by an image dislocation at the point $(r_1^2/R, \beta)$. The failure of the method of images is easily demonstrated in the case of a dislocation at $(a, 0)$ in a semi-infinite medium bounded by a free surface at $x=0$. If r_1 is distance from the image at $(-a, 0)$ and r_2 is distance from the original dislocation, the stress function is $cy[\ln(r_1/r_2)+\frac{1}{2}(r_2/r_1)^2]$; the image method gives only the first term, which satisfies the condition $X_x=0$, but not the condition $X_y=0$ at the boundary.

[12] The problem of a single dislocation in a cylinder can be solved more simply in bipolar coordinates: J. S. Koehler, Phys. Rev. **59**, 477A (1941); G. B. Jeffery, Phil. Trans. Roy. Soc. **A221**, 265 (1920). A different coordinate system is required for each dislocation, and there is, therefore, no advantage in introducing such coordinates in the present calculation.

$r_1-\delta<r<r_1$. The dislocations in A are indistinguishable, on the boundary, from a continuous distribution, and may therefore be treated as such in calculating the contribution of the boundary under their influence alone; the result is a good approximation in B as well as in A. This is not true of the dislocations in B. But the effect produced *in* A by a dislocation in B, in the presence of the boundary, is not appreciably affected by a slight change in the position of the dislocation. Therefore the dislocations in B may be replaced by a continuous distribution without greatly altering the stresses in A, though the stresses in the boundary region B are not given correctly by this method.

In the magnetic calculation it is convenient to treat the specimen as if it extended to infinity, but had at $r=r_1$ a boundary incapable of transmitting stress, with no dislocations outside the boundary. If the boundary could transmit stress, χ, in the external region, would be given by Eq. (4) summed over the dislocations. Except within a distance δ of the boundary, this may be replaced by its value for a continuous distribution, $-Nc\sin\theta\cdot[r\ln r+r_1^2/4r]$. The function $\chi=-c\sum_i s_i y_i'\ln r_i'+\chi_b'$, with

$$\chi_b'=+Nc\sin\theta\cdot[r\ln r+r_1^2/4r], \qquad (11)$$

is, therefore, a good approximation to the actual (zero) stress function for $r>r_1+\delta$. Thus the actual stresses in both regions may be approximated closely, everywhere except within a distance δ of either side of the boundary, by treating the dislocations as if they were surrounded by an infinite medium, but adding to the stress function a term χ_b for $r<r_1$ and a term χ_b' for $r>r_1$. The corresponding term in X_y for $r>r_1$ is

$$(X_y)_b'=\tfrac{1}{2}Nc[-r^{-1}(\cos\theta+\cos3\theta)+r_1^2r^{-3}\cos3\theta]. \qquad (12)$$

It is also convenient, in the magnetic calculation, to express X_y as a Fourier integral,

$$X_y=f(r,\theta)=(2\pi)^{-1}\int g(\rho,\phi)\exp[i\boldsymbol{\varrho}\cdot\mathbf{r}]d\boldsymbol{\varrho}, \qquad (13)$$

where

$$\mathbf{r}=r(\mathbf{i}\cos\theta+\mathbf{j}\sin\theta),\quad \boldsymbol{\varrho}=\rho(\mathbf{i}\cos\phi+\mathbf{j}\sin\phi),$$

and $d\boldsymbol{\varrho}=\rho d\rho d\phi$. The Fourier transform g is given by

$$g(\rho,\phi)=(2\pi)^{-1}\int f(r,\theta)\exp[-i\boldsymbol{\varrho}\cdot\mathbf{r}]d\mathbf{r}, \qquad (14)$$

where $d\mathbf{r}=rdrd\theta$. For a positive dislocation at the origin in an infinite medium,[13]

$$g=ic(-\cos\phi+\cos3\phi)/2\rho. \qquad (15)$$

For a dislocation at $\mathbf{R}$, an additional factor $\exp[-i\boldsymbol{\varrho}\cdot\mathbf{R}]$ must be inserted; a distribution of dislocations of signs s_i at points $\mathbf{R}_i$ requires a factor $\sum_i s_i\exp[-i\boldsymbol{\varrho}\cdot\mathbf{R}_i]$. The stress described by $(X_y)_b$ at interior points, and by $(X_y)_b'$ at exterior, has the Fourier transform

$$g=i(Nc/r_1)\rho^{-2}J_1(\rho r_1)(\cos\phi-\cos3\phi). \qquad (16)$$

2. Single Dislocations and Doublets

Suppose now that the specimen, with dislocation lines parallel to Oz, is subjected to a large magnetic field H parallel to Oy. This corresponds roughly to the situation in a small portion of a twisted wire, illustrated in Fig. 1(e); this same situation will now be supposed to prevail throughout the specimen.

The deviation of the magnetization vector from the field direction is measured by its direction cosine α with respect to the x axis. The equations that determine α were derived in an earlier article;[14] they are

$$\nabla^2\alpha-\partial u/\partial x-\eta\alpha=f_1, \qquad (17)$$

$$\nabla^2u=h\partial\alpha/\partial x, \qquad (18)$$

where $\eta=HJ_s/C$, $u=UJ_s/C$, $h=4\pi J_s^2/C$, $f_1=C^{-1}(dw/d\alpha)_{\alpha=0}$; C is a constant proportional to the strength of the interatomic coupling forces, U is the potential of the internal field produced

[13] The integration over θ may be carried out by taking as a new variable of integration the angle between $\boldsymbol{\varrho}$ and $\mathbf{r}$; the same method may be used for the integration over ϕ in §§3 and 4. The results may be expressed in terms of Bessel functions by means of formulas given by Watson, *Theory of Bessel Functions* (Cambridge, 1922), pp. 20–21. In the subsequent integration over r or ρ, only elementary properties of Bessel functions are required for Eqs. (15) and (16); but for such integrals as those of Eqs. (29) and (30), use must be made of special formulas given by Watson, Chapter XIII, §§13.4 ff., 13.51–13.53, 13.6. Partial fractions and the differentiation method of Eq. (47) are also useful.

[14] W. F. Brown, Jr., Phys. Rev. **58**, 736 (1940), Eqs. (50), with the change $(x, y, z)\rightarrow(z, x, y)$. Since w contains no linear term in γ, $f_3=0$ and (to the approximation adopted here) $\mathbf{J}$ remains in the xy plane.

by the non-uniform magnetization, and w is the anisotropy energy density associated with the stress. In Eq. (17), the first term represents the coupling torque exerted by neighboring atoms, the second the torque due to the component of internal field perpendicular to the magnetization, the third the torque due to the component of magnetization perpendicular to the external field; the sum of these must balance the anisotropy torque represented by f_1. Equation (18) is Poisson's equation. For $H \gg 4\pi J_s$ the internal field may be neglected; α is then determined by the equation

$$\nabla^2\alpha - \eta\alpha = f_1. \tag{17a}$$

For arbitrary direction cosines (α, β, γ) in a material with isotropic negative saturation magnetostriction $-\lambda_\infty$, w is given by[15]

$$w = \tfrac{3}{2}\lambda_\infty[X_x\alpha^2 + Y_y\beta^2 + Z_z\gamma^2 + 2(Y_z\beta\gamma + Z_x\gamma\alpha + X_y\alpha\beta)]; \tag{19}$$

when $Y_z = Z_x = 0$ and $\beta \doteq 1$, this becomes const. $+3\lambda_\infty X_y\alpha$, whence $f_1 = (3\lambda_\infty/C)X_y$. Insertion of the value of X_y from Eq. (3) gives, for a single positive dislocation at $x = y = 0$,

$$f_1 = k(\cos\theta + \cos 3\theta)/2r, \tag{20}$$

where $k = (3\lambda_\infty/C)c = 3\lambda_\infty G'\lambda_0/\pi C$. The solution of Eq. (17a), subject to finiteness conditions at $r = 0$ and $r = \infty$, is by direct integration

$$\alpha = (k/2\lambda')\{[K_1(\lambda' r) - 1/\lambda' r]\cos\theta - [K_3(\lambda' r) + 1/\lambda' r - 8/(\lambda' r)^3]\cos 3\theta\}, \tag{21}$$

where[16] $\lambda' = \eta^{\frac{1}{2}}$; or, by use of the Fourier expansion (15),

$$\alpha = (2\pi)^{-1}\int G \exp[i\boldsymbol{\varrho}\cdot\mathbf{r}]d\boldsymbol{\varrho}, \tag{22}$$

where

$$G = \tfrac{1}{2}ik(\cos\phi - \cos 3\phi)/\rho(\rho^2 + \lambda'^2). \tag{23}$$

The decay distance $1/\lambda'$ is about 500 lattice spacings for nickel at $H = 100$. For $r \leqq 1/\lambda'$ the coupling forces, which are responsible for the terms in $1/r^3$, K_1, and K_3, are important; but for $r \gg 1/\lambda'$ the value of α is the same as if the coupling forces were not present $(C = 0)$. The magnetization at any point is $J_s(1 - \frac{1}{2}\alpha^2)$. If an attempt is made to average this by integration over the xy plane, it is at once evident that the boundary must be taken into account, for the infinite integral diverges logarithmically at $r = \infty$.

If, however, the dislocations occur in pairs, with the positive one a short distance—$\mathbf{R} = \mathbf{i}X + \mathbf{j}Y$—from the negative, this difficulty does not occur. The value of α for such a *doublet* may be found by applying the operator $-\mathbf{R}\cdot\nabla$ to the value for a singlet. If the latter is expressed in the form (22), an additional factor $-i\boldsymbol{\varrho}\cdot\mathbf{R}$ in (23) gives G for a doublet, and

$$\int \alpha^2 d\mathbf{r} = \int |G|^2 d\boldsymbol{\varrho}. \tag{24}$$

The value of $(\alpha^2)_{Av}$ for n' dislocations per cm^2, distributed at random, is n' times this integral. The integration is straightforward and gives

$$1 - J/J_s = \tfrac{1}{2}(\alpha^2)_{Av} = n'k^2\pi(3X^2 + 5Y^2)/64\eta. \tag{25}$$

Such a distribution of dislocation doublets therefore gives a $1/H$ law of approach to saturation, provided H is high enough to justify the neglect of the internal field. The effect of the latter at lower H will be considered in §4.

3. Paired Dislocations

Consider, next, a more general distribution of dislocations, arbitrary except that equal numbers of positives and negatives are present in any macroscopic area of the xy plane. This restriction eliminates boundary difficulties and is probably not a bad approximation, for there is no physical reason why one type of dislocation should be produced faster than the other in the hardening process.

Superposition of the effects of all the dislocations gives α in the form (22), with G replaced by

$$G_1 = G\sum_i s_i \exp[-i\boldsymbol{\varrho}\cdot\mathbf{R}_i]. \tag{26}$$

Hence

$$\int \alpha^2 d\mathbf{r} = \int |G_1|^2 d\boldsymbol{\varrho} = \int |G|^2 \sum_i \sum_j s_i s_j \times \exp[i\boldsymbol{\varrho}\cdot\mathbf{R}_{ij}]d\boldsymbol{\varrho},$$

[15] Reference 1, p. 146.

[16] The symbols λ and k of reference 14 have been replaced by λ' and k' in the present article. The following must be distinguished: λ_0 = elementary slip distance, λ = elastic constant, λ_∞ = magnitude of saturation magnetostriction, $\lambda' = \eta^{\frac{1}{2}}$ = reciprocal of magnetic decay distance. A few symbols (β, γ, χ) have been used for different purposes in different parts of the discussion.

where $\mathbf{R}_{ij}=\mathbf{R}_j-\mathbf{R}_i$; or since $s_i=-\sum_j' s_j$,

$$\int \alpha^2 d\mathbf{r}=\int |G|^2 \sum_i s_i[s_i+\sum_j' s_j \exp(i\boldsymbol{\varrho}\cdot\mathbf{R}_{ij})]d\boldsymbol{\varrho}$$
$$=-\sum_i \sum_j' s_i s_j \int |G|^2[1-\exp(i\boldsymbol{\varrho}\cdot\mathbf{R}_{ij})]d\boldsymbol{\varrho}. \quad (27)$$

After integration over ϕ and transformation to a new variable of integration $x=R_{ij}\rho$, this becomes[13]

$$\int \alpha^2 d\mathbf{r}=-\tfrac{1}{2}\pi k^2 \sum_i \sum_j' s_i s_j R_{ij}^4\{f_0(\lambda' R_{ij})$$
$$-\tfrac{1}{2}f_2(\lambda' R_{ij})\cos 2\theta_{ij}$$
$$+f_4(\lambda' R_{ij})\cos 4\theta_{ij}+\tfrac{1}{2}f_6(\lambda' R_{ij})\cos 6\theta_{ij}\}$$
$$=-\tfrac{1}{2}\pi k^2 \sum_i \sum_j' s_i s_j F(\mathbf{R}_{ij}), \quad (28)$$

where $\theta_{ij}=\measuredangle(\mathbf{R}_{ij}, \mathbf{i})$, and

$$f_0(\mu)=\int_0^\infty [1-J_0(x)][x(x^2+\mu^2)^2]^{-1}dx, \quad (29)$$

$$f_n(\mu)=\int_0^\infty J_n(x)[x(x^2+\mu^2)^2]^{-1}dx \quad (n>0). \quad (30)$$

Integration gives[13]

$$2\mu^3 f_0(\mu)=K_1(\mu)+2\mu^{-1}K_0(\mu)$$
$$+2\mu^{-1}[(\gamma-\tfrac{1}{2})+\ln(\mu/2)], \quad (31)$$
$$2\mu^3 f_2(\mu)=K_1(\mu)+4\mu^{-1}K_2(\mu)+\mu^{-1}-8\mu^{-3},$$
$$2\mu^3 f_4(\mu)=-K_3(\mu)-6\mu^{-1}K_4(\mu)$$
$$+\tfrac{1}{2}\mu^{-1}-16\mu^{-3}+288\mu^{-5}, \quad (32)$$
$$2\mu^3 f_6(\mu)=K_5(\mu)+8\mu^{-1}K_6(\mu)+\tfrac{1}{3}\mu^{-1}$$
$$-24\mu^{-3}+1152\mu^{-5}-30{,}720\mu^{-7};$$

γ is Euler's constant. For $\mu\ll 1$,

$$f_0(\mu)=\tfrac{1}{8}\mu^2, \quad f_2(\mu)=\tfrac{1}{16}\mu^2,$$
$$f_4(\mu) \text{ and } f_6(\mu)\ll 1/\mu^2. \quad (33)$$

For $\mu\gg 1$,

$$f_0(\mu)=\mu^{-4}[(\gamma-\tfrac{1}{2})+\ln(\mu/2)],$$
$$2f_2(\mu)=4f_4(\mu)=6f_6(\mu)=\mu^{-4}. \quad (34)$$

In the case of f_0 and f_2, these approximations are reliable to within about 2 percent except in the range $\frac{1}{5}<\mu<5$. Use of (33) at $\mu=1$ results in an error of 16 percent in f_0 and 19 percent in f_2; (34) is useless below $\mu=3$ for f_0 and below $\mu=20$ for f_6.

Let n be the number of dislocations per cm² of the xy plane, and S the area of the specimen in this plane; then $\sum_i \sum_j' s_i s_j F(\mathbf{R}_{ij})$ may be replaced by $nS[s_i \sum_j' s_j F(\mathbf{R}_{ij})]_{Av}$, the average being taken over all dislocations i. Let the dislocations about any given one be divided into three groups: (1) those at a distance small enough to permit the use of the approximation (33) over the range of fields under investigation; (2) those at a distance large enough to permit the use of (34); (3) those at an intermediate distance. For rough calculations, if the chief contribution at large distances is from f_0, group 3 need include only values of R_{ij} between the smallest $1/\lambda'$ and the largest $3/\lambda'$ for the range.

For the first group,

$$F(\mathbf{R}_{ij})=\tfrac{1}{8}\lambda'^{-2}R_{ij}^2(1-\tfrac{1}{4}\cos 2\theta_{ij})$$
$$=(3X_{ij}^2+5Y_{ij}^2)/32\eta; \quad (35)$$

this makes a positive contribution to $(\alpha^2)_{Av}$ if dislocations i and j have opposite signs, a negative contribution if they have the same sign. Let f_1 be the average *net* number of dislocations j *of opposite sign* to dislocation i, in group 1; then the sum over all i's and over j's within group 1 gives

$$[(\alpha^2)_{Av}]_1=(1/64)\pi k^2 n f_1 \eta^{-1}(3X^2+5Y^2), \quad (36)$$

where X^2 and Y^2 are average values of X_{ij}^2 and Y_{ij}^2 for *near* pairs of dislocations.

For the second group,

$$F(\mathbf{R}_{ij})=\lambda'^{-4}\{[(\gamma-\tfrac{1}{2})+\ln(\lambda' R_{ij}/2)]-\tfrac{1}{4}\cos 2\theta_{ij}$$
$$+\tfrac{1}{4}\cos 4\theta_{ij}+\tfrac{1}{12}\cos 6\theta_{ij}\}; \quad (37)$$

and if f_2 is defined for this group as f_1 was for the first, the contribution to $(\alpha^2)_{Av}$ is

$$[(\alpha^2)_{Av}]_2=\tfrac{1}{2}\pi k^2 n f_2 \eta^{-2}[c_0+\ln(\lambda' R/2)], \quad (38)$$

where $\ln R$ is an average of the values of $\ln R_{ij}$ for this group, and

$$c_0=(\gamma-\tfrac{1}{2})-\tfrac{1}{4}(\cos 2\theta_{ij})_{Av}+\tfrac{1}{4}(\cos 4\theta_{ij})_{Av}$$
$$+\tfrac{1}{12}(\cos 6\theta_{ij})_{Av}. \quad (39)$$

If the distribution of dislocations j about a given dislocation i is approximately isotropic at large distances, as seems likely, the angular terms will be small, and $c_0=\gamma-\frac{1}{2}=0.0772$. In this case $\lambda' R$ must be at least 3 by the definition of this group;

but a larger order of magnitude than 10 for $\lambda' R$ would require appreciable noncancelling contributions to $\ln R$ from R_{ij}'s greater than the "block" dimensions or interflaw distances ($\geqq 10^{-4}$ cm). Such correlation of dislocation positions in different blocks seems unlikely, and it may therefore be assumed that $\lambda' R \leqq 10$; then $\ln(\lambda' R/2) \leqq 1$.

Thus, finally,

$$1-J/J_s=\tfrac{1}{2}(\alpha^2)_{Av}$$
$$=(1/128)\pi k^2 n f_1 \eta^{-1}(3X^2+5Y^2)$$
$$+\tfrac{1}{4}\pi k^2 n f_2 \eta^{-2}[c_0+\ln(\lambda' R/2)]+\psi(\eta), \quad (40)$$

where $\psi(\eta)$ is the contribution of dislocation pairs separated by intermediate distances and is a more complicated function than the other two terms; or

$$J=J_s-a/H-b/H^2-\chi(H), \quad (41)$$

where

$$a=nf_1\cdot 9(\lambda_x G'\lambda_0)^2(3X^2+5Y^2)/128\pi C, \quad (42)$$

$$b=nf_2\cdot 9(\lambda_x G'\lambda_0)^2[c_0+\ln(\lambda' R/2)]/4\pi J_s, \quad (43)$$

$$\lambda'=(HJ_s/C)^{\frac{1}{2}}, \quad (44)$$

and $\chi(H)$ is a more complicated function. If only group 1 contributes, the formula reduces to that for doublets, since $n=2n'$. It is clear that: (1) dislocations separated by distances smaller than the magnetic decay distance contribute a $1/H$ term to the law of approach to saturation; (2) dislocations separated by distances at least several times the magnetic decay distance contribute, not a $1/H^2$ term, but a term $b(H)/H^2$, in which $b(H)$ varies logarithmically with H; (3) dislocations separated by intermediate distances contribute a more complicated approach to saturation.

4. Effect of Magnetic Interactions and of the Boundary

To take account of the internal field, Eqs. (17) and (18) must be used instead of Eq. (17a). The factor $\rho^2+\lambda'^2$ in the denominator of G must then be replaced by $\rho^2+\lambda'^2+h\cos^2\phi=\rho^2+\lambda'^2\sin^2\phi+k'^2\cos^2\phi$, where $k'^2=\lambda'^2+h$. The calculation for the doublets of §2 is simple enough to be carried out without difficulty; the result is[17]

$$1-J/J_s=n'(\pi k^2 C/8J_s)[H^{\frac{1}{2}}+B^{\frac{1}{2}}]^{-4}$$
$$\times[(H+4H^{\frac{1}{2}}B^{\frac{1}{2}}+B)X^2$$
$$+(H+4H^{\frac{1}{2}}B^{\frac{1}{2}}+5B)Y^2], \quad (45)$$

where $B=H+4\pi J_s$ is the induction. This reduces to the previous formula for $H\gg 4\pi J_s$ and gives an approximately constant deviation from saturation for $H\ll 4\pi J_s$. In the range $0.1<H/4\pi J_s<1$, in which data are available, the right member of (45) is only very roughly equivalent to an expression of the form $a'/H+b'/H^2$; if it is fitted to such a formula as well as is possible, the required a' is of the same order of magnitude as a (though somewhat smaller), and the required b' is not large enough to affect the order of magnitude of the observed b.

To estimate the effect of the boundary when positive and negative dislocations are not exactly equal in numbers, consider the finite cylinder for which the stress problem was solved in §1. The direct effect of the boundary on α, for a given stress, is unimportant compared with its effect on the stress itself; the former is limited to a region within a distance $\delta' \leqq 1/\lambda'$ of the boundary,[14] the latter extends throughout the specimen. The specimen may, therefore, be considered infinite provided the extra boundary term of Eqs. (10), (12), (16) is added to the stress. The value of α calculated in this way is the correct value inside the actual specimen and vanishes outside, except within a distance $\delta+\delta'$ of the boundary. The calculation of $\int \alpha^2 d\tau$ proceeds as in §3. The correction to be added to the previous value, Eq. (28), includes terms of the form $\sum_i s_i F_n(R_i)\cos n\beta_i$, which may be neglected, and a term

$$\left[\int \alpha^2 d\tau\right]_b=\tfrac{1}{2}\pi k^2 N\int_0^\infty \{N+4N[J_1(\rho r_1)/\rho r_1]^2$$
$$-4[J_1(\rho r_1)/\rho r_1]\textstyle\sum_i s_i J_0(\rho R_i)\}$$
$$\times\rho^{-1}(\rho^2+\lambda'^2)^{-2}d\rho, \quad (46)$$

which may be evaluated approximately by re-

[17] The integration over ρ is elementary. The integration over ϕ may be carried out by expressing the numerator in the integrand as a sum of terms $A_n\cos^n\phi\cos n\phi$. See D. Bierens de Haan, *Nouvelles Tables d' Intégrales Définies* (Leyden, 1867), p. 77, Table 47, No. 20.

placing the sum by an integral.[18] The third term in braces becomes twice the negative of the second; the integral may be evaluated by operating with $-(1/2\mu)d/d\mu$ on the simpler integral[13]

$$\psi(\mu)=\int_0^\infty \{1-4[J_1(x)/x]^2\}x^{-1}(x^2+\mu^2)^{-1}dx$$
$$=\mu^{-2}\{(\gamma-\tfrac{1}{4})+\ln(\mu/2)+4\mu^{-2}[\tfrac{1}{2}-I_1(\mu)K_1(\mu)]\}. \quad (47)$$

Since $\lambda' r_1 \gg 1$, the correction to $1-J/J_s$ reduces to

$$[1-J/J_s]_b=(\pi k^2/4S)(N^2/\lambda'^4)\times(\gamma-\tfrac{3}{4}+\ln\tfrac{1}{2}\lambda' r_1), \quad (48)$$

which is of the same general form as the contribution of pairs of dislocations separated by a large distance. One may consider each unneutralized dislocation to be accompanied by an induced or image dislocation on or outside the boundary, although a quantitative calculation by the method of images is not possible.[11]

It has been assumed throughout §§2–4 that, despite the severe lattice distortion at the dislocation, the interatomic coupling forces are able to maintain approximate saturation there as elsewhere.[19] Any weakening of the interatomic forces at a dislocation would produce an appreciable effect only within a distance $1/\lambda'$ of the dislocation; it would not affect the contribution of distant pairs of dislocations, but might seriously alter the contribution of near pairs.

5. Interpretation of Experiments

The calculations of §§2–4 justify the following statements. (1) Even a drastically simplified model, in which it is assumed that $H \gg 4\pi J_s$ and that positive and negative dislocations are present in exactly equal numbers, leads to a more complicated law than the empirical one; but a/H and b/H^2 terms are definitely present and important. (2) Although b is not strictly a constant, it may be replaced by a constant over a limited range because of its slow variation with H. (3) The assumption of equal numbers of positive and negative dislocations is not a serious restriction, for the boundary terms introduced by a lack of such equality are of the same form as the terms due to dislocation pairs separated by large distances. (4) For $H<4\pi J_s$, the $a/H+b/H^2$ law becomes an even worse approximation because of magnetic interactions; but the empirical a and b in this range are probably of the same order of magnitude as the theoretical a and b calculated for $H \gg 4\pi J_s$. In view of (3) and (4), the numerical calculations will be based on the simplified model of §3.

Kaufmann's data on twisted nickel,[20] reproduced in Fig. 3 of reference 14, show an approximately linear increase of a with plastic twist. From the specimen dimensions (given in the caption of the same figure), twist may be converted to plastic shear γ averaged over the cross section. Thus $da/d\gamma=5.6\times10^4$ e.m.u. with torque still acting, $=3.3\times10^4$ after its release. Similarly, $db/d\gamma=8.2\times10^7$ e.m.u. with torque acting, $=1.70\times10^7$ after its release; the former value is largely due to *elastic* strain and is in fair agreement with the theoretical value.

Consider first the part of b not due to anisotropy or to elastic stress, of amount 1.70×10^7 per unit of plastic shear. If this is given by Eq. (43), then $nf_2/\gamma=4\pi J_s(db/d\gamma)/9(\lambda_\infty G'\lambda_0)^2(c_0+\ln\frac{1}{2}\lambda' R)$. For definiteness take $R=10^{-4}$ cm and $\lambda'^2=1000J_s/C$ (Kaufmann's field range was 600 to 6000 oersteds); $c_0=0.07$; $J_s=500$ e.m.u., $\lambda_\infty=3.9\times10^{-5}$, $\lambda_0=2\times10^{-8}$ cm, $G'=6.5\times10^{11}$ dynes/cm^2,

[18] This step requires defense for two reasons. (1) The terms in the integral do not converge separately at $\rho=0$; therefore a slight change in one term might conceivably introduce a large error. (2) The difference between a continuous and a discontinuous distribution of dislocations might be important at large ρ because of the oscillations in $J_0(\rho R_i)$. Objection (1) may be met by expanding the integrand in powers of ρ: it vanishes for $\rho=0$ by virtue of $\sum_i s_i=N$, whatever the distribution of dislocations. Objection (2) does not apply until $\rho \leqq 1/l$, where l is the distance between dislocations; but by then $\rho r_1 \gg 1$, so that the contribution to the integral from this range of ρ values is small compared with the contribution from the range where the substitution is permissible. A rigorous calculation shows that the error is of order of magnitude $2\sum_i s_i R_i^2/Nr_1^2-1$.

[19] The contrary possibility was suggested at the end of reference 14, because of an apparent failure of magnetostrictive forces alone to give a large enough order of magnitude. But in the tentative calculation given there, the forces were supposed to be concentrated in a cross-sectional area of atomic dimensions at the dislocation; when they are properly localized in the stress field about the dislocation, the difficulty disappears.

[20] A. R. Kaufmann, Phys. Rev. **57**, 1089A (1940) and private communication.

$C=10^{-5}$ erg/cm. Then $nf_2/\gamma=2\times10^{10}$ dislocations per cm² per unit of plastic shear.

Consider next the value of a after release of the applied torque. Here positive and negative dislocations seek equilibrium positions in the same vertical plane, so that, approximately, $X=0$. To explain the linearity of a with γ and hence with n on the basis of Eq. (42), it may be supposed that dislocations are produced at certain favored positions on "block" walls (planes perpendicular to Ox) and are propagated along Ox, positives to the right and negatives to the left from opposite walls, until they reach a common value of x and become caught in each other's attraction. The plastic shear is then $\gamma=n'\lambda_0 L$, where L is the block length and $n'=$number of doublets per cm²$=\frac{1}{2}nf_1$. Thus nf_1 is proportional to γ, but Y is determined by conditions at the block walls, and therefore $a\propto\gamma$. If a value of Y is assumed in Eq. (42), nf_1/γ may be calculated from the experimental $da/d\gamma$.

The largest Y that is consistent with $Y<1/\lambda'$ throughout the range is about 2×10^{-6} cm. If Y has this value, $nf_1/\gamma=3\times10^{12}$ dislocations per cm² per unit of plastic shear. Then $L=2\gamma/nf_1\lambda_0=\frac{1}{3}\times10^{-4}$ cm. A smaller assumed value of Y would increase still further the value of nf_1, which is already 100 times as large as nf_2. Thus it appears that $f_1\gg f_2$: that is, most of the dislocations are accompanied by a companion dislocation of opposite sign no more than 2×10^{-6} cm away. Very closely, therefore, $f_1=1$; and with Y as assumed, $n/\gamma=3\times10^{12}$, and $f_2=2\times10^{10}/3\times10^{12}=0.007$.

In these calculations, no use has been made of Taylor's formula for the stress produced by an array of dislocations or of Kaufmann's data on the applied torque required to produce the plastic twist. An independent calculation of n/γ and L may be made by using Taylor's formula and the torque data and by assuming that after plastic flow the stress due to the dislocations balances the applied stress. This calculation gives $n/\gamma=1.4\times10^{12}$, $L=0.4\times10^{-4}$. Taylor's formula, besides being subject to the error[21] pointed out in §1, is based on a somewhat different picture from the "doublet" picture adopted here;[22] consequently an agreement in order of magnitude is all that can be expected. The only unsatisfactory aspect of the theory is that to obtain such agreement, a value of Y must be assumed; and the value required, though reasonable in other respects, necessitates pushing the approximation (33) to the limit of its applicability.[23]

The larger value of a under applied stress may be due to a larger n or to a nonvanishing X. It should be possible to decide this question when more is known about the distribution of dislocations and about their behavior under applied stress.

Magnetic measurements at higher fields are desirable. The analysis of data in the range $H<4\pi J_s$ is complicated by another factor in addition to the necessity for taking account of magnetic interactions. The theory neglects second-order terms in α and therefore becomes a poor approximation if the value of α given by Eq. (21) is an appreciable fraction of unity for any value of r. It follows that k/λ' must be small, or $\sqrt{(H/H_1)}$ must be large, where $H_1=(3\lambda_x G'\lambda_0)^2/\pi^2 CJ_s\doteq50$ oersteds for nickel. This condition is not very well satisfied in the lower part of Kaufmann's range.

---

[21] This error has been corrected in calculations recently completed and briefly reported by J. S. Koehler, Phys. Rev. **59**, 943A (1941). I am indebted to Dr. Koehler and to Mr. H. B. Huntington for helpful discussions and for the opportunity to compare my stress formulas with theirs in advance of publication.

[22] The doublet picture would probably not lead to Taylor's parabolic relation between stress and plastic strain: see reference 2, p. 174. The experimental mechanical data plotted in reference 14, Fig. 3, show a small but systematic deviation from such a parabolic relation.—Taylor's stress formula, combined with Kersten's theory of the magnetic effect of internal stress, leads to a formula $b=c'n(\lambda_x G'\lambda_0)^2/J_s$, with $c'\doteq3/125=0.024$ (W. F. Brown, Jr., Phys. Rev. **59**, 528 (1941)). The factor in Eq. (43) that corresponds to c' is $(9f_2/4\pi)(c_0+\ln\frac{1}{2}\lambda' R)$, and its numerical value according to the calculations of the last paragraph is 0.013.

[23] The order of magnitude $Y\leqq10^{-6}$ cm may be arrived at by the following independent argument, which, however, is highly speculative. Suppose that the "favorable" points on block walls are distributed at random but with an average spacing (along y) of m atomic distances λ_0. Then one out of m of the favorable points on the left wall is in the same atomic plane with a favorable point on the right wall. On these particular atomic planes, positive and negative dislocations can be generated at opposite ends and combine in the middle, and a large slip can result; elsewhere, dislocations can be produced but not annihilated, and the process is that described before. The spacing of these doubly favored planes, $m^2\lambda_0$, may be identified with that of the slip bands, $D\leqq10^{-4}$ cm; then $m=\sqrt{(D/\lambda_0)}$ and $Y=m\lambda_0=\sqrt{(D\lambda_0)}\leqq10^{-6}$ cm.

Determination of the Residual Current of an Ionization Chamber and the True Conductivity of Dielectric Liquids

ANATOLE ROGOZINSKI
Laboratoire de Physique Cosmique de l'Observatoire de Meudon, France

(Received May 28, 1941)

A method is described to determine residual current due to phenomena inside of an ionization chamber which are found to be essential for intensity measurements of cosmic rays. In an ionization chamber containing a dielectric liquid, the residual current can be practically identified with the true conductivity of the liquid. It is found that in the case of liquid hexane, the residual current amounts only to one-sixth of the total current. The method to be described here permits one to decide whether or not the true conductivity of the liquid tends to zero, if we continue to purify the liquid, or whether the liquid behaves, with respect to ionizing radiations, as a high pressure gas.

CERTAIN particularities are found for currents in highly isolating dielectric liquids (e.g. saturated hydrocarbons, CS_2, CCl_4, isolating oils, etc.) which cannot be explained by assuming a well-determined conductivity of the studied substances. It has been shown by Jaffé[1] that the current in a liquid (hexane, heptane, etc.) becomes considerably reduced if the liquid is surrounded by a layer of lead. At least one part of the current has, therefore, to be ascribed to the influence of cosmic radiation and of radioactive phenomena. To all of these influences we shall refer as "cosmic radiation."

In order to know the current which is due exclusively to the conductivity of the liquid, we would have to protect our substance completely from cosmic radiation. The same problem arises if we want to determine the residual current which is due to phenomena originating in the interior of an ionization chamber. The main contribution in this case is due to α-particles from natural radioactive contamination in the chamber walls. Steinke, Kolhörster, Pforte, Compton and others[2] have resolved the problem by measuring the current in an ionization chamber in a deep mine, where the cosmic radiation becomes almost entirely absorbed by the matter above the apparatus. The radioactive radiation of the mine was absorbed by a thick lead screen. An analogous study has never been made with an ionization chamber containing a dielectric liquid.

Measurements in a deep mine present certain difficulties which may not be detailed here. We have replaced this method by another one, the principle of which shall be briefly described here.

Let us consider two points, where the intensity of the cosmic radiation I and I' are sensibly different. The currents i_e and i_e' which are produced in a gas-filled ionization chamber placed successively at the two points will be, to a first approximation, proportional to the intensity of the radiation. We should expect, therefore, to obtain a straight line parallel to the pressure axis if we plot the ratio of the two currents at different pressures in a gas chamber.[3] As a matter of fact, this straight line is found only at a pressure above about 10 atmos. This fact shows that there exists, beside the current induced by cosmic radiation, a residual current i_r which is independent of external radiations and has mainly to be ascribed to the action of α-particles from radioactive contamination in the chamber walls. It can be easily seen that the relative influence of the residual current diminishes with increasing pressure, because, while the cosmic-ray current increases with pressure, the current due to α-particles becomes reduced, since the lack of saturation affects, to a much higher degree, the second part of the current. *We are thus led to the conclusion that the ratio of the measured currents $i' : i$ tends, with increasing pressure, to the ratio $\theta = I' : I$ of the intensities of the corresponding cosmic radiation.* This conclusion remains valid even if the observed current is not saturated—as

[1] G. Jaffé, Ann. d. Physik **28**, 326 (1909).
[2] E. S. Steinke, Zeits. f. Physik **48**, 647 (1928); W. Kolhörster, Zeits. f. Geophys. **6**, 341 (1930); W. S. Pforte, Zeits. f. Physik **65**, 92 (1930); A. H. Compton, E. O. Wollan and R. D. Bennett, Rev. Sci. Inst. **5**, 415 (1934).
[3] We admit that each of the components of the radiation loses in the gas a small fraction of its energy.

is always the case in compressed gases, except in the extremely pure rare gases—since it has been shown experimentally that the current is proportional, over a wide range, to the intensity of cosmic radiation. We obtain, therefore, two equations: $i_r+i_e=i$ and $i_r+\theta i_e=i'$, from which $i_e=i[1-(i'/i)]/(1-\theta)$ and $i_r=i[(i'/i)-\theta]/(1-\theta)$. The knowledge of θ permits one to separate the residual and the cosmic components of the total current. It permits one further to measure the absolute intensity of cosmic rays with an ionization chamber containing a gas of about atmospheric pressure, in which we can obtain saturation with a comparatively weak electric field applied to the electrodes of the chamber.

In the case of a dielectric liquid, the residual current has practically to be ascribed to the true conductivity of the liquid only. Indeed, the fraction of this current resulting from natural radioactive contamination of the walls of the chamber would be negligible because of the very small proportion of the ions escaping from the recombination in the ionized columns, produced by the α-particles.

The measurements have been performed (1) in the laboratory (L) and (2) in a room (R) especially protected against natural radioactive radiations. A constant temperature of this room could be maintained for a long time. The room was screened by double walls 1 meter apart, the intervening space was filled with 50 tons of distilled, inactive water, which had a considerable thermal inertia.[4] The measurements in both rooms, (L) and (R), obtained with an ionization chamber filled with pure argon or nitrogen compressed up to 90 atmos.[5] furnished for the barometer effect of the radiation the respective values 2.5 percent and 5 percent per cm Hg. The ratio θ was found to be 0.44.

We have used this value in order to separate the two components, as indicated above, in a hexane chamber,[6] the isolated electrode of which was connected with the (floating) grid of one of the electrometer valves of a bridge device. The stability of the device was sufficient to detect voltage differences of the order of 10^{-4} volt per minute, which corresponds to less than 10^{-16} amp. The measured currents were of the order of 10^{-14} amp.

The temperature at (R) was constant and equal to 14°C, the temperature of (L) varied. A great number of measurements were made to determine the temperature coefficient of hexane. By successive approximations, taking into account the barometric effect of cosmic radiation, we found finally the following values, which are reduced to 760 mm Hg and 14°C: temperature coefficient, 2.2 percent per degree C; total current in (L), 9.0×10^{-4} volt per sec.; total current in (R), 4.8×10^{-4} volt per sec.

In calculating the two components of the current, we found that one-sixth of the total current measured is due to the residual current. Our ionization chamber was not especially designed for conductivity measurements of the investigated liquid and only one approximative value of the absolute conductivity has been obtained. It is of the order of 10^{-19} ohm$^{-1}\cdot$cm^{-1}.

We do not want to enter here into discussion of the origin of the conductivity of hexane. It may possibly be caused by some impurities of the substance. The hypothesis that the conductivity of *pure* hexane be zero has been put forward several times,[7] but it has, so far, never been proved unambiguously. As a matter of fact, even at a place where only very little radioactive radiation was present, e.g., in (L), the true conductivity represents only a small fraction of the current, even for a liquid, on which the limit of purification has not been obtained. We want to point out here that only measurements in deep mines, or measurements of the type indicated above, will finally permit us to decide to what extent pure hexane, or other substances with saturated molecules, behave like gases at high pressure.

This work was done in 1939 in the Laboratoire de Physique Cosmique de l'Observatoire de Meudon (near Paris). I am very grateful to Professor A. Dauvillier, Director of the Laboratory, for the opportunity he most kindly afforded me to carry out this research.

[4] A. Dauvillier, Bull. Astronomique **10**, 123 (1937).
[5] A. Dauvillier and A. Rogozinski, J. de phys. et rad. (7) **9**, 152 S (1938).
[6] A. Rogozinski, J. de phys. et rad. (7) **8**, 128 S (1937).
[7] G. Jaffé, reference 1; J. Adamczewski, Nature **137** 994 (1936).

On the Interaction of Mesotrons and Nuclei

J. R. OPPENHEIMER AND JULIAN SCHWINGER
Department of Physics, University of California, Berkeley, California
(Received June 19, 1941)

THE formalism of mesotron field theories was first developed in analogy either with the method of classical electrodynamics that involves the determination of fields produced by pregiven sources, or with the perturbation technique of quantum electrodynamics. This program not only has led to predictions in contradiction with experiment (the singular nature of nuclear forces, and large cross sections for mesotron scattering by nuclei) but is intrinsically inconsistent, for the methods of electrodynamics, involving the neglect of the reaction of field on source, and based on the small magnitude of the coupling between charges and the electromagnetic field, are here quite unjustified. This inconsistency is rendered far sharper by the charge- and spin-dependent couplings of the mesotron theory. These difficulties have led to two apparently unrelated suggestions for modifying the formal treatment of mesotron theory.

Thus Heisenberg has attempted a more complete solution of the mesotron equations by including, within the framework of a classical theory, the large reaction of the field on the emitting source. He treated the problem of a neutral vector field interacting with a fixed, spatially extended source to which is attached a classical spin. His calculations showed that the inertia of the spin, arising from the reaction of its proper field, would greatly reduce the spin-dependent mesotron scattering. A relativistic variant of this procedure has been elaborated by Bhabha, who based his work on Dirac's classical electron model. Those terms in the field reaction on the source which become singular as a, the spatial extension of the source, vanishes, are discarded and the finite terms are evaluated in the limit of point coupling. However, it is precisely these singular terms that are essential for Heisenberg's explanation of the small mesotron scattering. Furthermore, quite apart from the serious question of whether this method affords a classical description of elementary particles, it is so essentially restricted to the classical domain that it provides no basis for a correspondence treatment of the actual quantum-mechanical problems encountered in a discussion of the scattering of charged mesotrons and of nuclear forces.

For this reason Bhabha himself and Heitler suggested the alternative theory of proton isobars. They observed that, from the point of view of perturbation theory, the large scattering arising from charge- and spin-dependent couplings is a consequence of the prohibition of certain intermediate states in the scattering process by the conservation laws for charge and angular momentum. They therefore proposed a modification of the assumptions of mesotron theory by postulating the existence of slightly more massive nuclear particles with arbitrary integral charge and half-integral spin. By a suitable choice of the excitation energy of the lowest isobars—high enough to make them escape ready detection—the scattering cross section could be reduced sufficiently to avoid conflict with experiment.

The connection between these two sets of ideas lies in the circumstance that a field strongly coupled to a charge or spin-dependent source will itself possess states in which charge or angular momentum is bound to the source, with the energy of the system increasing quadratically in its dependence on the total charge or angular momentum. This has been shown in detail by Wentzel for the charged scalar field. Wentzel used a lattice space to achieve convergence and considered only the limit of strong coupling. Despite the fact that his theory predicted isobars, his calculations indicated an inacceptably large value for the mesotron scattering cross section.

The evidence of nuclear forces shows, however, that the mesotron coupling is spin dependent, and indicates that the coupling constant itself is not very large. In order to see how these facts would modify Wentzel's conclusions, we have investigated a class of problems that throws some light on the earlier work and that also offers promise of a limited but consistent description of

the mesotron, in agreement with experience: nuclear forces on the one hand, and, on the other, the small scattering, zero spin, and highly multiple production observed for mesotrons in cosmic rays. We have, in part, generalized Heisenberg's treatment, and considered the classical problem of the coupling of neutral and charged, scalar and pseudo-scalar mesotrons to an extended, spatially fixed source. These problems are all rigorously soluble, for all values of the coupling constant and source size. In addition, we have treated Wentzel's quantum problem of the charged scalar field,[1] using an extended source instead of a lattice space, in the limit where the coupling constant g is large, $\gamma = g^2/hc \gg 1$, and have made the analogous calculation for the neutral pseudo-scalar in the corresponding limit $\gamma \gg \kappa a$ (here $\kappa = \mu c/h$ and μ is the mesotron mass). The problem of the charged pseudo-scalar has not been solved quantum-mechanically even in this limit, nor has any quantum solution been found for intermediate values of γ, or $\gamma/\kappa a$; nor have the revisions in nuclear forces been calculated in detail.

Nevertheless, we believe our results to be of some interest. The classical solutions for the pseudo-scalar always give states of bound angular momentum if $\gamma/\kappa a$ is not too small; the energy of these states depends on the total angular momentum J, as

$$\tfrac{3}{2}(\kappa a/\gamma)\mu c^2(J^2-\tfrac{1}{4}).$$

Here a is defined by

$$a^{-1} = \int d\tau K(\mathbf{r}) |\mathbf{r}-\mathbf{r}'|^{-1} K(\mathbf{r}') d\tau'$$

and $K(\mathbf{r})$ is the source function. The symmetrical scalar and charged scalar theories give solutions with bound charge, the former only if $2\gamma > 1$; and here the mass of the normal state of an isobar, for $\gamma \gg 1$, depends on the charge Q as $(\mu/\gamma)(Q-\frac{1}{2})^2$. For the symmetrical pseudo-scalar the condition for the existence of bound spin and charge is $2\gamma > 3\kappa a$. The quantum solutions for $\gamma \gg 1$ (charged scalar) and $\gamma \gg \kappa a$ (neutral pseudo-scalar) agree in these conclusions.[2] This agreement confirms the *a priori* expectation that, for large enough coupling, the quantum fluctuations of the source will be negligible compared to the reaction of the source to the field.

Classical scattering formulae, applicable when the proton recoil is negligible, give for all pseudo-scalar theories a scattering vanishing with a^2: this is a direct consequence of the fact that, in these theories, only p states are coupled to the source. Thus, for $\gamma \gg \kappa a$, and a mesotron momentum $p < \hbar/a$, the scattering cross section for a charged mesotron on the symmetrical pseudo-scalar theory is

$$d\sigma = \tfrac{3}{5}a^2(pc/E)^4(1+2\cos^2\vartheta)d\Omega, \qquad (1)$$

whereas for a charged scalar with $\gamma \gg 1$, $a \to 0$, it is just

$$d\sigma = (hc/E)^2 d\Omega. \qquad (2)$$

The results of the quantum solution agree with (2) for the charged scalar, and are of the same form as (1) for the neutral pseudo-scalar.

It is thus clear that pseudo-scalar theories can give a scattering small enough to agree with that observed, but that scalar theories could, at most, do so with a choice of γ far too small to account for nuclear forces. In fact, the experimental scattering results demand a value of a of the order of the proton Compton wave-length h/Mc, or possibly slightly smaller. Indeed, this length marks the extreme limit of validity of the methods we are using, and of the classical localizability of the source.

With this small value of a, and a value $\gamma \sim \frac{1}{10}$, which is derived from the magnitude of nuclear forces in singlet states, the spin and charge isobars will have an excitation only somewhat smaller than the rest energy of the mesotron.

This small value of γ would at first sight seem to be inconsistent with the high multiplicity of mesotron production in high energy nuclear collisions; but for pseudo-scalar theories this is not so. We have made an admittedly crude estimate of this multiplicity by calculating classically the excitation of the mesotron field when a proton's velocity and spin are suddenly

[1] Julian Schwinger, to be published soon.

[2] G. Wentzel (Helv. Phys. Acta **13**, 269 (1940)) gives $\gamma\kappa a \gg 1$ as the condition for the validity of his solution and, for the isobar separation $(\mu/\gamma\kappa a)(Q-\frac{1}{2})^2$. In both results $\gamma\kappa a$ must be replaced by γ. Wentzel's conclusions were obtained by overlooking the contribution to the isobar energy of order g^{-1} in the expansion of the Hamiltonian in descending powers of g. For a detailed discussion see reference 1.

altered, and then limiting the actual spectrum to mesotrons of total energy equal to or lower than the energy loss ΔE of the proton. In this way one finds a multiplicity $N \sim \gamma^{\frac{1}{3}}(\Delta E/\mu c^2)^{\frac{1}{3}}$, with a value 10 for $\gamma = \frac{1}{10}$, and an energy loss of 10^{10} volts. Under these conditions, and with a comparable value of γ, a scalar theory would give practically no multiple production.

It will be observed that we have used a value of γ given by the perturbation theoretic evaluation of nuclear forces. This is because, for singlet states, our theories still give forces of range $h/\mu c$, which have an effective depth of the order $\gamma\mu c^2$, and which behave like g^2/a for $\gamma < a$. The detailed radial dependence, and in particular the form of the tensor forces, remains to be investigated.

In conclusion, we should like again to emphasize that our present methods involve, in their physical content, only a rather more complete effort to take into account the reaction of the source to the mesotron field than either Bhabha's classical methods or the *a priori* postulation of isobars afforded. But it would seem that these methods are sufficient to decide definitely in favor of a pseudo-scalar, rather than a scalar or vector, field and to fix roughly the values of the coupling constant and source size needed to make the model definite.

Letters to the Editor

PROMPT publication of brief reports of important discoveries in physics may be secured by addressing them to this department. Closing dates for this department are, for the first issue of the month, the eighteenth of the preceding month, for the second issue, the third of the month. Because of the late closing dates for the section no proof can be shown to authors. The Board of Editors does not hold itself responsible for the opinions expressed by the correspondents.

Communications should not in general exceed 600 words in length.

Azimuthal Variations of Cosmic Radiation for 60° Zenith Angle at 22° Latitude

P. S. GILL
Research Fellow of the University of Chicago, Forman Christian College, Lahore, India
June 19, 1941

THE theory of the effect of the earth's magnetic field on cosmic rays, as worked out by Lemaitre and Vallarta and their collaborators, predicts a variation of cosmic-ray intensity at a given point on the earth's surface and fixed zenith angle, but for different azimuths (azimuthal effect). Dr. Hutner[1] has made a quantitative study of the azimuthal effect for a constant zenith angle of 60°, at a geomagnetic latitude of 20°, and has thus suggested a possible method for determining the energy spectrum of primary cosmic rays. The present experiment at Lahore (geomagnetic latitude 22° N) is being carried out to find the azimuthal variation of cosmic radiation at a fixed zenith angle of 60°, in order to compare with the predicted effect. This is a preliminary report on the experiment.

Four cosmic-ray telescopes are used, each consisting of three triple coincidence G-M counter tubes with lead filter of 10.2 cm. The distance between the centers of the outer tubes is 20 cm in each case. The solid angle range covered by each telescope is 14.5° in the vertical and 65° in the lateral planes. The telescopes are mounted on four edges of a square table, which is rotated automatically back and forth through an angle of 180°, so that opposite telescopes interchange positions at regular intervals. Each telescope stays in one position for 35 minutes. The connections to the recorders are automatically changed, so that each counts rays from one direction only. The interchanging of opposite telescopes at regular intervals automatically corrects for the inevitable differences in counting rates of the two sets. Cosmic-ray intensities from two directions can thus be compared with an accuracy depending only upon the statistical fluctuations of the total number of rays counted and possible instrumental errors, provided the apparatus is shifted back and forth between the two opposite directions at frequent intervals.

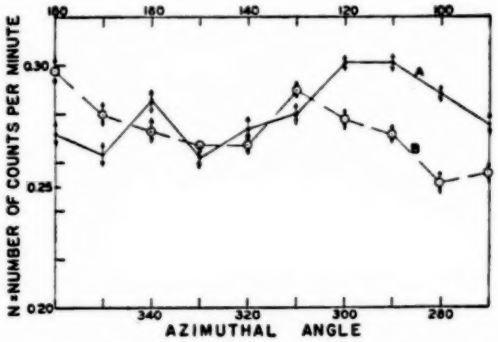

FIG. 1. Number of counts at various azimuthal angles.

The apparatus is installed in a special observatory constructed for the purpose on top of the new physics laboratory of Forman Christian College. The roof of the observatory is made of a single sheet of galvanized iron and is thus virtually open to the sky.

In Fig. 1, N, the number of counts per minute, is plotted against the azimuthal angle. Curve A represents the counts from the NW quadrant and curve B those from the SE quadrant. The probable error of each point is also shown in the figure. It is premature at this stage to compare the present data with Dr. Hutner's theoretical curve calculated for the energy distribution function $F(E)=B/E^{2.5}$. However, the directional asymmetries in NW and SE quadrants for zenith angle 60° at the latitude of Lahore are clearly shown by the two curves. The asymmetry 9.1 ± 0.8 percent for true magnetic north and south, can be compared with that calculated theoretically by Lemaitre and Vallarta[2] for 60° zenith angle and at 20 and 30 degree magnetic latitudes.

TABLE I. *Counts in NW quadrant (N_A) and in the SE quadrant (N_B)*

ANGLE	N_A	ANGLE	N_B	$\alpha=2\left(\frac{N_A-N_B}{N_A+N_B}\right)$
0	0.272 ±0.005	180	0.298 ±0.006	−0.091 ±0.008
350	0.263 ±0.005	170	0.280 ±0.005	−0.062 ±0.007
340	0.285 ±0.005	160	0.273 ±0.005	+0.043 ±0.007
330	0.262 ±0.005	150	0.267 ±0.005	−0.019 ±0.007
320	0.274 ±0.005	140	0.267 ±0.005	+0.026 ±0.007
310	0.280 ±0.004	130	0.290 ±0.004	−0.035 ±0.006
300	0.301 ±0.004	120	0.278 ±0.004	+0.080 ±0.006
290	0.301 ±0.004	110	0.272 ±0.004	+0.101 ±0.006
280	0.288 ±0.004	100	0.252 ±0.004	+0.133 ±0.006
270	0.276 ±0.004	90	0.256 ±0.004	+0.075 ±0.006

In Table I are given the counts per minute (N_A) for each angle in the NW quadrant while N_B represents the counts per minute in the SE quadrant. The asymmetry, $\alpha=2(N_A-N_B/N_A+N_B)$, is calculated at each 10° interval. The maxima of curve A (NW quadrant) corresponds to the maxima of Hutner's predicted theoretical curve, but is much less pronounced. In view of the fact that the resolving power of the telescopes is low, it is not to be expected that the curves should correspond closely. The experiment is being repeated with increased resolving power.

The author wishes to express his gratitude to the University of Chicago for supplying the apparatus. A grant from the Sir Dorabji Tata Trust is acknowledged. Forman Christian College has offered the facilities of the physics department.

[1] R. A. Hutner, Phys. Rev. **55**, 614 (1939).
[2] G. Lemaitre and M. S. Vallarta, Phys. Rev. **49**, 719 (1936).

Proper Lifetime of the Mesotrons

J. BARNÓTHY AND M. FORRÓ
Institute for Experimental Physics, University, Budapest, Hungary
May 25, 1941

EXPERIMENTS described in the present paper were designed to determine the average path length of the mesotrons before their decay, and thus the proper lifetime of the mesotrons. The experiments were performed in Budapest (124 m height, 47°30 geog. lat.). We used a twofold coincidence apparatus which had an angular aperture of 10×40 degrees and a sensitive area of 720 cm². The measurements were taken alternately in the vertical position of the counter telescope and at directions inclined 20 degrees to the north and south from the vertical. In order to cut out the soft component, 20 cm of lead was permanently placed between the counters. In the vertical position an additional absorber of 79 cm of wood was introduced between the counters; thus the absorbing power of the materials was the same in the vertical position as in the inclined direction, always being 1146 g/cm². In order to evaluate the required amount of wood absorber, we have assumed that the mesotrons are generated mainly at a height corresponding to 8 cm Hg pressure. The absorption power of the materials was computed in terms of equivalent electron densities. The mean barometric pressure at the place of the observations was 75 cm Hg. If we denote by J_0 the intensities, corrected for average barometric pressure and average temperature, in the vertical position, and by J_{20} the same quantity for the position inclined at 20°, we get from our measurements based on a total number of 2 3 million counts

$$J_0/J_{20}=1.060\pm0.002.$$

If l_0 and $l_{20}=1/\cos^{1.3}\vartheta$ denote the path length[1] of the mesotrons between the place where they were generated and the apparatus in the vertical and the inclined positions, respectively, then

$$J_0/J_{20}=\exp(l_{20}-l_0)/L$$

and the average path length of the mesotrons before decay (L) will be

$$L=1.45l_0=23 \text{ km}.$$

In order to evaluate the proper lifetime τ_0, the energy spectrum of the mesotrons must be taken into account:

$$J_0/J_{20}=\frac{\int_{E_1}^{\infty}\exp(-al_0/E)E^{-(\gamma+1)}dE}{\int_{E_1}^{\infty}\exp(-al_{20}/E)E^{-(\gamma+1)}dE}\;;\quad a=\frac{E_0}{c\tau_0},\qquad(1)$$

where E denotes the energy of the mesotrons at the place of their origin, E_1 the total energy loss throughout their path and $E_0=7\times10^7$ ev the energy of the mesotron when at rest. Assuming an energy loss of 2.4×10^6 ev (cm in air[2]) we have $E_1=2.8\times10^9$ ev. For all values of E coming into consideration, the exponent al/E will be $\leqq1$. Thus we have for $\gamma=1.7$ after developing in series $\tau_0=1.4\times10^{-6}$ sec. This value is, however, somewhat too low, because the mean energy with which a mesotron travels through the atmosphere is, on account of its energy loss in the air, 1.1×10^9 ev lower than its initial energy E. For the mean energy of the mesotrons of

$$\bar{E}=\frac{\int_{E_1}^{\infty}EdN}{\int_{E_1}^{\infty}dN}=\frac{\gamma}{\gamma-1}E_1=6.8\times10^9 \text{ ev},\qquad(2)$$

this will amount to 16 percent. Taking this into account we get, finally,

$$\tau_0=1.6\times10^{-6} \text{ sec}.$$

Because of the inaccurate knowledge of the height at which the mesotrons are generated, this value may be inaccurate to about 50 percent. For the sake of comparison, we collect here the values of the proper lifetime of the mesotrons found by other authors with similar methods. (All values are based on $E_0=7\times10^7$ ev.)

Rossi[3,4]	$\tau_0=1.5\times10^{-6}$ sec.
Pomerantz[5]	1.8×10^{-6} sec.
Barnóthy and Forró	1.6×10^{-6} sec.

We express our gratitude to the Hungarian Academy of Science and the Szécheny Scientific Society for the financial support of these investigations.

[1] J. Barnóthy and M. Forró, Nature **144**, 116 (1939).
[2] H. J. Bhabha, Proc. Roy. Soc. London **164**, 257 (1938).
[3] B. Rossi, Nature **142**, 993 (1938).
[4] In the quoted article Rossi assumes that the rest energy of the mesotron is 40 times smaller than the mean energy. We have estimated, with the help of Eq. (2), the mean energy in his case to be 3.8×10^9 ev and thus $E_0=9.5\times10^7$ ev.
[5] M. A. Pomerantz, Phys. Rev. **57**, 3 (1940).

The Effect of Temperature on the Secondary Electron Emission from Nickel

MONICA HEALEA AND CHARLOTTE HOUTERMANS
Vassar College, Poughkeepsie, New York
June 20, 1941

THE effect of the temperature of a nickel target on its secondary electron emission when it is bombarded with helium ions of about 1000-ev energy has been studied with the same apparatus and the same procedure used in previous work.[1-3] The temperature was varied gradually from about 900°C down through the Curie point nearly to room temperature. No change was found in the emission greater than the usual random variations of about 1 percent occurring in these measurements when the target is kept at a constant high temperature. This result is to be compared with that of Wooldridge[4] who studied the same effect with electrons of about 160-ev energy as primary bombarding particles. He obtained a very small temperature coefficient of secondary emission and a change due to the magnetic transformation of nickel of less than 0.3 percent. Since measurements made with an electron beam are more consistent than those made with an ion beam drawn from a gas discharge, the results of the two studies are in agreement within experimental error. It is interesting to note that this is true in spite of the difference in energy and kind of the primary particles.

[1] Monica Healea and E. L. Chaffee, Phys. Rev. **49**, 925 (1936).
[2] Monica Healea, Phys. Rev. **55**, 984 (1939).
[3] Monica Healea and Charlotte Houtermans, Phys. Rev. **58**, 608 (1940).
[4] D. E. Wooldridge, Phys. Rev. **58**, 316 (1940).

Total and Scattering Cross Sections for Slow Neutrons

MARTIN D. WHITAKER AND WILLIAM C. BRIGHT
New York University, University Heights, New York
June 27, 1941

WE have continued the work previously reported[1] on the angular distribution of slow neutrons scattered from various materials and are now able to separate the total interaction cross section of these samples into scattering and capture components with a fair degree of accuracy. The samples varied in transmission from 50 percent to 80 percent. In cases where only thick samples have been used (Mn compounds) some slight modification may later be necessary because of the multiple "scattering."

The apparatus used for the scattering measurements[1] can best be described as an annular ring arrangement. Large samples, in the form of cylinders 28 cm in diameter and of sufficient thickness to transmit the desired percentage of the incident thermal neutrons, were placed between a boron detector and a 400-mg radium-beryllium neutron source which was suitably placed in a paraffin "howitzer." The detector was shielded from the direct gamma- and neutron-radiation by means of cadmium, boron carbide, and lead shields, so that only neutrons scattered through selected angles could reach the detector. By varying the distance between detector and howitzer, and by varying the region of the sample that is irradiated with neutrons, it is possible to study the scattering in the various angular regions between 0° and 90°. A back scattering arrangement was used for the angles from 90° to 180°.

The observations consisted of comparing the number of neutrons scattered into a given angular region with the number scattered by a standard sample under the same geometrical conditions. Carbon, lead, and CS_2 were used at different times as the comparison materials. It is known that carbon does not capture slow neutrons, but its small mass causes the scattering to deviate from spherical symmetry slightly and there may be some deviation also due to Debye scattering. Lead is heavy enough to eliminate the first difficulty and one expects that there will be little Debye scattering because of the small amount of coherent scattering.[2] In the case of CS_2 no important crystal effects are to be expected, but the sulfur may capture slightly. An averaging of the scattering over various angular regions for these selected samples reduces the uncertainty of the results due to interference.

Measurements of total cross sections were made in the usual way with a parallel neutron beam. Of course, in all measurements mentioned here, observations with and without a cadmium filter were used to eliminate all counts except those due to thermal neutrons. While it is impossible to say that the scattering cross sections given here are those of an isolated nucleus, it is believed that the samples have been so selected and studied that the modification of the scattering interaction by interference[2,3] is very small. Values of the various cross sections are listed in Table I. The capture cross section was obtained by subtracting the scattering value from the total. The measurements are such that the uncertainties in the σ_c column should not be greater than about one unit.

TABLE I. *Values of total, scattering, and capture cross sections in units of 10^{-24} sq. cm.*

MATERIAL	σ_t	σ_s	σ_c	σ_c(COLTMAN)
C	4.5	4.5	0	....
Pb	10.0	9.0	1	....
CS_2	9.0	8.5	0.5	0.88
Fe	12.8	9.5	3.3	2.1
Ni	21.2	13.9	7.3	6.2
Cu	10.3	5.5	4.8	4.3
Mn	15.1	2.1	13	....

It should be pointed out that these results depend on the fact that carbon does not capture slow neutrons and on the assumption that the averaging over the various angles corrects the results for asymmetry in scattering due to any cause. The values of σ_c recently obtained by Coltman[4] are listed in column 5. Our value of σ_c for manganese is considerably higher than the 9.4 which Rasetti[5] found.

Financial support from the American Academy of Arts and Sciences is gratefully acknowledged.

[1] M. D. Whitaker and W. C. Bright, Phys. Rev. **57**, 1076 (1940).
[2] Franco Rasetti, Phys. Rev. **58**, 321 (1940).
[3] H. G. Beyer and M. D. Whitaker, Phys. Rev. **57**, 976 (1940).
[4] John W. Coltman, Phys. Rev. **59**, 917 (1941).
[5] Franco Rasetti, Phys. Rev. **58**, 869 (1940).

Artificial Radioactivity of Ti^{45}

J. S. V. ALLEN,* M. L. POOL, J. D. KURBATOV AND L. L. QUILL
The Ohio State University, Columbus, Ohio
June 30, 1941

A STRONG radioactive positron period of 3.08 hours has been produced both by proton and deuteron bombardment of scandium. The activity is assigned to Ti^{45} according to the nuclear reactions, $Sc^{45}(p, n)Ti^{45}$ and $Sc^{45}(d, 2n)Ti^{45}$.

The elements in the titanium region have been quite thoroughly examined by Walke[1,2] and others. However, no references are made to the above reactions.

By use of the method previously employed by one of us (J.D.K.)[3,4] the chemical procedure departed from the commonly used one in that the precipitation of titanium in the presence of scandium was performed without the addition of a titanium carrier. The large quantity of added inactive titanium which is normally used, and which impedes filtration and augments contamination due to its colloidal state, is thus avoided. Titanium in concentrations as low as 10^{-15} gram per liter has been successfully precipitated without a carrier.

If the logarithm of the half-life of Ti^{45} is plotted against its atomic number, the point falls very close to the curve given by Dickson and Konopinski[5] for nuclei with one excess neutron and an even atomic number.

It is a pleasure to acknowledge the help given by The Ohio State University Development Fund and Mr. Julius F. Stone.

* On sabbatical leave from Bethany College, Bethany, West Virginia.
[1] H. Walke, Phys. Rev. **51**, 1011A (1937).
[2] Walke, Williams, and Evans, Proc. Roy. Soc. **A171**, 360 (1939).
[3] J. Kurbatov, Am. J. Phys. Chem. **36**, 1241 (1932).
[4] J. D. Kurbatov, M. L. Pool, and H. B. Law, Phys. Rev. **59**, 919A (1941).
[5] G. R. Dickinson and E. J. Konopinski, Phys. Rev. **58**, 949 (1940).

Uranium Fission with Li–D Neutrons: Energy Distribution of the Fission Fragments

K. LARK-HOROVITZ AND R. E. SCHREIBER
Department of Physics, Purdue University, Lafayette, Indiana
June 17, 1941

THE energy distribution of the fission fragments from slow neutron bombardment has been reported by different observers (Jentschke and Prankl,[1a,1b] Haxel[2]). Two energy groups are found corresponding approximately to 60 and 95 Mev. These groups are separated by a valley about one-fourth the height of the peaks if the number of particles is plotted against energy. Some observers have also used fast neutrons (Ra-Be neutrons;[1] D – D neutrons, Kanner and Barschall[3]) and in this case the valley is considerably raised. One can, therefore, conclude that with fast neutrons symmetrical fission should be observed, and we started some time ago to investigate the energy distribution of the fission fragments with Li – D neutrons.[4]

The recoil energies were observed in an ionization chamber with a linear amplifier and recording oscillograph which was calibrated with alpha-particles and artificial pulses to extrapolate to the energy range used. Two different uranium samples were used: (a) uranium metal of 0.18 mg/cm² sputtered on an aluminum foil of 0.17 mg/cm², which was used both for measurements of total ionization and of single fragment energies, and (b) uranium oxide deposited electrolytically on a brass disk.

By surrounding the ionization chamber with 25 cm of paraffin and water, the fission with slow neutrons has been recorded and the results found in agreement with those of former investigators. Both types of targets show two peaks (with single particles) at 64 and 95 Mev.

The paraffin was then removed and the slow neutrons filtered out with cadmium shields. We now observed new modes of fission. Besides the two peaks observed before, there now appeared a peak corresponding to 86 Mev. This peak we assigned to the symmetrical fission. There also appeared peaks at 52 and 110 Mev[5], which apparently correspond to highly asymmetrical fission such as has been found by Nishina[6] who identified Hg and Bi among fission fragments from Li-D neutron bombardment.

About 5 percent of the total number of tracks give a peak of much higher energy, at 130 to 135 Mev, which we believe is due to a new type of fission as predicted by Present:[7] ternary or triple fission. Some fragments have even higher energy, 145 Mev, but are quite rare; they are 0.5 percent of the total number of tracks.[8]

By using the thin foil and observing the total ionization, these results are substantiated. With slow neutrons the main peak occurs at 164 Mev. With fast neutrons the main peak appears at 172 Mev and there is a definite indication of fragments of a still higher energy corresponding to 190 to 200 Mev.

The measurement of the energy distribution thus confirms the process of symmetrical fission corresponding to the chemical evidence in the experiments of Yasaki[9] and Segrè and Seaborg[10] and agrees also with the observation of the fission tracks on the photographic plate as described recently by Lark-Horovitz and Miller.[11]

The existence of high energy fragments in appreciable numbers is attributed to ternary fission. The masses of the fragments lie in the same region as those from ordinary asymmetric fission, therefore no chemical evidence is available. From Present's calculations,[7] about 20 Mev more energy should be released in this process. This is in agreement with our observations. It is not possible, however, to distinguish between triple fission and a binary fission with the fragment masses in the ratio 2 : 1 from ionization-chamber measurements alone. It will be necessary to use a cloud chamber or direct photographic detection. This work is now in progress.

[1a] W. Jentschke and F. Prankl, Akad. Wiss. Wien **148**, 372 (1939).
[1b] W. Jentschke and F. Prankl, Physik. Zeits. **40**, 706 (1939).
[2] O. Haxel, Zeits. f. Physik **112**, 681 (1939).
[3] M. H. Kanner and H. H. Barschall, Phys. Rev. **57**, 372 (1940).
[4] This conclusion has been confirmed since this work was begun by the discovery of fission products in the region between Pd and In by Yasaki (reference 9) and Segrè and Seaborg (reference 10).
[5] Pulses as high as 110 Mev have been observed by Kanner and Barschall (reference 3, p. 376).
[6] Y. Nishina, *et al.*, Nature **144**, 547 (1939).
[7] R. D. Present, Phys. Rev. **59**, 467 (1941).
[8] Jentschke and Prankl (reference 1a) record a few fragments of 140-Mev energy and attribute them to the total energy of both fragments even in a thick target experiment. This explanation is excluded by our experimental arrangement.
[9] T. Yasaki, Inst. Phys. Chem. Research Tokyo **37**, 457 (1940).
[10] E. Segrè and G. T. Seaborg, Phys. Rev. **59**, 212 (1941).
[11] K. Lark-Horovitz and W. A. Miller, Phys. Rev. **59**, 941 (1941).

On a Magneto-Acoustic Effect

M. RAMA RAO
Department of Physics, University of Mysore, Bangalore, S. India
April 29, 1941

IN recent years considerable interest has developed[1] among chemists and physicists in the determination of the velocity of sound in liquids by means of high frequency sound waves. These measurements are valuable for our knowledge of molecular properties. From a comparison of the velocity of sound in various homologous series, it is concluded that the spatial arrangement of the atoms in the liquid molecules plays the decisive part in the magnitude of velocity of sound. Thus aromatic compounds always have a higher velocity of sound than aliphatic compounds.

Cotton and Mouton discovered that when light traverses a liquid placed in a strong magnetic field in a direction transverse to the lines of force, the liquid exhibits a feeble birefringence. The double refraction exhibited by liquids when placed in a magneto-static field is ascribed, in the theory of Langevin, to an orientation of the molecules produced by the field, the orientative couple arising from an assumed magnetic anisotropy of the molecule. If an optical anisotropy of the molecule is postulated in addition, the birefringence of the liquid follows as a necessary consequence. A feeble birefringence is noticed when fluids are placed in an electrostatic field. This is known as the Kerr effect. Since the magnetic anisotropy of the molecules results in a tendency to orientate themselves relatively to the lines of force in a magnetic field, one would expect a change in the velocity of sound when the fluid is placed in a strong magnetic field. The change to be expected can be calculated by the well-known thermodynamic equations.

We have, considering unit mass of magnetic material in a field H,

$$TdS=du+Pdv-Hd\sigma,$$

where T = temperature, S = entropy, u = internal energy, P = external pressure, v = volume of the liquid, H = strength of magnetic field, σ = magnetic moment per unit mass of the liquid.

Assuming the validity of Curie's law for paramagnetic substances we have

$$\sigma/H=c/T \text{ where } c \text{ is a constant.}$$
$$(d\sigma/dT)_H=-cH/T^2,$$

substituting for $d\sigma$ one gets

$$TdS=(c_v+cH^2/T^2)dT+Pdv.$$

The effect of the magnetic field may be supposed to result in an increased value of c_v by an amount cH^2/T^2. From the equation of state of Van Laar,[2] which holds well for liquids, it can be shown from thermodynamics that the velocity of sound V is given by

$$V=(\gamma c_v/\alpha_P)^{\frac{1}{2}}[\tfrac{2}{3}(1+2b_0/v)/(1-b_0/v)\lambda]^{\frac{1}{2}},$$

where α_P is the coefficient of volume expansion, b_0 is the value of b when $v=v_0$ at absolute zero, λ is the ratio of the total to the translatory energy, γ is the ratio of specific heats. In the presence of a magnetic field we therefore have

$$V'=V[1+(cH^2/T^2c_v)]^{\frac{1}{2}},$$
$$(V'-V)/V=1\sigma H/2Tc_v$$

or the change in the velocity $=(1\sigma H/2Tc_v)V$. In the case of nitrobenzene, which is strongly anisotropic, one might expect, at ordinary temperatures, about 3 to 4 percent change. Dr. L. Sibaiya has promised me that he will carry out the experiments to verify the above conclusion. I thank him for very valuable suggestions in the course of this work.

[1] L. Bergmann, *Ultrasonics* (John Wiley and Sons, New York, 1939).
[2] Van Laar, Proc. Roy. Acad. Amst. **27**, 897 (1924).

The Mechanism of the Sodium Coulometer*

JOSEPH STEIGMAN
Pupin Physics Laboratories, Columbia University, New York, New York
May, 1941

BURT[1] has described a method of introducing metallic sodium electrolytically into a glass tube. The technique consists essentially of inserting an electric light bulb into molten sodium nitrate, and running the electrolysis current in such a direction that electrons from the filament are carried to the glass wall opposite the molten salt. After a few minutes, a metallic film of sodium metal becomes visible on the inside of the bulb. The system obeys Faraday's law to 1 part in 500,[1] and with adequate precautions, to 1 part in 10,000.[2]

A mechanism for this phenomenon has been proposed. Burt[1] postulates that sodium ions on the inside of the glass are neutralized and vaporized as metal, and that sodium ions from the fused salt replace those of the glass, and eventually migrate through it. The latter argument is supported by the work of Zworykin,[3] who finds that for a sodium-potassium glass immersed in molten potassium nitrate, the metal formed on the inside of the bulb is primarily sodium, and that the glass is enriched in potassium. The following experiment was performed with radioactive sodium (half-life 14.8 hours) in an attempt to confirm this mechanism.

One hundred and fifty grams of sodium nitrate (C.P.) were bombarded with slow neutrons. The nitrate was then fused in an iron crucible, and a G.E. Mazda T-10 clear 25-watt, 120-volt bulb was dipped into the molten salt to a depth of a half-inch. The lamp was connected to the 120-volt d.c. line through a 500-watt bulb which served as a series protective resistance. A copper rod attached to the positive lead from the line dipped into the nitrate bath. At the end of an hour of electrolysis, the bulb had gained 26 milligrams in weight. The activity of the sodium metal inside the bulb was tested by opening the bulb, removing the sodium and placing it on a Geiger-Müller counter. For comparison at the end of the electrolysis, a sample (of known weight) of the molten nitrate was ground and wrapped around the counter. The results are indicated below:

SAMPLE	ACTIVITY PER GRAM SODIUM
Sodium nitrate bath	17,800 counts/minute
Sodium deposited inside bulb	39 counts/minute

Were the mechanism of the process one of actual diffusion of the sodium ions from the fused nitrate directly through the glass, the activity per gram of the electrolytically deposited sodium should have been 17,800 counts per minute, whereas the observed activity is but 0.2 percent of this value. Actually, the activity of the 26 milligrams of sodium collected from the inside of the bulb was barely observable above the background of the counter.

The process therefore appears to be one of displacement as Burt has proposed, rather than one of simple diffusion. In this connection, the outer part of the glass bulb which had been dipped into the molten bath was quite radioactive, as would be expected. Because of the marked curvature of the bulb in that region, and because of the thickness of the glass, it was difficult to measure this activity accurately, but within the limits of error it was the correct value to be expected if sodium had gone into the glass from the bath in an amount corresponding to the sodium found on the inside of the bulb.

It should be pointed out that it is possible, through a modification of the technique used here, to measure the rate of diffusion of sodium ions through glass at various temperatures. That is to say, experiments comparing rates of ionic migration under differing electrical and thermal conditions are thus made possible.

* Publication assisted by the Ernest Kempton Adams Fund for Physical Research of Columbia University.
[1] R. C. Burt, J. Opt. Soc. Am. and Rev. Sci. Inst. **11**, 87 (1925).
[2] O. J. Stewart, J. Am. Chem. Soc. **53**, 3366 (1931).
[3] V. K. Zworykin, Phys. Rev. **27**, 813 (1926).

Proceedings of the American Physical Society

Minutes of the Pasadena, California, Meeting

June 18–20, 1941

THE 242nd regular meeting of the American Physical Society was held at the California Institute of Technology, Pasadena, California. On the afternoon of June 18 a joint session with the Astronomical Society of the Pacific was addressed by J. Holmboe, J. Strong, E. C. Slipher, and S. B. Nicholson, who spoke on various aspects of the dynamics of atmospheres. The afternoon session of June 19 consisted of a symposium on electron microscopes in which Otto Beeck, Alfred Marshak, and William V. Houston participated. A dinner for physicists, astronomers and guests on the evening of June 18 was attended by 100 persons. A physics luncheon on June 19 was addressed by President George B. Pegram. The thirty-five contributed papers abstracted and indexed below were presented in three morning sessions on June 18, 19, and 20. Numbers 5, 28, and 31 were read by title.

Paul Kirkpatrick
Local Secretary for the Pacific Coast
Stanford University, California

Abstracts

1. A Radiant Energy Theory of the Absorption of Primary X-Rays, Ionization and Photoelectron Emission. Samuel R. Cook, *Sacramento, California.*—An explanation of the absorption of primary x-rays by matter has been made, in accordance with the tenets of the radiant energy theory of primary x-rays. It has been shown that the products of the absorption of an x-ray or radiant energy quantum by an electron are a high speed beta-electron and an ionized molecule. It has also been shown that the high speed beta-electron, if it does not escape from the absorbing material, may make collision with a nucleus of the adsorbing material and generate secondary or fluorescent x-rays and that if it does escape it is what is known as a photoelectron, which explains photoelectron emission. Both ionization and photoelectron emission are, therefore, according to the tenets of the radiant energy theory, products of the absorption of x-rays. Equations for the absorption of x-rays were developed and it is shown that the equation for the absorption of a primary x-ray and the liberation of a beta-electron was identical with Einstein's equation for photoelectron emission which has been verified by Millikan and associates.

2. Internal Conversion in Photosynthesis. J. R. Oppenheimer, *California Institute of Technology.*—In some chlorophyll (cpl) containing algae, light absorbed by a fluorescent dye apparently produces photosynthesis. It has been suggested that this is because the cpl absorbs the fluorescent radiation of the dye, but the calculated absorption, using the known fluorescent yield, cpl concentration n and absorption coefficient σ, is far too small. We wish to point out that energy transfer from dye to cpl can be enormously enhanced by the fact that there are cpl oscillators far closer than a wave-length to the fluorescent source. This transfer gives a large scale model of the internal conversion of nuclear gamma-rays. A simple calculation gives, for the ratio of quanta transferred to cpl to those emitted in fluorescence, $no\lambda\!\!\!^{-4}/d^3$, where $2\pi\lambda\!\!\!^{-}$ is the fluorescent wave-length in water, and d the closest distance of approach of cpl and dye oscillators. With reasonable values for d this can explain a very high photosynthetic yield.

3. The Theory of Light Nuclei. Edward Gerjuoy and Julian Schwinger, *University of California.*—The existence of the deuteron quadrupole moment indicates the presence of tensor nuclear forces which destroy the constancy of orbital angular momentum, and thus necessitates a revision of the theory of light nuclei. In H^3, the tensor forces directly couple to the fundamental $^2S_{\frac{1}{2}}$ state a $^4D_{\frac{1}{2}}$ state, which in turn interacts with $^2P_{\frac{1}{2}}$ and $^4P_{\frac{1}{2}}$. To the fundamental $^1S_0$ state of He^4 is admixed a $^5D_0$ state which interacts with $^3P_0$. Thus all states consistent with the total angular momentum occur. These nuclei therefore constitute the simplest examples of the break-down of spin conservation laws. We have performed a variation calculation employing trial wave functions of the character $^2S_{\frac{1}{2}}+{}^4D_{\frac{1}{2}}$ for H^3, and $^1S_0+{}^5D_0$ for He^4, with simple Gaussian radial functions. Using the known force constants for rectangular well potentials, the calculations yield 40 and 50 percent of the binding energy for H^3 and He^4, respectively. A similar test calculation for H^2 gave 20 percent of the binding energy. The probability that these nuclei are in the D state was found to be 4 percent for all three nuclei; this value is in agreement with the exact deuteron computations. Calculations with improved trial functions are in progress.

4. Nuclear Electron Pairs from O^{16}. E. P. TOMLINSON, *California Institute of Technology.*—A magnetic electron pair spectrograph[1] has been used to investigate the energy of the excited pair-producing state of O^{16}.[2] A discussion of the data both for singles and coincidence measurements is presented. Comparison of the singles positron spectra of the nuclear pairs and of photoelectric pairs from the 6.2-Mev γ-rays of another excited state of O^{16} supports qualitatively the theoretical prediction for energy distribution discussed by J. R. Oppenheimer in paper No. 11 of this meeting. The energy of the pair producing state is found to be 6.0 ± 0.2 Mev above the ground state of O^{16}.

[1] E. P. Tomlinson, Phys. Rev. **59**, 216A (1941).
[2] Fowler and Lauritsen, Phys. Rev. **59**, 253 (1941).

5. Statistical Analysis of the Earth's Internal Magnetic Field. WALTER M. ELSASSER, *California Institute of Technology.*—In order to represent the irregular (non-dipole) part of the internal magnetic field of the earth the following model is considered. A finite number of dipoles are distributed with random positions inside a spherical shell concentric with the earth. Probabilities are calculated for the amplitudes with which the higher spherical harmonics appear in the field thus produced. The results are statistically compared with the harmonic components of the observed field of which 42 are numerically known, making a sufficiently large population to permit significant statistical inferences. The theory may be used to determine the outer radius of the spherical shell from the magnitude of the observed coefficients. This radius is found to be approximately $0.50R$ (where R is the earth's radius) and it is definitely not in excess of $0.55R$, the radius of the earth's core. The result is independent of the number of dipoles used to represent the irregular field, provided the latter is not excessively large.

6. The Latitude Effect of Primary Cosmic-Ray Intensity. SHUICHI KUSAKA, *University of California.*—Relative values of the total incident energy and the energy incident vertically of the primary cosmic rays have been calculated for the geomagnetic latitudes at which high altitude experiments were carried out by Pickering and Neher[1] in India. These calculations were based on the Lemaitre-Vallarta theory of the geomagnetic effect, and it was assumed that the distribution in number of the primaries was given by the inverse cube of the energy. The results of the calculation are:

Geomagnetic latitude	3°	17°	25°
Total incident energy	100	110	130
Vertically incident energy	100	108	125

The values given are relative values normalized to 100 at 3°. It may be noted that the approximate $\cos^4\lambda$ law for the variation of the minimum energy for vertical incidence gives much greater variation of the vertical intensities at 3° and 17°.

[1] W. H. Pickering and H. V. Neher, Bull. Am. Phys. Soc., Washington Meeting, May 1, 1941, No. 84.

7. The High Energy Soft Component of Cosmic Rays. R. F. CHRISTY AND J. R. OPPENHEIMER, *University of California.*—The recent proof[1] that the majority of the primary cosmic rays are not electrons necessitates an entirely different explanation of the atmospheric transition curve, and demands a separate source for the energetic soft radiation responsible for large showers and bursts at higher elevations and for Auger showers. Schein's suggestion that the primary protons are, in the stratosphere, almost entirely converted into preferentially low energy mesotrons which mostly decay in the atmosphere, is capable of accounting for the transition curve in air, but fails to explain the source of the energetic soft component. Apart from the possibility that a small but sufficient fraction of the primaries are electrons, two possibilities suggest themselves. There will be a weak radiation associated with the creation of mesotrons, analogous to the internal bremsstrahlung of electrons, although complicated by the probably multiple production of mesotrons. Or we may have to do with production, in numbers roughly equal to that of penetrating mesotrons, of fast-decaying mesotrons. Mesotrons decaying in $\sim10^{-8}$ sec. would account for the increase in large bursts and showers with elevation, as well as for β-decay lifetimes.

[1] M. Schein, W. P. Jesse and E. O. Wollan, Phys. Rev. **59**, 615 (1941).

8. On the Charged Scalar Mesotron Field. JULIAN SCHWINGER, *University of California.*—The charged nature of the mesotron field and the large magnitude of nuclear coupling prohibit both the conventional perturbation discussion and the classical approach to mesotron dynamics. This situation is particularly evident in the current treatment of the anomalously large theoretical scattering of charged mesotrons by nuclear particles. To circumvent these difficulties, Bhabha and Heitler have proposed the existence of slightly more massive states of the nucleon with charges of 2 and -1 units. However, such isobaric states may be expected to be a consequence of the large nuclear coupling binding mesotrons in stationary states around the nucleon. This has been investigated for the scalar mesotron field interacting with an infinitely massive nucleon through a finite-distance coupling, in the limit of large coupling strength. Stationary states of the system exist for all values of the total charge number Q, the energy exhibiting a quadratic charge dependence, $E=E_0+\frac{1}{2}\epsilon(Q-\frac{1}{2})^2$. The quantity ϵ varies inversely with the square of the coupling strength. The mesotron scattering cross section is of the order of nuclear dimensions for large coupling. The scattering is non-multiple, the scattered field consisting of equal numbers of positive and negative mesotrons.

9. Multiple Production of Mesotrons by Protons. E. C. NELSON AND J. R. OPPENHEIMER, *University of California.*—A puzzling feature of mesotrons is that their production in the upper atmosphere by primary cosmic rays (presumably protons[1]) in collisions with nuclei is copious, and probably highly multiple, while their subsequent absorption through nuclear scattering is apparently not multiplicative, and rare. This feature appears in a model in which

the mesotron field is strongly coupled to the proton,[2] instead of weakly coupled as is assumed in usual perturbation treatment of nuclear problems. A proton scattered by a nucleus radiates a mesotron field which is given, for short collision times, by the difference between the field of the proton before and after the collision. Calculation of the number of mesotrons emitted, using a charged, scalar mesotron field and determining the cut-off in momentum space by conservation of energy, gives for large energy loss of the proton a multiplicity

$$\frac{1}{3\pi}\frac{g^2}{\hbar c}\ln\left(\frac{10\Delta E}{\mu c^2}\right),$$

in close analogy to the corresponding radiation problem, and for

$$\frac{\Delta E}{\mu c^2}\frac{\hbar c}{g^2}\ll 1$$

a multiplicity $\Delta E/\mu c^2$.

[1] M. Schein, W. P. Jesse and E. O. Wollan, Phys. Rev. **59**, 615 (1941).
[2] See abstract No. 8 of this meeting.

10. Cloud Chamber for Cosmic-Ray Studies. CARL D. ANDERSON AND SETH H. NEDDERMEYER, *California Institute of Technology.*—A large cylindrical cloud chamber of 60-cm diameter and 7.5-cm depth has been constructed for observations on cosmic rays. It is mounted in an electromagnet capable of producing a field of 7000 gauss throughout the whole volume of the chamber at a power consumption of 60 kw. Higher field strengths (up to 12,000 gauss) are obtainable at the same power under conditions where the full vertical length of the chamber can be photographed, but where the horizontal width available for photography is limited. All the necessary operations are carried out automatically and Geiger counters are used for tripping the chamber. By means of two cameras, two views are taken and by reprojection through the same optical system the tracks are reproduced in space for stereoscopic measurements.

11. Long-lived Radioactive Cd from Deuteron Bombardment of Ag. A. C. HELMHOLZ, *University of California.*—In connection with work on the 40-sec. Ag isomer growing from the 6.7-hr. Cd activity,[1] a long period Cd also resulting from the Ag(d,2n)Cd reaction has been observed. Its half-life is 158±7 days. The radiations consist of soft electrons, x-rays and γ-rays, in agreement with the findings of Krishnan.[2] In addition it has been found that a 40±3 sec. Ag activity grows from this long-lived Cd. Attempts to find isomerism of the 158-day activity decaying to the 6.7-hr. activity have failed. Photographs taken with a β-ray spectrograph show for the short period a converted γ-ray of energy 92 kv, for the long period a converted γ-ray of 86 kv. It is believed that this difference is real. If so, both Ag^{107} and Ag^{109}, formed by K capture, have excited states which decay to the ground states with half-lives of about 40 sec. Both long and short periods have weak γ-rays of energy about 600 kv. A discussion of possible level schemes will be given.

[1] L. W. Alvarez, A. C. Helmholz and E. Nelson, Phys. Rev. **57**, 660 (1940).
[2] R. S. Krishnan, Proc. Camb. Phil. Soc. **36**, 500 (1940).

12. Circuit Independence of Charge in Fast Counter Pulses. H. G. STEVER, *California Institute of Technology.*—The mechanism of discharge of fast, or self-quenching, counters, which was postulated to explain the dead-time and associated phenomena,[1] demands efficient ionization in the neighborhood of the wire. This ionization must take place in a short time and be largely independent of the external circuit constants such as series resistance and capacity to ground of the wire system. The independence of amount of charge with respect to the external resistance is easily shown. The charge in a single pulse was measured for various values of resistance and voltage. At a particular voltage, the charge did not vary with series resistance. The charge did increase approximately linearly with over-voltage, or voltage above threshold. The independence of charge with respect to the wire-to-ground capacity was shown by varying both R and C to keep RC constant. The voltage pulse varied linearly with $1/C$ indicating independence of amount of charge with respect to capacity.

[1] H. G. Stever, Phys. Rev. **59**, 219 (1941).

13. The Energy Spectrum of H^3 β-Rays. CARL E. NIELSEN, *University of California (Introduced by R. B. Brode).*—H^3 is β-radioactive with long half-life; the maximum β-ray energy is of the order of 10 kev. The total ionization, hence the energy, of a low energy β-particle can be measured with the Wilson cloud chamber, if individual droplets can be counted, and if the correlation between droplets formed and ions present is known. The drop-ion correlation and the average energy loss per ion pair were determined from a study of the droplet clusters produced in the chamber by 8.86-kev x-ray photoelectrons. H^3 β-rays result in similar clusters. Count of the droplets gives the β-ray energy. 108 H^3 clusters photographed have a mean energy of 6.5 kev. For a Fermi distribution, the maximum energy is 9/5 of the mean; 9/5 of 6.5 kev is 11.7 kev. In disagreement with this value, linear extrapolation from the observed distribution indicates a maximum of 14.5 kev; and several clusters of 13.5 kev were observed. It is believed that the maximum energy is 14.5±1 kev.

14. Recoil from K Capture. L. W. ALVAREZ, A. C. HELMHOLZ AND B. T. WRIGHT, *University of California.*—Using a method similar to that used in the classical β recoil experiments,[1] we have exposed in vacuum a clean surface to a vacuum distilled layer of 6.7-hour Cd, formed by the Ag(d,2n)Cd reaction. We collected on this clean surface an activity of 40 seconds half-life, which must be the Ag activity known to be the daughter of the 6.7-hour Cd.[2] This passage of the Ag from one surface to the other may be due to (1) recoil from the neutrino emitted in the K capture of the Cd, (2) recoil from the x-ray following K capture, or (3) a change in the surface binding of the atom when it undergoes K capture.

[1] Philipp Donat, Zeits. f. Physik **45**, 512 (1927).
[2] L. W. Alvarez, A. C. Helmholz and E. Nelson, Phys. Rev. **57**, 660 (1940).

15. The Crystal Photo-Effect in d-Tartaric Acid. CHUNG KWAI LUI, *Oregon State College (Introduced by J. J. Brady).*—Brady and Moore[1] observed a crystal photo-effect in

tartaric acid. They reported that certain crystals which appeared to have flaws and were not very transparent gave a current response which started out in one direction just after the light was turned on, decreased rapidly with time of illumination, and then flowed in the opposite direction. This phenomenon has been investigated in detail. All clear well-formed single crystals exhibit this current-reversal phenomenon when light falls on certain points of the crystal surface. These points always lie between two regions which respond with normal current flows in opposite directions. The superposition of the two normal current-response curves gives a resultant which agrees with the observed current-reversal curve within the experimental error. The various current response curves for different illuminated faces of the crystal, including the current-reversal effect, are correlated by assuming a particular direction in the unit cell of the crystal for which the electrical conductivity is a maximum. The crystal photo-effect decreases rapidly as the temperature is raised above 23°C. At 50°C the photo-current approaches zero.

[1] James J. Brady and William H. Moore, Phys. Rev. **55**, 308 (1939).

16. Diffusion in Alloys and Mechanical Strength. S. KYROPOULOS, *California Institute of Technology.*—In general, the structure of cast alloys does not represent equilibrium conditions. Thus, solid solutions tend to approach equilibrium by diffusion. If its rate differs for the components, diffusion must result in local volume expansion and formation of gaps. An extreme case has been previously studied by Masing and Overlach. It suggested itself in a typical case of bearing failure by cracking. Preceding cracking, mostly individual crystallites rise from the surface and carry the load in nonfluid lubrication, reducing the available surface by about 50 percent. The crystal boundaries are richer in the faster diffusing Sn. Consequently, gaps must form at the boundaries causing there stress concentrations which explains the predominance of boundary cracks, previously communicated by the author. Volume expansion was demonstrated by an optical method and confirmed by density measurements on annealed specimens. The cracked alloys show typical annealing structure. The phenomenon is general with current bearing alloys and sets a basic limit to strength obtainable with multicomponent alloys. Due to its fundamental nature it may play a part in other fatigue phenomena.

17. Atmospheric Potential Gradient at Exposed Coastal Stations. E. J. FARRELL AND N. E. BRADBURY, *Stanford University.*—The diurnal variation in the fair-weather potential gradient of the earth involves two components. One of these, the unitary variation, changes simultaneously over the earth, and the other, the local variation, varies with local station time. Since the latter is primarily due to the normal daily convective cycle in the atmosphere over land stations, it should disappear over the open sea, and should be greatly reduced at exposed coastal stations subjected to a prevailing on-shore wind. Accordingly a portable recording potential gradient apparatus was constructed and set in operation on an exposed bluff near Golden Gate. The potential gradient values were compared with those recorded simultaneously at Stanford University. From the differences in the type of variation observed, an estimate of the magnitude of the effect of the unitary variation may be obtained.

18. Rapid Precision Gas Analysis by Infra-Red Absorption. R. ROBERT BRATTAIN AND O. BEECK, *Shell Development Company, Emeryville, California.*—Binary or, in some cases, multi-component mixtures of hydrocarbon gases are analyzed for a specific component by determination of the percent transmission at a single spectral position. Choice of this wave-length, which need not necessarily coincide with an absorption maximum of the component in question, and the method of finding the most favorable spectral slit width and specific adsorption path will be described. Application of this method in the analysis of two isomeric mixtures proved accurate to ± 0.5 percent for rapid routine analyses, but is more accurate under special precautions. One analysis (including sampling) takes about one-quarter man-hour as contrasted with 5 to 10 man-hours for the usual low temperature distillation. The method is easily adapted to continuous recording and to plant control for both gaseous and liquid streams. By selecting several suitable spectral positions more complicated mixtures could be completely analyzed. Although these analyses were performed on the research instrument described in abstract number 35, an inexpensive, simplified control instrument has already been constructed.

19. Direct Pen Recording of Galvanometer Deflections. D. J. POMPEO AND C. J. PENTHER, *Shell Development Company, Emeryville, California (Introduced by O. Beeck).*—A recorder is described which records directly the deflections of any instrument, using a light pointer, without recourse to photographic development processes. The recording is easily accomplished at pen speeds of 12.7 cm. per second across 25 cm. of chart without "hunting" taking place. The instrument has been satisfactorily used, with considerable saving in time, for recording current-voltage curves in polarographic analysis; for obtaining infra-red absorption curves; and for recording ion currents in mass-spectrographic work. Essentially the basic idea of this recorder is that the pen follows the light beam from an external galvanometer by mounting a double cathode photo-tube on the pen carriage so that both move as a unit. By means of vacuum tube amplifiers operating a reversible motor, the pen carriage moves to the left when the light beam deflects to the left on to the left photo-tube cathode and to the right when the right photo-tube cathode is exposed.

20. Infra-Red Reflectivities of Nickel at High Temperatures. CURTIS REID, *Oregon State College.*—The changes in the spectral reflectivity of nickel with temperature have been measured directly between 20° and 920°C in the region between 0.8 and 11μ. The reflectivities and their changes with temperature for wave-lengths longer than 5μ were found to be entirely in accord with Drude's formula $R=100-3650(\rho/\lambda)^{\frac{1}{2}}$; ($\lambda$ in microns, ρ in ohm-cm). In passing to shorter wave-lengths the reflectivity decreases more rapidly than the formula indicates and passes through

a sharp minimum of 58 percent at 1.0μ. The ratio of the reflectivity at 920°C to that at 20°C changes from 0.96 at 5μ through 1.00 at 2.15μ to 1.06 at 0.8μ. This corresponds to a change in the temperature coefficient of reflectivity from -4.4×10^{-5} per degree at 5μ through zero at 2.15μ to $+6.6\times10^{-5}$ per degree at 0.8μ.

21. Electrical Conduction and Crystallization Phenomena in Thin Films Deposited at Low Temperatures. EDGAR L. ARMI, *California Institute of Technology.*—An apparatus for depositing metal films by evaporation in high vacuum and measuring their electrical resistances up to 10^{15} ohms, previously described,[1,2] was redesigned for work at temperatures down to 14°K. After 4 minutes of deposition at low temperatures, at a rate of 2A/min., Pb films showed beginning of electrical conduction. When the molecular beam had been shut off, films 10A thick displayed the following behavior: Below 100°K, conductivities increased by a factor of several hundred towards stationary values, a phenomenon which was accelerated by raising the temperature. At ca. 100°K, decrease of conductivity set in and was greatly speeded up by higher temperatures, leading finally to complete destruction of conduction. To explain this behavior, it may be assumed that two different processes are occurring in the films: (1) formation of conductive metal from the deposited molecules, (2) agglomeration into crystallites, the latter process taking place at appreciable rates at temperatures only above 100°K.

[1] A. B. Anderson and A. Goetz, Phys. Rev. **45**, 293 (1934).
[2] M. G. Foster, Phys. Rev. **57**, 42 (1940).

22. A Carbon Carrier of Oligodynamically Active Silver for Water Disinfection. F. S. HARRIS, JR., A. GOETZ AND R. L. TRACY, *California Institute of Technology.*—A carbon carrier of active silver has been developed to utilize the disinfecting properties of oligodynamic silver ion concentrations (0.05–0.5 parts per million). A certain type of hard carbon, consisting mainly of lamp-black, was found to fulfill the prerequisite conditions of electrical conductivity and capacity for electrolytic adsorption. This material in the form of small cylinders is impregnated with silver by soaking it first in a silver nitrate solution. After air-drying the carbon is heated in a muffle furnace to reduce the silver to metallic form, finely dispersed throughout the body of the carrier. The silver is then "activated" by making the carrier anode in an electrolyte and charging with 50–60 coulombs/g carbon at a current density of about 7 ma/cm^2 for 30 minutes. Subsequently, the carbon-silver-carrier is rinsed, dried and ready for use. It is stable over very long periods of time, unaffected by temperatures ($<$300°C) and humidity. Upon immersion in water the carrier emits germicidally active silver; the emission, declining exponentially with time, is complete in a few hours. Water thus treated oligodynamically is nontoxic, tasteless and odorless.

23. Dependence of Band Absorption on Pressure. MARTIN SUMMERFIELD AND JOHN STRONG, *California Institute of Technology.*—Experiments on carbon dioxide,[1] water vapor,[2] and ozone[3] have yielded the result that, over a wide range of pressure, the infra-red absorption is proportional to the fourth-root of the total pressure. This fact suggested that the widths of infra-red lines are proportional to the square-root of the pressure, not to the first power, as the Lorentz theory requires. Formulas for the integrated absorption of a band[4] were applied to our measurements on ozone[5] and an "effective value" of the rotational spacing of the 9.6μ band was calculated. Using this value, it is shown that the empirical $p^{\frac{1}{2}}$ relation can be derived on the basis of Lorentz line broadening, and is consistent with the proportionality of width to pressure. This slower increase of absorption with pressure is due to the overlapping of the wings of lines, the fourth-root dependence appearing even though the width is less than 1/10 of the spacing.

[1] G. Hertz, Verh. deut. phys. Ges. **13**, 617 (1911).
[2] J. Kühne, Zeits. f. Physik **84**, 722 (1933).
[3] Strong and Watanabe, Phys. Rev. **57**, 1049 (1940).
[4] Elsasser, Phys. Rev. **54**, 126 (1938).
[5] Summerfield and Strong, Phys. Rev. **59**, 217A (1941).

24. X-Ray Studies of Magnesium Single Crystals at Low Temperatures. A. DEMBER AND A. GOETZ, *California Institute of Technology.*—The effect of temperature on the reflection of x-rays from Mg single crystals was investigated in the range from 14°K to 300°K. Intensity distributions (rocking curves) of the Mo $K\alpha$ doublet were obtained with a recording ionization spectrometer of the Bragg type. The crystal was mounted in a cryostat, previously described,[1] and could be maintained at constant temperature anywhere between the triple point of hydrogen and room temperature. Evaluation of the records enables one to determine the relative integrated intensities of reflection as well as the changes in lattice spacing. Measurements were made on planes perpendicular and parallel to the hexagonal axis for different orders of reflection. Characteristic temperatures (Θ_{II}, $\Theta_{\perp}$) and coefficients of thermal expansion (α_{II}, $\alpha_{\perp}$) were calculated and a discussion is given of their relation to data[2,3] (obtained by other methods) on thermal and electrical properties of single crystals and polycrystalline material.

[1] A. Goetz and A. Dember, Phys. Rev. **56**, 857 (1939).
[2] H. Ebert, Zeits. f. Physik **47**, 712 (1928).
[3] P. W. Bridgman, Proc. Am. Acad. **66**, 255 (1931); **67**, 29 (1932).

25. An Absolute Intensity Determination in the Continuous X-Ray Spectrum of Nickel. EDWARD SMICK AND PAUL KIRKPATRICK, *Stanford University.*—A sheet of nickel 506A thick, backed only by a film of cellulose acetate, was bombarded normally by 60 microamperes of electrons of 15.0-kev energy. X-rays leaving the target in a direction making a mean angle of 88° with the direction of motion of the electrons were analyzed with Ross filters of copper and nickel having a pass band at 1.431A and were then absorbed in a large standard ionization chamber filled with air. Absolute charge measurements were made with a calibrated electrometer. Corrections for absorption and other disturbing effects were applied. Taking the energy per ion pair as 33 electron volts these measurements give for the stated wave-length, emission angle, electron energy and target element a radiation output at the target of 2.2×10^{-50} ergs per unit frequency interval per steradian per bombarding electron per atom-per-square-centimeter of

target area. No quantitative theory fully applicable to these conditions is known, but Sauter's[1] treatment with a slight modification predicts the value 2.9×10^{-30}, agreeing with the experiment within the uncertainties of the two values.

[1] F. Sauter, Ann. d. Physik **20**, 408 (1934).

26. Further Experiments Concerning the Determination of h/e by the Short Wave-Length Limit of the Continuous X-Ray Spectrum. J. W. M. DuMond, W. K. H. Panofsky and A. E. S. Green, *California Institute of Technology.*—Recently, new results regarding the value of h/e as obtained by x-ray methods were obtained by Bearden and Schwarz[1] and Per Ohlin.[2] The experiments of Bearden and Schwarz reconfirm the value of h/e as obtained previously which lies about 0.2 percent lower than the value computed from indirect determinations. The value of Ohlin agrees with the preliminary results obtained by us and the indirectly computed values. In order to investigate the cause of these discordant results the influence on the shape and position of short wave-length limit isochromats of the following factors was noted: (1) the effect of deposits on the target was investigated by installing a device in the x-ray tube to clean the target in vacuum. (2) The effect of the slow decline of the monochromator pass band "wings" was investigated further by using a 2-crystal monochromator in conjunction with a set of balanced filters and by changing the wave-length separation between the filter edges and the crystal monochromator peak. The conclusion was reached that both factors will profoundly influence the value of h/e as obtained by short wave-length limit measurements.

[1] Bearden and Schwarz, Bull. Am. Phys. Soc., Washington Meeting, May 1–3, 1941.
[2] Per Ohlin, Arkiv Mat. Astro. Fysik, 27B, No. 10 (1940).

27. The Polarization of X-Rays from Thin Targets. Brewer F. Boardman, *Stanford University and Fresno State College* (*Introduced by Paul Kirkpatrick*).—The polarization of x-rays from thin nickel, silver, and lead targets is measured as a function of tube voltage for the wave-length band between 0.176 and 0.184A. The targets are thinner than 1000A, made by vacuum evaporation onto thin plastic films. The method is that of 90° scattering from paraffin as used in a previous study,[1] but the x-ray tube is redesigned to eliminate stray radiation at voltages above 110 kv and to use targets of large area. Corrections are calculated for secondary and tertiary scattering in the paraffin. The rays from silver show the same complete polarization at the quantum limit as those from Piston's 1700A foil, have slightly higher polarization between 70 and 90 kv and lower beyond 90 kv. Nickel gives similar results; and of two nickel films the thinner gives somewhat more polarized rays. X-rays from lead are apparently only three-quarters polarized at the limit, and depolarize more rapidly with increasing voltage than those from films of lower atomic number. The polarizations decrease more rapidly than is called for by Elwert's theoretical work.[2]

[1] Piston, Phys. Rev. **49**, 275 (1936).
[2] Elwert, Ann. d. Physik **34**, 178 (1939).

28. Extended X-Ray Absorption Fine Structure in Solutions. S. T. Stephenson, *State College of Washington.*—The extended K absorption structures of Cu and Se in $CuSeO_4$ solutions of about $1N$ concentration have been studied. Se shows a definite structure which is similar to that for the solid state.[1] This substantiates the view[1] that the immediate surroundings of the atom from which the K electron comes are more important in determining extended fine structure than the crystal lattice itself since Se still has its four O neighbors while in solution, but is no longer in a crystal lattice. Cu showed no extended fine structure pronounced enough to be observed. This can be expected because the Cu ion in solution lacks the close neighbors which it had in the solid state.

[1] S. T. Stephenson, Phys. Rev. **58**, 873 (1940).

29. Relative Intensities in the Nickel Continuous X-Ray Spectrum. Keith Harworth and Paul Kirkpatrick, *Stanford University.*—A sheet of nickel 199A thick, prepared by condensation upon a thin film of cellulose acetate, was bombarded normally with electrons in the energy range from 10 to 180 kev. X-radiation leaving the target in a direction making a mean angle of 93.5° with the direction of motion of the electrons was analyzed with Ross filters and an ionization chamber. (The apparatus resembled that of abstract 25 but was an entirely separate outfit.) Wave-length bands centered at 0.497A (Ag-Pd), 1.01A (Se-As) and 1.431A (Cu-Ni) were isolated by the filters and intensity measurements performed at voltages within the above range. The data were corrected for electron retardation and scattering in the target, for slight effects due to the backing film and other matter near the target, and for various absorptions to which the radiation was subject. Isochromats and spectrum curves for the independent nickel atom are in partial agreement with theoretical curves.

30. New Spectra in Nitrogen. Joseph Kaplan and Sidney M. Rubens, *University of California at Los Angeles.*—A tube, containing nitrogen at 50 mm and conditioned to produce a strong auroral afterglow when properly excited, has been studied when the discharge is weak. The weak discharge resembles the ozonizer used by Wulf and Melvin to excite the Vegard-Kaplan bands at atmospheric pressure. The green line is strong in the continuous "ozonizer" discharge and it is accompanied by the Vegard-Kaplan bands and by a set of five bands between 5000A and 6100A, one of which falls under the green line. The new bands and the green line disappear when enough oxygen is added to quench the auroral afterglow. The bands persist as the oxygen cleans up. The weak discharge is the most auroral-like source of the green line so far observed. The addition of helium reduces the intensity of both the green line and the new bands. The presence of these bands as well as the high efficiency of the green line excitation may thus be due to chemical action in the discharge, the green line due to excitation and dissociation of ozone and the new bands to N_3 or to a triatomic oxide of nitrogen.

31. Resonance Broadening of Homogeneous Caesium Vapor in Absorption. CHRIS GREGORY, *California Institute of Technology.*—The resonance broadening of homogeneous Cs vapor in absorption was studied by means of the contour method. The intensities were obtained via the method of "astigmatic photometry" by utilizing the astigmatism of the Rowland grating. The pressure of the homogeneous absorbing vapor ranged from 10^{-2} to 17.5 mm Hg. The half-breadth varied rather linearly with the number of atoms per unit volume, with $(\gamma_1/N)\times 10^7 = 1.45$, $(\gamma_2/N)\times 10^7 = 0.84$ for the $^2P_{3/2}$ and $^2P_{1/2}$ components, respectively, of the resonance lines. The average value of the ratio of half-breadths γ_1/γ_2 was found to be 1.8. The experimental half-width γ is found to be about $1\frac{1}{2}$ times larger than that predicted by Professor Houston. Below pressures of 10 mm Hg the lines exhibited symmetrical broadening according to the "dispersion" formula. At higher pressures indications of a violet and red asymmetry are present for the $^2P_{3/2}$ and $^2P_{1/2}$ components, respectively. A definite band on the red side of the $^2P_{3/2}$ and one on the violet side of the $^2P_{1/2}$ was observed.

32. The Quadrupole Moment of the Deuteron and the Range of Nuclear Forces. JULIAN SCHWINGER, *University of California.*—The quadrupole moment is a unique property of the deuteron, for its very existence demands a finite range of the forces. This is a simple consequence of the observation that the D wave function must vanish in the limit of zero range, for being of the form $e^{-\alpha r}(1+3/\alpha r+3/(\alpha r)^2)$, it possesses inadmissible singularities. This fact, combined with the upper limit to the amount of D state provided by magnetic moment measurements, sets a lower limit to the range of nuclear forces. This limitation can be placed in quantitative form with the aid of the approximate equations:

$$w_D=\frac{5}{3}\frac{\alpha r_0}{1+\alpha r_0}\chi^2, \quad Q=\frac{2^{\frac{1}{2}}}{6}\frac{r_0^2}{1+\alpha r_0}\chi,$$

which express the D state probability and the quadrupole moment in terms of the force range and the quantity χ, the ratio of the D to S wave function at the boundary of the well. Hence, $w_D=30\alpha r_0(1+\alpha r_0)(Q/r_0^2)^2$, an equation which is practically independent of any details of the interaction other than that both ordinary and tensor interactions possess the common range r_0. Thus the limitation $w_D<5$ percent implies $r_0>2.6\times 10^{-13}$ cm.

33. On the Internal Pairs from Oxygen. J. R. OPPENHEIMER, *California Institute of Technology.*—Because the pair producing fields are here limited to the interior of the nucleus, the energy and angle distribution of the internal pairs from excited O^{16} is quite different from that for pairs made by gamma-rays and by internal conversion. In deriving the distribution we can neglect the Coulomb field and the ratio of nuclear radius to wave-length. We then find, if $E\pm$, $p\pm$ are energy and momentum of positron and electron, and ϑ is the angle between them,

$$dN=dE_+d(\cos\vartheta)p_+p_-(E_+E_--m^2c^4+p_+p_-c^2\cos\vartheta).$$

34. On a Modification of Planck's Quantum Theory with Special Reference to an Explanation of His Oscillators. SAMUEL R. COOK, *Sacramento, California.*—A statement of Planck's quantum theory in the light of the tenets of the radiant energy theory of the geneses and absorption of primary x-rays is given and it is shown that, if the processes of geneses and absorption, as given in the radiant energy theory, be substituted for Planck's oscillators, Planck's quantum theory is very simply explained. It is also shown that the quantum concept is applicable both to geneses and absorption and that, with the modification of Planck's quantum theory, by the substitution of the radiant energy theory *processes* for Planck's *oscillators*, a quantum theory for all forms of radiation may be simply and scientifically explained.

35. An Automatic-Recording Vacuum Spectrograph for the 2μ to 27μ Region. R. ROBERT BRATTAIN, *Shell Development Company, Emeryville, California.*—An infra-red vacuum spectrograph, of the Wadsworth-Littrow type, which incorporates the following features, is described: (1) A double bilateral slit is opened automatically and continuously by a cam arrangement in such a manner that the energy remains constant when either the 2μ to 15μ or 14μ to 27μ region is mapped. (2) The prism is turned by another cam arrangement at such a rate that regardless of the variation of spectral slit-width with prism position and regardless of the variation of actual slit-width necessary to maintain constant energy, the prism turns through each spectral slit-width in constant time. (3) As a result of (1) and (2) an approximately constant spectral slit-width is maintained over a large part of the 2μ to 27μ region. (4) Absorption spectra are recorded directly and automatically in terms of percent transmission *versus* wave-length.

Author Index to Abstracts of Papers Presented at the Pasadena Meeting

Alvarez, L. W., A. C. Helmholz and B. T. Wright—No. 14
Anderson, Carl D. and Seth H. Neddermeyer—No. 10
Armi, Edgar L.—No. 21

Beeck, O.—see Brattain, R. Robert
Boardman, Brewer F.—No. 27
Bradbury, N. E.—see Farrell, E. J.
Brattain, R. Robert—No. 35
—— **and O. Beeck**—No. 18

Christy, R. F. and J. R. Oppenheimer—No. 7
Cook, Samuel R.—Nos. 1 and 34

Dember, A. and A. Goetz—No. 24
DuMond, J. W. M., W. K. H. Panofsky and A. E. S. Green—No. 26

Elsasser, Walter M.—No. 5

Farrell, E. J. and N. E. Bradbury—No. 17

Gerjuoy, Edward and Julian Schwinger—No. 3
Goetz, A.—see Dember, A.
—— see Harris, F. S., Jr.
Green, A. E. S.—see DuMond, J. W. M.
Gregory, Chris—No. 31

Harris, F. S., Jr., A. Goetz and R. L. Tracy—No. 22
Harworth, Keith and Paul Kirkpatrick—No. 29
Helmholz, A. C.—No. 11
—— see Alvarez, L. W.

Kaplan, Joseph and Sidney M. Rubens—No. 30
Kirkpatrick, Paul—see Harworth, Keith
—— see Smick, Edward
Kusaka, Shuichi—No. 6
Kyropoulos, S.—No. 16

Lui, Chung Kwai—No. 15

Neddermeyer, Seth H.—see Anderson, Carl D.
Nelson, E. C. and J. R. Oppenheimer—No. 9
Nielsen, Carl E.—No. 13

Oppenheimer, J. R.—Nos. 2 and 33
—— see Christy, R. F.
—— see Nelson, E. C.

Panofsky, W. K. H.—see DuMond, J. W. M.
Penther, C. J.—see Pompeo, D. J.
Pompeo, D. J. and C. J. Penther—No. 19

Reid, Curtis—No. 20
Rubens, Sidney M.—see Kaplan, Joseph

Schwinger, Julian—Nos. 8 and 32
——see Gerjuoy, Edward
Smick, Edward and Paul Kirkpatrick—No. 25
Stephenson, S. T.—No. 28
Stever, H. G.—No. 12
Strong, John—see Summerfield, Martin
Summerfield, Martin and John Strong—No. 23

Tomlinson, E. P.—No. 4
Tracy, R. L.—see Harris, F. S., Jr.

Wright, B. T.—see Alvarez, L. W.

Proceedings of the American Physical Society

MINUTES OF THE PROVIDENCE, RHODE ISLAND, MEETING

June 20–21, 1941

THE 243rd regular meeting of the American Physical Society occurred at Brown University, Providence, Rhode Island, on June 20 and 21, 1941.

A symposium on "The Philosophy of Physics" was held on the morning of June 21: the participants and titles of their papers were as follows:

The Relation of Theory to Experiment in Physics. W. F. G. SWANN, *Bartol Research Foundation of the Franklin Institute.*

The Place of Nuclear Physics Among Physical Theories. ENRICO FERMI, *Columbia University.*

Metaphysical Elements in Physical Theory. HENRY MARGENAU, *Yale University.*

Why do Scientists and Philosophers so often Disagree about the Merits of a New Theory? PHILIPP FRANK, *Harvard University.*

The abstracts of forty-two contributed papers, of which eight (Nos. 16, 29, 37, 38, 39, 40, 41, and 42) were read by title. These abstracts are herewith appended.

The meeting was distinguished rather by the quality than by the quantity of the attendance since only fifty-five were present at the dinner and probably not many more than one hundred at the sessions; this was attributed partly to the current preoccupations of many physicists and partly to the most unfavorable weather. After the dinner President Wriston of Brown University addressed the Society, and Dr. W. F. G. Swann and Mrs. Richard M. Bozorth played music of Bach, Bloch, Schumann, Van Goens and Boccherini for cello and piano.

At the dinner it was announced that Dean Pegram had resigned the presidency of the Society owing to the burden of duties connected with defense, and that by action of the Council Professor G. W. Stewart had succeeded him as President for the remainder of the year and Professor P. W. Bridgman had succeeded Professor Stewart as Vice President.

The Council met on Friday morning, June 20, 1941 and elected twenty-nine new Members, *viz.*: Heinrich H. Barschall, W. David Bemmels, Donald E. Brimley, Clinton M. Doede, Felix Ehrenhaft, Albert S. Eisenstein, William R. Kennedy, Arthur A. Klebba, James A. Krumhansl, Harvey M. Lashier, Herta Leng, Sister John Baptist Macelwane, Archie I. Mahan, Eugene C. Mallary, Edgar Meyer, Benjamin L. Moore, Nobuyosi Morita, Arnold P. G. Peterson, Frank W. Pote, Andre F. Reno, Frederick C. Roop, Vikram A. Sarabhai, Harold A. Sauer, Alfred Schild, Paul C. Sharrah, Everett P. Tomlinson, Kenichi Watanabe, Roger Williams, Jr., and Richard H. Woodward.

Word was received by the Council of the deaths of one Fellow (Frances G. Wick) and three Members (Richard Bär, Anna May Callan and James A. Chiles, Jr.).

KARL K. DARROW, *Secretary*
Columbia University, New York

ABSTRACTS

1. Diffusion of Thermal Neutrons. G. PLACZEK, *Cornell University.*—The transport equation for the diffusion of neutrons in an infinite medium in which scattering without velocity change, as well as capture, takes place has been solved for arbitrary distribution of isotropic sources in the cases of isotropic and of anisotropic scattering. The resulting distributions in time and space are compared with the results of the usual approximate treatment based on the diffusion equation. The relation of the solutions to the solution[1–3] of the problem of steady-state diffusion, with isotropic scattering, in a half-space bounded by a plane is discussed. In view of the fact that the scattering of thermal neutrons in paraffin seems to be rather anisotropic,[4] the application of the latter results to the diffusion of thermal neutrons in paraffin cannot be expected to yield complete agreement. This holds in particular for an attempt[2] to derive the ratio of capture and scattering cross sections.

[1] O. Halpern, E. A. Lueneburg and O. Clark, Phys. Rev. **53**, 173 (1938).
[2] E. A. Uehling and E. A. Schuchard, Phys. Rev. **58**, 611 (1940).
[3] E. A. Uehling, Phys. Rev. **59**, 136 (1941).
[4] N. Arley, Kgl. Dansk. Vid. Selsk. Medd. **16**, 1 (1938).

2. Angular Distribution of the *d-d* Neutrons. H. T. RICHARDS, *Rice Institute.*—In a recent calibration[1] of the stopping power of photographic emulsions for recoil protons, plates were placed at 0° and 90° to a heavy paraffin target 20 kev in thickness which was bombarded by 700-kev deuterons. Since the exposure conditions were identical for the plates at the two angles, the angular distribution of the neutrons from the *d-d* reaction may be inferred from the difference in number of recoil tracks on the two plates. The measured laboratory distribution $N(0°)/N(90°)=2.74$ was corrected for geometry and *n-p* scattering cross section.[1] The corrected distribution transformed to center of gravity coordinates gives $N(0°)/N(100°17')=2.62$. If the angular distribution of the neutrons is given by $N(\theta)=1+A\cos^2\theta$, then $A=1.84$ for 700-kev deuterons. At lower bombarding energies the angular distribution of the neutrons has been found[2] to be represented by the above expression with $A=0.7$ for 200-kev deuterons. Hence the angular distribution of the *d-d* neutrons is markedly dependent on the bombarding energy of the deuterons. This is similar to the result previously reported[3] for the protons from this same reaction.

[1] H. T. Richards, Phys. Rev. **59**, 796 (1941).
[2] Kempton, Browne and Maasdorp, Proc. Roy. Soc. **157**, 386 (1936).
[3] Huntoon, Ellett, Bayley and Van Allen, Phys. Rev. **59**, 97 (1940).

3. Yield of Neutrons and Beta-Rays from Li+H². W. E. BENNETT AND B. E. WATT, *Rice Institute.*—Measurements have been made on the yield of neutrons from lithium bombarded by deuterons. The targets of lithium hydroxide were less than 15 kev thick, and the neutrons were measured using a pressure electroscope of the Wulf type filled with methane. The excitation curve shows resonance peaks at 650 and at 1020-kev energy of the bombarding deuterons. The latter resonance is 80 kv broad and is more pronounced for neutrons in the forward direction than for neutrons at 90°. The yield of Li^8 from the same bombardment has been measured by coincidence counting of the high energy beta-rays. The yield curve shows the same resonance at 1020 kev as is shown by the neutrons. There is also a resonance at 750 kev, possibly the same as the broad 650-kev resonance for neutrons, but the peak is shifted to higher energy because Li^8 is produced by the emission of a low energy proton which must penetrate the potential barrier. A third resonance at 1350 kev is shown for beta-rays but not for neutrons.

4. 4.9-Mev Gamma-Ray from Li+H². T. W. BONNER AND H. T. RICHARDS, *Rice Institute.*—The gamma-rays from the bombardment of lithium by deuterons have been studied with Geiger counters. The energy was found, by measuring the range of Compton electrons in aluminum between coincidence Geiger counters, to be 4.9 ± 0.3 Mev. An absorption curve of the gamma-radiation in lead was taken to determine the ratio of intensities of the 4.9-Mev and the 440-kev radiation. The lower energy gamma-radiation is so much weaker that it was not detected. The yield of gamma-radiation as a function of bombarding energy was measured. The excitation curve was very similar to the neutron yield curve from the same bombardment. Since over 90 percent of the neutrons are from the disintegration of the Li^7 isotope, the neutron excitation curve is characteristic of Be^9 as the intermediate nucleus. Therefore the gamma-rays were not produced by the bombardment of the Li^6 isotope nor of any impurity in the target. However a similar yield curve would have been observed if the gamma-rays had been produced by inelastic scattering of the lithium neutrons in surrounding materials. This possibility was excluded by quantitative measurements.[1]

[1] Bennett, Bonner, Richards and Watt, Letter to the Editor, Phys. Rev., to be published.

5. Internal Conversion in Mercury. G. E. VALLEY,* *Harvard University.*—The radiation emitted by radioactive mercury formed by deuteron bombardment of gold will be discussed. It consists almost entirely of internal conversion lines lying in the energy region between 50 kev and 200 kev. The most intense of these fall at 63, 75, 84, 125 and 157 kev. Of these five at least the most energetic pair accompany the 25-hour decay period.

* National Research Fellow.

6. β-Spectra of Some Uranium Fission Products. G. L. WEIL, *Columbia University.*—The β-spectra of Kr^{88} ($T=3$ hr) and its daughter product Rb^{88} ($T=18$ min)[1] were investigated in a hydrogen-filled cloud chamber placed in a magnetic field. The radioactive krypton was extracted from a slow neutron irradiated uranyl nitrate solution and introduced into a thin-(12.4 mg/cm²) windowed cell located inside the cloud chamber. The electron spectrum of the composite source (Kr+Rb) shows a maximum at $H\rho$ 3500 and an end point at $H\rho$ 18,000. The spectrum clearly indicates the presence of at least two energy groups. Rb^{88} alone was obtained by collecting recoils from Kr^{88} disintegrations on thin aluminum foil (3.5 mg/cm²). Its spectrum shows a maximum at $H\rho$ 6000 and an end point at $H\rho$ 18,500 (5.06 ± 0.10 Mev). A straight line can be fitted to a Fermi plot[2] over the energy range 2.5 Mev to the end point. By subtraction of the rubidium spectrum from the composite (Kr+Rb) spectrum an end point of $H\rho$ 9200 (2.3 Mev) is obtained for Kr^{88}.

[1] G. N. Glasoe and J. Steigman, Phys. Rev. **58**, 1 (1940).
[2] F. N. D. Kurie, J. R. Richardson and H. C. Paxton, Phys. Rev. **49**, 368 (1936).

7. Nuclear Spin and Magnetic Moment of In^{113}. T. C. HARDY,* *The City College of New York,* AND S. MILLMAN,* *Queens College.*—The radiofrequency spectrum of the ground state of the indium atom has been studied in fields ranging from 3000 to 7000 gauss. Lines characterized by the transitions $\Delta F=0$, $\Delta m=\pm1$, have been observed for In^{113} as well as for In^{115}. The ratio of the depths of the resonance minima of a given transition observed in the two isotopes is in agreement with the known abundance ratio. The experiments give conclusive evidence that the spin of In^{113} is 9/2, the same as that of In^{115}. The ratio of the magnetic moments $\mu113/\mu115$, which is the same as the ratio of the hyperfine separations of the ground states of the two isotopes, is 0.998. The sign of the moment of In^{113} is positive, the same as that of In^{115}.

* Research done in laboratories of Columbia University.

8. The Nuclear Spin and Magnetic Moment of K^{40}. JERROLD R. ZACHARIAS,* *Hunter College.*—The molecular beam magnetic resonance method has been employed to observe the nuclear spin and the separation $\Delta\nu$ of the hyperfine-structure doublet of K^{40}. The apparatus and procedures used were different from those previously used by Kusch, Millman and Rabi[1] in their experiments with other alkali atoms because of the small natural abundance of K^{40} and because both the nuclear spin and the value of $\Delta\nu$ were previously unknown. The nuclear spin of K^{40} is shown to be 4 and the value of $\Delta\nu$ is 1285.65 ± 0.1 megacycles per second. The doublet is inverted. By comparison with the known nuclear magnetic moment and $\Delta\nu$ of K^{39}, the nuclear moment of K^{40} is shown to be -1.290 nuclear magnetons.

* Research done in laboratories of Columbia University.
[1] Kusch, Millman and Rabi, Phys. Rev. **57**, 765 (1940).

9. Interaction between Nuclear Spin and Molecular Rotation. HARVEY BROOKS, *Harvard University.*—The Hamiltonian for a diatomic molecule in a magnetic field contains coupling terms $-\mu H' \mathbf{I} \cdot \mathbf{J}$ for each nucleus where μ is the nuclear magnetic moment, $\mathbf{I}$ the nuclear spin operator, and $\mathbf{J}$ the angular momentum operator for molecular rotation. I have developed the quantum-mechanical formula for the constant H', which is

$$H' = \frac{Ze}{McR^3}\left[1 - \frac{R}{Zm}\frac{\langle L_1^2/r_1^3\rangle_{Av}}{\bar{E}}\right],$$

where M is the reduced mass, Z the nuclear charge, R the internuclear distance, and $\bar{E}$ a "centroid" frequency. In the expression $\langle L_1^2/r_1^3\rangle_{Av}$ L_1^2 is the electronic angular momentum about the nucleus rather than the molecular midpoint. I have calculated $\langle L_1^2/r_1^3\rangle_{Av}$ for H_2 with Nordsieck's wave function. $\bar{E}$ is estimated by comparison of "upstairs" and "downstairs" centroids as described previously.[1] The theoretical field H' is 24.6 gauss as compared with the observed 27.2. For HD and D_2 the experimental H' is proportional to M^{-1} as predicted by the theory.

[1] H. Brooks, Bull. Am. Phys. Soc., Washington Meeting, May 1, 1941, No. 57.

10. Angular Distribution of γ-Quanta Emitted Following β-Decay. DONALD R. HAMILTON,* *Harvard University.*—A nucleus left excited after β-decay emits one γ-quantum in the simplest case. One may investigate theoretically the probability, $W(\theta)$, that the direction of emission of this quantum will make an angle θ with that of the β-ray. The procedure is analogous to that used when a γ- instead of a β-ray is emitted in the first transition.[1] $W(\theta)$ depends on the γ-ray multipolarity, the angular momenta of the three nuclear levels involved, and the β-interaction. We have considered the Fermi and K–U interactions, using the plane wave electron approximation (light nuclei, high energies). $W(\theta)$ is uniform (independent of θ) for allowed transitions but non-uniform for "forbidden" transitions which are made possible by retardation of the electron waves across the nucleus. The non-uniformity is much greater for the Fermi interaction than for the K–U and is greatest, in either case, when the successive angular momenta are 0, 1, 0. Here (dipole γ-ray) $W(\theta) = 1 - 9/13\cos^2\theta$ (Fermi) or $1 - 1/11\cos^2\theta$ (K–U). In general, the non-uniformity is increased if only the higher energy electrons are considered.

* Society of Fellows.
[1] D. R. Hamilton, Phys. Rev. **58**, 122 (1940).

11. X-Ray Diffraction Analyses of Calcium Salts in Gallstones. R. PEPINSKY, *University of Chicago.**—In conjunction with studies on gallstone formation carried out in the University of Chicago Clinics by Dr. D. B. Phemister and his collaborators, x-ray diffraction analyses were made of forty-five stones from thirty-two cases showing precipitates rich in calcium salts. These analyses revealed two general and distinct types of aberrant calcium metabolism, the more common resulting in precipitation of one or more of the three polymorphic forms of calcium carbonate, and the other in the deposition of an apatite-like carbonate-phosphate similar to the material of bone or teeth. In the case of the carbonate precipitates, the polymorphs—calcite, aragonite and vaterite—appeared singly, or all three together, or in the combinations calcite-aragonite or calcite-vaterite, indicating specifically-differing precipitation conditions. Vaterite was apparently stabilized by the presence of bile pigments, and was often found free or almost free of the other forms. Four cases of phosphate precipitation, in the form of very finely-divided crystals, were observed, and in each of these the bladder was packed with large stones showing increasing pigmentation from duct to fundus. The value of compound and phase identification as a key to precipitation conditions, and the identification of organic constituents by the diffraction method, will be discussed.

* Now at U. S. Rubber Company, Providence, Rhode Island.

12. Fine Structure in the Diffraction of Low Speed Electrons. H. E. FARNSWORTH AND W. E. JOHNSON, *Brown University.*—Fine structure of electron diffraction beams has been observed by one of us[1] for a wide range of angle of incidence including normal incidence. For the case of symmetrical reflection, at a particular angle of incidence, from planes parallel to the crystal surface, the structure is observed by noting the variation of reflected intensity as the incident voltage is changed. Laschkarew[2] has suggested that, for several particular voltages, reflections from other sets of planes will occur besides those from the set under consideration; and these additional reflections may occur partially at the expense of the symmetrical reflection, thus resulting in depressions at several voltages. We have carried out more detailed computations than those of Laschkarew and find that such reflections are not adequate to account for the fine structure observed. Also, the fine structure characteristics from a single crystal face in different azimuths are found to be the same.[3] This would not be expected from the considerations of Laschkarew.

[1] H. E. Farnsworth, Phys. Rev. **40**, 684 (1932); **43**, 900 (1933).
[2] W. E. Laschkarew, Trans. Faraday Soc. **31**, 1081 (1935).
[3] H. E. Farnsworth, Phys. Rev. **49**, 598 (1936).

13. Optical Filtration in Stratified Media. R. B. LINDSAY, *Brown University.*—The transmission of light at normal incidence through a stratified medium consisting of alternate plane parallel layers of two different substances is closely analogous to the transmission of elastic waves through non-homogeneous media. In the optical case the electrical and magnetic field vectors play roles corresponding to the pressure and volume current, respectively, in the acoustical case. The theory of elastic wave filtration[1] can at once be applied and leads to the characteristic function for the equivalent infinite structure

$$\cos W=\cos 2k_1l_1\cdot\cos 2k_2l_2-\tfrac{1}{2}\left(\frac{n_1}{n_2}+\frac{n_2}{n_1}\right)\sin 2k_1l_1\cdot\sin 2k_2l_2,$$

where $2l_1$ and $2l_2$ are the layer thicknesses respectively, while n_1 and n_2 are the absolute indices of refraction of the two substances. As usual $k_1=\omega/c_1$ and $k_2=\omega/c_2$, where c_1 and c_2 are the light velocities in the two layers and $\omega/2\pi$ is the frequency. If the layers are composed of crown glass and air of thickness 0.008 cm and 0.001 cm, respectively, the transmission bands in the yellow part of the spectrum are approximately 10A wide and the attenuation bands approximately 1.0A wide. It is comparatively easy to observe the bands by passing white light through a pile of microscope cover glasses and examining it by means of a reflection grating of moderate resolving power.

[1] Cf. J. Acous. Soc. Am. **5**, 202 (1934).

14. The Absorption of Alkali Halides in the Extreme Ultraviolet. EDWIN G. SCHNEIDER, *Stevens Institute of Technology.*—Absorption measurements on thin films of alkali halides have been extended into the region between 400 and 1000A. Difficulties due to overlapping orders of spectra were avoided by using a speculum grating at normal incidence, the low reflecting power for the short wave-lengths furnishing a convenient lower limit to the spectrum. The salts were deposited on thin films of Formvar, a plastic made by the Shawinigan Products Corporation, prepared by placing a drop of a chloroform solution of the plastic on water. A number of intense narrow bands are evident. Some of these are identified as transitions from the inner shells of electrons in the atoms to discrete excited states while others are probably caused by structure in the continuous absorption region.

15. Selection Rule for Collisions of the Second Kind. J. G. WINANS, *University of Wisconsin.*—The sensitized fluorescence spectrum of tin in Hg vapor at about one-cm pressure excited by 2536 showed 3034 ($^3P_0-^3P_1$) much stronger than 3009 ($^3P_1-^3P_1$). The carbon arc spectrum of tin showed these lines with about equal intensity. The corresponding lines of lead 3683 ($^3P_0-^3P_1$) and 3639 ($^3P_1-^3P_1$) appeared with nearly equal intensity in both sensitized fluorescence and carbon arc spectra. However, sensitized fluorescence of lead at high mercury pressures (15 to 40 cm) gave 3683 as the only lead line with appreciable intensity, and therefore much stronger than 3639. The unequal excitation of these lines may be attributed to 6^3P_0 Hg atoms since, at high pressure, Hg 6^3P_1 would be quenched by collisions with Hg atoms and at low pressure with tin by transfer of energy to those tin levels which have very low energy discrepancy. The selection rule which appears to be followed is: For change of J from 0 to 0 in Hg, a collision of the second kind is more likely if a change in J from 0 to 0 takes place in Sn or Pb. The more general rule may be ΔJ equals zero where J is the resultant angular momentum vector for the quasi-molecule formed upon impact of Hg with Sn or Pb. If excitation is from Hg_2' $^1\Sigma$ from $^1S_0$ and $^3P_0$, the same selection rule is indicated.

16. A Radiant Energy Theory of the Absorption of Primary X-Rays, Ionization and Photoelectron Emission. SAMUEL R. COOK, *Sacramento, California.*—An explanation of the absorption of primary x-rays by matter has been made, in accordance with the tenets of the radiant energy theory of primary x-rays. It has been shown that the product of the absorption of a radiant energy quantum is a high speed beta-electron, and that the liberation of the electron from a molecule produced ionization of the absorbing material. It was also shown that the high speed beta-electron, which was the direct product of the absorption of a primary x-ray, was, when liberated from the absorbing material, a photoelectron, which explained photoelectron emission. Equations for the absorption were developed and it appeared that the equation for absorption of a primary x-ray and the liberation of a beta-electron was identical with Einstein's equation for photoelectron emission.

17. Phenomena of Photophoresis and Special Application for the System Sun-Earth. LEO BANET (*Introduced by W. F. G. Swann*).—A short description of the phenomena of longitudinal photophoresis, electro-photophoresis and magneto-photophoresis (i.e. the movement of small particles in the beam of light itself and the movement of such particles under the influence of electric and magnetic fields) will be given. Considering the fact that the phenomena have not been clearly explained by mechanical or radiometer forces, an interpretation on the basis of electric and magnetic forces will be given. Some applications for the phenomena on the Sun and on the Earth will be cited where photophoretic effects are observed. The influence of the sunspot cycle on the terrestrial phenomena as well as the general influence of the radiation of the Sun on the Earth's magnetism will be described. The possibility of finding an explanation of the cause of the Earth's magnetism in terms of the photophoretic influence will be discussed.

18. Photophoresis: Applications and the Question of the Existence of Unipolar Magnetism. FELIX EHRENHAFT (*Introduced by W. F. G. Swann*).—The interpretation of the phenomena of photophoresis leads to new consequences. Such are the "trembling-effect" discovered in the observation of magneto-photophoresis, the coagulation of matter under the influence of the light, the growth of some crystals toward the light, the influence of the light on Brownian movement and diffusion, etc. On the hypothesis of a unipolar magnetic "ion" it is also possible to determine from those measurements the magnitude of its magnetic charge. The question of the existence of unipolar magnetism is discussed, and the insufficiency of experimental evidence against it is indicated.

19. Operational Details of the Bartol Electrostatic Generator. W. E. DANFORTH AND EMMETT L. HUDSPETH, *Bartol Research Foundation of the Franklin Institute.*—A vertical pressure Van de Graaff generator has been completed and is now delivering two million volts. The unit is patterned after the compact x-ray generators of Trump and has been adapted for positive ion acceleration. A tank 13 feet in over-all height and 44 inches in diameter, which will withstand a pressure of 200 pounds, encloses an accelerating tube of twenty porcelain cylinders, each of which is $6\frac{1}{2}$ inches I.D. and $3\frac{1}{4}$ inches in height. Fifty-two equipotential rings of 24-inch diameter surround the accelerating tube; uniform potential distribution is obtained by connecting adjacent rings through a 500-megohm IRC power resistor. The ion source assembly is supplied by a 120-v d.c. generator and a 110-v a.c. converter. Controls for the apparatus in the high potential spinning are connected by flexible shafting to textolite rods which run to a gear box and more flexible shafting at the bottom of the tube. Small lamps, connected in the separate circuits of the ion source, are focused on photoelectric cells at the lower end of the tube. Variation of the respective intensities of the lamps yields corresponding photoelectric currents. These have been suitably calibrated to give reliable readings of instruments in the high-potential spinning.

20. Consequences of the Assumption of a Single Primary Component in the Cosmic Radiation. W. F. G. SWANN, *Bartol Research Foundation of the Franklin Institute.*—The paper comprises an extension of the discussions already made by the writer of the effect of energy combined with mean life considerations in determining the degree of asymmetry in electron emission at different altitudes. When the logarithm of the mesotron intensity is plotted against altitude, the relation is linear for low altitudes when the altitude is expressed in terms of actual distance, but it is non-linear when expressed in terms of water equivalent distance. The reverse is true at higher altitudes where linearity occurs when water equivalent distance is used. The relation of these facts to the relative parts played by mean life considerations and ionization loss is discussed. The bearing of the sea-level latitude effect in relation to the initial energy of the mesotrons and of their parents is examined.

21. On the Theory of the Photo-Effect in Semi-Conductors. V. F. WEISSKOPF AND L. W. APKER, *University of Rochester.*—The surface photo-effect in metals has so far been calculated by using Sommerfeld's assumption of completely free electrons within the metal. This assumption is justified for good conductors in which the characteristic energy bands are half-filled. In the case of semi-conductors, however, it is assumed that the energy bands are completely filled and the free electron theory is no longer adequate. The number of electrons $N(E)dE$ emitted with a given energy E by light of frequency ν is proportional to the number of electrons with an equivalent energy ϵ within the material and proportional to the transition probability P. If the electrons emitted come from states in the upper edge of a filled band, as it is in the case of a semi-conductor, we can make use of the fact that the density of states near the upper edge is known to be const. $(\epsilon_0-\epsilon)^{\frac{1}{2}}d\epsilon$ where ϵ_0 is the highest energy in the band. We further assume that the probability P is proportional to the velocity of the "hole" created by the removal of the electron, which carries away the charge, and obtain $N(E)dE=\text{const.}\ (h(\nu-\nu_{th})-E)^2dE$ where ν_{th} is the threshold frequency. This distribution should be independent of the temperature. Measurements to verify this distribution are under way in this laboratory.

22. Preparation of Tungsten Single Crystal Faces for Thermionic Emission Studies. A. A. BROWN, *Brown University (Introduced by H. E. Farnsworth).*—For obtaining thermionic work functions of different faces of single crystals, it is desirable to obtain smooth plane surfaces parallel to the desired set of crystallographic planes and exposing the undistorted crystalline lattice. A method of doing this is described for the (110) and (100) faces of single crystals of tungsten. An etching solution of equal parts of boiling 30 percent $K_3Fe(CN)_6$ and 10 percent NaOH exposed only (110) type faces. Using a goniometer, the lattice orientation was then determined uniquely and a thin diamond saw used to cut parallel to the desired planes. The saw marks were removed by grinding and the surface polished with dry levigated alumina on a hard surfaced lap. This left a disturbed layer which had to be removed. No chemical reagent could be found which would etch parallel to the surface without excessive pitting. A few attempts at heat treatment produced only a mosaic surface composed of randomly oriented crystallites. Satisfactory surfaces were finally obtained by partially removing the disturbed surface by electrolytic polishing with NaOH followed by heat treatment at 2600°K. It was determined by very slight chemical etching that this exposed the undistorted lattice.

23. Attenuated Superconductors. II. Pb, Sn, Cb and Ta. W. F. BRUCKSCH, JR., W. T. ZIEGLER, F. H. HORN AND DONALD H. ANDREWS, *The Johns Hopkins University.*—Measurements previously reported[1] on films have been extended by using films of Pb from 0.02μ to 1μ thick. The same technique was also applied to fine wires of Pb, Sn, Cb and Ta with diameters ranging from 26μ to 260μ. Variation of resistance with temperature was studied in the neighborhood of the superconducting transition point, with magnetic fields ranging from zero to ninety oersteds and with currents from 10^{-5} to 0.3 amp. All the samples of lead studied including evaporated films, drawn wires, and capillary-moulded wires had transition temperatures identical to within 0.05°, the probable experimental error. The width of the transition zone varied from 0.02° for a film 0.6μ thick to 0.08° for a film 0.02μ thick. Critical current values increased and approached the bulk metal value as thickness increased. In contrast with Sn and Pb, the hard metals Cb and Ta showed a depression of the transition temperature as the wire diameter was reduced. Cb wire, 25μ diam., had a transition at about 7°K and showed a residual resistance of 1 percent below this temperature. Ta wire, 25μ diam., failed to become superconducting even at 3.2°K. An x-ray study showed it to be polycrystalline.

[1] Phys. Rev. **59**, 688 (1941).

24. Young's Modulus of NaCl Near the Melting Point. LLOYD HUNTER, *Carnegie Institute of Technology*, AND SIDNEY SIEGEL, *Westinghouse Research Laboratories.*—Measurements of Young's modulus were made on several different NaCl crystals cut in {100} and {110} orientations. The temperature range covered was 290°K to 1077°K, the melting point of NaCl. The method used was a piezoelectric oscillator method. The oscillator consisted of a quartz crystal driver, a long fused silica rod which extended into the high temperature furnace, and the NaCl specimen. This arrangement made it possible to keep the quartz crystal near room temperature and at the same time drive a specimen at high temperature, thus obviating any difficulties due to the quartz crystallographic change at 849°K. It was found that for the {100} orientation the Young's modulus decreases from 4.440×10^{11} dynes/cm² at 290°K to 1.527×10^{11} dynes/cm² at the melting point. The Young's modulus of the {110} orientation does not change as rapidly, decreasing from 3.490×10^{11} dynes/cm² at 290°K to 2.062×10^{11} dynes/cm² at the melting point. The Young's modulus is the same for both orientations at 653°K, thus showing that NaCl is elastically isotropic at this temperature.

25. Theory of Cathode Sputtering in Low Voltage Glow Discharges. C. H. TOWNES, *Bell Telephone Laboratories.*—Cathode sputtering has been shown to involve the release of atomic material from the cathode by an impinging positive ion and the subsequent diffusion of this material to surfaces surrounding the cathode. To determine the amount of sputtering in a glow discharge three functions must be known: the number of ions of a given energy striking the cathode, the amount of material released from the cathode by each ion, and the fraction of material released from the cathode which diffuses away. Estimates are made of these, and an expression is obtained giving the dependence of the total rate of sputtering on the geometry of the discharge, pressure, cathode fall, current, and constants of the gas and cathode surface. It is most accurate for very low voltage, high pressure discharges. Comparisons with data will be given.

26. Visualizing Airflow. ERWIN J. SAXL, *Providence, Rhode Island.*—Bullets passing through air at great velocity are known to set up compression and decompression waves that can be made visible under certain conditions of spark photography. Inversely, air passing objects at great velocities produces upon them distinct disturbances that possibly are at the root of the vortices, and discontinuities that peal off subsequently from such surfaces and greatly reduce the potential speed of fast aircraft as observed on a larger scale in wind-tunnel experiments. A new technique was developed by the writer whereby the origin of such vortices can be made visible directly. Wave phenomena of a recurring geometrical pattern were recorded. The method lends itself to the investigation of surfaces and objects of every description. Photographs of air moving in the neighborhood of sound velocity relative to objects have been made, particularly of air escaping orifices at approximately sonic speed. A peculiar wave pattern is recorded within that air stream. The speed of the air was calculated from the pressure of the gases before leaving the throat. The theoretical fundamentals are discussed that underlie the phenomena recorded and suggestions are made as to the utilization of the facts observed with particular reference to today's high speed airplanes, internal combustion engines and other instances where gases travel at high relative speeds.

27. Acoustic Filtration in Parallel Conduit Structures. L. W. LABAW, *Brown University* (*Introduced by R. B. Lindsay*).—The acoustical structure consisting of parallel conduits (Quincke-Herschel tubes) combined in series by means of single conduit connectors has been studied theoretically, and found to be a band pass acoustic filter.[1] By varying the dimensions of the conduits, nearly any frequency region up to 10,000 cycles may be attenuated. The energy transmission between the attenuation bands depends on the number of sections and the type of ending. Measurements of the transmitted power were made by recording on an oscillograph the amplified voltage from a small Rochelle salt crystal sound cell which was used as a detector and constructed to fit in the connecting conduit with its length along the tube axis and its width along the tube diameter. The number of experimental peaks in the transmission regions, and the position of the attenuation bands agree with the predictions of the theory. The values of the curve minima in the transmission bands are in excellent agreement up to 5000 cycles. The change of phase over the filter was also measured and found to correspond closely to the theory.

[1] L. W. Labaw, J. Acous. Soc. Am. **12**, 232 (1940).

28. Molar Refraction of Carbon Dioxide as a Function of Density. F. B. OLESON AND C. E. BENNETT, *University of Maine.*—Recent measurements on carbon dioxide have not only confirmed the results of preliminary work recently reported by the senior author[1] but have extended the density values to 0.0448 gram per cc. Whereas Keyes and Oncley[2] report an increase in molar polarization with density at large density values, the present findings, based upon precise optical measurements at lower densities, indicate a definite decrease of this quantity when the density values are computed by the Keyes equation of state. It is noted, however, that the results are changed somewhat by the use of the Beattie-Bridgeman equation of state, but not enough to conclude that the molar refraction at zero frequency increases with density. The question is thus raised whether or not molar refraction at zero frequency is the same as molar polarization of carbon dioxide. The best value of molar refraction at zero frequency (referred to by some authors as the L–L function) found by displacement interferometry is between 6.55 and 6.65 when extrapolated to zero density.

[1] C. E. Bennett, Phys. Rev. **58**, 263 (1940).
[2] F. G. Keyes and J. L. Oncley, Chem. Rev. **19**, 3, 195 (1936).

29. Vapor Pressure Determination of HTO and DTO. W. F. LIBBY AND R. CORNOG, *University of California.*—The vapor pressure of HTO in H_2O and DTO in D_2O has been measured as a function of temperature in the range of

25°C to the boiling point under one atmosphere. Because of the sensitivity of the radioactive method employed, it has been possible to check the accuracy of Henry's law at dilutions of one part in ten million. It is also possible, assuming a perfect solution, to compute that the boiling point of pure HTO under a pressure of one atmosphere is less than that of H_2O.

30. Turbulent Flow of Argon in a Hot-Wire Clusius and Dickel Column. RALPH SIMON, *Yale University.*—The "hot wall" of a 22-mm diameter glass column two meters long is a 20-mil tungsten wire. Following the method of Onsager and Watson,[1] the pressure at which lamellar flow breaks up into turbulence is determined at various wire temperatures from 400° to 1700°K. The curve of critical pressure *versus* temperature has a minimum at 650°±50°K. From this fact it is possible to estimate the value of the exponent in the viscosity law $\eta = cT^n$ in fair agreement with viscosity measurements. The Reynolds' number for the hot-wire type of convective flow is found to be much less than that for pressure flow through cylindrical tubes. A preliminary investigation of this type should prove extremely valuable in the design of a thermal diffusion apparatus because the onset of turbulence (the avoidance of which is essential for efficient operation) sets an upper limit to the usable value of Kc/Kd, the ratio of remixing by convection and by diffusion. It is planned to construct an apparatus for the concentration of the A^{36} isotope.

[1] L. Onsager and W. W. Watson, Phys. Rev. **56**, 474 (1939).

31. Correlations in Dielectric Data. ROBERT H. COLE, *Harvard University.*—It is well known that it is possible to calculate the transient current in a dielectric as a function of time after application of a constant potential difference if the frequency dependence of the complex dielectric constant is known, and vice versa. The fact that either the real or the imaginary part of the complex dielectric constant may be used for this calculation suggests that either one of these quantities is determined if the complete frequency dependence of the other is known. Integral equations expressing this correlation have been given by Kramers for the case of optical dispersion.[1] It will be shown that these relations may be derived (a) from the expressions for the transient current by use of Fourier transforms, or (b) as a special case of the Hilbert transforms. A knowledge of either the real or imaginary parts of the complex dielectric constant *versus* frequency or the transient current *versus* time thus specifies completely the dielectric properties at a given temperature of a substance for which the superposition principle is valid. Possible applications of these relations and their bearing on some previous attempts to correlate dielectric data will be discussed.

[1] H. A. Kramers, Atti Congr. dei Fisici, Como (1927), p. 545.

32. A Derivation of the Thermodynamic Equations for the Heats of Reaction of Saturated Weston and Clark Standard Cells. F. G. BRICKWEDDE AND L. H. BRICKWEDDE, *National Bureau of Standards.*—Saturated cells involving the formation of *hydrated* salts are either neglected or incorrectly treated in even the most recent texts on thermodynamics. The Gibbs-Helmholtz equation relating the heat of the cell reaction to the free energy changes is not directly applicable to the electromotive force of cells in which the concentration of a solution entering the cell reaction changes with temperature. Only in Jellinek's *Lehrbuch der physikalischen Chemie* (1930) have we found a derivation of the equation $Q/2\mathbf{F} = E - T(dE/dT)$ for such saturated cells, where Q is the heat of the complete cell reaction and E is the e.m.f. of the saturated cell. A simpler and more satisfactory derivation of this equation will be given. Equations are obtained relating the e.m.f. of a *saturated* cell with the heat changes of the various parts of the cell reaction. For example, for the reaction Cd (2-phase amalgam) $+ Hg_2SO_4(c) = 2Hg(l) + CdSO_4$ (dissolved in sat. soln.) the equation is

$$Q' = 2\mathbf{F}\left[E - T\left(\frac{dE}{dT}\right)_{\text{sat.}} + T\left(\frac{\partial E}{\partial m}\right)_T \left(\frac{dm}{dT}\right)_{\text{sat.}} - T\left(\frac{\partial E}{\partial p}\right)_T \left(\frac{dp}{dT}\right)_{\text{sat.}}\right],$$

where m and p are the concentrations of the aqueous solution and solid amalgam, respectively.

33. Optimum Design of Physical Apparatus. R. C. SPENCER, *University of Nebraska.*—A distortionless apparatus would be one for which the output function $G_1(x)$, after correction for a possible shift h in the origin, is proportional to the input function $G_0(x)$. Thus, $G_0(x) = e^{hD}G_1(x)$, where the relative impedance e^{hD} is the Heaviside shift operator. The optimum design for low values of hD is obtained by expanding the operator for the apparatus into a power series $\Sigma a'_n D^n$ and then equating the first few coefficients to those of e^{hD}. There are four equivalent[1] conditions. (1) $a'_n = a'^n_1/n!$ (2) Each reduced coefficient is zero. (3) The moments μ'_n of the response of the apparatus to a unit impulse are given by $\mu'_n = \mu'^n_1$. (4) Each reduced moment is zero. Only underdamped systems satisfy these conditions so that a static system whose response is essentially positive must be coupled to an underdamped dynamic system. This method satisfies the two conditions of constant amplitude response and linear phase response necessary in television. Although ideal for low frequencies, the method introduces resonance peaks at the higher frequencies. The theory is illustrated by examples from spectroscopy, statistics and television.

[1] R. C. Spencer, Phys. Rev. **55**, 239A (1939).

34. The Principle of the Unobservable. H. M. DADOURIAN, *Trinity College.*—After analyzing the concept of the unobservable, Herbert Dingle has reached the conclusion that we must either presume omniscience, or abandon our belief in the external world, if we accept the principle: *That which is unobservable is not significant.* As the first alternative is untenable, Dingle has faced us with the dilemma of either accepting a form of solipsism or abandoning a principle which has proved to be of great value. Dingle's dilemma is due to his tacit assumption that the principle states a logical proposition. The dilemma disappears if the principle of the unobservable is taken to be what it really is—an heuristic principle, a useful and convenient rule of action for investigators.

35. Physical Theory and a Monistic Conception of the Universe. ENOS E. WITMER, *University of Pennsylvania.*—In this paper an attempt is made to interpret the theory of relativity and quantum mechanics from a more general point of view, into which the facts of biology and psychology can be fitted in a satisfactory manner.

36. Physics as "Useful Fiction." G. A. FINK, *C. K. Williams and Co.*—Some of the sources of the philosophical theory to be presented, and some of its resemblances to others, are noted. Definitions of science, physics, philosophy, fiction and usefulness are given. The science of physics, considered as a human activity which has evolved from crude beginnings, is discussed from an esthetic and psychological point of view. The characteristics desirable for a physical theory—agreement of its predictions with experiment, logical coherence, simplicity and use of familiar space-time concepts with a minimum of modification—are discussed, and explained by the "useful fiction" theory. The fictional nature of all physical concepts is emphasized and illustrated, using "force" as the chief example. The spirit of the present theory is well illustrated by the following excerpt from the chapter on "The Art of Thinking" in Havelock Ellis' *The Dance of Life:* "thinking we may regard as fiction that helps us to live." And thinking is the most essential part of the activity we call science.

37. On a Modification of Planck's Quantum Theory with Special Reference to an Explanation of His Oscillators. SAMUEL R. COOK, *Sacramento, California.*—The paper consists of a statement of Planck's quantum theory in the light of the tenets of the radiant energy theory of the genesis and absorption of primary x-rays.

38. Velocity of Sound in Gases at Temperatures Below the Ice Point. THOMAS H. QUIGLEY, *College of the Holy Cross.**—The fixed path acoustic interferometer possesses distinct advantages for work at low temperatures, such as absence of moving parts with the avoidance of leaks and contaminations of material, and the elimination of the necessity of piston rods or guides for a moving reflector. The interferometer unit consists of a ring of fused quartz with optically plane parallel faces, separating a plane fused quartz reflector and a piezoelectric quartz X cut plate with condensed gold film electrodes. This, with thermocouples, is assembled inside a copper cylinder which is supported at the bottom of a cryostat. Temperature equilibrium is maintained by balancing cooling by evaporation of liquid nitrogen and heating produced electrically in a Nichrome wire wound around the copper cylinder. Temperature is varied until a value for resonance is determined with precision. Sound velocities for 17 temperatures for air and for 12 temperatures for methane between 90°K and the ice point have been determined. These are of great self-consistency, but for each gas lead to a slightly smaller value of sound velocity at 0°C than that commonly accepted; for air, 330.6; for methane, 427.2 m/sec. A detailed analysis of the results will be published.

* The work here reported was done in the Laboratory of Physics of the Johns Hopkins University.

39. The Neutrino Concept. ALEXANDER W. STERN, *Brooklyn, New York.*—The evolution of the neutrino is traced from its conception by Pauli in 1931 to its recent application in the theory of stellar explosions.[1] While originally the neutrino was evoked to save the conservation laws in the beta-disintegration process, it is now called in to rationalize the hypothesis[1] of the *disappearance* of energy from exploding stars. With regard to these stellar bodies there is no conservation of energy—in fact, the star ultimately "dies" (astrophysically) from lack of energy conservation. But the nonconservation of energy is here achieved by purely conventional and accepted means—the intervention of the neutrino to "kidnap" the energy from the star. Even if the neutrino were found to exist, a process such as that envisaged by Gamow and Schoenberg would mean a violation of the conservation laws as far as the stellar bodies in question are concerned. It is interesting to note that heretofore the neutrino appeared only in a secondary role, as a "by-product" of beta-disintegration, and its emission had no physical consequence. Here its role is of primary importance and it is one of the contributing causes of the phenomenon investigated.

[1] G. Gamow and M. Schoenberg, Phys. Rev. **59**, 539 (1941).

40. Magnetic Rotatory Power of Crystalline Nickel Sulfate in the Ultraviolet Region. J. J. O'CONNOR, C. BECK, AND N. UNDERWOOD, *Vanderbilt University.*—Previous measurements of the magnetic rotatory power of crystalline α-$NiSO_4 \cdot 6H_2O$ in the visible region of the spectrum and at one point in the ultraviolet have been extended into the ultraviolet as far as the 2537A line of the mercury spectrum. An unsymmetrical anomaly has been found at the strong 3850A absorption band. The constants in the equation for the magnetic rotatory dispersion have been evaluated so that Verdet constants calculated from the equation agree with the experimental values throughout the visible and ultraviolet except within the 3850A absorption band. The equation is

$$\alpha = \frac{(n^2+2)^2}{9n} \frac{0.00509\lambda^2}{(\lambda^2-0.123^2)^2}.$$

α is in minutes per oersted-cm, n is index of refraction and λ is in microns.

41. Scattering of Protons from 200 to 300 kev. H. MACK THAXTON, *The Agricultural and Technical College, Greensboro, North Carolina.*—G. L. Ragan, W. R. Kanne and R. F. Taschek[1] have observed the scattering of protons in hydrogen from 200 to 300 kev. Theoretical calculations have been made for comparison with these experiments at 10-kev intervals in this energy region for potentials, Gauss[2] error ($A \exp[-\alpha r^2]$); meson[3] ($Ce^{-r/a}/r/a$); exponential[4] ($Be^{-2r/b}$); Morse[5] $D(e^{-4r/a}-2e^{-2r/a})$; and square well[2] with depth 10.5 Mev. Phase shifts have been calculated for each energy and are, for example, 8.82°; 8.67°; 9.11°; 9.02°; 8.83°; respectively, for the potentials above and the energy 250 kev. The Mott ratios are calculated for all angles from 15° to 45° and graphs of these ratios and quantities easily comparable with experiment are given as functions of angle and energy. In addition, tabulated values of all mathe-

matical quantities necessary for direct comparison with the experimental data are given. The presence of the phase shift K_1 has been investigated and is negligible for all potentials at 300 kev.

[1] K. S. Cole and R. F. Baker, Phys. Rev. **59**, 685A (1941).
[2] G. Breit, H. M. Thaxton and L. E. Eisenbud, Phys. Rev. **55**, 1018 (1939).
[3] L. E. Hoisington, S. S. Share and G. Breit, Phys. Rev. **56**, 884 (1939).
[4] W. Rarita and R. D. Present, Phys. Rev. **51**, 793 (1937).
[5] H. M. Thaxton and D. M. Monroe, Phys. Rev. **57**, 246 (1940).

42. Total Atomic Scattering Cross Sections for Fast Electrons. L. I. SCHIFF, *University of Pennsylvania.*—Marton[1] has recently suggested that the thicknesses of electron microscope objects can be determined by measuring the transmission of the electron beam through them. To correlate transmission and thickness it is necessary to know the scattering cross sections of the atoms involved. Calculation shows that the inelastic (small energy loss) and elastic scattering are of comparable importance, and that the angular aperture of the electron microscope is so small that total cross sections can be used to calculate the diminution of intensity of the electron beam. Results have been obtained for a large number of atoms and ions using Hartree wave functions and the Thomas-Fermi model for elastic scattering, and Slater wave functions for the inelastic scattering. These will be published soon, together with a discussion of the related experiments, in collaboration with L. Marton in the *Journal of Applied Physics.*

[1] L. Marton, Bull. Am. Phys. Soc., Washington Meeting, May 1, 1941, No. 77.

Author Index to Abstracts of Papers Presented at the Providence Meeting

Andrews, Donald H.—see Brucksch, W. F., Jr.
Apker, L. W.—see Weisskopf, V. F.

Banet, Leo—No. 17
Beck, C.—see O'Connor, J. J.
Bennett, C. E.—see Oleson, F. B.
Bennett, W. E. and B. E. Watt—No. 3
Bonner, T. W. and H. T. Richards—No. 4
Brickwedde, F. G. and L. H. Brickwedde—No. 32
Brickwedde, L. H.—see Brickwedde, F. G.
Brooks, Harvey—No. 9
Brown, A. A.—No. 22
Brucksch, W. F., Jr., W. T. Ziegler, F. H. Horn and Donald H. Andrews—No. 23

Cole, Robert H.—No. 31
Cook, Samuel R.—Nos. 16 and 37
Cornog, R.—see Libby, W. F.

Dadourian, H. M.—No. 34
Danforth, W. E. and Emmett L. Hudspeth—No. 19

Ehrenhaft, Felix—No. 18

Farnsworth, H. E. and W. E. Johnson—No. 12
Fermi, Enrico—No. II
Fink, G. A.—No. 36
Frank, Philipp—No. IV

Hamilton, Donald R.—No. 10
Hardy, T. C. and S. Millman—No. 7
Horn, F. H.—see Brucksch, W. F., Jr.
Hudspeth, Emmett L.—see Danforth, W. E.
Hunter, Lloyd and Sidney Siegel—No. 24

Johnson, W. E.—see Farnsworth, H. E.

Labaw, L. W.—No. 27
Libby, W. F. and R. Cornog—No. 29
Lindsey, R. B.—No. 13

Margenau, Henry—No. III
Millman, S.—see Hardy, T. C.

O'Connor, J. J., C. Beck and N. Underwood—No. 40
Oleson, F. B. and C. E. Bennett—No. 28

Pepinsky, R.—No. 11
Placzek, G.—No. 1

Quigley, Thomas H.—No. 38

Richards, H. T.—No. 2
—— see Bonner, T. W.

Saxl, Erwin, Jr.—No. 26
Schiff, L. I.—No. 42
Schneider, Edwin G.—No. 14
Siegel, Sidney—see Hunter, Lloyd
Simon, Ralph—No. 30
Spencer, R. C.—No. 33
Stern, Alexander W.—No. 39
Swann, W. F. G.—Nos. I and 20

Thaxton, H. Mack—No. 41
Townes, C. H.—No. 25

Underwood, N.—see O'Connor, J. J.

Valley, G. E.—No. 5

Watt, B. E.—see Bennett, W. E.
Weil, G. L.—No. 6
Weisskopf, V. F. and L. W. Apker—No. 21
Winans, J. G.—No. 15
Witmer, Enos E.—No. 35

Zacharias, Jerrold R.—No. 8
Ziegler, W. T.—see Brucksch, W. F., Jr.